DIETARY TOMATO CAROTENOIDS AND β-CAROTENE-15,15'-DIOXYGENASE (*Bco1*) GENOTYPE ALTER ANDROGEN METABOLISM, LIPID METABOLISM, AND PROSTATE CANCER PROGRESSION IN MICE

BY

JOSHUA WILLIAM SMITH

DISSERTATION

Submitted in partial fulfillment of the requirements
for the degree of Doctor of Philosophy in Nutritional Sciences
in the Graduate College of the
University of Illinois at Urbana-Champaign, 2016

Urbana, Illinois

Doctoral Committee:

Professor Emerita Elizabeth H. Jeffery, Chair
Professor Emeritus John W. Erdman, Jr., Director of Research
Professor William G. Helferich
Assistant Professor Eric C. Bolton

ABSTRACT

β-carotene-15,15'-dioxygenase (BCO1) cleaves dietary carotenoids at the central 15,15' double bond, most notably acting on β-carotene to yield retinal. Much work has gone into the description of enzymatic carotenoid cleavage activities of the enzyme, but although pleiotropic effects of *Bco1* loss on lipid and cholesterol metabolism *in vivo* have occasionally been described, few investigators have reported extensively on this. Furthermore, given the intersections of lipid metabolism, cholesterol/steroid metabolism, and carotenoid transport and distribution, functions of BCO1 within these interdependent realms is of clear physiological relevance. Moreover, since observational data in humans have repeatedly demonstrated that tomato carotenoid intake is associated with a reduced risk of primary prostate cancer (PCa), fundamental knowledge of the role of BCO1 on steroid and lipid metabolism is imperative for proper interpretation of epidemiological and experimental data demonstrating a protective role of dietary tomato. Thus, using animal models, we sought to: elucidate the carotenoid cleavage-independent role of Bco1 on circulating testosterone and prostatic androgen signaling; determine the impact of Bco1 on lipid, cholesterol, and retinoid metabolism in the liver, a key organ in the metabolism and biodistribution of dietary carotenoids; and evaluate the effects of dietary tomato feeding in an animal model of PCa and determine its efficacy in preventing disease progression.

In Chapter 2, using the *Bco1*$^{-/-}$ mouse model, we sought to probe the effects of *Bco1* ablation on testicular steroidogenesis, serum testosterone levels, and prostatic androgen signaling. Male wild-type (WT) and *Bco1*$^{-/-}$ mice were raised on carotenoid-free AIN-93G diets before sacrifice between 10-14 weeks of age. We observed a significant reduction in serum testosterone levels due to *Bco1*$^{-/-}$ genotype, accompanied by significantly reduced weights of the prostate and seminal vesicles. This reduction in serum testosterone may have been driven by

significant reductions in the expression of a testicular steroidogenic gene (*Hsd17b3*) and/or Leydig cell populations. Concomitantly, we observed reductions in markers of androgen signaling, proliferation, and cell cycle progression in the prostate. Together, these data support a hypothesis that *Bco1*$^{-/-}$ mice exhibit reduced testicular testosterone synthesis, concomitant with a lowering of circulating testosterone, resulting in depressed prostatic androgen signaling, proliferation, and organ weight.

In Chapter 3, in order to further probe the impacts of *Bco1* loss on lipid and retinoid metabolism, we again utilized the carotenoid-free *Bco1*$^{-/-}$ mouse model. We found that, first, adult male *Bco1*$^{-/-}$ mice accumulate 2-6-fold more hepatic retinyl esters than do WT mice and that this accumulation is highly dependent on developmental age, as juvenile mice demonstrated significant *decreases* in retinyl esters as a result of *Bco1* loss. Additionally, patterns of hepatic lipid esterification are altered by *Bco1* loss in adult mice, as evidenced by alterations in unique fatty acid species, most notably being a two-fold increase in cholesteryl palmitate. Finally, PPAR/RXR signaling may explain at least a portion of the hepatic lipid phenotype observed in *Bco1*$^{-/-}$ mice, including the steatosis reported by several independent investigators. In summary, we report that *Bco1* loss interacts with developmental age to alter hepatic retinyl ester accumulation, even when maintained on a carotenoid-free, vitamin A-sufficient diet. This effect may in turn result in altered RXR/PPAR signaling and a disruption of hepatic lipid metabolism.

In Chapter 4, we sought to determine whether dietary tomato treatments could reduce the PCa progression in a mouse model of lethal PCa. This was provoked by the observation that although epidemiological studies continue to find strong protection against advanced and lethal PCa with increased tomato consumption, no animal studies have examined the effects of dietary tomato on castration-resistant prostate cancer (CRPC), which constitutes the late and lethal stage

of human PCa. Therefore, we used a mouse model, the transgenic adenocarcinoma of the mouse prostate (TRAMP), to probe this gap in the literature. TRAMP mice (n=30/treatment) were treated with either control AIN-93G diet (CON) or 10% w/w lyophilized tomato paste (TP) from 4 weeks of age until euthanization. A third group, modeling adjuvant dietary intervention, consumed CON diet from 4 weeks of age until 12 weeks of age, and then 10% w/w lyophilized tomato paste from week 12 until euthanization (TP-I). To induce castration-resistant tumors, all animals were castrated at 12 weeks of age. Beginning at 10 weeks of age, mice were monitored longitudinally with biweekly ultrasound scans for tumor detection and measurement of tumor growth rate. Using this experimental design, we have shown for the first time that dietary tomato can reduce CRPC progression in an animal model. CRPC tumor volume and rate of CRPC tumor growth were significantly reduced nearly 50% by adjuvant dietary tomato intervention following surgical castration. In addition, compared to control feeding, adjuvant tomato treatment reduced distant gross metastasis to the lungs, and increased gonadal adipose depot and body weights. Importantly, CRPC progression was reduced with achievable levels of dietary tomato intake, and through the use of a common tomato food source that is already commercially available to consumers. These effects should be replicated and extended in future animal studies to assess their potential for clinical translation in men with CRPC.

In conclusion, this work has revealed that BCO1, a key enzyme involved in carotenoid metabolism, impacts steroid, lipid, and retinoid metabolism *independent of its role in carotenoid cleavage*. Further work in animal models and humans is needed, but we have shed additional light on a somewhat unexamined corner of the carotenoid field. Future work should utilize our findings in mice and assess their relevance in humans. Secondly, we have demonstrated that a relevant level and source of dietary tomato can reduce cancer progression in a mouse model of

human CRPC. This work requires confirmation and further expansion in order to be considered for translation to humans. In total, this dissertation has contributed novel findings to our understanding of carotenoid metabolism and bioactivity *in vivo*.

ACKNOWLEDGEMENTS

Throughout the course of my doctoral training, I have been fortunate enough to enjoy opportunities for guidance and mentorship from many excellent scientists. First, I would like to thank Dr. Erdman. When I started this degree, I did not fully understand the investment, and yes, the gamble, made by advisors when bringing on a new student. I am in debt to him for his belief in my potential and for his continued guidance, without which my growth as a scientist would have been impossible.

I also owe sincere gratitude to Dr. Martha Belury of The Ohio State University. While I have always loved science, I never believed it could become my career until I came under her mentorship. It was through Dr. Belury's guidance that I first realized I loved *doing* science, and that I was capable of it. The alternative trajectory of my career would be much different without her example and advice. An additional thank you to Dr. Joshua Bomser and Dr. Michael Stout; their friendship, encouragement, and support while at Ohio State were instrumental to my decision to pursue a Ph.D.

I would like to thank the members of my doctoral committee: Dr. Elizabeth Jeffery, Dr. William Helferich, and Dr. Eric Bolton. They have continually challenged me and I am a much-improved scientist for it. Additional thanks are owed to Dr. Steven Clinton; as with previous students from the Erdman lab, he has gone above and beyond his role as a collaborator to serve as a demanding, but crucial mentor. Many other scientists have brightened my experiences in graduate school: Dr. Janice Bahr taught me, with kindness and rigorous expectations of quality, radioimmunoassay techniques; Dr. Matthew Wallig performed histology on several studies and has always been willing to stop and chat about our mutual love, cycling; Dr. Rita Miller has spent innumerable hours with me doing ultrasound scans and has, to my knowledge, not yet

grown sick of my company. Dr. Bill O'Brien has provided the generous guidance and collaboration that was essential to the completion of Chapter 4 of this dissertation. Dr. Jennifer Thomas-Ahner has often provided insight and critique, which has improved my thinking and writing. Dr. Nancy Moran has not only been a helpful editor and sounding board, but a friend, mentor, and role model.

Thank you to members of the Erdman lab, past and present, for making ours a collegial, collaborative, and fun place to work. Special thanks are owed to all who have assisted with animal studies and lab work, and in particular, Taylor Durkin and Connor Buchweitz.

Despite all of the professional support provided by the above-named mentors, surviving the gauntlet run that is a Ph.D. would not have been possible without the support of my friends and family. To Brandon Gifford, Charlie Able, Andrew Murray, Dan Kavouras, Mike Babin, Keira Gifford, Zach Healy, Sarah Walter, Michele Trecaso, Ashleigh Galizio and Max Markovich, thank you for your support from afar. Friendships are often strained over time and distance, but with you guys, it's never been work. To Jen Barnes, Alex Benavente, Gabe Chiu, Nick Dietz, Ross DeAngelis, Pat Gavin, Hannah Holscher, Naiman Khan, Chris Moulton, Jon Mun, Lauren Panasevich, Matt Panasevich, Nate Pratt, Lauren Raine, Ginger Reeser, Katie Robinson, Tim Robinson, Mina Sohaj, and Krystle Zuniga, thank you for your friendship throughout these six years. I have simultaneously made colleagues and friends for life. To Brooke, thank you for your love and selfless support of my ambitions, even when those ambitions serve to increase the miles that separate us. I count myself as a lucky man. Finally, an incalculable thank you to my parents, Bill and Peg, and to my sister, Em, for your unconditional love and support; it leaves me humbled. I will try to live up to the pride you have in me.

TABLE OF CONTENTS

CHAPTER 1: Literature Review.....1

CHAPTER 2: Serum testosterone and prostatic androgen receptor signaling are reduced in mice lacking the carotenoid cleavage enzyme β-carotene-15,15'-dioxygenase.....67

CHAPTER 3: Loss of β-carotene-15,15'-dioxygenase alters hepatic vitamin A and lipid metabolism in mice.....109

CHAPTER 4: Dietary tomato reduces castration-resistant prostate cancer progression in the TRAMP model.....155

CHAPTER 5: Summary and future directions.....196

APPENDIX A: Supplemental tables and figures for Ch. 2.....209

APPENDIX B: Supplemental tables and figures for Ch. 3.....230

APPENDIX C: Supplemental tables and figures for Ch. 4.....241

CHAPTER 1

Literature Review

Introduction

Carotenoids are ubiquitous in our environment, with over 600 identified in nature [1]. Their incredible variety is outweighed still by their sheer abundance – chlorophyll is surely the most common pigment on planet Earth and yet both it and carotenoids can be measured in deciduous leaves on the level of milligrams per gram [2]. Carotenoids' accumulation indicates their importance to the photosynthetic process, in which they have been likened to lightning rods, dissipating excess energy whenever more has been absorbed than can be safely harnessed [3]. higher-order plants are the first to mind and the most commonly celebrated for the carotenoid content of their fruits and autumnal foliage, unicellular algae are capable of similarly impressive feats. Some strains of *Dunaliella salina*, which thrive in otherwise inhospitably saline conditions, produce copious levels of β-carotene to protect against damage by light and oxidative stress [4]. In fact, 14% of the total *D. salina* dry biomass present in the appropriately named Pink Lake in Victoria, Australia comes from β-carotene [4]. Similarly, the colorful bacterial mats surrounding the Firehole Pool hot spring in Yellowstone National Park, Wyoming have been shown to produce a polar hydroxylated carotenoid thought to be lycoxanthin [5]. Whereas some rare species in the kingdom Animalia are capable of carotenoid biosynthesis *de novo* [6], all other animals must acquire carotenoids from their diet. Perhaps the most elegant examples of animals' abilities to harness dietary carotenoids have been described in studies of the feather pigmentation and visual systems of birds. The colorful plumage displayed by many birds is a result of sequestration of dietary carotenoids in feathers, and the sexually dimorphic nature of this coloration (i.e., that males often have more brightly and intricately colored plumage) is due to sex-dependent

differences in feather carotenoid deposition [7]. Additionally, the cone photoreceptors of the avian retina possess richly pigmented oil droplets in their inner segment. These oil droplets accumulate distinct carotenoid species in a cell-type-specific manner, where they serve as highly sophisticated band-specific lenses that fine-tune spatial and color discriminatory visual abilities [8]. With carotenoids so abundant throughout nature and with the clearly evolved functions that various animal species have developed for use of dietary carotenoids, it is no wonder that these compounds have been proposed to have bioactivity in humans, notably in lowering the risk of chronic diseases such as cardiovascular disease and cancer [9,10].

Carotenoid Structure

The biochemical actions of carotenoids as a class of compounds, as well as the differences in function of individual carotenoid species, depend first and foremost on their chemical structure (**Fig. 1.1**). At their most basic level, carotenoids are members of the terpenoid (also known as isoprenoid) family, to which cholesterol and its derived steroids also belong. The basic building block of these compounds is the 5-carbon isoprene, or 2-methyl-2,3-butadiene (PubChem CID: 6557). Terpene consists of the condensation of two isoprene subunits. Triterpenes, like the cholesterol precursor squalene, consist of three terpene (six isoprene) molecules, and thus are 30-carbon terpenoid polymers. Carotenoids belong to the tetraterpene subfamily and thus normally contain 40 carbons [11] . This basic structure of long hydrocarbon backbones with repeating conjugated double bonds gives carotenoids two of their most fundamental properties: hydrophobicity and strong absorbance of light, respectively. The basic backbone can be modified, however, as is the case with end-group cyclization of lycopene to β-carotene, or the addition of oxygen-containing functional groups, as is the case with the

dihydroxylation of β-carotene to form zeaxanthin [12]. These structural modifications can result in drastic changes in chemical properties. For example, lycopene is produced from phytofluene in tomatoes through the addition of three double bonds by two enzymes [13]. This shifts the ultraviolet-visible (UV-vis) absorption spectra of the compound from a λ_{max} of 348 nm, invisible to the human eye, to 472 nm, producing a deep red pigment. It is also this highly conjugated double bond structure that makes lycopene an incredibly effective antioxidant [11,14]. Changes to the double bond structure of the molecule affect not only chemical properties, but also biological functions. β-carotene is a key provitamin A carotenoid, due to its yield of two molecules of retinal upon cleavage at the central 15,15' double bond [15,16]. Retinal is then further converted to retinol. However, changing the 5,6 double bond β-ring of retinol to a 4,5 double bond ε-ring yields α-retinol, which has only half of the vitamin A capacity [17]. The *in vivo* provitamin A capacities of β-carotene (two β-rings) and α-carotene (one β-ring, one ε-ring) reflect this structural difference. Other structural changes result in alteration of both chemical and biological properties. Hydroxylation of β-carotene at the 3 position of one of its two β-ionone rings yields β-cryptoxanthin [12]. Not only does this result in a more polar molecule - and now classifies it as a xanthophyll carotenoid instead of as a hydrocarbon carotene - but it also modifies its provitamin A potential [18]. Finally, due to the isomerism possible around double bonds and the high degree of unsaturation present within carotenoids, many structural isomers are possible for each carotenoid. In fact, Olson and Krinsky estimate that the permitted isomerization states of the ≥600 natural carotenoids allow for over 200,000 unique carotenoid structures [1]. Of course, the vast majority of these possible isomers are neither abundant nor present in either the human food supply or the human body. Selected isomers of certain carotenoids, though, are both present in consumed foods and have biological relevance. Lycopene, for example, has many structural

isomers that can be measured in human blood samples [19]. Broadly, they can be classified by *cis*/*trans* conformational identify; all-*trans* lycopene is the "parent" form and the isomer that is overwhelmingly found in foods (80 - 90%), whereas at least half of the lycopene in human circulation or tissues is in the *cis* conformation [20,21]. Evidence suggests that these *cis* isomers may be more bioavailable than the all-*trans* configuration [22,23], but isotopic labeling studies convincingly show that *cis*-to-*trans* isomerization *in vivo*, and not differential bioavailability, likely explains the majority of the differential biodistribution of lycopene isomers [24,25]. Conversely, it seems that all-*trans* β-carotene is more bioavailable than the 9-*cis* form [26], demonstrating the complex biochemistry of carotenoid absorption *in vivo*.

Carotenoid Absorption in the Gastrointestinal Tract

Prior to any *in vivo* digestion, aspects of the preparation and delivery of the carotenoid-containing meal play a large role in eventual absorption – for instance, food matrix [27], heat processing [28], and the co-consumption with dietary fat [29] all modulate the bioaccessibility and bioavailability of lycopene. In addition, the type of lipid co-consumed with carotenoids may impact bioavailability and eventual tissue distribution [30]. Although differences in bioavailability exist among the carotenoids, regardless of isomeric conformation or even identity, all carotenoids share the same mechanisms and routes of digestion and absorption. Following ingestion, carotenoids must be: freed from the food matrix through physical, chemical, and enzymatic digestion; hydrolyzed from esterified fatty acids, if present; solubilized in lipid droplets or mixed micelles; absorbed into the enterocyte *via* micelle uptake, passive transport, or active transport (through SR-BI or CD36); packaged into chylomicrons; secreted into the lymph; and united with venous blood for distribution to peripheral tissues [31]. Recently, genetic

regulation of active transport of carotenoids has been described [32]. Through this mechanism, vitamin A inhibits intestinal expression of SR-BI via intestine-specific homeobox (ISX), a retinoic acid receptor (RAR) target gene. This system functions as a negative feedback loop to inhibit the absorption of provitamin A carotenoids and prevent retinoic acid-induced hypervitaminosis. However, as lycopene and other non-provitamin A carotenoids are also absorbed *via* SR-BI [33], retinoid signaling through this network serves to inhibit all carotenoid absorption, regardless of vitamin A potential. It is for this reason that we and others have utilized reduced (but sufficient) levels of dietary preformed vitamin A when examining the absorption and metabolism of carotenoids *in vivo* [34–36]. Somewhat ironic, then, is the fact that since preformed dietary vitamin A is not absorbed through SR-BI and its uptake is seemingly dependent on either facilitated or passive diffusion [37], excess intake causes toxicity. This occurs even while the RAR – ISX – SR-BI cascade efficiently inhibits the absorption of provitamin A and non-provitamin A carotenoids alike.

Bioaccumulation of Dietary Carotenoids, Particularly those of the Tomato, in Peripheral Tissues

Distribution of carotenoids to peripheral tissues is achieved through the same route of lipoprotein metabolism that is utilized by dietary fatty acids. As carotenoids are effluxed within chylomicrons from intestinal enterocytes into the lymph, they bypass the portal circulation and hepatic “first-pass” metabolism. After chylomicron remnants return to the liver following peripheral off-loading of prandial triglycerides, they are re-packaged as very low-density lipoproteins (VLDL) and exported back to the periphery. While in circulation, VLDLs lose triglycerides, becoming low-density lipoproteins (LDL), which are the vehicles most responsible for delivery of carotenoids to peripheral tissues. In fact, carotenoids do not distribute to various

peripheral tissues in equal amounts [30,38–40], which may be explained by the relative tissue expression levels of LDL receptor [41]. Liver tissue invariably accumulates the largest mass of carotenoids, which is not surprising, but other tissues show striking differences. For example, the adrenals and testes, both steroidogenic organs, accumulate divergent levels of total carotenoids (adrenals high, testes low; [30,39,40]). Moreover, the profile of carotenoid distribution is also tissue-specific – even when provided with higher serum concentrations of phytoene than of lycopene, the prostate and seminal vesicles accumulate lycopene but not phytoene [39]. It is currently unknown what tissue-specific mechanisms of carotenoid uptake mediate these effects, but their elucidation would fortify arguments in favor of evolved bioactive functions of these compounds in humans.

Carotenoid Metabolism – Carotenoid Oxygenases: the Early Days

Investigations of carotenoid metabolism have roots as far back as the early twentieth century; at that point, scientists were primarily concerned with the identities and metabolism of vitamin A and "carotene" [42]. Scientists had questioned the logic that "the fat-soluble vitamine" and carotenoids were related [43], arguing that raising rodents on diets free of carotenoids produced no ill effects, whereas vitamin A-deficient animals suffered well-documented symptoms of deficiency [44]. However, in 1930, Moore proposed that "carotene" could be converted to vitamin A *in vivo*, thus beginning the modern era of research on provitamin A carotenoids [45]. In 1949, the work of Thompson, Ganguly, and Kon demonstrated that in addition to the liver, the intestine had a capacity for conversion of β-carotene to vitamin A [46]. A true watershed moment for carotenoid research came in 1965, with the independent discovery by two laboratories of the enzymatic cleavage of β-carotene to retinal using crude intestinal and hepatic purifications [47,48].

Olson and Hayaishi called their enzyme β-carotene-15,15′-oxygenase, while Goodman and Huang provided no suggestion as to naming. Although we now know that the enzyme they discovered cleaves other carotenoids in addition to β-carotene [49], modern investigators have retained Olson and Hayaishi's β-carotene-specific nomenclature for the enzyme.

One year after their initial discovery, Goodman et al. utilized double labeling experiments to propose that the enzymatic cleavage mechanism was that of a dioxygenase [50]. These results were not unequivocal, however, as the authors used ^{14}C and ^{3}H labels, rather than labeled oxygen. Concrete assignment of a dioxygenase reaction mechanism would require confirmation that the oxygen atoms in the two retinal products originated exclusively from molecular oxygen, and not from water. Subsequent work using $H_2{}^{18}O$ suggested that the reaction mechanism was a monooxygenase cleavage (i.e., one molecule of retinal deriving its oxygen from water and one from molecular oxygen), but that study was plagued by methodological issues that likely allowed molecular exchange of isotopic oxygen label with the aqueous reaction medium [51]. Nevertheless, the enzyme was subsequently categorized as a monooxygenase (EC 1.14.99.36) and the enzyme became known as β-carotene-15,15′-monooxygenase (BCMO1). However, in 2014, a carefully controlled experiment presented the most convincing evidence to date regarding the enzymatic mechanism of central β-carotene cleavage, clearly reestablishing the enzyme as a dioxygenase [52]. The approved human gene symbol (*BCO1*) provided by the Human Genome Organization (HUGO) Gene Nomenclature Committee (HGNC) attempts to avoid the confusion that has resulted from the various mechanism-derived names that this enzyme has been given over its four decades of study (BCMO1, CMO1, CMO-I, BCDO, BCDO1). For clarity and congruity with HGNC standards, the enzyme will therefore be referred to in this document only as β-

carotene-15,15′-dioxygenase or BCO1, even in cases where primary authors utilized other names.

Following the discovery of BCO1, the Olson group described its substrate specificity, demonstrating a preference for the 15,15′ central bond, but also arguing that enzyme activity was maximal for the β-carotene metabolite β-apo-10′-carotenal [15]. This latter claim would be found to be inaccurate, as the availability of a highly purified human enzyme 45 years later revealed that conversion of β-carotene was much higher than that of equimolar concentrations of β-apo-10′-carotenal, even accounting for the two-fold difference in provitamin A potential between the two substrates [49]. Still, other revelations by the Olson group regarding BCO1 have proved prescient, such as use of chelating agents to predict that the enzyme requires non-heme iron as a cofactor, as well as the realization that intestinal purifications from felines demonstrated no catalytic activity [53]. Indeed, other obligate carnivores such as the ferret (*Mustela putoius furo*) are not effective converters of β-carotene to vitamin A [54].

Carotenoid Metabolism – Molecular Identification and Characterization of Carotenoid Oxygenases

Despite thorough characterization of tissue purifications of BCO1, its sequence identity remained a mystery until the turn of the 21st century. This changed in early 2000, when two groups separately reported the cloning of two eukaryotic β-carotene-15,15′-dioxygenases within two months of one another [55,56]. On par with the 1965 discovery of enzymatic β-carotene cleavage by Olson and Hayaishi and Goodman and Huang, this was another seminal moment in carotenoid research. However, armed with cDNA sequences and predicted primary protein structures, subsequent advances came in greater number and more rapidly. Whereas the original

reports identified the sequences of *Drosophila* [56] and chicken [55] genes, Redmond et al. subsequently identified the first mammalian β-carotene-15,15′-dioxygenase in mice [57]. Several months later, in the same journal, the Blaner group replicated the finding [58]. This was followed shortly by recombinant expression, purification, and biochemical characterization of the human BCO1 enzyme by Lindqvist and Andersson [59]. In agreement with the early purifications of BCO1 from tissue homogenate supernatant [47,48], investigators consistently found that the cloned and recombinant enzymes were present in the cytoplasm, rather than other cellular compartments [55,57,59].

Given the function of BCO1 in cleavage of dietary provitamin A carotenoids, obvious functions outside of the liver and gastrointestinal (GI) tract were not clear and expression was expected to be largely limited to those tissues. Using two unique monoclonal antibodies directed against the human enzyme, Lindqvist et al. provided what remains as the most comprehensive screen of BCO1 expression in human tissues [60,61]. This led to the realization that BCO1 was expressed more broadly than previously anticipated. While high levels of staining were indeed found in hepatocytes and throughout the GI tract, exocrine epithelia of the pancreas (acinar cells) and uterus (endometrium) also demonstrated high levels of BCO1 expression. Interestingly, the pancreatic endocrine epithelium (islet cells) does not express BCO1, and other endocrine cell types in the adrenals, ovaries and testes stained positively for BCO1, but only weakly to moderately. Glandular epithelia in the prostate expressed only low levels of BCO1, and the stroma lacked expression altogether. Similarly, stromal cells in the uterus, heart, and skeletal muscle all lacked staining for BCO1 or expressed only low levels of the protein. Finally, skin and ocular epithelium demonstrated strong BCO1 staining. Three broad themes can be gleaned from these data: 1) as expected, BCO1 expression is highest in tissues involved in carotenoid

metabolism [GI tract, liver]; 2) generally, epithelial cells strongly express BCO1, with few exceptions (e.g., prostatic epithelia); 3) cells of mesodermal origin [stroma, muscle, gonads] do not express BCO1 strongly. Epithelial cells are broadly known to be sensitive to retinoid signaling - thus, expression of BCO1 in epithelial cells outside of the liver and GI tract may provide "backup" capacity for local conversion of β-carotene to retinal in tissues such as the retina and epidermis, which have heightened sensitivity to retinoid status. Additionally, although testicular Leydig and Sertoli cells displayed only moderate BCO1 staining, they showed stronger expression than any other cell type of mesodermal origin examined [60,61]. This is consistent with the well-established sensitivity of testicular development and function on retinoid status [62–65]. These results from tissue expression studies suggest that not only does BCO1 function in central carotenoid metabolism, but also may have important functions in peripheral tissues.

Clearly, carotenoid oxygenases play critical roles in the formation and metabolism of bioactive carotenoid metabolites. The metabolite of central β-carotene cleavage by BCO1, retinal, has bioactivity due to its downstream conversion to retinoic acid, as well as the indispensable role of its metabolite 11-*cis*-retinal in the visual cycle [66]. All-*trans* retinoic acid (RA) mediates the classical functions of vitamin A through high-affinity binding to retinoic acid receptors (RAR), whereas the RA metabolite 9-*cis*-RA is an endogenous ligand for the retinoid X receptors (RXR) [67–69]. Carotenoid oxygenases mediate the production of both of these important signaling molecules, as well as other potentially bioactive carotenoid metabolites. Studies of BCO1 enzyme kinetics have demonstrated that 9-*cis*-RA is not formed from central cleavage of full-length 9-*cis*-β-carotene, but rather must result from the isomerization of all-*trans*-RA (atRA) to the 9-*cis* conformation [49]. Thus, in conjunction with an as-yet-unidentified isomerase, BCO1 regulates production of the RXR ligand 9-*cis*-RA from β-carotene. Eccentric

β-carotene metabolites (i.e., derived from cleavage at bonds other than the central 15,15′ bond) have previously been identified and it has been proposed that a "stepwise" pathway might exist alongside the central cleavage mechanism for the production of retinal from these asymmetric metabolites [70]. Although its cleavage activity is strictly limited to the central 15,15′ double bond, BCO1 has been shown to yield retinal and varying-length isoprene fragments from the cleavage of β-apo-8′-carotenal, β-apo-10′-carotenal, β-apo-12′-carotenal, and β-apo-14′-carotenal [49]. When intact, these eccentric carotenoid metabolites – which are naturally present in foods [71] or formed from β-carotene through the action of the second mammalian carotenoid oxygenase β-carotene-9′,10′-dioxygenase (BCO2) [72,73] – antagonize RAR [74] and RXR [75] activity. Thus, bioactive carotenoid metabolites are formed and interconverted by the endogenous mammalian carotenoid oxygenases, BCO1 and BCO2.

Bioactivity of carotenoid metabolites is not limited to provitamin A-derived compounds, however, as eccentric cleavage products of lycopene have been shown to exhibit bioactivity both *in vitro* and *in vivo*. BCO2 degrades lycopene *in vivo* [35] through cleavage at the 9′,10′ double bond [73,76]. Apo-10′-lycopenoic acid inhibited cell cycle progression and activated RARβ promoter activity in both normal human bronchial epithelial cells and non-small cell lung cancer cells, and reduced lung tumorigenicity *in vivo* [77]. The corresponding aldehyde (apo-10′-lycopenal) and alcohol (apo-10′-lycopenol) also exhibited bioactive effects in bronchial cells *in vitro*, modulating redox status through glutathione and reactive oxygen species generation [78]. The same group has also reported that apo-10'-lycopenoic acid reduces high-fat diet/diethylnitrosamine-induced liver cancer in mice [79]. Interestingly, the metabolite (apo-10′-lycopenoic acid) and the parent carotenoid (lycopene) may have differential effects *in vivo* [80] and these effects may be dependent on BCO2 genotype [81]. Our own group has shown that lycopene

and apo-12′-lycopenal both inhibit DU145 prostate cancer cell cycle progression and proliferation *in vitro* [82], suggesting that differential effects of parent and metabolite may be highly dependent on structure. Early reports on BCO1 reported that viable substrates must have at least one unsubstituted β-ionone ring [59], but others have reported that the enzyme is able to cleave lycopene, producing acycloretinal [49,57]. *In vitro* studies using acycloretinal have failed to demonstrate effects with physiologically relevant concentrations or that were specific to the acycloretinal itself, however (i.e., not also induced by the parent lycopene) [83,84]. In summary, both BCO1 and BCO2 produce bioactive carotenoid metabolites from provitamin A carotenoids, but current data suggest that only BCO2 may be able to directly produce physiologically relevant metabolites from acyclic carotenoids like lycopene. Regardless of their source, due to the presence of endogenous antioxidants at vastly higher concentrations *in vivo* (e.g., α-tocopherol), it seems that the bioactivity of these lycopene metabolites must be mediated through impacts on cellular pathways of molecular biology, rather than through modification of general redox status [85–87].

Carotenoid Metabolism – Studies In Vivo

Despite advancement of the field through enzymatic characterization of purified BCO1 protein, identification of reaction products *in vitro*, and immunohistochemical assessment of its tissue distribution, there remained a desire to experimentally manipulate BCO1 function *in vivo*. Answering that call, Hessel et al. successfully generated the *Bco1*$^{-/-}$ mouse in 2007 and experimentally demonstrated that genomic disruption of *Bco1* prevented the conversion of β-carotene to retinal *in vivo* [88]. The creation of the *Bco1*$^{-/-}$ mouse model has been of great utility to the carotenoid research community and twenty published studies have utilized the strain since its

creation in 2007 [32,34,36,88–104]. It remains, to our knowledge, the only existing animal model of disrupted *Bco1* function. Ten studies using this strain have replicated the original finding of Hessel et al., providing convincing experimental evidence that *Bco1* expression is necessary for production of retinal from provitamin A carotenoids [34,36,89–93,96,97,99]. Coincidentally, only six days prior to the original report on the *Bco1*$^{-/-}$ mouse model, Lindqvist et al. reported a loss-of-function mutation in *BCO1* [105] in a woman who had been diagnosed with familial hypercarotenemia and hypovitaminosis A nearly 40 years earlier [106]. The missense mutation resulted in the replacement of a highly conserved threonine residue with methionine and decreased enzymatic activity of a recombinant clone by 90% [105]. Subsequently, single nucleotide polymorphisms (SNPs) in the human *BCO1* gene have been shown to modulate the metabolism and distribution of provitamin A carotenoids and retinol [107–110], as well as other carotenoids – including lycopene [108–112]. The combined evidence in these observational and experimental reports strongly support a central role for BCO1 in carotenoid metabolism.

Carotenoid Metabolism – Alternative Functions of Carotenoid Oxygenases?

Carotenoid cleavage is very likely to be the role for which BCO1 has been evolutionarily conserved. However, it has become increasingly clear that loss of *Bco1* function impacts a myriad of physiological endpoints even when mice are fed diets devoid of carotenoids. Evidence for this was present even in the very first report on the *Bco1*$^{-/-}$ model, when it was shown that liver steatosis occurred in *Bco1*$^{-/-}$ mice provided a vitamin A-sufficient, β-carotene-free diet, and that high-fat diet feeding further exacerbated this metabolic perturbation [88]. Elevations in serum free fatty acids were also observed in *Bco1*$^{-/-}$ mice; uptake of these non-esterified fatty acids into tissues is unregulated and may have contributed to the observed phenotype. Dysregulation of

lipid metabolism in *Bco1*$^{-/-}$ mice is not limited to the liver, however, as Lee and colleagues have shown that *Bco1* loss resulted in elevated cardiac non-esterified fatty acid and ceramide levels, alterations in markers of retinoid metabolism, and impairment of cardiac function [102]. Furthermore, disruption of normal lipid metabolism by *Bco1* loss extends throughout the lifespan, as reports from the Quadro group have demonstrated altered retinol, cholesterol, and lipid esterification in *Bco1*$^{-/-}$ embryos [101,104]. It seems likely that these effects may involve alterations in nuclear signaling by the peroxisome proliferator-activated receptor family [88,99,101,102]; these nuclear transcription factors play central roles in lipid metabolism and *BCO1* is known to be regulated by one member, PPARγ [113]. It is unknown whether direct reciprocal regulation of PPARγ by *BCO1* occurs, but PPARs do heterodimerize with the retinoid-responsive RARs and RXRs [69], and *Bco1* loss has been shown to affect retinoid status even in mice provided with adequate dietary levels of preformed vitamin A [101,104]. This suggests that modulation of BCO1 status may alter mammalian biology not only through the production of bioactive molecules from exogenous carotenoids, but also through modulation of cellular sensitivity to endogenous levels of nuclear receptor ligands. Clearly, much work is still needed to elucidate the impact of BCO1 on mammalian physiology *in vivo*, especially in "basal" conditions devoid of cleavage substrates.

Prostate Cancer – Statistics of Incidence, Staging at Diagnosis, and Mortality

It is likely that more than 1 in 3 U.S. women and nearly half of American men will be diagnosed with cancer in their lifetime [114]. More common in males than any other cancer, prostate cancer (PCa) singlehandedly accounts for 20 - 30% of all new cancers and is the second-leading cause of cancer death in this population [114–116]. In probabilistic terms, the most recent

estimates suggest that 1 in 7 men is likely to be diagnosed with the disease at some point in their life [114]. Projections for the current year suggest that nearly 181,000 American men will be diagnosed with PCa in 2016 and 14% of these men (an estimated 26,160) will die as a direct result of the disease [114]. Fortunately, 80% of cases are diagnosed when the disease is still localized to the prostate gland, a stage at which five-year relative survival is 99% or greater. Data from the Surveillance, Epidemiology, and End Results (SEER) database demonstrate that this is part of a larger trend, as survival has increased in each of the assessment periods since 1975, when overall five-year relative PCa survival was only 68% [114]. Although comparable survival in men with distant (metastatic) PCa at diagnosis (28%) sharply contrasts with the prognosis of men with localized disease, advanced disease at diagnosis comprises only 4% of overall cases, and so all-stage survival rates are the same as those for localized cancer [114].

Prostate Cancer – Structure, Function, and Carcinogenesis of the Prostate Gland

To best understand the malignant transformation, progression, and lethal metastasis of PCa, it is necessary to understand the structure, development, and function of the organ in its normal, non-neoplastic state. The prostate is an accessory sex organ present only in male mammals, which contributes to the composition of semen and critically relies on androgens for development and organ maintenance [117]. In 1968, McNeal developed an anatomical model of the human prostate, describing the presence of peripheral, central, and transition zones, a model which is now widely accepted worldwide [118]. The peripheral zone occupies 70% of the mass of the gland and accounts for nearly 75% of the cancers that arise [119]. In contrast, the rodent prostate is distinctly lobular, consisting of the anterior, ventral, dorsal, and lateral lobes; the latter two are often grouped together as the dorsolateral lobe (**Fig. 1.2**). Molecular studies have

suggested that the mouse dorsolateral lobe is the closest homologue to the human peripheral zone [120], although it was the consensus opinion of a National Cancer Institute-directed expert panel, convened to assess mouse models of human prostate cancer, that there is not "evidence for a direct relationship between the specific mouse prostate lobes and specific zones in the human prostate" [121]. Regardless, both the human and rodent benign prostrates share general features of glandular structure, with ductal branching and two types of epithelial cell - basal and luminal [121]. Luminal cells, the differentiated cells responsible for secretion of the prostatic components of semen into the ductal lumen, are tall columnar cells lining the ducts in a continuous layer and can be identified by immunostaining for cytokeratins 8 and 18. Basal epithelial cells line the basement membrane (discontinuously in mice and in a continuous layer in humans) and can be distinguished histologically by their expression of p63 and the cytokeratins 5 and 14 [122,123]. The mesenchymal or stromal compartment of the prostate is largely composed of smooth muscle cells, characteristically expressing smooth muscle actins, desmin, and vimentin [124], although morphological differences exist between the human and murine organ. The stromal layer in the human prostate is much thicker than that of the mouse, yielding a higher stromal:epithelial cell ratio [125].

Development, growth, and function of the prostate are highly dependent upon androgens. Some of the earliest accounts of androgen-regulated growth of the prostate were observations that eunuchs had small and underdeveloped prostates. In experiments in animals, castration causes regression of the prostate due the apoptosis of the epithelial cell compartment [126]. This regression is rapid, as it can be detected within one day and can result in a loss of two-thirds of epithelial cells within one week [127]. The involution of the prostate is fully reversible and repletion of androgen status with exogenous testosterone results in rapid proliferation of

epithelial cells and reestablishment of a gland of normal size [128]. Circulating androgens control the development of the prostate and are supplied almost entirely by the testes, even during the fetal period [129,130]. One of the first androgen-driven responses of the developing prostate is the elevated expression of the homeobox gene Nkx3.1 in the fetal urogenital sinus epithelium (UGE) [131]. *Nkx3.1* expression is also dramatically reduced (~8-fold) following castration of adult mice. In contrast to other homeobox gene families, the Nkx family of genes controls *tissue-specific* organogenesis; loss of *Nkx2.1* is embryonically lethal and results in the absences of the thyroid gland and lung parenchyma [132], whereas loss of *Nxk2.5* results in an embryonic-lethal disruption in heart development [133]. Nkx3.1 maps to chromosomal position 8p21, a locus that frequently suffers a loss of heterozygosity in PCa [134]. Additionally, *Nkx3.1*$^{-/-}$ mice exhibit epithelial hyperplasia, which increases in severity with age [135,136], suggesting that Nkx3.1 plays a key role in androgen-driven establishment and maintenance of differentiated prostate structure and function.

Paracrine Androgen Signaling in Prostatic Development and Carcinogenesis

In contrast to androgens' direct pro-differentiative influence on Nkx3.1 in the epithelia, many androgenic effects in the prostate are mediated through stromal-epithelial interactions. In a series of elegant and seminal experiments starting in the 1970s, Cunha et al. began to describe the central role played by stromal-epithelial paracrine signaling in prostatic organogenesis and function. Using tissue recombination approaches, they demonstrated that 1) stromal signals control epithelial differentiation and function, and 2) functional androgen receptor (AR) in the stroma is necessary for prostatic differentiation, morphogenesis, and proliferation. When *ventral* prostate fetal urogenital sinus mesenchyme (UGM) was combined with UGE from a *mix of*

dorsal and ventral prostate lobes, the tissue recombinant formed differentiated prostate glandular ducts that displayed molecular signatures characteristic of *only the ventral* prostate [137]. In direct contrast, mixed UGM from the dorsal and ventral lobes combined with adult ventral epithelium formed tissue recombinants with molecular signatures characteristic of not only the ventral lobe, but also the dorsal and anterior lobes [138]. Fascinatingly, prostatic UGM recombined with adult bladder epithelium also resulted in the formation of differentiated prostatic tissue. However, it seems that this effect is limited to cell types of similar embryological origin – recombination of UGM with epithelia from other anatomical locations, such as the salivary gland and esophagus, only form differentiated epithelia reflective of their site of origin and cannot be "reprogrammed" as prostatic tissue [139]. Regardless, despite the aforementioned anatomical differences of the prostate between species, it appears that the paracrine signals involved in prostatic development and differentiation are widely conserved: in almost all combinations of UGM and UGE or adult bladder epithelium from human, mouse, rat, or rabbit sources, differentiated glandular prostatic tissue arose [140].

Androgenic control of this paracrine signaling system was demonstrated by use of stromal or epithelial tissue from *Tfm* mice, which carry an X-linked AR mutation that results in a premature stop codon and severe decrease (~10%) in androgen responsiveness [141]. In these experiments, as previously demonstrated, UGM and UGE from wild-type animals recombined to form functional and differentiated glandular prostatic-like tissue. However, when mesenchyme from *Tfm* mice (lacking a functional AR) was recombined with wild-type UGE, vaginal-like morphology resulted, demonstrating a need for stromal AR function in prostatic differentiation [142]. Additionally, using the reciprocal combination (*Tfm* epithelia and wild-type stroma) in this

and another paper [143], Cunha et al. crucially demonstrated that epithelial AR function was not necessary for prostatic morphogenesis, given a functional stromal AR.

Clearly, androgen signaling supports prostatic development, differentiation, and proliferation to yield the normal functions of a healthy organ. However, androgenic stimulation has been alleged to play key roles in the malignant transformation, progression, and metastasis of PCa [144]. How the normal androgen signaling program in the prostate becomes corrupted is clearly of interest to cancer biologists and nutritionists concerned with identifying dietary strategies for PCa prevention. As in the normal prostate, stromal-epithelial interactions are involved in malignant transformation and carcinogenesis. Ricke et al. [145] demonstrated this using tissue recombinants of mouse stroma and human benign prostate epithelia grafted into castrated athymic host mice, which were then treated with testosterone and estradiol for two to four months to stimulate proliferation and carcinogenesis. When the investigators combined wild-type stroma and either wild-type benign epithelia or benign epithelia with AR knocked-down through small hairpin RNA, they observed the development of large invasive tumors. Conversely, loss of AR in the stroma (using stroma from AR-knockout mice) prevented the malignant transformation when recombined with wild-type benign human prostate epithelium. Using a different paradigm, the authors recombined wild-type mouse stroma with mouse epithelium from *Pten* and *Tp53* double heterozygote mice ($Pten^{+/-}$, $p53^{+/-}$) and implanted grafts into castrated or intact athymic mice. In castrated animals, the recombinants were histologically benign and similar to recombinants with wild-type epithelium. In intact animals, however, carcinogenesis occurred. Data such as these demonstrate that stromal androgen-mediated signaling is necessary for malignant transformation of prostatic epithelium, even with diminished function of major tumor suppressor genes.

In support of this hypothesis, Ricke et al. found that testosterone treatment increased stromal expression of major paracrine peptides such as fibroblast growth factor (FGF) 2, FGF7, FGF10, transforming growth factor β (TGF-β), and hepatocyte growth factor (HGF). Demonstrating that androgen-dependent paracrine signaling can also enhance progression of previously transformed PCa cells, in an *in vitro* co-culture model using human-derived cancer-associated fibroblasts (CAFs), the human PC3 PCa cell line grew more slowly and displayed less invasive potential when co-cultured with CAFs that had AR knocked down with siRNA, compared to control CAFs [146]. Knockdown of AR also resulted in a significant decrease in CAF mRNA expression of several paracrine growth factors, including FGF-7, FGF-10, HGF, TGF-βII, insulin-like growth factor (IGF) 1, and stromal cell-derived factor 1 (SDF1). The sum of the studies above shows that whereas androgens are necessary for the development and differentiated normal function of the prostate, abnormal androgenic stimulation can both induce malignant transformation and also enhance cancer progression.

Relationships between Circulating Hormone Levels and Prostate Carcinogenesis

First, it is important to note that differences between human and rodent endocrinology exist. In humans, up to half of the androgen available to the prostate gland is the product of local conversion of adrenal steroids, with the remainder directly supplied as testosterone from the testes [147]. This is in contrast to the endocrinology of rodents, which do not produce much of the androgen precursors dehydroepiandrosterone (DHEA) or androstenedione (AE) [148], relying instead on gonadal testosterone for androgenic stimulation of the prostate. This species-specific difference owes itself to divergent adrenal expression and activity of cytochrome P450 17A1 (CYP17A1). In both humans and rodents, CYP17A1 possesses dual enzymatic functions: the

17α-hydroxylation of 21-carbon steroids, as well as 17,20-lyase activity to produce the 19-carbon androgens [149]. Whereas the human adrenal gland utilizes the 17α-hydroxylation capacity of CYP17A1 to provide substrate (17α-OH-progesterone) for the eventual formation of cortisol, the major human glucocorticoid, it also harnesses CYP17A1's lyase activity to convert 17α-OH-pregnenolone to the 19-carbon androgen precursor DHEA. Rodents, on the other hand, do not express CYP17A1 in the adrenal gland [150]. The major glucocorticoid produced by the rodent adrenal gland is corticosterone, rather than cortisol, and it produces very little of the androgen precursors DHEA or AE [150,151]. Once circulating testosterone (or DHEA or AE in humans) reaches the prostate, it is free to diffuse into prostatic cells, where it is converted to dihydrotestosterone (DHT) by 5α-reductase, type 2 (SRD5A2) [152–154]. DHT is 10-fold more potent than testosterone, primarily due to a 10-fold lower rate of dissociation from the AR, and thus a much higher overall affinity [154]. Once bound to DHT, AR dimerizes, is phosphorylated, translocates to the nucleus, and binds AR response elements on AR-target genes (AREs), recruits transcriptional co-activators, and initiates gene transcription patterns collectively referred to as "androgen signaling" (reviewed in [155,156]).

Circulating androgens or androgen precursors, produced by the testes in mice and both the testes and adrenals in humans, have long been investigated as risk factors in the development of PCa. In fact, the recognition that PCa was responsive to manipulation of systemic androgen levels (*via* castration) won Charles Huggins a 50% share of the 1966 Nobel Prize in Physiology or Medicine for work he had done in the 1940s [157]. In 1990, the first prospective analysis of PCa risk relative to endogenous sex hormone levels suggested that men in the highest tertile of serum AE levels compared to the those in the lowest tertile were at a roughly 2-fold increased risk of total PCa [158]. In 1996, another prospective study found no relationships between individual

hormones and PCa risk, but when adjusted for concentrations of other circulating hormones, testosterone was positively associated with overall PCa risk [159]. A meta-analysis of three studies (including the 1996 study) found an association between endogenous levels of testosterone and PCa risk [160]. However, subsequent studies, including a large pooled analysis of 18 prospective studies, found no effect of any endogenous sex hormone and PCa risk [161]. Some investigators expressed concerns about exposure to *exogenous* testosterone, whether through dietary supplements [162,163], illegal anabolic steroids [164], or pharmacological agents to treat age-related hypogonadism [165]. Clearly, much confusion was present in the literature. Moreover, it had remained difficult to align the demographics of PCa incidence (highest incidence in aging males concomitantly experiencing declining androgen levels) with a model that proposed elevated androgen levels to be a causative factor.

A unifying theory arrived in 2006, when Morgenthaler proposed the saturation model [166]. Further refined in 2009, the saturation model posits that both the prostate's exquisite sensitivity to castration as well as its ambivalence to high levels of endogenous testosterone can be explained by recalling the basic biochemical principles of high-affinity ligand-receptor binding [167]. With castration, the androgen-dependent prostate rapidly and dramatically experiences apoptosis-mediated involution, as reviewed above. With systemic testosterone repletion, through the high-affinity binding of DHT to prostatic AR, the prostate is sensitive even to minute changes in circulating testosterone concentration, as long as concentrations remain near castrate levels. As intracellular DHT concentrations rise along with higher serum concentrations of testosterone, the prostate begins to approach a boundary to its androgen-induced response – the limited number of available AR binding sites become increasingly occupied by high-affinity DHT ligand. At a certain point of tissue DHT concentration, within the low nM range [168], all

binding sites are occupied and additional androgen achieves no further androgen-mediated response. In support of the saturation model, pharmacological inhibition of testosterone-to-DHT conversion forces the AR to bind lower-affinity ligand testosterone, receptor saturation does not occur, and prostatic growth tracks with serum testosterone across a wide range of concentrations [169]. Thus, without the need for novel mechanisms, the saturation model simultaneously describes the established effects of castration and testosterone repletion on androgen-dependent prostatic growth, while also explaining the lack of association observed between PCa and high endogenous levels of testosterone.

Prostate Cancer Epidemiology – Factors that Modulate Risk

Beyond the coarse-grained summary of PCa incidence and survival presented earlier, observational data have identified risk factors that significantly increase a man's risk of PCa diagnosis, or which may put an individual at higher risk of developing lethal disease. Factors that modulate these risks can be broadly classified into two groups: non-modifiable and modifiable.

A truly defining characteristic of PCa may be the "dose-response" in incidence observed in relation to age. Based on population-level statistics, whereas the percent likelihood of developing PCa before the age of 50 is less than 1%, the probability of a PCa diagnosis between the ages of 60 to 69 *alone* is >5%, and is 10% for all years at or above the age of 70 [114]. These statistics are borne out in autopsy studies, which consistently find that histological evidence of PCa tracks strongly with age at death from other causes. Indeed, at the upper end, 87% of men 81-95 years of age showed histological evidence of prostatic adenocarcinoma [170]. Surprisingly, even men in their 3rd decade of life (20-29 years of age) exhibit focal pre-neoplastic or neoplastic lesions [171],

demonstrating that although this is commonly perceived as a disease of older age, its etiology may be traced to events or conditions present at earlier stages of life.

Like the inevitable aging process, family medical history and racial background are factors that are not modifiable for the management of disease risk. Positive diagnosis in African-American men is 50-66% more common than in Caucasians and they are 200% more likely to die from PCa [172]. In contrast, Japanese and Chinese men in their native country enjoy low rates of PCa; strikingly, however, immigrants to the U.S. from these countries experience an elevated risk for PCa that increases in concordance with the length of their American residence [172–174]. Racial background thus seems to interact with environmental factors to modulate risk of PCa. While it follows, then, that a family's history of PCa is necessarily intertwined with its ethnic history, medical histories can still be independent predictors of PCa risk, even across groups with diverse ethnic backgrounds. Men with an immediate relative with PCa (i.e., in a father, brother, or son) or even a second-degree relative (cousin, uncle, grandfather) may have up to a three-fold increased risk of developing PCa themselves [172,175]. Additionally, whereas PCa is very rare in men below 50 - 55 years of age (≤1%), a positive family history can raise their risk probability to nearly 50% [173]. Of course, underlying the contribution that family histories provide to PCa risk are the inherited genetic variations that presumably mediate disease etiology. A thorough discussion of this entire body of literature is beyond the scope of the current review, but of note are studies that have investigated polymorphisms in genes governing steroid hormone metabolism. As PCa is in many ways governed by endocrine factors [144], it seems logical that polymorphisms in genes controlling androgen [176–178] and estrogen [179] metabolism may modulate disease risk. Moreover, a polymorphic polyglutamine sequence in the human androgen receptor (AR) may alter PCa risk [180] and its prevalence in the African-American population may account,

at least in part, for the increased PCa risk observed in that population [181]. However, it must be noted that hereditary factors account for only ~9% of PCa cases [172], and thus it seems that environmental factors or spontaneous genomic lesions may account for most of the observed PCa burden.

At the behest of the U.S. Congress, Doll and Peto estimated in 1981 that 35% of cancers could be attributed to dietary factors – albeit with a confidence interval of 10 - 70% [182]. Thirty-five years later, others have proposed that a more accurate number may be closer to 20%, but that Doll's and Peto's estimates "generally have held true" [183]. Of course, dietary components may either increase or decrease risk. Indeed, the 2007 World Cancer Research Fund/American Institute for Cancer Research joint report declared that foods containing lycopene, foods containing selenium, and selenium supplementation at a dose of 200 μg/day were associated with "probable decreased risk" of PCa, whereas diets high in calcium were linked to a "probable increase in risk" [184]. This judgment was based on synthesis of many observational individual studies, but individual cohort or case-control investigations have also proposed an increased risk of PCa with high levels of α-linolenic acid [175], calcium [175,185], whole milk [186], phosphorous [185], and total energy [175] intakes. Other dietary components, such as fiber [187], soy [174,188], cruciferous vegetables [188,189], and total vegetables [189,190], have been associated with decreased risk of total or aggressive prostate cancer. Notable though, and of interest to our research, has been the repeated observation that dietary lycopene or tomato products are associated with reduced risks of both total and lethal PCa.

Prostate Cancer Epidemiology – Tomatoes, Lycopene, and Prostate Cancer

The first study to propose an inverse relationship between dietary lycopene and PCa dates to 1995, when a landmark study of 47,894 men found that estimated lycopene intake was associated with a 31% reduced risk of prostate cancer diagnosis [173]. Internally consistent with this, tomato products (which provide >80% of U.S. lycopene intake [191]), but not 41 of the other 42 fruits or vegetables investigated, were significantly associated with lower rates of PCa. Furthermore, lycopene was unique among carotenoids in its protective effect, suggesting that the finding was not simply indicative of a biomarker for intake of vegetables or other potentially healthful foods, but rather that it may have communicated some truth about a meaningful biological relationship. Indeed, subsequent studies have repeatedly found an inverse association between dietary lycopene or tomato intake and PCa [175,192–195]. Often, the strongest protective effects of lycopene have been found in relation to advanced PCa [173,175,192–194,196]. Furthermore, meta- or combined analysis of studies has further supported a protective effect of lycopene and tomato intake [195,197]. Some researchers have suggested that dietary recall methods are inadequate for accurate estimation of dietary composition [198,199] and although methods for self-reported estimation of dietary carotenoids have been validated [200], some authors' concerns remain. Allaying this concern, then, should be studies in which direct measurements in the serum have revealed inverse associations between elevated levels of circulating lycopene and risks of total or lethal PCa [201,202].

Cancer is a complex disease, driven by many possible foundational and driver mutations, inhibitory and progression factors, environmental agents, and inherent variability in the patient's own physiology. Diet, too, is intricately complicated; dietary patterns may vary widely or not at all between assessments, varying food composition may confound similar outcomes of food item

intakes, and interactions between food components may cloud mechanistic insight. Given these challenges, it is not surprising that some observational studies have not reported significant associations between dietary lycopene/tomato exposure and PCa. Moreover, aspects of trial design may have biased several reports against detection of differences in PCa incidence or advanced disease. One trial in particular, the Prostate Cancer Prevention Trial (PCPT), was a placebo-controlled clinical trial to test the effect of a pharmacological inhibitor of androgen metabolism, finasteride, on prevention of primary prostate cancer [203]. A nested case-control study was performed within the PCPT to assess if dietary lycopene/tomato or serum lycopene could prevent prostate cancer. In two publications, Kristal et al. reported that dietary or supplemental lycopene did not modulate prostate cancer risk [204] and that serum concentrations of lycopene were not associated with lower risk of PCa [205]. Notably, the authors of this report made the following statement regarding the impact they interpreted from their findings:

> *"Scientists and the public should understand that early studies supporting an association of dietary lycopene with reduced prostate cancer risk have not been replicated in studies using serum biomarkers of lycopene intake. Recommendations of professional societies to the public should be modified to reflect the likelihood that increasing lycopene intake will not affect prostate cancer risk."*
>
> *– Kristal A.R. et al., Cancer Epidemiol Biomarkers Prev; 20(4); 638–46, 2011*

Such a statement would indeed be prudent if confronted with new and convincing evidence demonstrating an obvious futility of dietary lycopene or tomato in the prevention of PCa; however, their data do not, in fact, provide said convincing evidence. First, in clarification, "early studies supporting an association of dietary lycopene with reduced prostate cancer risk" indeed have been replicated in studies using serum biomarkers of lycopene intake [201,202]. Secondly, the PCPT, from which Kristal et al. obtained data for their nested case-control study,

is quite unique in design and requires careful analysis. Men 55 years of age or older were enrolled into a placebo or finasteride (5 mg/day) study arm, with intent-to-treat for seven years [203]. Monitoring of PCa in these men was accomplished through yearly digital rectal exams (DREs) and measurement of prostate-specific antigen (PSA), which is a prostatic-specific seminal protease that is released into the circulation as a result of neoplastic, but also non-cancerous, insults [206]. PSA screening has become a topic of fierce debate in the PCa community and only more so following the U.S. Preventative Services Task Force's 2008 and 2011 decisions to recommend against all PSA screening due to concerns of harms from over-diagnosis and overtreatment vs. limited perceived benefit [207,208]. Indeed, many clinicians have balked at the recommendation [209–211]. Analysis of PSA screening is beyond the current scope of this review, but nevertheless, its inclusion on the PCPT trial protocol is an important detail. Abnormal DRE or PSA findings in PCPT yearly screenings prompted needle core biopsy and evaluation of prostatic pathology; 571/1,934 (29.5%) men in the placebo group who underwent biopsies in this fashion were diagnosed with PCa. Cancers diagnosed in this fashion can be classified as "for-cause", as they were identified in response to subjects' clinical presentation. Following the seven-year study period, men in the PCPT who had not been diagnosed with PCa were given the option of receiving biopsies, *whether or not* their clinical presentation would have called for biopsy while on study; 576/3,820 (15%) of men in the placebo group who underwent these biopsies were subsequently diagnosed with PCa. These PCa diagnoses can be classified as "not for-cause" – they were identified not on the basis of clinical presentation, but as a byproduct of greatly elevated biopsy screening at the end of the PCPT trial. Strikingly, nearly two times as many men in the PCPT placebo group were screened "not for-cause" as "for-cause" (3,820 vs. 1,934), resulting in an overrepresentation of indolent, low-grade, localized, and asymptomatic

PCa diagnoses within the PCPT trial [212]. Surely, these "for-cause" and "not for-cause" cancers in the PCPT do not represent the same tumor phenotype. Similarly, the latent and focal lesions identified in 20-30-year-old men in autopsy studies are surely not of the same phenotype as those presenting as clinically urgent tumors in men over the age of 60. Thus, when Kristal et al. combine "for-cause" and "not for-cause" diagnoses and conclude that lycopene does not protect against PCa risk [205], they ignore this critical dichotomy present within the PCPT trial population. Indeed, their own data show that higher levels of serum lycopene in both quartile-based and continuous variable analyses provide a significant protective effect against "for-cause" cancers, but not "not for-cause" cancers; however, this was not reflected in their conclusions [205]. A separate re-analysis of the data from Kristal et al. by Giovannucci concurs with this [213]. A similar analytical approach draws into question the conclusions made from their analysis of dietary tomato and lycopene intake in the PCPT trial [204]. These are significant limitations to the conclusions drawn. Other studies finding no link between PCa and lycopene/tomato intake or serum lycopene have also drawn their study populations from large longitudinal DRE/PSA-based screening trials (e.g., the Prostate, Colorectal, Lung, and Ovarian [PLCO] Cancer Screening Trial) [214,215]. Although the PLCO and other trials did not utilize the unique end-of-study biopsy protocol that the PCPT did, reliance on PSA screening resulted in the diagnosis of many more low-grade, indolent cancers than would have otherwise been detected [208]. Without careful accounting for this PSA-bias, effects of dietary lycopene on clinically relevant cancers are likely to be "washed out" by the abundance of screening-detected cancers. Giovannucci convincingly argued this point in 2011 [213] and Wei and Giovannucci provided a thorough analysis of this problem in 2012 [216].

To summarize the body of epidemiological evidence linking lycopene/tomato intake and PCa, multiple reports, from multiple laboratories, suggest that tomato or lycopene intake is inversely associated with total PCa incidence. Moreover, lycopene or tomato intake appears to be linked most strongly with a lower risk of aggressive or lethal PCa, suggesting that lycopene/tomato may inhibit cancer progression. As cancer etiology and the composition of a human diet are both incredibly dynamic and complex ecological problems, it is not surprising that variability exists in the observational literature. Moreover, bias present within trial datasets, like the PCPT, has clouded or obscured relationships between dietary tomato/lycopene and PCa where they do or may exist. Whether dietary lycopene/tomato prevents the formation of initial carcinogenic lesions, inhibits the progression of extant lesions to clinically relevant and life-threatening stages, or both, are answers unavailable to the techniques at the disposal of observational investigation. Experimental studies, past and present, have used these questions as a foundation for inquiry.

The Transgenic Adenocarcinoma of the Mouse Prostate (TRAMP) Model

The transgenic adenocarcinoma of the mouse prostate (TRAMP) model was developed in the 1990s in the lab of Norman Greenberg as a model of human prostate carcinogenesis [217]. The model relies on prostate epithelium-specific expression of the simian virus 40 large and small T antigens (SV40 Tag), driven by the androgen-regulated rat probasin promoter, which directs transgene expression to the dorsal and ventral prostate lobes. The viral large T antigen inhibits the tumor suppressors p53 and Rb, two genes commonly lost in human PCa, whereas the small t antigen inhibits protein phosphatase 2A, a negative regulator of the pro-proliferative MAP kinase pathway. The result of these effects is prostatic hyperplasia and neoplasia in the TRAMP mouse

as early as 10 weeks of age. In subsequent papers, the Greenberg group documented progression of this model through primary disease, metastasis [218], and castration-resistant disease [219,220]. Additionally, they developed a histological pathology grading system for the model [221], which has been modified by Clinton and colleagues [222]. To date, the TRAMP model has been used extensively – over 440 original articles appear on PubMed as of March 17, 2016. Several aspects of the TRAMP model make it an appropriate model of human PCa and especially CRPC. The model demonstrates a progression from early low-grade hyperplasia through to metastasis, resembling development of the human disease. Castration initially induces prostatic or tumoral regression before selecting for castration-resistant disease, and some tumors exhibit AR mutations [223], as in humans (reviewed in [224,225]). Despite many similarities to the human disease, as with any animal model, the TRAMP model is not a perfect representation of human PCa. A commonly voiced concern over use of this model has been the presence of a neuroendocrine phenotype within some tumors. Some authors have claimed that malignancies in the TRAMP model are primarily of neuroendocrine phenotype and in fact are of neuroendocrine origin [226], but we and others feel that this is an extreme view. Studies of human PCa demonstrate that focal neuroendocrine differentiation is present in 45%-50% of tumor biopsies (as determined by synaptophysin immunoreactivity) and correlates with increasing Gleason score [227,228]. In the TRAMP model, similarly, many poorly differentiated tumors display focal synaptophysin immunostaining, but this occurs very rarely in less severe lesions [229]. Additionally, the fact that early prostatic intraepithelial neoplasia (PIN) lesions do not display synaptophysin staining contradicts arguments in favor of a neuroendocrine origin of disease in TRAMP mice. It seems that in the TRAMP model, as in human PCa, foci of neuroendocrine differentiation may be a natural function of disease progression.

Dietary Tomato or Lycopene in Animal Models of Prostate Cancer

This section will focus only on the use of rodent models for the investigation of PCa prevention by dietary tomato and lycopene. Use of available animal models for more general investigation of human PCa has been thoroughly reviewed elsewhere [224,230–232]. Additionally, despite much work that has been done on the effects of tomato carotenoids on PCa cell lines *in vitro,* these studies will not be addressed in depth here. Readers interested in summaries of *in vitro* reports of lycopene bioactivity are directed to the reviews by Holzapfel et al. and van Breemen and Pajkovic [233,234].

Although the TRAMP model is now the most common animal model for investigation of PCa, other models preceded its introduction. To our knowledge, the first report of the use of tomato or lycopene in an animal model of prostate carcinogenesis was a report in 2001 by Imaida and colleagues [235], but they failed to observe a preventative effect of lycopene on PCa incidence in their model of carcinogen-induced general carcinogenesis. Subsequently, our own group, using a carcinogen + testosterone model designed to specifically induce prostatic carcinogenesis, observed a significantly increased proportion of survival in rats fed tomato paste (10% w/w, 13 mg/kg diet), but not a ~10-fold higher dose of purified lycopene [236]. This was the first experimental report to show a protective effect of tomato feeding *in vivo* and, importantly, the source and level of tomato inclusion were chosen to approximate realistic intakes in humans. Furthermore, this study suggested a synergistic effect of compounds within the whole tomato, which was not matched by feeding of single purified bioactive compound (lycopene).

However, subsequent studies would provide conflicting data: Pannellini et al. demonstrated that a 10% tomato paste diet reduced cancer incidence in TRAMP mice [237], whereas Konijeti et al. reported no effect on TRAMP carcinogenesis with a 12.8% tomato paste

diet, but a significant reduction in cancer incidence (-35%, $p < 0.002$) in mice fed purified lycopene [238]. The reasons for these inconsistencies are unclear, as molecular endpoints (prostatic lycopene levels, serum growth factors, and markers of DNA damage) did not differ between the lycopene- and tomato paste-fed animals groups in the Konijeti report. Venkateswaran et al. demonstrated that lycopene in combination with vitamin E and selenium reduced carcinogenesis in the *Lady* model (which is a less-aggressive derivative of the TRAMP model) [239], and that lycopene was an essential component of this antioxidant mixture for prevention of carcinogenesis [240]. Our own lab has published two studies on the effects of tomato feeding in TRAMP mice. In the first, 10% tomato powder feeding significantly reduced PCa incidence by nearly 40%, and by 55% when combined with a 2% soy germ diet [241]. This combinatorial effect was less than additive, however, which might have been explained by the reduced carotenoid bioavailability observed when co-feeding soy [40]. In contrast, Conlon et al. failed to demonstrate a protective effect of 10% tomato feeding in TRAMP mice [242]. Despite the fact that the tomato diet provided by Conlon et al. contained ~20-fold lower levels of lycopene than was fed by Zuniga (24 μmol lycopene/kg vs. 500 μmol lycopene/ kg diet, respectively), prostatic accumulation in the anterior prostate of the Conlon study was actually higher (0.4 ± 0.1 nmol/g) than was accumulation in the tumors of the Zuniga study (0.25 ± 0.05 nmol/g). Serum concentrations were practically identical, at 0.66 ± 0.15 μM and 0.67 ± 0.07 μM, respectively. This suggests that, due to tissue saturation, vastly different dietary exposures may not have mediated the difference in effect. However, whereas the Zuniga study initiated feeding at weaning, the study by Conlon et al. was designed to assess whether tomato diet intervention at 8 weeks of age (during the window of SV40Tag-induced transformation) would be effective. It is possible that in primary TRAMP prostate cancers, there exists a critical window for intervention before neoplastic transformation

and while the Zuniga study intervened within this window, the treatment initiated by Conlon et al. was too late. Examining this question, we have demonstrated that markers of early prostate carcinogenesis are evident at 10 weeks of age in the TRAMP mouse and that although initiation of tomato and lycopene diets after weaning similarly impact gene expression, the effects are modest when compared to manipulation of TRAMP genotype or castration status [243]. Nonetheless, tomato and lycopene feeding both reduced mRNA expression of the DHT-biosynthetic enzyme 5α-reductase, as well as two AR coactivators (SREBP and paxillin) [243], suggesting that tomato intake may impact PCa carcinogenesis through modulation of androgen status. A later intervention (e.g., at 8 weeks as in Conlon et al.) would thus likely be at a distinct disadvantage in preventing early carcinogenic transformation and later PCa progression.

Other studies have utilized tumorigenesis models to demonstrate a protective effect of lycopene or tomato on PCa progression *in vivo*. Siler et al. showed that purified dietary lycopene induced necrosis in the Dunning transplantable tumor and modulated expression of genes involved in paracrine androgen signaling [244]. Our own lab has demonstrated that tomato feeding in combination with dietary broccoli reduced Dunning tumor weights, increases apoptosis, and inhibited proliferation [245].

Animal models have provided crucial opportunities for experimental testing of hypotheses generated by observational studies. Many studies have demonstrated efficacy of purified lycopene and/or tomato, but have not provided clarification as to what components of tomatoes may contribute to the occasionally differential impacts of purified lycopene and whole tomato. More studies focused on specific mechanisms are needed, but studies to this point have suggested that lycopene and/or tomato may alter androgen metabolism or signaling within tumors. Additionally, as efficacy has been demonstrated in both carcinogenesis and

tumorigenesis studies, lycopene and/or tomato may impact prostate cancer at multiple levels, preventing both initial lesions as well as disease progression.

Development, Treatment, and Prevention of Castration-Resistant Prostate Cancer

Whereas treatment for mild, primary disease is often radiation or prostatectomy (removal of the prostate), advanced cancers that progress after primary treatments fail require alternative treatment strategies. Androgen deprivation therapy (ADT), accomplished through pharmacological blockade of androgen synthesis or ligand binding (and formerly by surgical castration) is currently the first-line therapy for these aggressive cancers [155]. Since the prostate and prostatic neoplasms are initially dependent on circulating androgens, tumors often regress following ADT, but the disease recurs as castration-resistant prostate cancer (CRPC) in 80% - 90% of patients. CRPC is an advanced and lethal form of recurrent PCa that has a median survival of only 2.5 years [246]. CRPC development is facilitated by the selection via evolutionary pressure of existing "androgen-independent" clonal populations [247], acquisition of novel-function androgen receptor (AR) mutations [248–250], or the capacity for local *de novo* androgen synthesis [251–254]. Medical oncologists have long been searching for ADT regimes that will delay CRPC occurrence and prolong survival, whether through testing of new temporal [255] or pharmacological [246] schemes of treatment. However, as with primary PCa, dietary approaches may hold great promise in the prevention of disease progression. In fact, others have argued that the protective effects of lycopene and tomato intake on *primary* PCa may actually be through the reduction of disease progression and therefore clinical symptoms [213]. Supporting this, a prospective study in 1,202 men with PCa from the Health Professionals Follow-up cohort found that high consumption of tomato sauce *after* diagnosis was linked to lower rates of PCa progression [196].

Aims of Dissertation

Much has been discovered regarding the metabolism of tomato carotenoids and their protective effects against PCa incidence and mortality, but much still remains to be clarified. In particular, although BCO1 is known to play a key role in the metabolism of dietary carotenoids, it also appears to impact aspects of physiology independent from carotenoid cleavage. In order to fully understand how human genetic variation in *BCO1* may impact carotenoid metabolism – and potentially modulate relationships between dietary lycopene and PCa risk – a more thorough understanding of the cellular and physiological role of BCO1 is necessary. Specifically, elucidating the impact(s) of BCO1 on prostatic physiology and hepatic lipid metabolism will be important to understanding the complex interplay between carotenoid metabolism and prostatic disease. Secondly, although much epidemiological and animal work has focused on the effects of dietary tomato carotenoids on primary PCa, little is known about the effects on CRPC, which represents the lethal phase of the disease. Therefore, the aims of this dissertation are the following:

1. Elucidate the impact of *Bco1* loss on prostatic physiology, with a focus on androgen responsiveness,

2. Determine the impact of *Bco1* loss on lipid, cholesterol, and retinoid metabolism in the liver, a key organ in the metabolism and biodistribution of dietary carotenoids, and

3. Evaluate the effects of dietary tomato feeding on an animal model of CRPC and determine its efficacy in preventing disease progression.

References cited

1. Olson, J. A. & Krinsky, N. I. Introduction: The colorful, fascinating world of the carotenoids: Important physiologic modulators. *FASEB J.* **9,** 1547–1550 (1995).
2. Goodwin, T. W. The changes in carotenoid and chlorophyll pigments in the leaves of deciduous trees during autumn necrosis. *Biochem. J.* **68,** 503–511 (1958).
3. Demmig-Adams, B. & Adams, W. W. Antioxidants in photosynthesis and human nutrition. *Science.* **298,** 2149–53 (2002).
4. Oren, A. A hundred years of Dunaliella research: 1905-2005. *Saline Systems* **1,** 2 (2005).
5. Bauman, A. J. & Simmonds, P. G. Fatty acids and ploar lipids of extrememly thermophilic filamentous bacterial masses from two Yellowstone hot springs. *J. Bacteriol.* **98,** 528–531 (1969).
6. Moran, N. A. & Jarvik, T. Lateral transfer of genes from fungi underlies carotenoid production in aphids. *Science* **328,** 624–627 (2010).
7. McGraw, K. J., Hill, G. E., Stradi, R. & Parker, R. S. The effect of dietary carotenoid access on sexual dichromatism and plumage pigment composition in the American goldfinch. *Comp. Biochem. Physiol. B.* **131,** 261–269 (2002).
8. Toomey, M. B. *et al.* A complex carotenoid palette tunes avian colour vision. *J. R. Soc. Interface* **12,** 20150563 (2015).
9. Mein, J. R., Lian, F. & Wang, X.-D. Biological activity of lycopene metabolites: implications for cancer prevention. *Nutr. Rev.* **66,** 667–83 (2008).
10. Voutilainen, S., Nurmi, T., Mursu, J. & Rissanen, T. H. Carotenoids and cardiovascular health. *Am. J. Clin. Nutr.* **83,** 1265-1271 (2006).

11. Britton, G. Structure and properties of carotenoids in relation to function. *FASEB J.* **9,** 1551–1558 (1995).

12. *Carotenoids Handbook*. Britton, G., Liaaen-Jenson, S. & Pfander, H., Eds. (Springer Basel AG, 2004).

13. Engelmann, N. J., Rogers, R. B., Lila, M. A. & Erdman Jr., J. W. Herbicide treatments alter carotenoid profiles for 14C tracer production from tomato (Solanum lycopersicum cv. VFNT cherry) cell cultures. *J. Agric. Food Chem.* **57,** 4614–4619 (2009).

14. Müller, L. *et al.* Comparative study on antioxidant activity of lycopene (Z)-isomers in different assays. *J. Agric. Food Chem.* **59,** 4504-4511 (2011).

15. Lakshmanan, M. R., Pope, J. L. & Olson, J. A. The specificity of a partially purified carotenoid cleavage enzyme of rabbit intestine. *Biochem. Biophys. Res. Commun.* **33,** 347–352 (1968).

16. Barua, A. B. & Olson, J. A. Beta-carotene is converted primarily to retinoids in rats in vivo. *J. Nutr.* **130,** 1996–2001 (2000).

17. Riabroy, N., Dever, J. T. & Tanumihardjo, S. A. α-Retinol and 3,4-didehydroretinol support growth in rats when fed at equimolar amounts and α-retinol is not toxic after repeated administration of large doses. *Br. J. Nutr.* **111,** 1373–81 (2014).

18. Burri, B. J. & Clifford, A. J. Carotenoid and retinoid metabolism: insights from isotope studies. *Arch. Biochem. Biophys.* **430,** 110–9 (2004).

19. Wu, K. *et al.* Variations in plasma lycopene and specific isomers over time in a cohort of U.S. men. *J. Nutr.* **133,** 1930–6 (2003).

20. Clinton, S. K. *et al.* cis-trans lycopene isomers, carotenoids, and retinol in the human prostate. *Cancer Epidemiol. Biomarkers Prev.* **5,** 823–833 (1996).

21. Grainger, E. M. *et al.* A comparison of plasma and prostate lycopene in response to typical servings of tomato soup, sauce or juice in men before prostatectomy. *Br. J. Nutr.* **114,** 596-607 (2015).

22. Unlu, N. Z. *et al.* Lycopene from heat-induced cis-isomer-rich tomato sauce is more bioavailable than from all-trans-rich tomato sauce in human subjects. *Br. J. Nutr.* **98,** 140–146 (2007).

23. Cooperstone, J. L. *et al.* Enhanced bioavailability of lycopene when consumed as cis-isomers from tangerine compared to red tomato juice, a randomized, cross-over clinical trial. *Mol. Nutr. Food Res.* **59,** 658–669 (2015).

24. Ross, A. B. *et al.* Lycopene bioavailability and metabolism in humans: an accelerator mass spectrometry study. *Am. J. Clin. Nutr.* **93,** 1263-1273 (2011).

25. Moran, N. E. *et al.* Compartmental and noncompartmental modeling of 13C-lycopene absorption, isomerization, and distribution kinetics in healthy adults. *Am. J. Clin. Nutr.* **102,** 1436–1449 (2015).

26. Gaziano, J. M. *et al.* Discrimination in absorption or transport of a-carotene isomers after oral supplementation with either all-trans- or 9-cis-B-carotene. *Am. J. Clin. Nutr.* **61,** 1248–52 (1995).

27. Porrini, M., Riso, P. & Testolin, G. Absorption of lycopene from single or daily portions of raw and processed tomato. *Br. J. Nutr.* **80,** 353–361 (1998).

28. Periago, M. J., Bravo, S., García-Alonso, F. J. & Rincón, F. Detection of key factors affecting lycopene in vitro accessibility. *J. Agric. Food Chem.* **61,** 3859–3867 (2013).

29. Unlu, N. Z., Bohn, T., Clinton, S. K. & Schwartz, S. J. Carotenoid absorption from salad and salsa by humans is enhanced by the addition of avocado or avocado oil. *J. Nutr.* **135,** 431–436 (2005).

30. Conlon, L. E., King, R. D., Moran, N. E. & Erdman, J. W. Coconut oil enhances tomato carotenoid tissue accumulation compared to safflower oil in the mongolian gerbil (meriones unguiculatus). *J. Agric. Food Chem.* **60,** 8386–8394 (2012).

31. Reboul, E. & Borel, P. Proteins involved in uptake, intracellular transport and basolateral secretion of fat-soluble vitamins and carotenoids by mammalian enterocytes. *Prog. Lipid Res.* **50,** 388–402 (2011).

32. Widjaja-Adhi, M. A. K., Lobo, G. P., Golczak, M. & Von Lintig, J. A genetic dissection of intestinal fat-soluble vitamin and carotenoid absorption. *Hum. Mol. Genet.* **24,** 3206–19 (2015).

33. Moussa, M. *et al.* Lycopene absorption in human intestinal cells and in mice involves scavenger receptor class B type I but not Niemann-Pick C1-like 1. *J. Nutr.* **138,** 1432–6 (2008).

34. Lindshield, B. L. *et al.* Lycopene biodistribution is altered in 15,15'-carotenoid monooxygenase knockout mice. *J. Nutr.* **138,** 2367–2371 (2008).

35. Ford, N. A., Clinton, S. K., Lintig, J. Von, Wyss, A. & Erdman Jr., J. W. Loss of carotene-9',10'-monooxygenase expression increases serum and tissue lycopene concentrations in lycopene-fed mice. *J. Nutr.* **140,** 2134–2138 (2010).

36. Amengual, J. *et al.* Two carotenoid oxygenases contribute to mammalian provitamin A metabolism. *J. Biol. Chem.* **288,** 34081–96 (2013).

37. Harrison, E. H. Mechanisms involved in the intestinal absorption of dietary vitamin A and provitamin A carotenoids. *Biochim. Biophys. Acta - Mol. Cell Biol. Lipids* **1821,** 70–77 (2012).

38. Kaplan, L.A, Lau, J. M., & Stein, E. A. Carotenoid composition, concentrations, and relationships in various human organs. *Clin. Physiol. Biochem.* **8,** 1–10 (1990).

39. Moran, N. E., Clinton, S. K. & Erdman Jr., J. W. Differential bioavailability, clearance, and tissue distribution of the acyclic tomato carotenoids lycopene and phytoene in mongolian gerbils. *J. Nutr.* **143,** 1920–1926 (2013).

40. Zuniga, K. E. & Erdman, J. W. Combined consumption of soy germ and tomato powders results in altered isoflavone and carotenoid bioavailability in rats. *J. Agric. Food Chem.* **59,** 5335–41 (2011).

41. Erdman, J. W. How do nutritional and hormonal status modify the bioavailability, uptake, and distribution of different isomers of lycopene? *J. Nutr.* **135,** 2046S–2047S (2005).

42. Sourkes, T. L. The discovery and early history of carotene. *Bull. Hist. Chem* **34,** 32–38 (2009).

43. Palmer, L. S. Carotenoids as fat-soluble vitamine. *Science.* **50,** 501–502 (1919).

44. Palmer, L. S. & Kennedy, C. The relation of plant carotinoids to growth and reproduction of albino rats. *J. Biol. Chem.* **46,** 559–577 (1921).

45. Moore, T. The absence of the liver oil vitamin A from carotene and the conversion of carotene to vitamin A in vivo. *Biochem. J.* **24,** 692–702 (1930).

46. Thompson, S. Y., Ganguly, J. & Kon, S. K. The conversion of beta-carotene to vitamin A in the intestine. *Br. J. Nutr.* **3,** 50–78 (1949).

47. Olson, J. A. & Hayaishi, O. The enzymatic cleavage of beta-carotene into vitamin A by soluble enzymes of rat liver and intestine. *Proc. Natl. Acad. Sci.* **54,** 1364–1370 (1965).

48. Goodman, D. S. & Huang, H. S. Biosynthesis of vitamin A with rat intestinal enzymes. *Science.* **149,** 879–880 (1965).

49. dela Seña, C. *et al.* Substrate specificity of purified recombinant human β-carotene 15,15'-oxygenase (BCO1). *J. Biol. Chem.* **288,** 37094–103 (2013).

50. Goodman, D. S., Huang, H. S. & Shiratori, T. Mechanism of the biosynthesis of vitamin A from beta-carotene. *J. Biol. Chem.* **241,** 1929–1932 (1966).

51. Leuenberger, M. G., Engeloch-Jarret, C. & Woggon, W.-D. The reaction mechanism of the enzyme-catalyzed central cleavage of beta-carotene to retinal. *Angew. Chemie* **40,** 2613–2617 (2001).

52. dela Seña, C. *et al.* The human enzyme that converts dietary provitamin a carotenoids to vitamin A is a dioxygenase. *J. Biol. Chem.* **289,** 13661–13666 (2014).

53. Lakshmanan, M. R., Chansang, H. & Olson, J. A. Purification and properties of carotene 15,15'-dioxygenase of rabbit intestine. *J. Lipid Res.* **13,** 477–482 (1972).

54. Lederman, J. D. *et al.* Ferrets (Mustela putoius furo) inefficiently convert beta-carotene to vitamin A. *J. Nutr.* **271,** 280–286 (1998).

55. Wyss, A. *et al.* Cloning and expression of β,β-Carotene 15,15′-dioxygenase. *Biochem. Biophys. Res. Commun.* **271,** 334–336 (2000).

56. von Lintig, J. & Vogt, K. Filling the gap in vitamin A research. Molectular identification of an enzyme cleaving beta-carotene to retinal. *J. Biol. Chem.* **275,** 11915–11920 (2000).

57. Redmond, T. M. *et al.* Identification, expression, and substrate specificity of a mammalian beta-carotene 15,15'-dioxygenase. *J. Biol. Chem.* **276,** 6560–5 (2001).

58. Paik, J. *et al.* Expression and characterization of a murine enzyme able to cleave β-carotene. The formation of retinoids. *J. Biol. Chem.* **276,** 32160–32168 (2001).

59. Lindqvist, A. & Andersson, S. Biochemical properties of purified recombinant human beta-carotene 15,15'-monooxygenase. *J. Biol. Chem.* **277,** 23942–8 (2002).

60. Lindqvist, A. & Andersson, S. Cell type-specific expression of beta-carotene 15,15'-mono-oxygenase in human tissues. *J. Histochem. Cytochem.* **52,** 491–499 (2004).

61. Lindqvist, A., He, Y.-G. & Andersson, S. Cell type-specific expression of beta-carotene 9',10'-monooxygenase in human tissues. *J. Histochem. Cytochem.* **53,** 1403–12 (2005).

62. Livera, G., Rouiller-Fabre, V., Durand, P. & Habert, R. Multiple effects of retinoids on the development of Sertoli, germ, and Leydig cells of fetal and neonatal rat testis in culture. *Biol. Reprod.* **62,** 1303–1314 (2000).

63. Livera, G., Rouiller-Fabre, V. & Habert, R. Retinoid receptors involved in the effects of retinoic acid on rat testis development. *Biol. Reprod.* **64,** 1307–1314 (2001).

64. Livera, G., Rouiller-Fabre, V., Pairault, C., Levacher, C. & Habert, R. Regulation and perturbation of testicular functions by vitamin A. *Reproduction* **124,** 173–180 (2002).

65. Hogarth, C. A., Amory, J. K. & Griswold, M. D. Inhibiting vitamin A metabolism as an approach to male contraception. *Trends Endocrinol. Metab.* **22,** 136–44 (2011).

66. von Lintig, J. Colors with functions: Elucidating the biochemical and molecular basis of carotenoid metabolism. *Annu. Rev. Nutr.* **30,** 35–56 (2010).

67. Ziouzenkova, O. & Plutzky, J. Retinoid metabolism and nuclear receptor responses: New insights into coordinated regulation of the PPAR-RXR complex. *FEBS Lett.* **582,** 32–38 (2008).

68. Shirakami, Y., Lee, S. A., Clugston, R. D. & Blaner, W. S. Hepatic metabolism of retinoids and disease associations. *Biochim. Biophys. Acta - Mol. Cell Biol. Lipids* **1821,** 124–136 (2012).

69. Evans, R. M. & Mangelsdorf, D. J. Nuclear receptors, RXR, and the Big Bang. *Cell* **157,** 255–66 (2014).

70. Olson, J. A. The Alpha and the Omega of vitamin A metabolism. *Am. J. Clin. Nutr.* **22,** 953–962 (1969).

71. Fleshman, M. K. *et al.* Carotene and novel apocarotenoid concentrations in orange-fleshed Cucumis melo melons: determinations of β-carotene bioaccessibility and bioavailability. *J. Agric. Food Chem.* **59,** 4448–54 (2011).

72. Harrison, E. H., dela Seña, C., Eroglu, A. & Fleshman, M. K. The formation, occurrence, and function of B-apocarotenoids: B-carotene metabolites that may modulate nuclear receptor signaling. *Am. J. Clin. Nutr.* **96,** 1189S–1192S (2012).

73. Kiefer, C. *et al.* Identification and characterization of a mammalian enzyme catalyzing the asymmetric oxidative cleavage of provitamin A. *J. Biol. Chem.* **276,** 14110–6 (2001).

74. Eroglu, A. *et al.* Naturally-occurring eccentric cleavage products of provitamin A beta-carotene function as antagonists of retinoic acid receptors. *J. Biol. Chem.* **287,** 15886–15895 (2012).

75. Ziouzenkova, O. *et al.* Asymmetric cleavage of beta-carotene yields a transcriptional repressor of retinoid X receptor and peroxisome proliferator-activated receptor responses. *Mol. Endocrinol.* **21,** 77–88 (2007).

76. Hu, K.-Q. *et al.* The biochemical characterization of ferret carotene-9',10'-monooxygenase catalyzing cleavage of carotenoids in vitro and in vivo. *J. Biol. Chem.* **281,** 19327–38 (2006).

77. Lian, F., Smith, D. E., Ernst, H., Russell, R. M. & Wang, X.-D. Apo-10'-lycopenoic acid inhibits lung cancer cell growth in vitro, and suppresses lung tumorigenesis in the A/J mouse model in vivo. *Carcinogenesis* **28,** 1567–74 (2007).

78. Lian, F. & Wang, X.-D. Enzymatic metabolites of lycopene induce Nrf2-mediated expression of phase II detoxifying/antioxidant enzymes in human bronchial epithelial cells. *Int. J. Cancer* **123,** 1262–8 (2008).

79. Ip, B. C. *et al.* Lycopene metabolite, apo-10′-lycopenoic acid, inhibits diethylnitrosamine-initiated, high fat diet-promoted hepatic inflammation and tumorigenesis in mice. *Cancer Prev. Res.* **6,** 1304–1316 (2013).

80. Ip, B. C., Liu, C., Lichtenstein, A. H., Lintig, J. Von & Wang, X. Lycopene and apo-10 ' -lycopenoic acid have differential mechanisms of protection against hepatic steatosis in beta-carotene-9',10'- oxygenase knockout male mice. *J. Nutr.* **145,** 268–276 (2015).

81. Ip, B. C., Liu, C., Ausman, L. M., Von Lintig, J. & Wang, X. D. Lycopene attenuated hepatic tumorigenesis via differential mechanisms depending on carotenoid cleavage enzyme in mice. *Chest* **146,** 1219–1227 (2014).

82. Ford, N. A., Elsen, A. C., Zuniga, K. E., Lindshield, B. L. & Erdman, J. W. Lycopene and apo-12'-lycopenal reduce cell proliferation and alter cell cycle progression in human prostate cancer cells. *Nutr. Cancer* **63,** 256–263 (2011).

83. Stahl, W., Laar, J. Von, Martin, H.-D., Emmerich, T. & Sies, H. Stimulation of gap junctional communication: Comparison of acyclo-retinoic acid and lycopene. *Arch. Biochem. Biophys.* **373,** 271–274 (2000).

84. Ben-Dor, A. *et al.* Effects of acyclo-retinoic acid and lycopene on activation of the retinoic acid receptor and proliferation of mammary cancer cells. *Arch. Biochem. Biophys.* **391,** 295–302 (2001).

85. Lindshield, B. L., Canene-Adams, K. & Erdman, J. W. Lycopenoids: Are lycopene metabolites bioactive? *Arch. Biochem. Biophys.* **458,** 136–40 (2007).

86. Erdman, J. W., Ford, N. A. & Lindshield, B. L. Are the health attributes of lycopene related to its antioxidant function? *Arch. Biochem. Biophys.* **483,** 229–35 (2009).

87. Wang, X. Lycopene metabolism and its biological significance. *Am. J. Clin. Nutr.* **96,** 1214S–1222S (2012).

88. Hessel, S. *et al.* CMO1 deficiency abolishes vitamin A production from beta-carotene and alters lipid metabolism in mice. *J. Biol. Chem.* **282,** 33553–61 (2007).

89. Fierce, Y. *et al.* In vitro and in vivo characterization of retinoid synthesis from beta-carotene. *Arch. Biochem. Biophys.* **472,** 126–38 (2008).

90. Lobo, G. P. *et al.* ISX is a retinoic acid-sensitive gatekeeper that controls intestinal beta,beta-carotene absorption and vitamin A production. *FASEB J.* **24,** 1656–66 (2010).

91. Shmarakov, I. *et al.* Hepatic stellate cells are an important cellular site for β-carotene conversion to retinoid. *Arch. Biochem. Biophys.* **504,** 3–10 (2010).

92. van Helden, Y. G. J. *et al.* Knockout of the Bcmo1 gene results in an inflammatory response in female lung, which is suppressed by dietary beta-carotene. *Cell. Mol. Life Sci.* **67,** 2039–56 (2010).

93. van Helden, Y. G. J. *et al.* Downregulation of Fzd6 and Cthrc1 and upregulation of olfactory receptors and protocadherins by dietary beta-carotene in lungs of Bcmo1-/- mice. *Carcinogenesis* **31,** 1329–1337 (2010).

94. Amengual, J. *et al.* Beta-carotene reduces body adiposity of mice via BCMO1. *PLoS One* **6,** e20644 (2011).

95. Kim, Y.-K. *et al.* β-Carotene and its cleavage enzyme β-carotene-15,15'-oxygenase (CMOI) affect retinoid metabolism in developing tissues. *FASEB J.* **25,** 1641–1652 (2011).

96. van Helden, Y. G. J. *et al.* Beta-carotene affects gene expression in lungs of male and female Bcmo1 (-/-) mice in opposite directions. *Cell. Mol. Life Sci.* **68,** 489–504 (2011).

97. van Helden, Y. G. J. *et al.* Gene expression response of mouse lung, liver and white adipose tissue to β-carotene supplementation, knockout of Bcmo1 and sex. *Mol. Nutr. Food Res.* **55,** 1466-1474 (2011).

98. Ford, N. A., Moran, N. E., Smith, J. W., Clinton, S. K. & Erdman Jr., J. W. An interaction between carotene-15,15'-monooxygenase expression and consumption of a tomato or lycopene-containing diet impacts serum and testicular testosterone. *Int. J. Cancer* **131,** E143–8 (2012).

99. Ford, N. A., Elsen, A. C. & Erdman Jr., J. W. Genetic ablation of carotene oxygenases and consumption of lycopene or tomato powder diets modulate carotenoid and lipid metabolism in mice. *Nutr. Res.* **33,** 733–42 (2013).

100. van Helden, Y. G. J., Godschalk, R. W. L., van Schooten, F. J. & Keijer, J. Organ specificity of beta-carotene induced lung gene-expression changes in Bcmo1-/- mice. *Mol. Nutr. Food Res.* **57,** 307–319 (2013).

101. Dixon, J. L., Kim, Y.-K., Brinker, A. & Quadro, L. Loss of β-carotene 15,15'-oxygenase in developing mouse tissues alters esterification of retinol, cholesterol and diacylglycerols. *Biochim. Biophys. Acta* **1841,** 34–43 (2014).

102. Lee, S.-A. *et al.* Cardiac dysfunction in Beta-carotene-15,15'-dioxygenase-deficient mice is associated with altered retinoid and lipid metabolism. *Am. J. Physiol. - Hear. Circ. Physiol.* **307,** H1675–H1684 (2014).

103. Piga, R., Van Dartel, D., Bunschoten, A., Van der Stelt, I. & Keijer, J. Role of Frizzled6 in the molecular mechanism of beta-carotene action in the lung. *Toxicology* **320,** 67–73 (2014).

104. Kim, Y.-K., Zuccaro, M. V., Costabile, B. K., Rodas, R. & Quadro, L. Tissue- and sex-specific effects of β-carotene 15,15′ oxygenase (BCO1) on retinoid and lipid metabolism in adult and developing mice. *Arch. Biochem. Biophys.* **572,** 11–18 (2015).

105. Lindqvist, A., Sharvill, J., Sharvill, D. E. & Andersson, S. Loss-of-function mutation in carotenoid 15,15'-monooxygenase identified in a patient with hypercarotenemia and hypovitaminosis A. *J. Nutr.* **137,** 2346–2350 (2007).

106. Sharvill, D. E. Familial Hypercarotinemia and Hypovitaminosis A. *Proc. R. Soc. Med.* **63,** 3–4 (1970).

107. Leung, W. C. *et al.* Two common single nucleotide polymorphisms in the gene encoding beta-carotene 15,15'-monoxygenase alter beta-carotene metabolism in female volunteers. *FASEB J.* **23,** 1041–53 (2009).

108. Ferrucci, L. *et al.* Common variation in the beta-carotene 15,15'-monooxygenase 1 gene affects circulating levels of carotenoids: A genome-wide association study. *Am. J. Hum. Genet.* **84,** 123–33 (2009).

109. Hendrickson, S. J. *et al.* Beta-Carotene 15,15'-monooxygenase 1 single nucleotide polymorphisms in relation to plasma carotenoid and retinol concentrations in women of European descent. *Am. J. Clin. Nutr.* **96,** 1379–1389 (2012).

110. Wang, T. T. Y., Edwards, A. J. & Clevidence, B. A. Strong and weak plasma response to dietary carotenoids identified by cluster analysis and linked to beta-carotene-15,15' monooxygenase 1 single nucleotide polymorphisms. *J. Nutr. Biochem.* **24,** 1538–46 (2013).

111. Borel, P. *et al.* Human fasting plasma concentrations of vitamin E and carotenoids, and their association with genetic variants in apo C-III, cholesteryl ester transfer protein, hepatic lipase, intestinal fatty acid binding protein and microsomal triacylglycerol transfer p. *Br. J. Nutr.* **101,** 680–7 (2009).

112. Meyers, K. J. *et al.* Genetic determinants of macular pigments in women of the Carotenoids in Age-Related Eye Disease Study. *Invest. Ophthalmol. Vis. Sci.* **54,** 2333–45 (2013).

113. Gong, X., Tsai, S.-W., Yan, B. & Rubin, L. P. Cooperation between MEF2 and PPARgamma in human intestinal beta,beta-carotene-15,15'-monooxygenase gene expression. *BMC Mol. Biol.* **7,** 7 (2006).

114. Siegel, R. L., Miller, K. D. & Jemal, A. Cancer Statistics, 2016. *CA. Cancer J. Clin.* **66,** 7–30 (2016).

115. Siegel, R. L., Ma, J., Zou, Z. & Jemal, A. Cancer Statistics, 2014. *CA. Cancer J. Clin.* **64,** 9–29 (2014).

116. Siegel, R. L., Miller, K. D. & Jemal, A. Cancer Statistics, 2015. *CA. Cancer J. Clin.* **65,** 21254 (2015).

117. Wilson, J. D. The critical role of androgens in prostate development. *Endocrinol. Metab. Clin. North Am.* **40,** 577–590 (2011).

118. Myers, R. P. Structure of the adult prostate from a clinician's standpoint. *Clin. Anat.* **13,** 214–215 (2000).

119. Garcia, J. J. *et al.* Do prostatic transition zone tumors have a distinct morphology? *Am. J. Surg. Pathol.* **32,** 1709–1714 (2010).

120. Berquin, I. M., Min, Y., Wu, R., Wu, H. & Chen, Y. Q. Expression signature of the mouse prostate. *J. Biol. Chem.* **280,** 36442–51 (2005).

121. Shappell, S. B. *et al.* Prostate pathology of genetically engineered mice: Definitions and classification. The consensus report from the Bar Harbor Meeting of the Mouse Models of Human Cancer Consortium Prostate Pathology Committee. *Cancer Res.* **64,** 2270–2305 (2004).

122. Verhagen, A. P. M., Ramaekers, F. C. S., Aalders, T. W. & Schalken, J. A. Colocalization of basal and luminal cell-type cytokeratins in human prostate cancer. *Cancer Res.* **52,** 6182–6187 (1992).

123. Goldstein, A. S., Huang, J., Guo, C., Garraway, I. P. & Witte, O. N. Identification of a cell of origin for human prostate cancer. *Science.* **329,** 568–71 (2010).

124. Shukla, C. J. *et al.* Laser-capture microdissection in prostate cancer research: Establishment and validation of a powerful tool for the assessment of tumour-stroma interactions. *Br. J. Urol. Int.* **101,** 765–74 (2008).

125. Marker, P. C., Donjacour, A. A., Dahiya, R. & Cunha, G. R. Hormonal, cellular, and molecular control of prostatic development. *Dev. Biol.* **253,** 165–174 (2003).

126. Kerr, J. F. R. & Searle, J. Deletion of cells by apoptosis during castration-induced involution of the rat prostate. *Virchows Arch. B* **13,** 87–102 (1973).

127. Kyprianou, N. & Isaacs, J. T. Activation of programmed cell death in the rat ventral prostate after castration. *Endocrinology* **122,** 552–562 (1988).

128. Evans, G. S. & Chandler, J. A. Cell proliferation studies in the rat prostate: II. The effects of castration and androgen-induced regeneration upon basal and secretory cell proliferation. *Prostate* **11,** 339–51 (1987).

129. Pointis, G., Latreille, M.-T. & Cedard, L. Gondo-pituitary relationships in the fetal mouse at vaious times during sexual differentiation. *J. Endocrinol.* **86,** 483–488 (1980).

130. Siiteri, P. K. & Wilson, J. D. Testosterone formation and metabolism during male sexual differentiation in the human embryo. *J. Clin. Endocrinol. Metab.* **38,** 113–125 (1974).

131. Sciavolino, P. J. *et al.* Tissue-specific expression of murine Nkx3.1 in the male urogenital system. *Dev. Dyn.* **209,** 127–38 (1997).

132. Kimura, S. *et al.* The T/ebp null mouse: thyroid-specific enhancer-binding protein is essential for the organogenesis of the thyroid, lung, ventral forebrain, and pituitary. *Genes Dev.* **10 ,** 60–69 (1996).

133. Lyons, I. *et al.* Myogenic and morphogenetic defects in the heart tubes of murine embryos lacking the homeo box gene Nkx2-5. *Genes Dev.* **9,** 1654–1666 (1995).

134. He, W. W. *et al.* A novel human prostate-specific, androgen-regulated homeobox gene (NKX3.1) that maps to 8p21, a region frequently deleted in prostate cancer. *Genomics* **43,** 69–77 (1997).

135. Bhatia-Gaur, R. *et al.* Roles for Nkx3.1 in prostate development and cancer. *Genes Dev.* **13,** 966–77 (1999).

136. Kim, M. J. *et al.* Nkx3.1 mutant mice recapitulate early stages of prostate carcinogenesis. *Genes Dev.* **62,** 2999–3004 (2002).

137. Timms, B. G., Lee, C. W., Aumüller, G. & Seitz, J. Instructive induction of prostate growth and differentiation by a defined urogenital sinus mesenchyme. *Microsc. Res. Tech.* **30,** 319–32 (1995).

138. Hayashi, G. R., Parker, M. N. & Cunha, G. R. Permissive and instructive induction of adult rodent prostatic epithelium by heterotypic urogenital sinus mesenchyme. *Epithelial Cell Biol.* **2,** 66–78 (1993).

139. Cunha, G. R. *et al.* The endocrinology and developmental biology of the prostate. *Endocr. Rev.* **8,** 338–362 (1987).

140. Cunha, G. R., Sekkingstad, M. & Meloy, B. A. Heterospecific induction of prostatic development in tissue recombinants prepared with mouse, rat, rabbit and human tissues. *Differentiation* **24,** 174–180 (1983).

141. Gaspar, M. L., Meo, T., Bourgarel, P., Guenet, J. L. & Tosi, M. A single base deletion in the Tfm androgen receptor gene creates a short-lived messenger RNA that directs internal translation initiation. *Proc. Natl. Acad. Sci.* **88,** 8606–10 (1991).

142. Cunha, G. R. & Lung, B. The possible influence of temporal factors in androgenic responsiveness of urogenital tissue recombinants from wild-type and androgen-insensitive (Tfm) mice. *J. Exp. Zool.* **205,** 181–193 (1978).

143. Cunha, G. R. & Chung, L. W. Stromal-epithelial interactions-I. Induction of prostatic phenotype in urothelium of testicular feminized (Tfm/y) mice. *J. Steroid Biochem.* **14,** 1317–24 (1981).

144. Taplin, M. E. & Ho, S. M. The endocrinology of prostate cancer. *J. Clin. Endocrinol. Metab.* **86,** 3467–77 (2001).

145. Ricke, E. A. *et al.* Androgen hormone action in prostatic carcinogenesis: stromal androgen receptors mediate prostate cancer progression, malignant transformation and metastasis. *Carcinogenesis* **33,** 1391–1398 (2012).

146. Yu, S. *et al.* Androgen receptor in human prostate cancer-associated fibroblasts promotes prostate cancer epithelial cell growth and invasion. *Med. Oncol.* **30,** 674 (2013).

147. Labrie, F. *et al.* Is dehydroepiandrosterone a hormone? *J. Endocrinol.* **187,** 169–96 (2005).

148. van Weerden, W. M., Blerings, H. G., van Steenbrugge, G. J., de Jong, F. H. & Schröder, F. H. Adrenal glands of mouse and rat do not synthesize androgens. *Life Sci.* **50,** 857–861 (1992).

149. Brock, B. J. & Waterman, M. R. Biochemical differences between rat and human cytochrome P450c17 support the different steroidogenic needs of these two species. *Biochemistry* **38,** 1598–606 (1999).

150. Perkins, L. M. & Payne, A. H. Quantification of P450(scc), P450(17alpha), and iron sulfur protein reductase in Leydig cells and adrenals of inbred strains of mice. *Endocrinology* **123,** 2675–2682 (1988).

151. Touitou, Y., Auzeby, A. & Bogdan, A. Cortisol and cortisone production in rat and mouse adrenal incubations. *J. Steroid Biochem. Mol. Biol.* **37,** 279–284 (1990).

152. Kokontis, J. M. & Liao, S. Molecular action of androgen in the normal and neoplastic prostate. *Vitam. Horm.* **55,** 219–307 (1999).

153. Luu-The, V., Bélanger, A. & Labrie, F. Androgen biosynthetic pathways in the human prostate. *Best Pract. Res. Clin. Endocrinol. Metab.* **22,** 207–21 (2008).

154. Sherbet, D. P. & Auchus, R. J. in *Contemp. Endocrinol. Leydig Cell Heal. Dis.* Payne, A. H. & Hardy, M. P., Eds. 181–188 (Humana Press, 2007).

155. Feldman, B. J. & Feldman, D. The development of androgen-independent prostate cancer. *Nat. Rev. Cancer* **1,** 34–45 (2001).

156. Chen, Y., Sawyers, C. L. & Scher, H. I. Targeting the androgen receptor pathway in prostate cancer. *Curr. Opin. Pharmacol.* **8,** 440–8 (2008).

157. Huggins, C. Endocrine-induced regression of cancers. *Cancer Res.* **27,** 1925–1930 (1967).

158. Barrett-Connor, E., Garland, C., McPhillips, J. B., Khaw, K.-T. & Wingard, D. L. A prospective, population-based study of androstenedione, estrogens, and prostatic cancer. *Cancer Res.* **50,** 169–173 (1990).

159. Gann, P. H., Hennekens, C. H., Ma, J., Longcope, C. & Stampfer, M. J. Prospective study of sex hormone levels and risk of prostate cancer. *J. Natl. Cancer Inst.* **88,** 1118–1126 (1996).

160. Shaneyfelt, T., Husein, R., Bubley, G. & Mantzoros, C. S. Hormonal predictors of prostate cancer: a meta-analysis. *J. Clin. Oncol.* **18,** 847–53 (2000).

161. Roddam, A. W., Allen, N. E., Appleby, P. & Key, T. J. Endogenous sex hormones and prostate cancer: a collaborative analysis of 18 prospective studies. *J. Natl. Cancer Inst.* **100,** 170–83 (2008).

162. Shariat, S. F., Lamb, D. J., Roehrborn, C. G. & Slawin, K. M. Potentially harmful effect of a testosterone dietary supplement on prostate cancer growth and metastasis. *Arch. Intern. Med.* **168,** 235–236 (2008).

163. Shariat, S. F., Lamb, D. J., Iyengar, R. G., Roehrborn, C. G. & Slawin, K. M. Herbal/hormonal dietary supplement possibly associated with prostate cancer progression. *Clin. Cancer Res.* **14,** 607–11 (2008).

164. Roberts, J. T. & Essenhigh, D. M. Adenocarcinoma of prostate in 40-year-old body-builder. *Lancet* 742 (1986).

165. Rhoden, E. L. & Morgentaler, A. Risks of testosterone-replacement therapy and recommendations for monitoring. *N. Engl. J. Med.* **350,** 482–92 (2004).

166. Morgentaler, A. Testosterone and prostate cancer: An historical perspective on a modern myth. *Eur. Urol.* **50,** 935–939 (2006).

167. Morgentaler, A. & Traish, A. M. Shifting the paradigm of testosterone and prostate cancer: the saturation model and the limits of androgen-dependent growth. *Eur. Urol.* **55,** 310–20 (2009).

168. Ho, S. M., Damassa, D., Kwan, P. W., Seto, H. S. & Leav, I. Androgen receptor levels and androgen contents in the prostate lobes of intact and testosterone-treated Noble rats. *J. Androl.* **6,** 279–90 (1985).

169. Wright, A. S., Douglas, R. C., Thomas, L. N., Lazier, C. B. & Rittmaster, R. S. Androgen-induced regrowth in the castrated rat ventral prostate: Role of 5-alpha-reductase. *Endocrinology* **140,** 4509–4515 (1999).

170. Soos, G. *et al.* The prevalence of prostate carcinoma and its precursor in Hungary: An autopsy study. *Eur. Urol.* **48,** 739–44 (2005).

171. Sakr, D. J. *et al.* High grade prostatic intraepithelial neoplasia (HGPIN) and prostatic adenocarcinoma between the ages of 20-69: An autopsy study of 249 cases. *In Vivo.* **8,** 439–443 (1994).

172. Chan, J. M., Stampfer, M. J. & Giovannucci, E. L. What causes prostate cancer? A brief summary of the epidemiology. *Semin. Cancer Biol.* **8,** 263–73 (1998).

173. Giovannucci, E. L. *et al.* Intake of carotenoids and retinol in relation to risk of prostate cancer. *J. Natl. Cancer Inst.* **87,** 1767–76 (1995).

174. Clinton, S. K. & Giovannucci, E. L. Diet, nutrition, and prostate cancer. *Annu. Rev. Nutr.* **18,** 413–40 (1998).

175. Giovannucci, E. L., Liu, Y., Platz, E. A., Stampfer, M. J. & Willett, W. C. Risk factors for prostate cancer incidence and progression in the health professionals follow-up study. *Int. J. Cancer* **121,** 1571–8 (2007).

176. Setlur, S. R. *et al.* Genetic variation of genes involved in dihydrotestosterone metabolism and the risk of prostate cancer. *Cancer Epidemiol. Biomarkers Prev.* **19,** 229–39 (2010).

177. Park, J. *et al.* Deletion polymorphism of UDP-glucuronosyltransferase 2B17 and risk of prostate cancer in African American and Caucasian men. *Cancer Epidemiol. Biomarkers Prev.* **15,** 1473–8 (2006).

178. Park, J. Y. *et al.* Association between polymorphisms in HSD3B1 and UGT2B17 and prostate cancer risk. *Urology* **70,** 374–9 (2007).

179. Tang, L. *et al.* Repeat polymorphisms in estrogen metabolism genes and prostate cancer risk: results from the Prostate Cancer Prevention Trial. *Carcinogenesis* **32,** 1500–6 (2011).

180. Giovannucci, E. L. *et al.* The CAG repeat within the androgen receptor gene and its relationship to prostate cancer. *Proc. Natl. Acad. Sci.* **94,** 2106–2110 (1997).

181. Robins, D. M. Androgen receptor gene polymorphisms and alterations in prostate cancer: Of humanized mice and men. *Mol. Cell. Endocrinol.* **352,** 26–33 (2012).

182. Doll, R. & Peto, R. The quantitative of cancer causes of cancer: Estimates of avoidable risks in the United States today. *J. Natl. Cancer Inst.* **66,** 1192–1308 (1981).

183. Blot, W. J. & Tarone, R. E. Doll and Peto's quantitative estimates of cancer risks: Holding generally true for 35 years. *J. Natl. Cancer Inst.* **107,** djv044–djv044 (2015).

184. World Cancer Research Fund/American Institute for Cancer Research. *Full report - food, nutrition, physical activity, and the prevention of cancer: A global perspective*. (2007).

185. Wilson, K. M., Shui, I. M., Mucci, L. A. & Giovannucci, E. L. Calcium and phosphorus intake and prostate cancer risk: A 24-y follow-up study. *Am. J. Clin. Nutr.* **101,** 173–183 (2015).

186. Pettersson, A. *et al.* Milk and dairy consumption among men with prostate cancer and risk of metastases and prostate cancer death. *Cancer Epidemiol. Biomarkers Prev.* **21,** 428–36 (2012).

187. Sawada, N. *et al.* Fiber intake and risk of subsequent prostate cancer in Japanese men. *Am. J. Clin. Nutr.* **101,** 118–125 (2015).

188. Kolonel, L. N. *et al.* Vegetables, fruits, legumes and prostate cancer: A multiethnic case-control study. *Cancer Epidemiol. Biomarkers Prev.* **9,** 795–804 (2000).

189. Kirsh, V. A. *et al.* Prospective study of fruit and vegetable intake and risk of prostate cancer. *J. Natl. Cancer Inst.* **99,** 1200–9 (2007).

190. Hardin, J., Cheng, I. & Witte, J. S. Impact of consumption of vegetable, fruit, grain, and high glycemic index foods on aggressive prostate cancer risk. *Nutr. Cancer* **63,** 860–72 (2011).

191. Clinton, S. K. Lycopene: Chemistry, biology, and implications for human health and disease. *Nutr. Rev.* **56,** 35–51 (1998).

192. Giovannucci, E. L., Rimm, E. B., Liu, Y., Stampfer, M. J. & Willett, W. C. A prospective study of tomato products, lycopene, and prostate cancer risk. *J. Natl. Cancer Inst.* **94,** 391–8 (2002).

193. Zu, K. *et al.* Dietary lycopene, angiogenesis, and prostate cancer: A prospective study in the prostate-specific antigen era. *J. Natl. Cancer Inst.* **106,** djt430 (2014).

194. Vogt, T. M. *et al.* Serum lycopene, other serum carotenoids, and risk of prostate cancer in U.S. blacks and whites. *Am. J. Epidemiol.* **155,** 1023–1032 (2002).

195. Etminan, M., Takkouche, B. & Caamaño-Isorna, F. The role of tomato products and lycopene in the prevention of prostate cancer: A meta-analysis of observational studies. *Cancer Epidemiol. Biomarkers Prev.* **13,** 340–345 (2004).

196. Chan, J. M. *et al.* Diet after diagnosis and the risk of prostate cancer progression, recurrence, and death (United States). *Cancer Causes Control* **17,** 199–208 (2006).

197. Key, T. J. *et al.* Carotenoids, retinol, tocopherols, and prostate cancer risk: Pooled analysis of 15 studies. *Am. J. Clin. Nutr.* **102,** 1142-1157 (2015).

198. Dhurandhar, N. V. *et al.* Energy balance measurement: When something is not better than nothing. *Int. J. Obes.* **39,** 1109-1113 (2014).

199. Subar, A. F. *et al.* Addressing current criticism regarding the value of self-report dietary data. *J. Nutr.* **145,** 2639-2645 (2015).

200. George, S. M. *et al.* Strength of the relationships between three self-reported dietary intake instruments and serum carotenoids: The Observing Energy and Protein Nutrition (OPEN) Study. *Public Health Nutr.* **15,** 1000–1007 (2012).

201. Gann, P. H. *et al.* Lower prostate cancer risk in men with elevated plasma lycopene levels: Results of a prospective analysis. *Cancer Res.* **59,** 1225–1230 (1999).

202. Wu, K. *et al.* Plasma and dietary carotenoids, and the risk of prostate cancer: A nested case-control study. *Cancer Epidemiol. Biomarkers Prev.* **13,** 260–269 (2004).

203. Thompson, I. M. *et al.* The Influence of Finasteride on the Development of Prostate Cancer. *N. Engl. J. Med.* **349,** 215–224 (2003).

204. Kristal, A. R. *et al.* Diet, supplement use, and prostate cancer risk: Results from the prostate cancer prevention trial. *Am. J. Epidemiol.* **172,** 566–77 (2010).

205. Kristal, A. R. *et al.* Serum lycopene concentration and prostate cancer risk: Results from the prostate cancer prevention trial. *Cancer Epidemiol. Biomarkers Prev.* 638–646 (2011).

206. Sriprasad, S., Feneley, M. R. & Thompson, P. M. History of prostate cancer treatment. *Surg. Oncol.* **18,** 185–191 (2009).

207. Screening for Prostate Cancer: U.S. Preventative Task Force Recommendation Statement. *Ann. Intern. Med.* **149,** 185–192 (2008).

208. Moyer, V. A. Screening for Prostate Cancer: U.S. Preventative Task Force Recommendation Statement. *Ann. Intern. Med.* **157,** 120–134 (2012).

209. Miller, D. C. & Hollenbeck, B. K. Missing the mark on prostate-specific antigen screening. *J. Am. Med. Assoc.* **306,** 2719–20 (2011).

210. Kim, J. & Davis, J. W. Prostate cancer screening – time to abandon one-size-fits-all approach? *J. Am. Med. Assoc.* **306,** 2717–8 (2011).

211. Volk, R. J. & Wolf, A. M. D. Grading the new us preventive services task force prostate cancer screening recommendation. *J. Am. Med. Assoc.* **306,** 2715–2716 (2012).

212. Thompson, I. M. *et al.* Long-term survival of participants in the prostate cancer prevention trial. *N. Engl. J. Med.* **369,** 603–10 (2013).

213. Giovannucci, E. L. Commentary: Serum lycopene and prostate cancer progression: A re-consideration of findings from the prostate cancer prevention trial. *Cancer Causes Control* **22,** 1055–1059 (2011).

214. Kirsh, V. A. *et al.* A prospective study of lycopene and tomato product intake and risk of prostate cancer. *Cancer Epidemiol. Biomarkers Prev.* **15,** 92–8 (2006).

215. Peters, U. *et al.* Serum lycopene, other carotenoids, and prostate cancer risk: A nested case-control study in the prostate, lung, colorectal, and ovarian cancer screening trial. *Cancer Epidemiol. Biomarkers Prev.* **16,** 962–8 (2007).

216. Wei, M. Y. & Giovannucci, E. L. Lycopene, tomato products, and prostate cancer incidence: A review and reassessment in the psa screening era. *J. Oncol.* **2012,** 271063 (2012).

217. Greenberg, N. M. *et al.* Prostate cancer in a transgenic mouse. *Proc. Natl. Acad. Sci.* **92,** 3439–3443 (1995).

218. Gingrich, J. R. *et al.* Metastatic prostate cancer in a transgenic mouse. *Cancer Res.* **56,** 4096–4102 (1996).

219. Gingrich, J. R. *et al.* Androgen-independent prostate cancer progression in the TRAMP model. *Cancer Res.* **57,** 4687–4691 (1997).

220. Eng, M. H. *et al.* Early castration reduces prostatic carcinogenesis in transgenic mice. *Urology* **54,** 1112–1119 (1999).

221. Gingrich, J. R., Barrios, R. J., Foster, B. A. & Greenberg, N. M. Pathologic progression of autochthonous prostate cancer in the TRAMP model. *Prostate Cancer Prostatic Dis.* **2,** 70–75 (1999).

222. Berman-Booty, L. D. *et al.* A review of the existing grading schemes and a proposal for a modified grading scheme for prostatic lesions in TRAMP mice. *Toxicol. Pathol.* **40,** 5–17 (2012).

223. Han, G. *et al.* Hormone status selects for spontaneous somatic androgen receptor variants that demonstrate specific ligand and cofactor dependent activities in autochthonous prostate cancer. *J. Biol. Chem.* **276,** 11204–13 (2001).

224. Jeet, V., Russell, P. J. & Khatri, A. Modeling prostate cancer: A perspective on transgenic mouse models. *Cancer Metastasis Rev.* **29,** 123–42 (2010).

225. Abate-Shen, C. & Shen, M. M. Mouse models of prostate carcinogenesis. *Trends Genet.* **18,** S1–S5 (2002).

226. Chiaverotti, T. *et al.* Dissociation of epithelial and neuroendocrine carcinoma lineages in the transgenic adenocarcinoma of mouse prostate model of prostate cancer. *Am. J. Pathol.* **172,** 236–46 (2008).

227. Segawa, N. *et al.* Prognostic significance of neuroendocrine differentiation, proliferation activity and androgen receptor expression in prostate cancer. *Pathol. Int.* **51,** 452–459 (2001).

228. Bollito, E. *et al.* Relationship between neuroendocrine features and prognostic parameters in human prostate adenocarcinoma. *Ann. Oncol.* **12,** S159–S164 (2001).

229. Kaplan-Lefko, P. J. *et al.* Pathobiology of autochthonous prostate cancer in a pre-clinical transgenic mouse model. *Prostate* **55,** 219–37 (2003).

230. Navone, N. M., Logothetis, C. J., von Eschenbach, A. C. & Troncoso, P. Model systems of prostate cancer: Uses and limitations. *Cancer Metastasis Rev.* **17,** 361–71 (1999).

231. Shirai, T. *et al.* Experimental prostate carcinogenesis - rodent models. *Mutat. Res.* **462,** 219–26 (2000).

232. Valkenburg, K. C. & Williams, B. O. Mouse models of prostate cancer. *Prostate Cancer* **2011,** 1–22 (2011).

233. Holzapfel, N. P. *et al.* The potential role of lycopene for the prevention and therapy of prostate cancer: From molecular mechanisms to clinical evidence. *Int. J. Mol. Sci.* **14,** 14620–14646 (2013).

234. van Breemen, R. B. & Pajkovic, N. Multitargeted therapy of cancer by lycopene. *Cancer Lett.* **269,** 339–51 (2008).

235. Imaida, K. *et al.* Lack of chemopreventive effects of lycopene and curcumin on experimental rat prostate carcinogenesis. *Carcinogenesis* **22,** 467–472 (2001).

236. Boileau, T. W.-M. *et al.* Prostate carcinogenesis in N-methyl-N-nitrosourea (NMU)-testosterone-treated rats fed tomato powder, lycopene, or energy-restricted diets. *J. Natl. Cancer Inst.* **95,** 1578–1586 (2003).

237. Pannellini, T. *et al.* A dietary tomato supplement prevents prostate cancer in TRAMP mice. *Cancer Prev. Res.* **3,** 1284–91 (2010).

238. Konijeti, R. *et al.* Chemoprevention of prostate cancer with lycopene in the TRAMP model. *Prostate* **70,** 1547–54 (2010).

239. Venkateswaran, V., Fleshner, N. E., Sugar, L. M. & Klotz, L. H. Antioxidants block prostate cancer in Lady transgenic mice. *Cancer Res.* **64,** 5891–5896 (2004).

240. Venkateswaran, V. *et al.* A combination of micronutrients is beneficial in reducing the incidence of prostate cancer and increasing survival in the Lady transgenic model. *Cancer Prev. Res.* **2,** 473–83 (2009).

241. Zuniga, K. E., Clinton, S. K. & Erdman, J. W. The interactions of dietary tomato powder and soy germ on prostate carcinogenesis in the TRAMP model. *Cancer Prev. Res.* **6,** 548–57 (2013).

242. Conlon, L. E., Wallig, M. A. & Erdman, J. W. Low-lycopene containing tomato powder diet does not protect against prostate cancer in TRAMP mice. *Nutr. Res.* **35,** 882–890 (2015).

243. Wan, L. *et al.* Dietary tomato and lycopene impact androgen signaling- and carcinogenesis-related gene expression during early TRAMP prostate carcinogenesis. *Cancer Prev. Res.* **7,** 1228–1239 (2014).

244. Siler, U. *et al.* Lycopene and vitamin E interfere with autocrine/paracrine loops in the Dunning prostate cancer model. *FASEB J.* **18,** 1019–21 (2004).

245. Canene-Adams, K. *et al.* Combinations of tomato and broccoli enhance antitumor activity in Dunning R3327-H prostate adenocarcinomas. *Cancer Res.* **67,** 836–43 (2007).

246. Antonarakis, E. S. & Eisenberger, M. A. Expanding treatment options for metastatic prostate cancer. *N. Engl. J. Med.* **364,** 2055–8 (2011).

247. Fiñones, R. R. *et al.* Early human prostate adenocarcinomas harbor androgen-independent cancer cells. *PLoS One* **8,** e74438 (2013).

248. O'Mahony, O. A. *et al.* Profiling human androgen receptor mutations reveals treatment effects in a mouse model of prostate cancer. *Mol. Cancer Res.* **6,** 1691–701 (2008).

249. Wang, Q. *et al.* Androgen receptor regulates a distinct transcription program in androgen-independent prostate cancer. *Cell* **138,** 245–56 (2009).

250. Guo, Z. *et al.* A novel androgen receptor splice variant is up-regulated during prostate cancer progression and promotes androgen depletion-resistant growth. *Cancer Res.* **69,** 2305–13 (2009).

251. Cai, C. *et al.* Intratumoral de novo steroid synthesis activates androgen receptor in castration-resistant prostate cancer and is upregulated by treatment with CYP17A1 inhibitors. *Cancer Res.* **71,** 6503–13 (2011).

252. Locke, J. A. *et al.* Androgen levels increase by intratumoral de novo steroidogenesis during progression of castration-resistant prostate cancer. *Cancer Res.* **68,** 6407–15 (2008).

253. Chang, K.-H. *et al.* Dihydrotestosterone synthesis bypasses testosterone to drive castration-resistant prostate cancer. *Proc. Natl. Acad. Sci.* **108,** 13728-13733 (2011).

254. Montgomery, R. B. *et al.* Maintenance of intratumoral androgens in metastatic prostate cancer: A mechanism for castration-resistant tumor growth. *Cancer Res.* **68,** 4447–54 (2008).

255. Jain, H. V., Clinton, S. K., Bhinder, A. & Friedman, A. Mathematical modeling of prostate cancer progression in response to androgen ablation therapy. *Proc. Natl. Acad. Sci.* **108,** 19701–19706 (2011).

256. Abate-Shen, C. Molecular genetics of prostate cancer. *Genes Dev.* **14,** 2410–2434 (2000).

Figures

Figure 1.1.

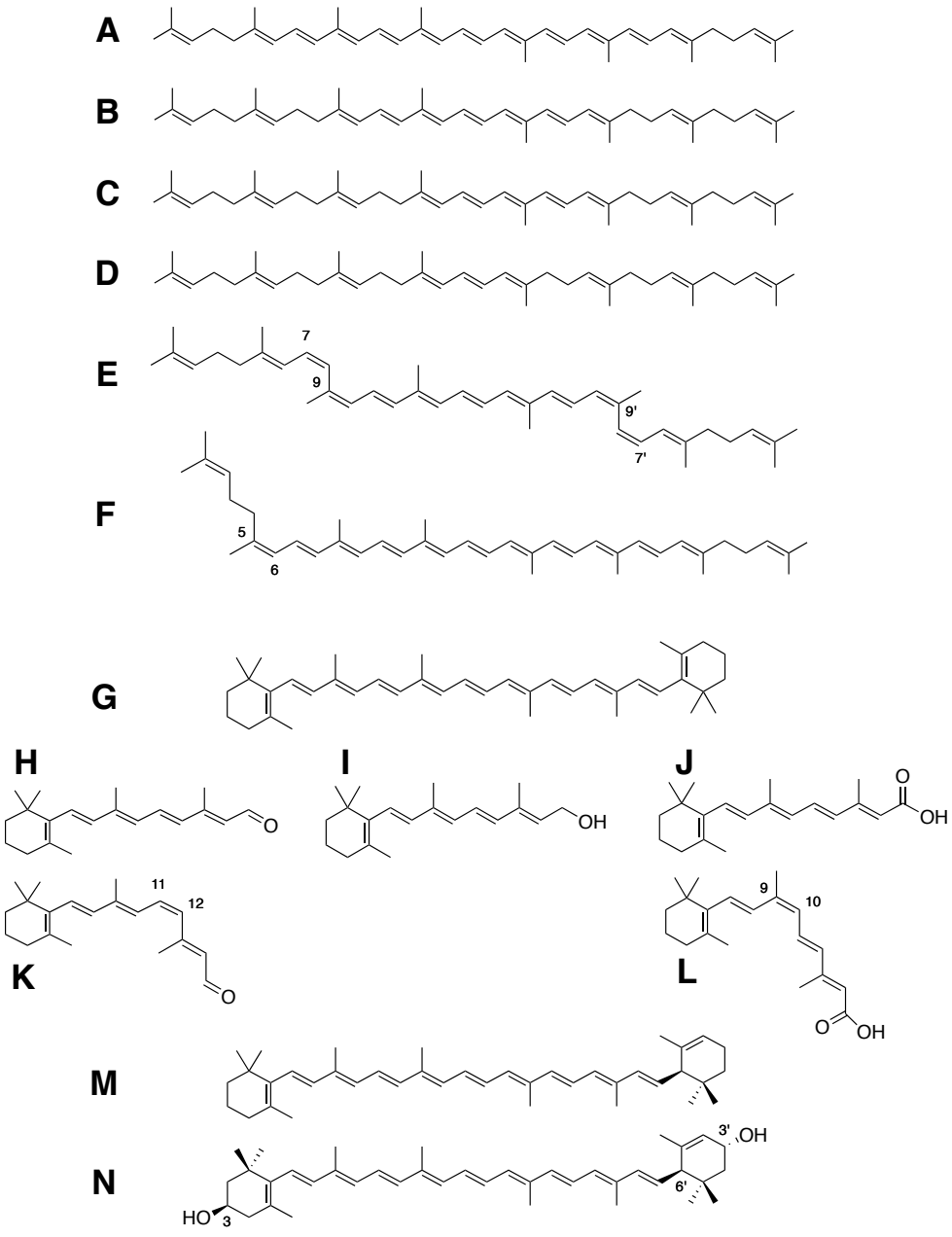

Figure 1.1. Structures of major dietary carotenoids and biologically active retinoids. **A** all-*trans* lycopene, **B** all-*trans* ζ-carotene, **C** all-*trans* phytofluene, **D** all-*trans* phytoene, **E** tetra-*cis* (7,9,7′,9′) lycopene, **F** 5-*cis* lycopene, **G** all-*trans* β-carotene, **H** all-*trans* retinal, **I** all-*trans* retinol, **J** all-*trans* retinoic acid, **K** 11-*cis* retinal, **L** 9-*cis* retinoic acid, **M** α-carotene, **N** lutein.

Figure 1.2.

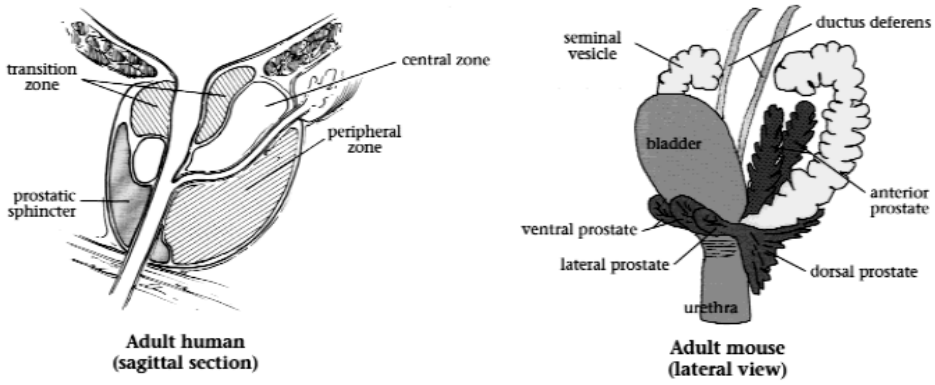

Figure 1.2. The anatomies of the adult human (left) and adult mouse (right) prostates. Reproduced from [256].

CHAPTER 2

Serum testosterone and prostatic androgen receptor signaling are reduced in mice lacking the carotenoid cleavage enzyme β-carotene-15,15'-dioxygenase

Abstract

β-carotene-15,15'-dioxygenase (BCO1) cleaves dietary carotenoids at the central 15,15' double bond, most notably acting on β-carotene to yield retinal. However, *Bco1* ablation also impacts diverse physiologic endpoints independent of dietary carotenoid feeding, including expression of genes controlling androgen metabolism. Using the *Bco1*$^{-/-}$ mouse model, we sought to probe the effects of *Bco1* ablation on testicular steroidogenesis, serum testosterone levels, and prostatic androgen signaling. Male wild-type (WT) and *Bco1*$^{-/-}$ mice were raised on carotenoid-free AIN-93G diets before sacrifice between 10-14 weeks of age. *Bco1* gene ablation significantly decreased serum testosterone concentrations and altered prostatic homeostasis. Organ weights of the prostate and seminal vesicles were significantly lower in *Bco1*$^{-/-}$ than in WT mice (-18% and -29%, respectively). Serum testosterone levels in *Bco1*$^{-/-}$ mice were significantly reduced by 73%. *Bco1* ablation reduced Leydig cell number and decreased testicular mRNA expression of *Hsd17b3* while increasing *Hsd17b2* expression, suggesting a possible inhibition of testicular testosterone synthesis. Immunofluorescent staining of the androgen receptor (AR) in the dorsolateral prostate lobes of *Bco1*$^{-/-}$ mice revealed a modest decrease in AR nuclear localization and analysis of prostatic H&E morphology suggested decreases in gland size. These findings were supported by a reduction in immunofluorescent labeling of the proliferation marker Ki67 in *Bco1*$^{-/-}$ prostates. Expression analysis of 200 prostate cancer- and androgen-related genes suggested that *Bco1* loss significantly disrupted prostatic androgen receptor signaling, cell cycle progression, and proliferation. This is the first demonstration that *Bco1*

ablation impacts murine prostatic cell proliferation and androgen receptor signaling, further supporting the role of this gene in processes more diverse than carotenoid cleavage.

Introduction

Experimental evidence demonstrating that β-carotene is a precursor to vitamin A, and therefore serves as a provitamin, dates to the late 1920s. However, elucidation of the mechanism of action of this conversion remained a mystery until 1965, when two independent reports demonstrated the enzymatic cleavage of β-carotene to retinal and retinol using extracts of rat liver and intestine [1,2]. Additional studies over the next several decades determined the characteristics and specificity of this new enzyme [3], identified iron as a required cofactor [4], and proposed central cleavage metabolites as the main reaction products [5]. Still, the molecular identity of this crucial enzyme remained unknown for 35 years, until the cloning of the *Drosophila* ortholog of human BCO1 in 2000 [6]. Biochemical characterization of recombinant mammalian enzymes [7,8], tissue-specific expression in humans [9], and description of mutational events [10] followed in short order. The mechanism of its enzymatic activity was debated for an additional 14 years, until careful double-labeling experiments confirmed that BCO1 is a dioxygenase [11]. Genomic research has now identified single nucleotide polymorphisms (SNPs) in the human *BCO1* gene, which result in altered accumulation of dietary carotenoids, including β-carotene [12–14].

Meanwhile, carefully controlled studies in mice lacking functional copies of this enzyme demonstrate the importance of BCO1 in carotenoid cleavage. These mice experience dramatic accumulation of β-carotene and are unable to generate vitamin A when fed a diet providing β-carotene as the predominant or only source of vitamin A [15,16]. However, these mice often present

additional phenotypes independent of their dietary vitamin A status, including altered lipid metabolism [15], impaired lipid, cholesterol, and retinol esterification [17], cardiac dysfunction [18], elevated insulin and leptin levels [19], and changes in expression of genes controlling steroid metabolism [20]. A preponderance of evidence now suggests that whereas central cleavage of provitamin A carotenoids to yield retinal represents the main evolutionary function of BCO1, this enzyme likely plays a broader role in an array of physiological processes. Given the demonstrated effect of *Bco1* ablation on the expression of genes responsible for steroid metabolism [20] and our group's longstanding interest in the role of dietary carotenoids in prostate carcinogenesis [21,22] – which is driven by androgens – we questioned the extent to which *Bco1* ablation and dietary tomato carotenoids may alter androgen biology in male mice. Therefore, in this report, we have assessed the impact of homozygous genomic *Bco1* deletion and short-term dietary lycopene or tomato feeding on serum concentrations of sex steroids (testosterone and estradiol), testicular morphology, genes controlling testicular steroid and cholesterol metabolism, prostatic morphology, prostatic androgen receptor signaling, and prostatic cell proliferation.

Materials and Methods

Animals and study designs

All animal procedures were approved by the University of Illinois Institutional Animal Care and Use Committee.

Generation of *Bco1*$^{-/-}$ animals has been described previously [15]. C57BL/6J x 129/SvJ F1 cross and C57BL/6J mice were purchased from The Jackson Laboratory (Bar Harbor, ME). Mice were housed in shoebox cages in a temperature- and humidity-controlled facility with *ad libitum*

access to water. Mice were acclimated to powdered AIN-93G diet for two to three weeks before exposure to experimental diets.

Three studies were completed to investigate the effects of tomato carotenoid feeding and *Bco1* loss on prostatic and androgen biology. Study 1 and Study 2 examined interactions between *Bco1* status and short-term tomato carotenoid feeding, whereas Study 3 was designed to investigate only *Bco1* genotype effects.

The experimental design for Study 1 has been described previously [23]. Nine- to twelve-week-old male wild-type (WT; C57BL/6J x 129/SvJ F1) or *Bco1*$^{-/-}$ mice were randomly assigned to one of two study arms, consisting of a tomato powder (TP) or lycopene (LYC) diet group and their respective control diet group (**Appendix Fig. A.1**). TP diet consisted of powdered, modified AIN-93G diet with 10% w/w tomato powder (Futureceuticals, Momence, IL). LYC diet consisted of powdered, modified AIN-93G diet with the addition of 0.1% w/w water-soluble beadlets containing purified lycopene (10% w/w, DSM, Basel, Switzerland). Control diets for the TP and LYC diets consisted of powdered, modified AIN-93G (CON) and powdered, modified AIN-93G + 0.1% w/w placebo beadlets (CON+P), respectively. Diets were formulated to be isocaloric and balanced for levels of protein, fat, carbohydrates, and fiber (**Appendix Table A.1**). Mice (n = 25 per genotype/diet) consumed the experimental diets *ad libitum* for four days, after which they were fasted for three hours, asphyxiated with CO_2, and blood collected via cardiac puncture. Tissues were collected, frozen in liquid nitrogen, and stored at -80 ˚C until analysis.

Study 2 was designed to replicate Study 1, with slight modifications. Ten- to thirteen-week-old male WT (C57BL/6J) and *Bco1*$^{-/-}$ mice were randomized onto one of three powdered AIN-93G-based diets: 10% w/w tomato powder + 0.1% w/w placebo beadlets (TP+P), 0.1% w/w

lycopene beadlet (LYC), or control diet + 0.1% w/w placebo beadlets (CON+P) (**Appendix Fig. A.1**). Inclusion of placebo beadlets in the control and tomato diets allowed statistical comparison across all three diet groups. Tomato powder and beadlet sources were the same as in Study 1. Mice (n = 15 per genotype/diet) consumed the experimental diets for four days *ad libitum* and were euthanized in the same manner as in Study 1. One testicle per mouse was fixed in 10% neutral-buffered formalin for 24 h, whereas all other tissues were frozen in liquid nitrogen and stored at -80 ˚C until analysis.

In Study 3, Ten-week-old WT (C57BL/6J) and *Bco1*$^{-/-}$ mice (n = 10 - 11/genotype) consumed CON+P diet for four days *ad libitum* and were euthanized in the same manner as in Study 1. Only the CON+P diet was fed in Study 3 (**Appendix Fig. A.1**), as this study was designed to examine only the effects of *Bco1* ablation. One lobe of the anterior, dorsolateral, and ventral prostate per mouse was fixed in 10% neutral-buffered formalin for 24, whereas all other tissues were frozen in liquid nitrogen and stored at -80 ˚C until analysis.

In all three studies, mice were euthanized between 13:00 and 16:00 U.S. Central Time to control for diurnal variation in hormone levels. Designs of all three studies are shown in **Appendix Fig. A.1**.

In Study 1, the LYC diet provided 248 nmol lycopene/g diet, whereas TP diet provided 204 nmol lycopene/g diet, 10.1 nmol phytoene/g diet, 2.6 nmol phytofluene/g diet, and 0.8 nmol beta-carotene/g diet. In Study 2, LYC diet contained 185 nmol lycopene/g diet whereas TP+P provided 214 nmol lycopene/g diet, 24.6 nmol phytoene/g diet, 14.6 nmol phytofluene/g diet, and 1.9 nmol beta-carotene/g diet **Appendix Table A.1**. All diets were reduced in vitamin A content to 1500 IU retinyl palmitate/kg in order to ensure intestinal carotenoid absorption while

not resulting in vitamin A deficiency [15,16]. Diets were formulated every one to two months and stored in the dark at 4 ˚C. Fresh diet was provided to animals each study day.

Serum testosterone and estradiol analysis

Serum steroids were extracted with diethyl ether and lipids were removed with a biphasic hexane-methanol extraction. Briefly, 150 μL of serum was spiked with approximately 1000 cpm of tritiated testosterone (Perkin-Elmer, Waltham, MA) and vortexed for 3 minutes with 6 mL diethyl ether (Sigma, St. Louis, MO). The aqueous phase was frozen in dry ice-cooled methanol and the ether extract was removed and evaporated. Hexane and methanol (1.5 mL each; Sigma) were added to each tube and vortexed for 3 minutes. The hexane and methanol layers were allowed to separate for 30 minutes and the bottom methanol layer was removed and dried. Samples were reconstituted in phosphate-buffered saline + 1% w/v gelatin. 15 μL was removed for scintillation counting and calculation of extraction efficiency, which averaged 75% for both the testosterone and estradiol assays. In Study 2, serum testosterone was quantified with a radioimmunoassay (RIA) kit (TKTT1 Coat-A-Count Total Testosterone, Siemens, Malvern, PA) per manufacturer's instructions, but with a customized standard curve. In Study 3, due to manufacturer's discontinuation of the RIA, serum testosterone was measured using a coated-plate ELISA, per manufacturer's instructions (Arbor Assays, Ann Arbor MI). Inter-assay %CV was 14% for the RIA; intra-assay %CV was 5% for the RIA and 17% for the ELISA. Serum estradiol was quantified with an RIA (KE2D1 Double Antibody Estradiol, Siemens) per manufacturer's instructions, but with a customized standard curve.

Gene expression

Total RNA was extracted from pooled prostate (Study 1) and dorsolateral prostate (Study 2) using RNEasy Mini spin columns (Qiagen, Valencia, CA) according to manufacturer's

instructions. cDNA was synthesized using the High-Capacity Reverse Transcription Kit (Life Technologies, Grand Island, NY). qPCR was carried out with SYBR Green chemistry (Life Technologies) on an ABI 7900 HT qPCR platform (Life Technologies), using pre-designed primer assays (*Cyp17a1*, *Hsd17b2*, *Hsd17b3*, *Scarb1, Hmgcr, Vim,* and *Actb*; SA Biosciences, Valencia, CA) or custom-designed oligonucleotide primers (Integrated DNA Technologies (IDT), Coralville, IA) (**Appendix Table A.2**). Oligonucleotide primers were validated for specificity and amplification efficiency.

NanoString nCounter technology was used for prostatic gene expression analysis on a custom-designed 200-gene codeset (**Appendix Table A.3**), which has been described previously [24]. RNA was extracted from the dorsolateral prostates of mice from Study 3 as described above and 100 ng total RNA was used directly for gene expression analysis [25]. Data were subjected to global normalization (global mean fold-change = 1.06; 95% confidence interval: 0.97, 1.14). Transcripts with expression below negative control group means were excluded from further analysis. A heat map was constructed in the nSolver Analysis Software by subjecting Z-scored samples (columns) and genes (rows; labels not shown) to Ward's minimum distance linkage within Pearson's correlation hierarchical clustering.

Protein expression

Tissues were lysed in RIPA buffer with the addition of Halt Protease Inhibitor Cocktail, EDTA-Free (Pierce Thermo Scientific, Rockford, IL), and protein quantified using the BCA assay (Pierce Thermo Scientific). After SDS-PAGE and transfer onto PVDF membranes (0.45 μm Immobilon-P, Millipore), blots were blocked with 5% nonfat dry milk and probed for Cyp11a1 (sc-18043, Santa Cruz Biotechnology, Dallas, TX; 1:200 dilution) with GAPDH (#5174, Cell Signaling Technology, Danvers, MA; 1:4000 dilution) as the loading control.

Androgen receptor (#06-680, Millipore; 1:500) was measured relative to histone H3 (#4499, Cell Signaling; 1:2000) as the loading control. HMG-CoA reductase expression was probed (sc-33827, Santa Cruz; 1:1000) with GAPDH as the loading control. Detection was with donkey anti-goat (sc-2020, Santa Cruz; 1:5000) and goat anti-rabbit (#7074, Cell Signaling; 1:2000) HRP-linked secondary antibodies, SuperSignal Molecular Weight Protein Ladder (Pierce Thermo Scientific), and Amersham ECL Prime Western Blotting Reagent (GE Life Sciences, Pittsburgh, PA) on an ImageQuant LAS 4000 imaging station (GE Life Sciences). Relative band densitometry was performed in ImageJ software (Rasband, W.S., ImageJ, U. S. National Institutes of Health, Bethesda, Maryland, USA, http://imagej.nih.gov/ij/) by integration of intensity profile area-under-the-curve.

Histology

Testes from Study 2 and prostate from Study 3 were fixed in 10% neutral-buffered formalin for 24 hours, transferred to 70% ethanol until embedding in paraffin blocks, and cut into five-micron sections. Cross-sectional testicular sections were stained with periodic acid-Schiff-hematoxylin (PAS-H) and prostatic sections were stained with hematoxylin and eosin (H&E). Staining was done in the Comparative Biosciences Histology Laboratory at the College of Veterinary Medicine, University of Illinois at Urbana-Champaign. Slides were digitized with a NanoZoomer 2.0-HT slide scanner (Hamamatsu, Bridgewater, NJ) equipped with an Olympus Uplansapo 10X objective (Tokyo, Japan). Images were captured with NDP View software (Hamamatsu).

A blinded evaluator with expertise in comparative pathology (Matthew A. Wallig, Ph.D., D.V.M.) assessed testicular and prostatic pathology. Testes were graded on the basis of seminiferous tubule contraction/dilation and the vacuolation, apoptosis, necrosis, and size of

Sertoli and Leydig cells (score 1 = <5% affected, 2 = 5-25% affected, 3 = 26-50% affected, 4 = 51-75% affected, 5 = >75% affected). Prostates were graded on the basis of gland size (score 0 = normal, 1 = slight decrease, 2 = decrease, 3 = marked decrease) and abundance of glandular secretion (score 0 = 0% decrease, 1 = <20% decrease, 2 = 20-40% decrease, 3 = >40% decrease).

Testicular morphology (seminiferous tubule number, total tubule size, tubule lumen area, and tubule epithelial area) was measured in Fiji using the following method: 1) representative frames of H&E-stained testicular sections were captured at 10x optical magnification; 2) circumference of individual seminiferous tubules which were no less than 80% within frame was manually traced and total tubule area [lumen + epithelium; *ta*] calculated in μm^2; 3) lumen circumference of individual seminiferous tubules was manually traced and lumen area [*la*] calculated in μm^2; 5) epithelial cell layer area [*ea*] of individual seminiferous tubules was calculated as $ea = ta - la$; 6) seminiferous tubules measured in this fashion were counted; 7) *TA*, *LA*, and *EA* were calculated as the averages of *ta*, *la*, and *ea,* respectively, across all counted seminiferous tubules; 8) Leydig cells were counted and expressed as cell count/1000 μm^2 *TA*. All calculations were subsampled across 6 - 7 seminiferous tubules/frame and 2 - 3 frames/slide. Averages for an entire slide (i.e., animal/experimental unit) were used for statistical analysis.

Immunofluorescence imaging

Formalin-fixed, paraffin-embedded prostatic sections from Study 3 used for immunofluorescence imaging. Background Punisher blocking agent (Biocare Medical, Concord, CA) was used to reduce non-specific binding. Sections were probed for AR or Ki67 with primary (AR: 1:100, Millipore; Ki67: 1:600, #9129, Cell Signaling) and secondary antibodies (DyLight 488, 1:200, #111-487-03-03, Jackson ImmunoResearch Laboratories, West Grove, PA). Nuclei were stained with 4',6-diamidino-2-phenylindole (DAPI, 1:1000, #32670, Sigma-Aldrich).

Negative controls were created for each sample by omission of the primary antibody; non-specific staining was revealed to be minimal (data not shown). Slides were imaged on a Zeiss LSM 700 confocal microscope at the Core Facilities of the University of Illinois Carl R. Woese Institute for Genomic Biology.

Nuclear AR staining was scored on a qualitative three-point scale; a score of 1 indicating predominantly diffuse cellular AR localization with the absence of punctate nuclear staining, and a score of 3 corresponding to predominantly nuclear staining, at times with cytoplasmic exclusion. Scores from subsample images (2 - 4/prostate lobe/mouse) were averaged and rounded to the nearest integer. A similar approach has been demonstrated previously [26].

Ki67 quantitation was performed on 20x confocal images in Fiji using a thresholding-watershed cell counting method (Fiji. Nuclei Watershed Separation. Available from http://fiji.sc/Nuclei_Watershed_Separation. Accessed Nov 2, 2015).

Statistical analysis

Data are presented as mean ± SEM. With the exception of the NanoString gene expression analysis, all data were analyzed with two-way ANOVA and results were considered statistically significant at $p \leq 0.05$. Data were transformed logarithmically when normality assumptions were violated. Individual group variances were used in place of the pooled variance when homogeneity of variance assumptions were violated. In Study 1, the CON/TP and CON+P/LYC study arms were analyzed as separate 2x2 factorial designs. Where appropriate, data were blocked by study cohort, assay batch, or sacrifice order. ANOVA analysis was done in SAS v9.3 (SAS Institute, Cary, NC). For NanoString expression analysis, calculations of fold regulation by *Bco1*$^{-/-}$ genotype (relative to WT) were done within the NanoString nSolver Analysis Software (NanoString Technologies, Seattle, WA). Pairwise T-tests were considered

significant at α = 0.005. False discovery rate (FDR) at α = 0.005 was estimated to be FDRhat = 0.060 (95% confidence interval: 0.053, 0.068) using the method of Storey [27,28].

Results

Effects of dietary tomato or lycopene

Short-term tomato or lycopene feeding had no effect on most of the endpoints measured. As a result, only main effects of *Bco1* genotype in animals fed the CON+P diet will be addressed in this chapter, with two exceptions. Testicular expression of 3-hydroxy-methylglutaryl-coenzyme A reductase (HMG-CoA reductase) protein and testicular mRNA expression of steroidogenic acute regulatory protein (*Star*), were impacted by tomato or lycopene feeding, effects which were modulated by *Bco1* genotype. Those results are displayed in **Appendix A** (**Appendix Fig. A.4A-D**) and interpreted in the discussion. Data of outcomes with dietary treatments, rather than the genotype-only data presented in this section, are displayed in **Appendix A** and referenced throughout.

Prostate and seminal vesicle weights are decreased in *Bco1*$^{-/-}$ *mice*

We observed no effect of *Bco1* ablation on body weight or testicular weight (**Fig 2.1C, D; Appendix Fig. A.2C, D**). *Bco1* ablation reduced prostate weight as a percentage of total body weight (%BW). Total prostate %BW was significantly decreased by 18% in *Bco1*$^{-/-}$ mice compared to WT ($p < 0.001$, **Fig. 2.1A**), an effect replicated in a second independent trial (-14%, $p < 0.001$, **Appendix Fig. A.2E**).

The seminal vesicles, like the prostate, are dependent upon androgens for growth; similarly, *Bco1*$^{-/-}$ mice were found to have statistically significant decreases in seminal vesicle

%BW, compared to WT (-29%, $p < 0.001$, **Fig. 2.1B).** A second study confirmed these observations (-18%, $p < 0.001$, **Appendix Fig. A.2F**).

Serum testosterone is decreased in *Bco1*$^{-/-}$ mice

Given the significant reductions in the weights of the prostate and seminal vesicles, we measured circulating concentrations of the sex steroids testosterone and estradiol. Serum testosterone levels were significantly lower in *Bco1*$^{-/-}$ mice than in WT mice, as measured by RIA (3.9 ± 0.3 nM vs. 14.6 ± 5.4 nM, respectively, $p < 0.05$; **Fig 2.2**). This observation was replicated in a second independent trial, as measured by ELISA (4.1 ± 0.9 nM in WT vs. 2.5 ± 0.5 nM in *Bco1*$^{-/-}$, $p < 0.001$; **Appendix Fig. A.3B**). Serum concentrations of estradiol, as measured by RIA, were unchanged by genotype (99.3 ± 5.0 pM in WT vs. 100.7 ± 4.8 pM in *Bco1*$^{-/-}$, **Appendix Fig. A.3C, D**).

Bco1 ablation alters testicular morphology and reduces Leydig cell number

Morphological assessment of testicular sections from WT and *Bco1*$^{-/-}$ mice (**Fig. 2.3C**) revealed an increase in total seminiferous tubule area as a result of *Bco1* ablation (**Fig. 2.3A**). Pathological grading corroborated this finding, suggesting a modest increase in tubule dilation in *Bco1*$^{-/-}$ mice compared to WT mice (data not shown). Necrosis, apoptosis, vacuolation of Sertoli or Leydig cells, and alterations in Leydig cell size were all determined to be minimal/normal (data not shown). The increase in seminiferous tubule area was driven by expansion of the epithelial compartment, rather than an increase in tubule lumen area (**Fig. 2.3A**). Counting of Leydig cells (normalized to tubule area) revealed a 44% decrease in Leydig cell number in *Bco1*$^{-/-}$ mice, compared to WT (**Fig. 2.3B**).

Testicular androgen biosynthetic capacity at the mRNA level is reduced in *Bco1*$^{-/-}$ mice

Testicular Leydig cells obtain cholesterol substrate for testosterone synthesis via lipoprotein import or through *de novo* synthesis. Seven key mediators of testicular cholesterol acquisition (*de novo* and selective uptake), steroidogenesis, and androgen metabolism were assayed to determine the effects of *Bco1* ablation on testicular steroidogenic potential (**Fig. 2.4**). No differences in expression of genes or proteins controlling testicular *de novo* cholesterol synthesis (*Hmgcr* transcript, HMG-CoA reductase protein), cholesterol uptake (*Scarb1*), cholesterol transport (*Star*), or general steroidogenesis (CYP11A1 protein, *Cyp17a1* transcript) were observed. However, transcript levels of *Hsd17b3*, which encodes an enzyme responsible for the final reduction of androstenedione to testosterone [29], were significantly decreased by *Bco1* ablation (69% of WT, $p < 0.01$). Conversely, the enzyme produced by the *Hsd17b2* gene catalyzes the reverse reaction, converting testosterone back to its less active precursor [30]; testicular *Hsd17b2* mRNA expression was significantly upregulated 34% ($p < 0.05$) in *Bco1*$^{-/-}$ mice (**Fig. 2.4**).

Prostatic androgen receptor signaling and markers of cellular proliferation are reduced in *Bco1*$^{-/-}$ mice

Concurrent observations of decreased prostatic weight and reduced serum testosterone concentrations suggest that *Bco1* ablation may alter prostatic biology through androgen-dependent pathways. We explored this hypothesis by examining prostatic androgen receptor (AR) expression and subcellular localization, the expression of AR-target genes, and the expression of genes controlling apoptosis, cell cycle progression, and cellular proliferation.

We performed confocal fluorescence microscopy to evaluate the effect of *Bco1* ablation on prostatic AR nuclear localization. Representative confocal microscopy images are shown in

Fig. 2.5Ai, ii, vi, and viii, demonstrating a modest reduction in nuclear AR staining in dorsolateral prostate sections from *Bco1*$^{-/-}$ mice, compared to WT. As seen in **Fig. 2.5Aiii** and **2.5Aviii**, *Bco1* ablation reduced qualitative scores of nuclear localization. Moreover, morphological assessment of H&E-stained dorsolateral prostate sections (**Fig. 2.5Aiv, ix**) revealed a similar shift, resulting in smaller gland structures in *Bco1*$^{-/-}$ mice, compared to WT (**Fig. 2.5Av, x**). These effects were limited to the dorsolateral prostate, and were not observed in the ventral or anterior prostate lobes (data not shown).

Although *Bco1* loss appeared to decrease nuclear localization of the AR, total levels of AR mRNA or protein were unchanged (**Fig. 2.5B, Appendix Fig. A.7**).

Due to the morphological changes we observed in the prostates of *Bco1*$^{-/-}$ mice, we assessed proliferation through immunofluorescent labeling of Ki67 protein. Ki67 labeling (as a percentage of total nuclei) was reduced by nearly half in the dorsolateral prostate of *Bco1*$^{-/-}$ mice (1.85% ± 0.19% in WT vs. 0.98% ± 0.11% in *Bco1*$^{-/-}$, $p < 0.001$) and trended lower in the anterior prostate (2.56% ± 0.78% in WT vs. 1.01% ± 0.17% in *Bco1*$^{-/-}$, $p = 0.09$) (**Fig. 2.5C**).

We hypothesized that the reduced prostatic weight and proliferation in *Bco1*$^{-/-}$ mice resulted from decreased prostatic AR signaling, potentially impacting the expression of genes involved in growth and proliferation. Therefore, using a previously described custom NanoString gene expression array [24], we measured the dorsolateral prostate expression of 200 genes involved in androgen synthesis, AR signaling, apoptosis, cell cycle progression, proliferation, and prostate carcinogenesis. *Bco1* ablation significantly ($p < 0.005$) modulated 13 genes of the 200-gene codeset (**Fig. 2.6B and Table 2.1**). The entire dataset is presented in **Appendix Table A.3**. Among the 13 genes significantly altered were genes involved in proliferation (*Ki67*, -44%; *Pcna*, -12%), G2 to M cell cycle progression (*Aurkb*, -54%; *Ccnb2*, -51%), apoptosis (*Bax*, -

18%), and cell-cell communication, intracellular signaling, or gene transcription (*Kras*, -89%; *Tgfb2*, -59%; *Met*, +66%; *Esr2*, +60%; *Vegfa*, +51%). To further elucidate prostatic pathways and biological processes potentially regulated by *Bco1*$^{-/-}$ genotype, the heat map of the entire 200-gene code set (**Fig. 2.6A**) was visually inspected to identify signatures of differential regulation. Three gene clusters, assembled during heat map creation through minimum-distance clustering based on gene expression correlation, were identified as displaying potentially differential regulation due to *Bco1* status. The 36 genes contained within these three clusters, along with their fold change, raw p-values, and gene ontology functional classifications [31,32], are presented in **Table 2.1**.

To support our NanoString gene expression data, we used qPCR to measure the mRNA expression of an androgen-induced gene, *Msmb*, and a stromal marker not responsive to androgen, *Vim*. As expected, *Msmb* expression was significantly decreased (66% ± 10% of WT), whereas *Vim* expression remained unchanged by *Bco1* knockout (**Fig. 2.6C, Appendix Fig. A.8)**.

Discussion

This work sought to investigate the effects of disrupted *Bco1* function on androgen status and prostatic androgen receptor signaling in mice. We observed a reduction in serum testosterone levels due to *Bco1*$^{-/-}$ genotype, accompanied by reduced weights of the prostate and seminal vesicles. This reduction in serum testosterone may be driven by a reduction in testicular steroidogenic genes and/or reduced Leydig cell populations. Concomitantly, we observed reductions in markers of androgen signaling, proliferation, and cell cycle progression in the prostate. Together, these data support a hypothesis that *Bco1*$^{-/-}$ mice exhibit reduced testicular

testosterone synthesis, thereby lowering circulating testosterone, resulting in depressed prostatic androgen signaling, proliferation, and organ weight.

Both the prostate and seminal vesicles, as male sex accessory glands, are dependent upon androgens for growth and homeostasis. As clearly demonstrated by rodent castration studies, removal of circulating testosterone induces involution of the organ [33]. In fact, prostatic regression after androgen deprivation is such a well-characterized response that it has been directly implemented as an assay to investigate the activity of putative AR agonists [34]. Seminal vesicular response to androgen is very similar to that of the prostate [35]. Rodent castration studies report reductions in prostate weight between 40% and 80% [36–38], and reductions in seminal vesicle weight of approximately 70% [36]. Our results (-14% to -18% in total prostate weight, -18% to -29% in seminal vesicle weight) are more modest than found in castration studies, but this is expected, as the reductions in serum testosterone observed in our mice (-39% to -73%) are not as severe as reductions achieved by castration (-90% to undetectable levels; [39–41]). However, since testosterone serves as a substrate for local prostatic synthesis of the most active androgen, dihydrotestosterone (DHT) [30], and prostatic DHT levels in mice correlate significantly with serum testosterone across a >100-fold range of concentrations [41], it is likely that both castration and *Bco1* ablation serve to reduce the amount of testosterone available for local DHT synthesis in the prostate.

In men, it is estimated that up to half of the androgen in the prostate is derived from local conversion of adrenal steroid precursors, whereas the remainder is supplied directly as testicular-derived testosterone [42]. Rodents, however, secrete very little adrenal androgen precursors and the prostate in these species relies on testicular testosterone for virtually all androgenic activity [43,44]. Testicular steroidogenesis is a multistep process that is dependent upon several key enzymes for

acquisition of cholesterol substrate. Whether cholesterol is synthesized *de novo* through the rate-limiting step of HMG-CoA reductase (gene name *Hmgcr*), or is imported from circulating HDL via scavenger receptor class B, type 1 (SR-B1, gene name *Scarb1*), steroidogenic acute regulatory protein D1 (StAR) transports cholesterol across the outer mitochondrial membrane to the inter-membrane space for side-chain cleavage by the rate limiting enzyme for all steroid synthesis, CYP11A1 [29]. HMG-CoA reductase is well-known to be regulated both transcriptionally and translationally [45,46], whereas testicular levels of *Scarb1 and Star* are primarily under transcriptional control by cAMP-mediated, hormone-stimulated signaling [47,48]. Expression of *Scarb1* and *Hmgcr* mRNA, and HMG-CoA reductase protein, were not altered by the main effect of genotype (**Fig. 2.4**). However, we did observe a significant interaction in testicular HMG-CoA reductase protein expression between diet and genotype, such that dietary lycopene depressed expression in WT mice, but elevated expression in *Bco1*$^{-/-}$ mice (**Appendix Fig. A.4B**). A similar, but non-significant, trend was observed when mice were fed tomato powder (**Appendix Fig. A.4A**). This was an intriguing result, as other groups have found lycopene to reduce HMG-CoA reductase activity in cultured macrophages [49] and that several plant-derived terpenes (the chemical family to which lycopene and all carotenoids belong) reduced translation of *Hmgcr* transcript [50]. Additionally, testicular *Star* mRNA expression was significantly reduced by a main effect of tomato feeding and a main effect of *Bco1* ablation significantly increased expression across both the CON and TP diets (**Appendix Fig. A.4C**). However, this genotype effect did not reach significance in the CON+P-fed (**Fig. 2.4**) and LYC-fed groups (**Appendix Fig. A.4D**).

On one hand, these results suggest that 1) short-term tomato carotenoid feeding may alter expression of enzymes controlling cholesterol substrate acquisition for testicular steroidogenesis,

2) these may represent primary targets of lycopene action, and 3) *Bco1* status may modify the effects of tomato carotenoid feeding. In opposition to such a hypothesis, however, is the observation that the effects seen are small and very likely not physiologically relevant. Indeed, when levels of testicular cholesterol were measured, levels of total (**Appendix Fig. A.5A-B**) and free (**Appendix Fig. A.5C-D**) cholesterol were unaltered by either *Bco1* genotype or dietary treatment. Paradoxically, levels of esterified cholesterol were lower in *Bco1*$^{-/-}$ mice than in WT mice (**Appendix Fig. A.5E-F**), despite a lack of effect on the mRNA expression of two enzymes controlling cholesterol esterification, *Soat1* and *Soat2* (**Appendix Fig. A.6A-D**), and the increased expression of a third, *Lcat* (**Appendix Fig. A.6E**). Perhaps a longer period of dietary exposure to tomato carotenoids would induce greater and more consistent differences across the endpoints in testicular cholesterol metabolism that we measured here. Alternatively, the minor alterations in testicular cholesterol metabolism observed in this study may be secondary to perturbations in other organs, such as the liver. Regardless, the present data clearly do not support the hypothesis that *Bco1* ablation or short-term tomato carotenoid feeding reduce serum testosterone through direct modulation of testicular cholesterol uptake, esterification, or *de novo* synthesis.

In mice and humans, subsequent to cholesterol side-chain cleavage by CYP11A1, the cholesterol-derived sterol backbone is transported to the ER, where CYP17A1 catalyzes the production of several possible intermediate steroids, which are dedicated to sex steroid synthesis [29]. No differences in expression (Cyp11a1 protein, *Cyp17a1* transcript) were detected for either of these enzymes, suggesting that decreases in serum testosterone in *Bco1*$^{-/-}$ mice are likely due to alterations specifically in androgen biosynthesis, rather than impacts at earlier stages of testicular steroidogenesis.

The final step of testosterone synthesis involves the reduction of the inactive androgen, androstenedione, to testosterone via 17β-hydroxysteroid dehydrogenase, isoform 3 (gene name *Hsd17b3*) [29,51]. The importance of this enzyme in testosterone synthesis is made clear by observations that mutations in the human *HSD17B3* gene result in male pseudohermaphroditism and an inability to produce testosterone [52]. Conversely, Hsd17b2 catalyzes the reverse, oxidative reaction, converting testosterone back to inactive androstenedione [53]. Relative to WT, transcript levels of *Hsd17b3* were decreased 32% by *Bco1*$^{-/-}$ genotype, whereas *Hsd17b2* was induced by 34%. Using a basic ratio operation, we can calculate an *Hsd17b3* / *Hsd17b2* value of 0.51 (0.68/1.34), suggesting that, at the transcript level, capacity for inactivation of testosterone to androstenedione is roughly double the biosynthetic capacity. However, this is a simplistic model, not accounting for the absolute level of expression for each gene: although *Hsd17b3* is highly expressed in the testes, *Hsd17b2* is not. In our data, average *Hsd17b3* Ct was 22.6 and average *Hsd17b2* Ct equaled 29.0; the absolute difference between these two values, and thus the exponential difference in transcript abundance of the two genes, is 6.4 Ct units. Computed, this corresponds to >84-fold difference in transcript abundance ($2^{6.4}$ = 84.4). Threshold values and cycling parameters were set equal for the two genes, and the difference in expression of the housekeeping gene, *Actb,* was <1-fold. Both primers were validated for amplication efficiency (data not shown). Therefore, we propose that although both *Hsd17b3* and *Hsd17b2* were significantly modulated by *Bco1* ablation to putatively alter testosterone biosynthetic capacity, due to absolute transcript abundance, the observed decrease in serum testosterone was likely due to inhibition of *Hsd17b3*, whereas catabolic *Hsd17b2* contribution was likely negligible. However, the mechanism by which *Bco1* ablation impacts expression of *Hsd17b3* and *Hsd17b2* in the testes remains to be determined.

In the testes, testosterone is produced by Leydig cells [54], as they express all of the necessary enzymes required for androgen synthesis [29,55]. Experimental evidence demonstrates that reductions in Leydig cell number, through either apoptosis or necrosis, result in reduced testosterone production [56–58]. Thus, we examined the testes of WT and *Bco1*$^{-/-}$ to determine whether altered morphology or decreased Leydig cell populations may help to explain the observed reduction in serum testosterone. We found that loss of *Bco1* increased total seminiferous tubule area, driven by an increase in seminiferous epithelial area, rather than lumen area. Additionally, Leydig cell number, normalized to tubule area, was lower in *Bco1*$^{-/-}$ testes than in WT testes. Leydig cell counts were normalized to tubule area, rather than total area or tubule count, because variation in tubule diameter necessarily alters tubule packing density, and therefore, the volume of interstitial space where Leydig cells reside. No overt differences in Leydig apoptosis or necrosis were observed between groups. It may seem apparent that the observed reduction in serum testosterone levels would be a consequence of diminished Leydig cell number, it is not clear whether the reduction in Leydig cells is causative or a simply associated with other morphological changes in the testes. In addition, although expression of *Hsd17b3* was reduced, other steroidogenic enzymes were unchanged, such as *Cyp17a1* and CYP11A1, and yet others were induced (*Star* and *Hsd17b2*) - suggesting that a decrease in Leydig cell number did not reduce steroidogenic capacity *en bloc.*

The testicular seminiferous epithelium consists predominantly of germ cells (spermatogonia, spermatocytes, spermatids, and spermatozoa), with the much less-common somatic Sertoli cells present on the basal perimeter [59]. While it has been shown that global AR loss results in altered Sertoli cell number in the adult mouse testes [60], due to the small number of Sertoli cells normally present, such changes are not likely to impact seminiferous epithelium

thickness directly. Rather, perturbations in germ cell development can meaningfully influence composition and size of the epithelium. Typically, upon inhibition of testosterone secretion or in mice lacking functional AR, investigators have observed drastically reduced populations of spermatocytes and spermatids [61]. In contrast, we observe reductions in serum testosterone in conjunction with a 24% increase in seminiferous epithelial area. Analysis of germ cells in testicular sections revealed a moderate decrease in spermatocyte apoptosis, which may explain these results, although the cause of this effect remains unclear. This study was not designed to allow for a comprehensive assessment of spermatogenesis and fertility, so firm conclusions would be improper at this point. Focused work in this area would be required to fully address questions regarding the impact of *Bco1* genotype on spermatogenesis and fertility.

Androgens mediate their actions at target tissues (such as the prostate) through specific binding to the AR and subsequent transcriptional regulation of genes containing androgen response elements (AREs). Unliganded AR exists as a monomer primarily localized to the cytoplasm [62]. Upon ligand binding, AR undergoes a conformational change, dissociates from cytosolic chaperones, translocates to the nucleus, dimerizes, binds androgen response elements (AREs) on AR-target genes, and recruits transcriptional machinery to initiate a transcriptional program collectively referred to as 'AR signaling' [63,64]. Genes activated in this AR signaling program serve to, among other functions, maintain epithelial differentiation, stimulate release of stromal-derived growth factors, and inhibit epithelial apoptosis [65–67]. Translocation of ligand-bound AR from the cytoplasm to the nucleus during AR signaling is thus a necessary step in androgen-dependent maintenance of the prostate; this process can serve as one marker of prostatic androgen status [62,68]. WT animals displayed both nuclear and cytoplasmic AR staining within dorsolateral prostate luminal epithelia, but many *Bco1*$^{-/-}$ sections lacked the punctate

nuclear AR localization characteristic of active AR signaling. Ablation of *Bco1* thus induced a downward shift in qualitative nuclear AR staining scores. This qualitative analysis suggests modest effects of *Bco1* ablation on dorsolateral prostate nuclear AR localization, rather than drastic "on/off" regulation; such an effect aligns with the modest reductions seen in prostatic organ weight and serum testosterone levels. Similar methods of qualitative nuclear staining scoring have been previously used to describe modulation of nuclear AR localization within the rat prostate during castration and DHT administration [26]. AR mRNA and total protein expression remained unchanged, suggesting that any androgen-regulated effects on the dorsolateral prostate of *Bco1*$^{-/-}$ mice may have been due to diminished AR activation, and not reduced expression of the receptor. This supports the hypothesis that *Bco1* ablation impacts prostatic androgen status through depression of testicular testosterone synthesis, rather than through direct perturbation of the prostate. Indeed, in humans, BCO1 is not highly expressed in the prostatic epithelium, but greater expression is seen in both testicular Sertoli cells and the testosterone-producing Leydig cells [9].

Previously, in the transgenic adenocarcinoma of the mouse prostate (TRAMP) model of prostate cancer, our group has found that castration significantly reduced prostatic mRNA expression of cell growth and proliferation markers (*Mki67, Aurkb, Ccnb2, Ccne2, Foxm1,* and *Birc5*), which, with the exception of *Foxm1*, were also upregulated by TRAMP genotype during early carcinogenesis [24]. Additionally, Wan et al. [24] reported that castration, as expected, modulated classical androgen-regulated genes, including down regulation of *Nkx3.1* and induction of *Igfbp3*. We have obtained very similar results in the dorsolateral prostates of *Bco1*$^{-/-}$ mice. *Msmb* is an androgen-regulated gene known to be strongly repressed by castration and induced by testosterone repletion [69–72]; in single-gene qPCR analysis, *Bco1*$^{-/-}$ genotype

significantly reduced *Msmb* expression, suggesting that *Bco1* ablation impacted prostatic androgen receptor signaling. NanoString analysis revealed that markers of cell growth and proliferation (*Pcna, Mki67, Aurkb, Ccnb2*) were significantly reduced ($p < 0.005$), with several others (*Aurka, Birc5, Ccne2, Foxm1*) inhibited at $0.005 < p < 0.05$ (**Table 2.1**). Moreover, Wan et al. reported that prostatic Ki67 protein expression (gene name *Mki67*), as measured by immunofluorescent staining, was reduced by castration, but induced in early carcinogenesis [24]. Similarly, we found that *Bco1*$^{-/-}$ genotype significantly reduced Ki67 labeling in the dorsolateral prostate, and trended towards a reduction in the anterior prostate. Although the fold-change differences were predictably higher in the castration and cancer model used by Wan et al., our results here show that *Bco1*$^{-/-}$ genotype not only mimicked decreases in proliferation seen with castration (both at the level of gene and protein expression), but also inhibited the expression of genes that are induced during early carcinogenesis.

Unexpectedly, *Bco1* mRNA expression was increased 8.2-fold ($p = 0.0001$) in *Bco1*$^{-/-}$ mice compared to WT mice (**Table 2.1**). When this genetically engineered mouse model was created, disruption of *Bco1* gene function was achieved through homozygous replacement of exons 2 and 3 of the *Bco1* gene (approximately 8.8 kb) with *IRES-lacZ* and a *neomycin*^{R} cassette [15]. This was confirmed by PCR genotyping (see also **Appendix Fig. A.9**). Mice of this strain do not express BCO1 protein [15] and they accumulate intact β-carotene when fed tomato powder [16], consistent with a lack of BCO1 cleavage function. However, the *Bco1* probe used in this NanoString array targets 100 nt within exons 9 and 10 (see footnote † at **Appendix Table A.3**) – a portion of the gene that was not modified during generation of this model. The increased mRNA transcript expression detected with this specific *Bco1* probe is likely a feedback response

to the absence of functional BCO1 protein. *Bco1*$^{-/-}$ genotype of mice in this study was confirmed by PCR (**Appendix Fig. A.9**).

After unguided visual inspection of the NanoString heat map (**Fig. 2.6A**), three gene clusters were identified as being potentially differentially regulated by *Bco1*$^{-/-}$ genotype (**Table 2.1**). All 13 genes that were significantly regulated by *Bco1* ablation ($p \leq 0.005$) were included within these three clusters, representing 36% of the 36 total genes in the three clusters combined. In contrast, a random sample of 36 genes from the entire 200-gene code set would be expected to contain ~7% significant genes (13 / 200), or only 2 - 3 genes. The fact that these three clusters not only contained all of the significantly regulated genes in the entire analysis, but also represented a >5-fold enrichment of significantly regulated genes (36% / 7% = 5.1), suggests that they are the most biologically informative group of genes examined. Gene ontology classifications from the PANTHER database [31,32] demonstrates that cluster 1 predominantly contains genes involved in the regulation of proliferation, cell cycle regulation, and apoptosis, whereas clusters 2 and 3 contain genes implicated in cell-cell-communication, intracellular signaling, and gene transcription (**Table 2.1**).

Conclusions

Together, these data suggest that lowered prostatic AR activation, mediated by reductions in serum testosterone due to *Bco1* ablation, results in decreased AR signaling within the prostate, reduced cellular proliferation, and a decreased rate of growth of the prostate. Moreover, the gene and protein expression patterns observed in *Bco1*$^{-/-}$ mice demonstrate a similar, although less dramatic, phenotype as that observed after castration. Previous work in mice shows that adiposity [73], diet-induced obesity [15], hepatic steatosis [15], adipocyte gene expression [15,73],

cholesterol esterification [17], triglyceride and phospholipid metabolism [17], serum insulin, leptin, and cholesterol [19], and cardiac lipid metabolism [18] are all impacted by *Bco1* loss. In conjunction with this previous work, our findings continue to build a convincing argument for the existence of functions of BCO1 that are independent of carotenoid cleavage. Eleven studies [12–14,74–81] have investigated the impact of single nucleotide polymorphisms (SNPs) in the human *BCO1* gene. These SNPs are common (most with a minor allele frequency between 0.25 and 0.50) and have been shown to impact carotenoid metabolism and distribution. However, only three of the studies [74,77,78] investigated endpoints other than carotenoid metabolism and distribution. Greater understanding of the consequences of *Bco1* ablation in this model may not only help to uncover new aspects of carotenoid metabolism, but it may inform the scientific community of the potential physiologic repercussions of natural genomic variation in the human *BCO1* gene. This report adds novel data to the growing body of evidence demonstrating that, although cleavage of dietary carotenoids seems to be the major function of BCO1, its pleiotropic roles in mammalian physiology may extend far beyond carotenoid metabolism.

References cited

1. Goodman, D. S. & Huang, H. S. Biosynthesis of vitamin A with rat intestinal enzymes. *Science.* **149,** 879–880 (1965).
2. Olson, J. A. & Hayaishi, O. The enzymatic cleavage of beta-carotene into vitamin A by soluble enzymes of rat liver and intestine. *Proc. Natl. Acad. Sci.* **54,** 1364–1370 (1965).
3. Lakshmanan, M. R., Pope, J. L. & Olson, J. A. The specificity of a partially purified carotenoid cleavage enzyme of rabbit intestine. *Biochem. Biophys. Res. Commun.* **33,** 347–352 (1968).
4. Lakshmanan, M. R., Chansang, H. & Olson, J. A. Purification and properties of carotene 15,15'-dioxygenase of rabbit intestine. *J. Lipid Res.* **13,** 477–482 (1972).
5. Barua, A. B. & Olson, J. A. Beta-carotene is converted primarily to retinoids in rats in vivo. *J. Nutr.* **130,** 1996–2001 (2000).
6. von Lintig, J. & Vogt, K. Filling the gap in vitamin A research. Molecular identification of an enzyme cleaving beta-carotene to retinal. *J. Biol. Chem.* **275,** 11915–11920 (2000).
7. Lindqvist, A. & Andersson, S. Biochemical properties of purified recombinant human beta-carotene 15,15'-monooxygenase. *J. Biol. Chem.* **277,** 23942–8 (2002).
8. Poliakov, E., Gentleman, S., Cunningham, F. X., Miller-Ihli, N. J. & Redmond, T. M. Key role of conserved histidines in recombinant mouse beta-carotene 15,15'-monooxygenase-1 activity. *J. Biol. Chem.* **280,** 29217–23 (2005).
9. Lindqvist, A. & Andersson, S. Cell type-specific expression of beta-carotene 15,15'-mono-oxygenase in human tissues. *J. Histochem. Cytochem.* **52,** 491–499 (2004).

10. Lindqvist, A., Sharvill, J., Sharvill, D. E. & Andersson, S. Loss-of-function mutation in carotenoid 15,15'-monooxygenase identified in a patient with hypercarotenemia and hypovitaminosis A. *J. Nutr.* **137,** 2346–2350 (2007).

11. dela Seña, C. *et al.* The human enzyme that converts dietary provitamin A carotenoids to vitamin A is a dioxygenase. *J. Biol. Chem.* **289,** 13661–13666 (2014).

12. Ferrucci, L. *et al.* Common variation in the beta-carotene 15,15'-monooxygenase 1 gene affects circulating levels of carotenoids: A genome-wide association study. *Am. J. Hum. Genet.* **84,** 123–33 (2009).

13. Leung, W. C. *et al.* Two common single nucleotide polymorphisms in the gene encoding beta-carotene 15,15'-monoxygenase alter beta-carotene metabolism in female volunteers. *FASEB J.* **23,** 1041–53 (2009).

14. Hendrickson, S. J. *et al.* Beta-carotene 15,15'-monooxygenase 1 single nucleotide polymorphisms in relation to plasma carotenoid and retinol concentrations in women of European descent. *Am. J. Clin. Nutr.* **96,** 1379–1389 (2012).

15. Hessel, S. *et al.* CMO1 deficiency abolishes vitamin A production from beta-carotene and alters lipid metabolism in mice. *J. Biol. Chem.* **282,** 33553–61 (2007).

16. Lindshield, B. L. *et al.* Lycopene biodistribution is altered in 15,15'-carotenoid monooxygenase knockout mice. *J. Nutr.* **138,** 2367–2371 (2008).

17. Dixon, J. L., Kim, Y.-K., Brinker, A. & Quadro, L. Loss of β-carotene 15,15'-oxygenase in developing mouse tissues alters esterification of retinol, cholesterol and diacylglycerols. *Biochim. Biophys. Acta* **1841,** 34–43 (2014).

18. Lee, S.-A. *et al.* Cardiac dysfunction in beta-carotene-15,15'-dioxygenase-deficient mice is associated with altered retinoid and lipid metabolism. *Am. J. Physiol. - Hear. Circ. Physiol.* **307,** H1675–H1684 (2014).

19. Ford, N. A., Elsen, A. C. & Erdman Jr., J. W. Genetic ablation of carotene oxygenases and consumption of lycopene or tomato powder diets modulate carotenoid and lipid metabolism in mice. *Nutr. Res.* **33,** 733–42 (2013).

20. van Helden, Y. G. J. *et al.* Beta-carotene affects gene expression in lungs of male and female Bcmo1 (-/-) mice in opposite directions. *Cell. Mol. Life Sci.* **68,** 489–504 (2011).

21. Clinton, S. K. *et al.* cis-trans lycopene isomers, carotenoids, and retinol in the human prostate. *Cancer Epidemiol. Biomarkers Prev.* **5,** 823–833 (1996).

22. Boileau, T. W.-M. *et al.* Prostate carcinogenesis in N-methyl-N-nitrosourea (NMU)-testosterone-treated rats fed tomato powder, lycopene, or energy-restricted diets. *J. Natl. Cancer Inst.* **95,** 1578–1586 (2003).

23. Ford, N. A., Moran, N. E., Smith, J. W., Clinton, S. K. & Erdman Jr., J. W. An interaction between carotene-15,15'-monooxygenase expression and consumption of a tomato or lycopene-containing diet impacts serum and testicular testosterone. *Int. J. Cancer* **131,** E143–8 (2012).

24. Wan, L. *et al.* Dietary tomato and lycopene impact androgen signaling- and carcinogenesis-related gene expression during early TRAMP prostate carcinogenesis. *Cancer Prev. Res.* **7,** 1228–1239 (2014).

25. Geiss, G. K. *et al.* Direct multiplexed measurement of gene expression with color-coded probe pairs. *Nat. Biotechnol.* **26,** 317–25 (2008).

26. Paris, F., Weinbauer, G. F., Blum, V. & Nieschlag, E. The effect of androgens and antiandrogens on the immunohistochemical localization of the androgen receptor in accessory reproductive organs of male rats. *J Steroid Biochem Mol Biol* **48,** 129–137 (1994).

27. Osborne, J. A. Estimating the false discovery rate using SAS. In *Proc. Thirty-first Annu. SAS Users Gr. Int. Conf.* 190–31 (SAS Institute, Inc., 2006).

28. Storey, J. D. A direct approach to false discovery rates. *J. R. Stat. Soc. B.* **64,** 479–498 (2002).

29. Payne, A. H. & Hales, D. B. Overview of steroidogenic enzymes in the pathway from cholesterol to active steroid hormones. *Endocr. Rev.* **25,** 947–70 (2004).

30. Luu-The, V. & Labrie, F. in *Prog. Brain Res.* **181,** 177–192 (Elsevier, 2010).

31. Mi, H., Muruganujan, A., Casagrande, J. T. & Thomas, P. D. Large-scale gene function analysis with the PANTHER classification system. *Nat. Protoc.* **8,** 1551–66 (2013).

32. Mi, H., Muruganujan, A. & Thomas, P. D. PANTHER in 2013: Modeling the evolution of gene function, and other gene attributes, in the context of phylogenetic trees. *Nucleic Acids Res.* **41,** D377–D386 (2013).

33. Kerr, J. F. R. & Searle, J. Deletion of cells by apoptosis during castration-induced involution of the rat prostate. *Virchows Arch. B* **13,** 87–102 (1973).

34. Suzuki, Y., Nakagawa, M., Sato, F., Iichikawa, Y. & Mizushima, Y. A primary adrenal steroid, 11-beta-hydroxyandrostenedione, has an osteotropic effect and little androgenic activity. *J. Steroid Biochem. Mol. Biol.* **74,** 203–11 (2000).

35. Terada, N., Ogasawara, Y., Yamane, T., Matsumoto, K. & Kitamura, Y. Heterogeneity in mouse seminal vesicle epithelial cells responding to androgen as evaluated by incorporation of 125I-iododeoxyuridine. *Endocrinology* **116,** 1466–72 (1985).

36. Mahendroo, M. S., Cala, K. M., Hess, D. L. & Russell, D. W. Unexpected virilization in male mice lacking steroid 5-alpha-reductase enzymes. *Endocrinology* **142,** 4652–62 (2001).

37. Nantermet, P. V *et al.* Identification of genetic pathways activated by the androgen receptor during the induction of proliferation in the ventral prostate gland. *J. Biol. Chem.* **279,** 1310–22 (2004).

38. Bruni-Cardoso, A., Augusto, T. M., Pravatta, H., Damas-Souza, D. M. & Carvalho, H. F. Stromal remodelling is required for progressive involution of the rat ventral prostate after castration: Identification of a matrix metalloproteinase-dependent apoptotic wave. *Int. J. Androl.* **33,** 686–695 (2010).

39. Kyprianou, N. & Isaacs, J. T. Activation of programmed cell death in the rat ventral prostate after castration. *Endocrinology* **122,** 552–562 (1988).

40. Campbell, J. K., Stroud, C. K., Nakamura, M. T., Lila, M. A. & Erdman, J. W. Serum testosterone is reduced following short-term phytofluene, lycopene, or tomato powder consumption in F344 rats. *J. Nutr.* **136,** 2813–9 (2006).

41. McNamara, K. M. *et al.* Measurement of sex steroids in murine blood and reproductive tissues by liquid chromatography-tandem mass spectrometry. *J. Steroid Biochem. Mol. Biol.* **121,** 611–8 (2010).

42. Labrie, F. *et al.* Is dehydroepiandrosterone a hormone? *J. Endocrinol.* **187,** 169–96 (2005).

43. van Weerden, W. M., Blerings, H. G., van Steenbrugge, G. J., de Jong, F. H. & Schröder, F. H. Adrenal glands of mouse and rat do not synthesize androgens. *Life Sci.* **50,** 857–861 (1992).

44. Brock, B. J. & Waterman, M. R. Biochemical differences between rat and human cytochrome P450c17 support the different steroidogenic needs of these two species. *Biochemistry* **38,** 1598–606 (1999).

45. Azhar, S. & Reaven, E. in *Contemp. Endocrinol. Leydig Cell Heal. Dis*. 135–48 (Humana Press, 2007).

46. Goldstein, J. L. & Brown, M. S. Regulation of the mevalonate pathway. *Nature* **343,** 425–430 (1990).

47. Azhar, S. & Reaven, E. Scavenger receptor class BI and selective cholesteryl ester uptake: partners in the regulation of steroidogenesis. *Mol. Cell. Endocrinol.* **195,** 1–26 (2002).

48. Manna, P. R., Wang, X.-J. & Stocco, D. M. Involvement of multiple transcription factors in the regulation of steroidogenic acute regulatory protein gene expression. *Steroids* **68,** 1125–1134 (2003).

49. Fuhrman, B., Elis, A. & Aviram, M. Hypocholesterolemic effect of lycopene and beta-carotene is related to suppression of cholesterol synthesis and augmentation of LDL receptor activity in macrophages. *Biochem. Biophys. Res. Commun.* **233,** 658–62 (1997).

50. Peffley, D. M. & Gayen, A. K. Plant-derived monoterpenes suppress hamster kidney cell 3-hydroxy-3-methylglutaryl coenzyme A reductase synthesis at the post-transcriptional level. *J. Nutr.* **133,** 38–44 (2003).

51. Baker, P. J., Sha, J. H. & O'Shaughnessy, P. J. Localisation and regulation of 17-beta-hydroxysteroid dehydrogenase type 3 mRNA during development in the mouse testis. *Mol. Cell. Endocrinol.* **133,** 127–33 (1997).

52. Geissler, W. M. *et al.* Male pseudohermaphroditism caused by mutations of testicular 17-beta-hydroxysteroid dehydrogenase 3. *Nat. Genet.* **7,** 34–39 (1994).

53. Luu-The, V., Bélanger, A. & Labrie, F. Androgen biosynthetic pathways in the human prostate. *Best Pract. Res. Clin. Endocrinol. Metab.* **22,** 207–21 (2008).

54. Prince, F. P. in *Contemp. Endocrinol. Leydig Cell Heal. Dis.* 71–89 (Humana Press, 2007).

55. Payne, A. H. in *Contemp. Endocrinol. Leydig Cell Heal. Dis.* 157–71 (Humana Press, 2007).

56. Liu, J. *et al.* Icariside II reduces testosterone production by inducing necrosis in rat Leydig cells. *J. Biochem. Mol. Toxicol.* **27,** 243–250 (2013).

57. Liu, S. *et al.* Citrinin reduces testosterone secretion by inducing apoptosis in rat Leydig cells. *Toxicol. Vitr.* **26,** 856–61 (2012).

58. Kim, J.-H., Park, S.-J., Kim, T.-S., Kim, J.-M. & Lee, D.-S. Testosterone production by a Leydig tumor cell line is suppressed by hyperthermia-induced endoplasmic reticulum stress in mice. *Life Sci.* **146,** 184–191 (2015).

59. Parvinen, M. Regulation of the seminiferous epithelium. *Endocr. Rev.* **3,** 404–417 (1982).

60. Johnston, H. *et al.* Regulation of Sertoli cell Nnmber and activity by follicle-stimulating hormone and androgen during postnatal development in the mouse. *Endocrinology* **145,** 318–329 (2004).

61. O'Shaughnessy, P. J. Hormonal control of germ cell development and spermatogenesis. *Semin. Cell Dev. Biol.* **29,** 55–65 (2014).

62. Gerdes, M. J., Dang, T. D., Larsen, M. & Rowley, D. R. Transforming growth factor-beta1 induces nuclear to cytoplasmic distribution of androgen receptor and inhibits androgen response in prostate smooth muscle cells. *Endocrinology* **139,** 3569–77 (1998).

63. Shang, Y., Myers, M. & Brown, M. Formation of the androgen receptor transcription complex. *Mol. Cell* **9,** 601–10 (2002).

64. Basu, S. & Tindall, D. J. Androgen action in prostate cancer. *Horm. Cancer* **1,** 223–8 (2010).

65. Bolton, E. C. *et al.* Cell- and gene-specific regulation of primary target genes by the androgen receptor. *Genes Dev.* **21,** 2005–17 (2007).

66. Berry, P. a., Maitland, N. J. & Collins, A. T. Androgen receptor signalling in prostate: Effects of stromal factors on normal and cancer stem cells. *Mol. Cell. Endocrinol.* **288,** 30–37 (2008).

67. Kurita, T. *et al.* Paracrine regulation of apoptosis by steroid hormones in the male and female reproductive system. *Cell Death Differ.* **8,** 192–200 (2001).

68. Wilson, J. D. The critical role of androgens in prostate development. *Endocrinol. Metab. Clin. North Am.* **40,** 577–590 (2011).

69. Wang, X.-D. *et al.* Expression profiling of the mouse prostate after castration and hormone replacement: implication of H-cadherin in prostate tumorigenesis. *Differentiation* **75,** 219–34 (2007).

70. Love, H. D. *et al.* Androgen regulated genes in human prostate xenografts in mice: relation to BPH and prostate cancer. *PLoS One* **4,** e8384 (2009).

71. Yu, S. *et al.* Androgen receptor in human prostate cancer-associated fibroblasts promotes prostate cancer epithelial cell growth and invasion. *Med. Oncol.* **30,** 674 (2013).

72. Le, H., Arnold, J. T., McFann, K. K. & Blackman, M. R. DHT and testosterone, but not DHEA or E2, differentially modulate IGF-I, IGFBP-2, and IGFBP-3 in human prostatic stromal cells. *Am. J. Physiol. Endocrinol. Metab.* **290,** E952–60 (2006).

73. Amengual, J. *et al.* Beta-carotene reduces body Aaiposity of mice via BCMO1. *PLoS One* **6,** e20644 (2011).

74. Perry, J. R. B. *et al.* Circulating beta-carotene levels and type 2 diabetes – cause or effect? *Diabetologia* **52,** 2117–21 (2009).

75. Borel, P. *et al.* Genetic variants in BCMO1 and CD36 are associated with plasma lutein concentrations and macular pigment optical density in humans. *Ann. Med.* **43,** 47–59 (2011).

76. Lietz, G., Oxley, A., Leung, W. & Hesketh, J. Single nucleotide polymorphisms upstream from the beta-carotene-15,15'-monooxygenase gene influence provitamin A conversion efficiency in female volunteers. *J. Nutr.* **142,** 161S–165S (2012).

77. Clifford, A. J. *et al.* Single nucleotide polymorphisms in CETP, SLC46A1, SLC19A1, CD36, BCMO1, APOA5, and ABCA1 are significant predictors of plasma HDL in healthy adults. *Lipids Health Dis.* **12,** 66 (2013).

78. Hendrickson, S. J. *et al.* Plasma carotenoid- and retinol-weighted multi-snp scores and risk of breast cancer in the national cancer institute breast and prostate cancer cohort consortium. *Cancer Epidemiol. Biomarkers Prev.* **22,** 927–936 (2013).

79. Lobo, G. P. *et al.* Genetics and diet regulate vitamin A production via the homeobox transcription factor ISX. *J. Biol. Chem.* **288,** 9017–27 (2013).

80. Wang, T. T. Y., Edwards, A. J. & Clevidence, B. A. Strong and weak plasma response to dietary carotenoids identified by cluster analysis and linked to beta-carotene 15,15'-monooxygenase 1 single nucleotide polymorphisms. *J. Nutr. Biochem.* **24,** 1538–46 (2013).

81. Feigl, B., Morris, C. P., Voisey, J., Kwan, A. & Zele, A. J. The relationship between BCMO1 gene variants and macular pigment optical density in persons with and without age-related macular degeneration. *PLoS One* **9,** e89069 (2014).

Figures

Figure 2.1.

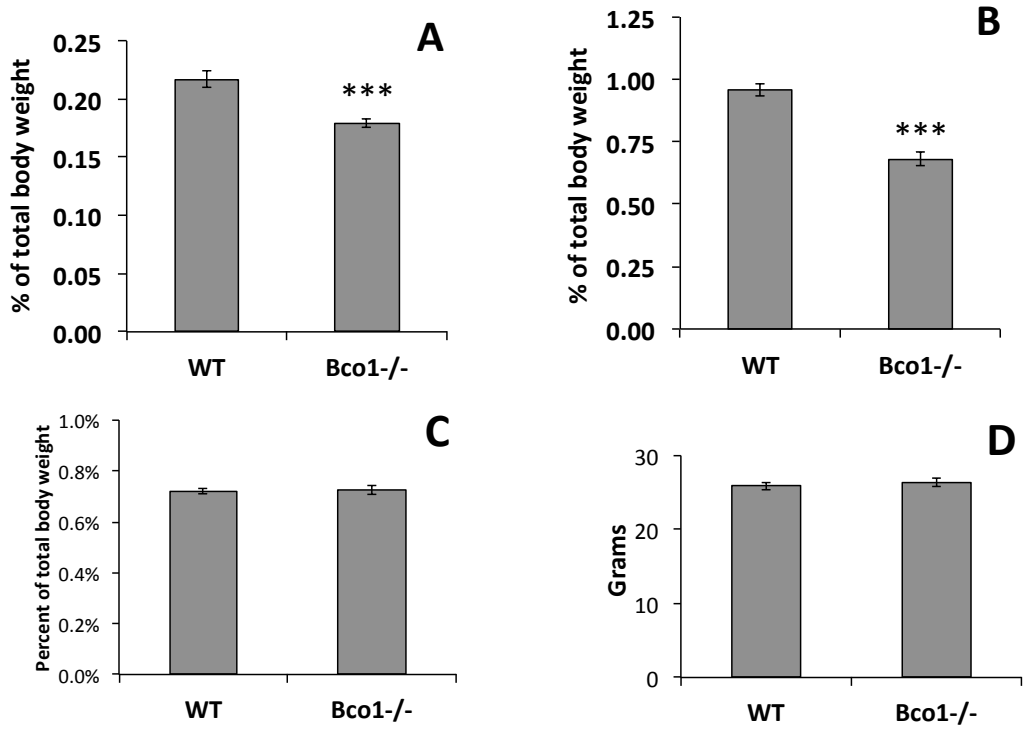

Figure 2.1. *Bco1*$^{-/-}$ loss reduces seminal vesicular and prostate weight as a percent of body weight. Total prostate (**A**), seminal vesicle (**B**), testes weight (**C**), as percent of total body weight (%BW). Body weight (**D**). Data are presented as group mean %BW ± SEM. n = 15, ***p < 0.001.

Figure 2.2.

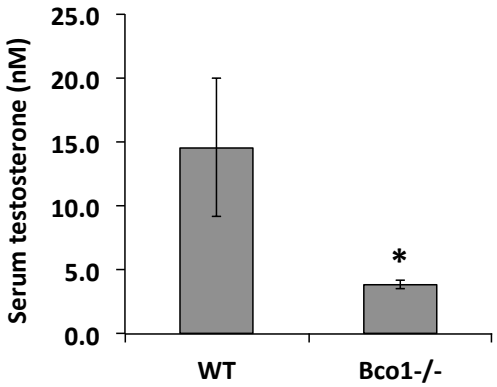

Figure 2.2. Serum testosterone is reduced by *Bco1* ablation. Data are presented as means ± SEM; n = 11-13. *$p < 0.05$.

Figure 2.3.

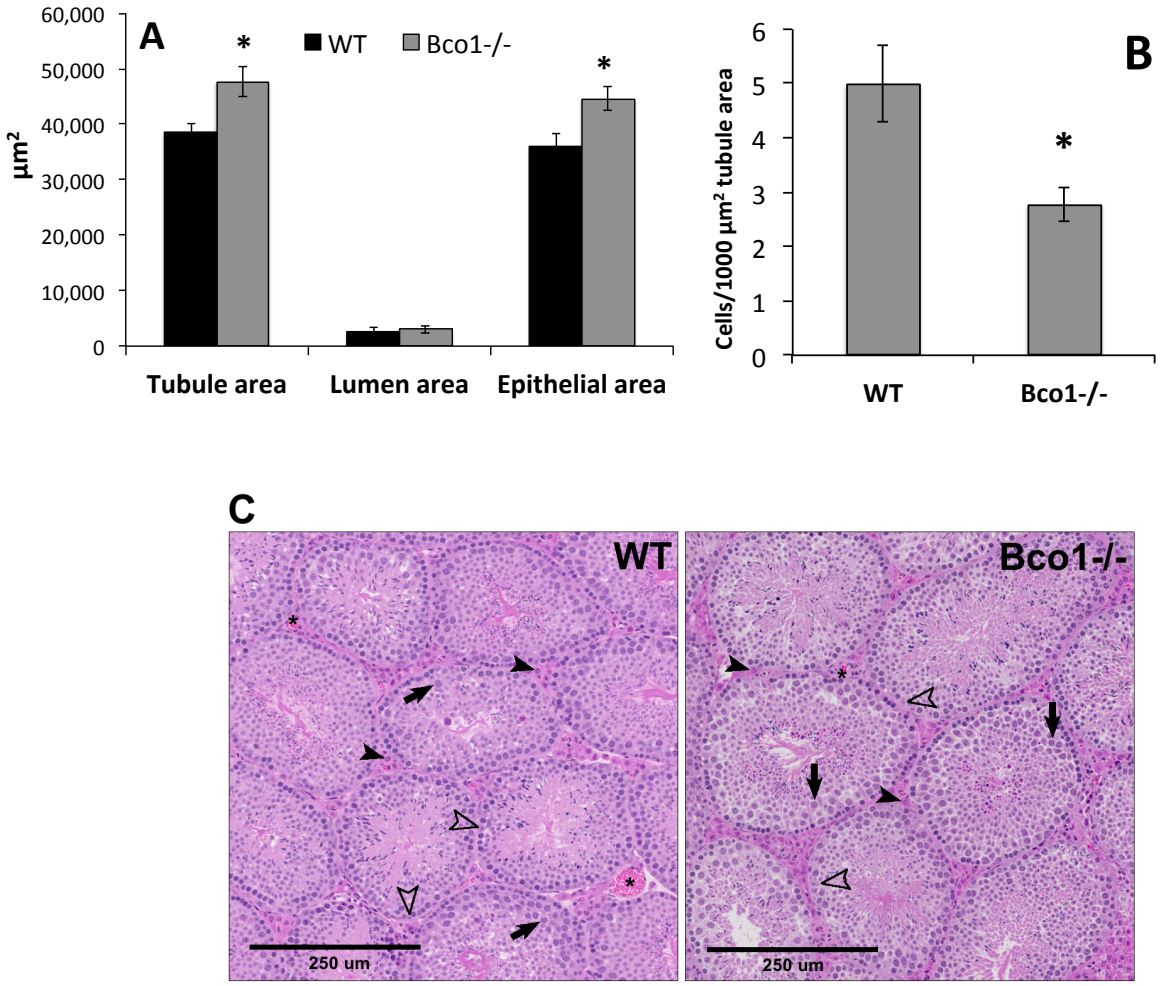

Figure 2.3. *Bco1* ablation increased seminiferous tubule total and epithelial areas (**A**) and decreased Leydig cell number (**B**). Representative images are shown in (**C**). Leydig cells (filled arrowheads) reside in the interstitial space between seminiferous tubules, often alongside blood vessels (asterisks). Cells within the seminiferous tubules include Sertoli cells (open arrowheads) and spermatocytes (filled arrows). *$p \leq 0.05$.

Figure 2.4.

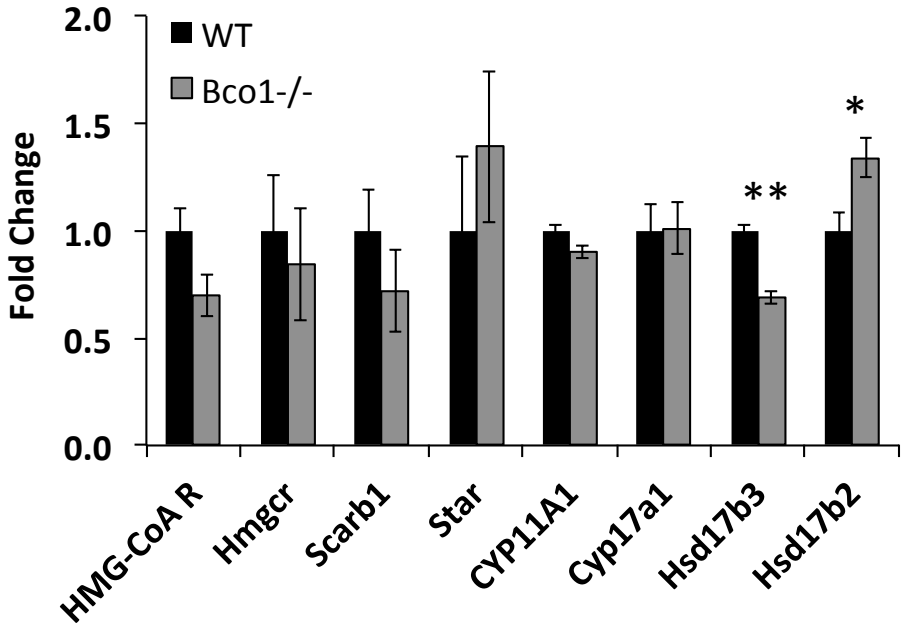

Figure 2.4. *Bco1* ablation does not significantly affect testicular protein expression of HMG-CoA reductase (HMG-CoA R) or CYP11A1, and does not alter mRNA expression of *Hmgcr, Scarb1, Star,* or *Cyp17a1*. Expression of *Hsd17b3* is significantly decreased, while *Hsd17b2* expression is induced by *Bco1* ablation. HMG-CoA reductase and CYP11A1 protein expression was measured by Western blot and *Hmgcr, Scarb1, Star, Cyp17a1, Hsd17b3,* and *Hsd17b2* mRNA expression was determined by qPCR. Data are presented as means ± SEM, n = 6 - 10, *$p < 0.05$, **$p < 0.01$.

Figure 2.5.

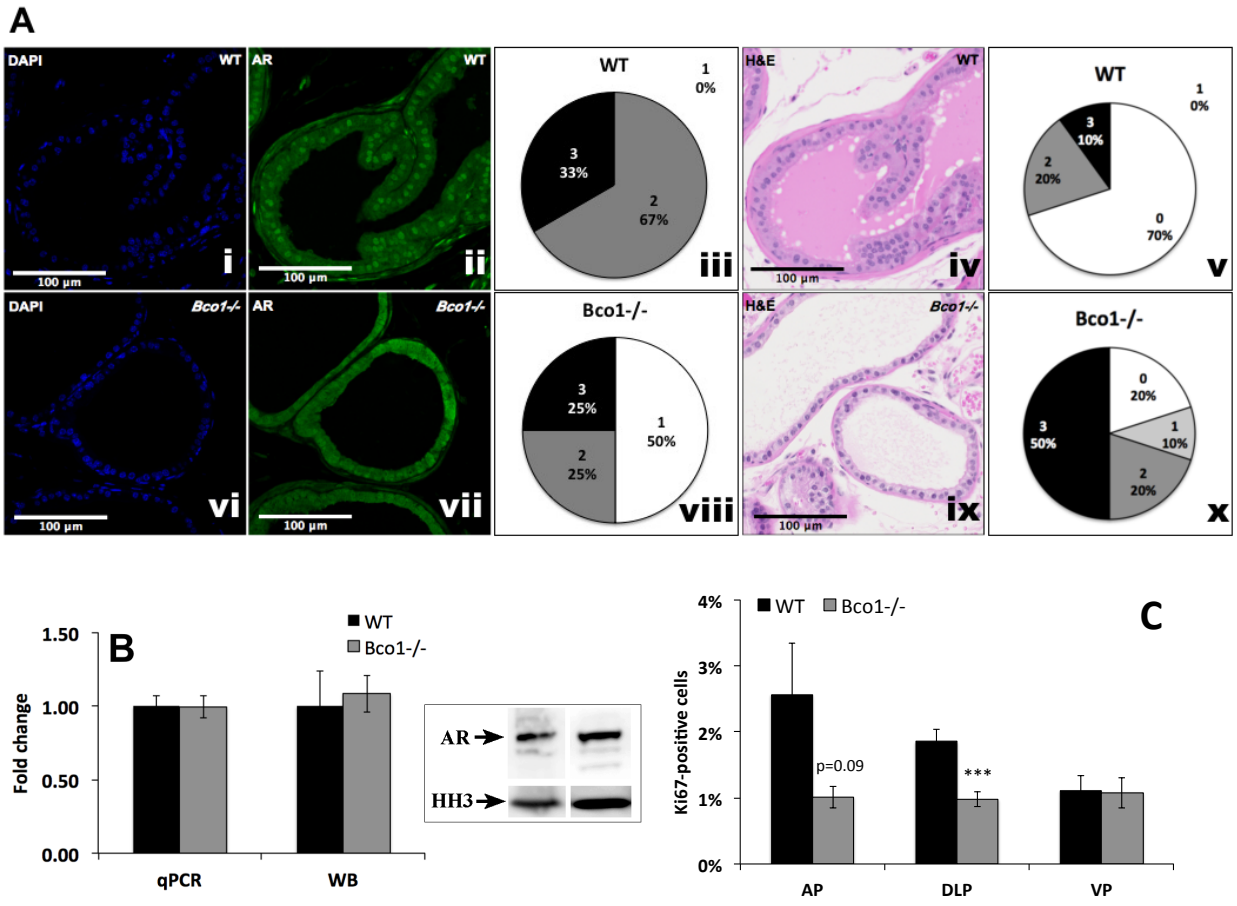

Figure 2.5. *Bco1* ablation alters prostatic morphology, AR localization, and proliferation, but does not impact AR expression. *Bco1* ablation impacts nuclear AR localization within the dorsolateral prostate lobe (**Aii, Avii**), as well as alters dorsolateral prostate morphology (**Aiv**, **Aix**). Qualitative grading of immunofluorescent androgen receptor nuclear staining demonstrates a shift from high or moderate nuclear localization (score = 3 or 2) in WT mice (**Aiii**) to weak nuclear localization (score = 1) in *Bco1*$^{-/-}$ mice (**Aviii**). Qualitative grading of prostatic morphology reveals a shift from predominantly normal glandular size (score = 0) in WT mice to markedly decreased size (score = 3) in *Bco1*$^{-/-}$ (**Av**, **Ax**). Data in (**Ai, Aii, Aiii, Avi, Avii, Aviii**) are representative of 2 - 4 images in n=3 - 4 mice per genotype; data in (**Aiv, Av, Aix, Ax**) are representative of n = 9-10 mice/genotype. AR mRNA and protein expression is unchanged in *Bco1*$^{-/-}$ mice (**B**). Data are presented as means ± SEM; n = 11 - 14 for qPCR and n = 5 for Western blotting (WB). AR mRNA expression was normalized to Rpl19 and histone H3 (HH3) was used as a loading control for WB. *Bco1* loss reduces Ki67 protein (as detected with immunofluorescent labeling) in the dorsolateral prostate (**C**); ***p < 0.001, n = 4 - 6. AP: anterior prostate; DLP: dorsolateral prostate; VP: ventral prostate.

Figure 2.6.

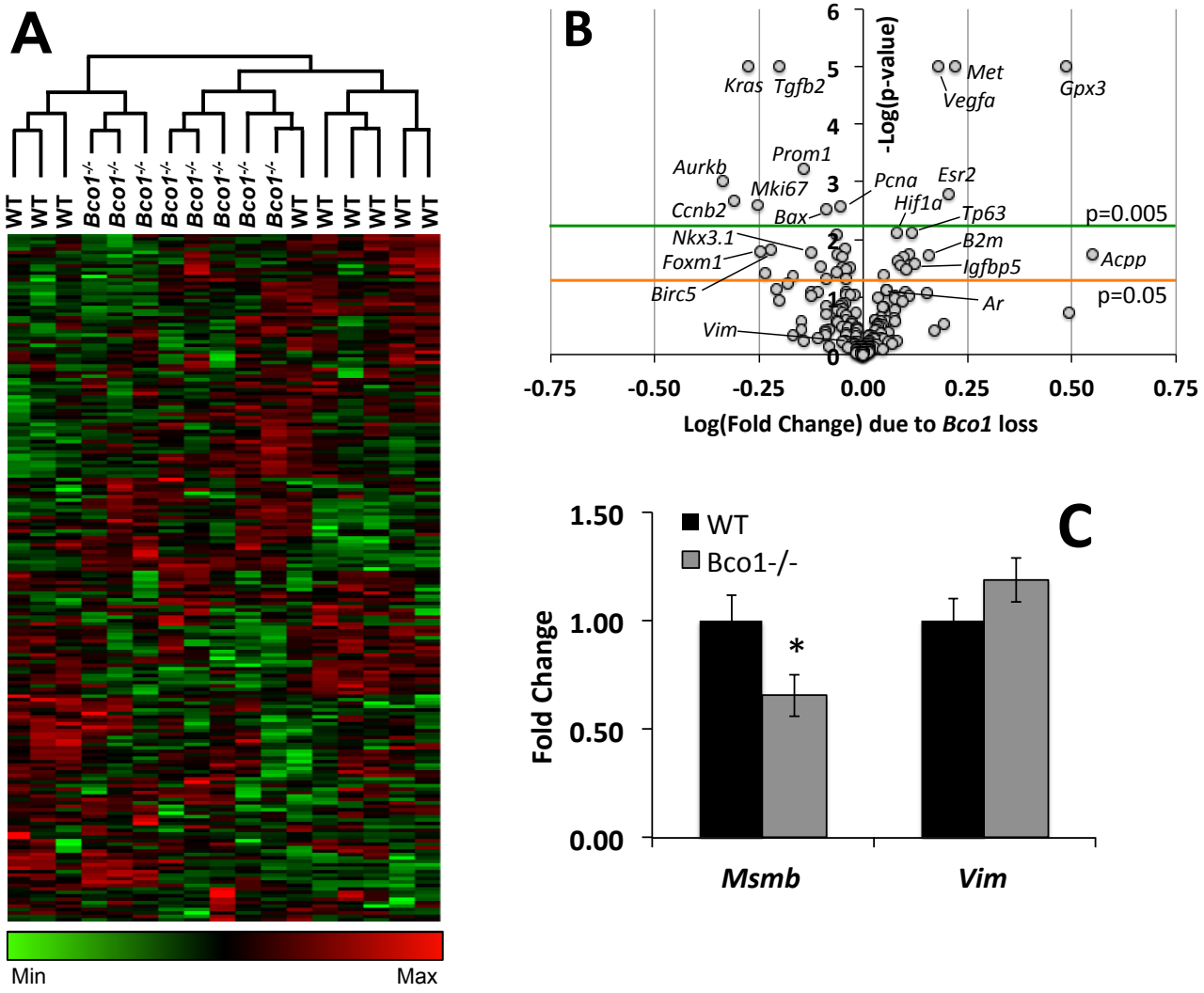

Figure 2.6. Prostatic androgen- and proliferation-related expression is altered in *Bco1*$^{-/-}$ mice. NanoString quantitative gene expression analysis for 200 proliferation-, androgen- and cancer-related genes WT or *Bco1*$^{-/-}$ mice (n = 8 - 9) displayed in a heat map (**A**) and volcano plot (**B**). Z-scored samples (columns) and genes (rows; labels not shown) were subjected to Ward's minimum distance linkage within Pearson's correlation hierarchical clustering (**A**). Absolute log(fold-change) values of 0.25 and 0.50 approximately equal absolute fold-change values of 1.8 and 3.2, respectively (**B**). qPCR-based single gene expression of *Msmb* and *Vim* in the prostates of mice (**C**); n = 7 - 14, *p < 0.05 vs. WT.

Table 2.1.

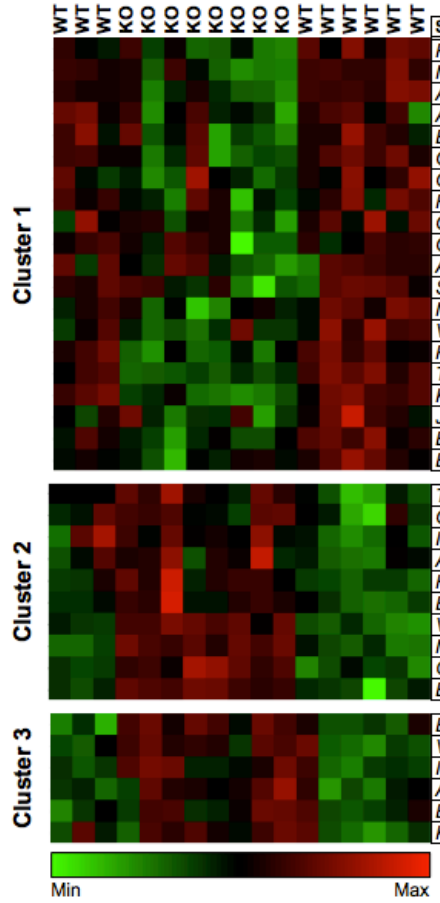

Symbol	Gene Name	Gene Ontology process	Fold Change	p-value
Pcna	Proliferating Cell Nuclear Antigen	Proliferation (DNA replication)	-1.13	0.0027
Mki67	Antigen Identified By Monoclonal Antibody Ki 67	Proliferation (rRNA synthesis)*	-1.77	0.0025
Aurka	Aurora Kinase A	Cell cycle regulation (chromatin organization)	-1.48	0.0449
Aurkb	Aurora Kinase B	Cell cycle regulation (chromatin organization)	-2.19	0.0005
Birc5	Baculoviral Iap Repeat-Containing 5 (Survivin)	Apoptosis	-1.65	0.0154
Ccnb2	Cyclin B2	Cell cycle regulation (Entry to M)	-2.03	0.0021
Ccne2	Cyclin E2	Cell cycle regulation (Entry to S)	-1.27	0.0291
Foxm1	Forkhead Box M1	Transcription factor	-1.75	0.0157
Casp3	Caspase 3	Apoptosis	-1.08	0.0320
Cdc25c	Cell Division Cycle 25C	Cell cycle regulation (mitosis)	-1.58	0.1108
Arntl	Aryl Hydrocarbon Receptor Nuclear Translocator-Like Protein	Transcription factor	-1.21	0.1430
Selp	Selectin, Platelet	Cell communication; Cell-cell adhesion	-1.73	0.0401
Mcl1	Myeloid Cell Leukemia Sequence 1	Apoptosis	-1.11	0.0146
Vegfb	Vascular Endothelial Growth Factor B	Cell communication (Growth factor); Angiogenesis	-1.14	0.0179
Prom1	Prominin 1 (Cd133)	Intracellular protein transport	-1.38	0.0006
Tgfb2	Transforming Growth Factor, Beta 2	Proliferation; Apoptosis; Differentiation	-1.59	<0.0001
Kras	V-Ki-Ras2 Kirsten Rat Sarcoma Viral Oncogene Homolog	Intracellular signaling	-1.89	<0.0001
Jun	Jun Proto-oncogene	Transcription factor (AP-1); Intracellular signaling	-1.23	0.0484
Bax	BCL2-associated X protein	Apoptosis	-1.21	0.0030
Egfr	Epidermal Growth Factor Receptor	Proliferation; Apoptosis	-1.16	0.0376
Tp63	Transformation Related Protein 63 (p63)	Transcription factor; Apoptosis; Cell cycle regulation	1.31	0.0079
Casp2	Caspase 2	Apoptosis	1.14	0.0758
Igfbp3	Insulin-Like Growth Factor Binding Protein 3	Cell communication (Growth factor regulation)	1.19	0.1092
Ar	Androgen Receptor	Transcription factor (Nuclear hormone receptor)	1.14	0.0778
Hif1a	Hypoxia Inducible Factor 1, Alpha Subunit	Transcription factor (VEGF signaling)	1.20	0.0078
B2m	Beta 2-Microglobulin	Cellular defense response (MHC complex)	1.44	0.0190
Vegfa	Vascular Endothelial Growth Factor A	Cell communication (Growth factor); Angiogenesis	1.51	<0.0001
Met	Met Proto-oncogene (Hepatocyte Growth Factor Receptor)	Cell communication (Growth factor receptor)*	1.66	<0.0001
Gpx3	Glutathione Peroxidase 3	Catalytic activity (Antioxidant activity)	3.06	<0.0001
Bco1	Beta-Carotene Oxygenase 1	Catalytic activity (Vitamin biosynthesis)	8.21	0.0001
Esr2	Estrogen Receptor 2 (Beta)	Transcription factor (nuclear hormone receptor)*	1.60	0.0016
Vdr	Vitamin D Receptor	Transcription factor (nuclear hormone receptor)	1.21	0.0232
Igf1r	Insulin-Like Grwoth Factor 1 Receptor	Cell communication (Growth factor receptor)	1.25	0.0196
Akt2	V-Akt Murine Thymoma Viral Oncogene Homolog 2	Catalytic activity (Kinase); Apoptosis	1.23	0.0276
Erbb2	Erythroblastic Leukemia Viral Oncogene Homolog 2 (Her2/Neu)	Proliferation; Apoptosis; Cell-cell adhesion	1.12	0.1489
Krt5	Keratin 5	Cytoskeleton (Basal cell marker)	1.29	0.0943

Table 2.1. *Bco1* ablation alters the prostatic expression of genes involved in cell cycle progression, proliferation, apoptosis, and cellular signaling pathways. Clusters were selected from gene subfamilies by visual inspection of the entire 200-gene heat map (**Fig. 5B**). Gene names and symbols were obtained from the Online Mendelian Inheritance in Man (OMIM) database. Gene ontology process classification was done according to annotations in the PANTHER Classification System; asterisks (*) denote genes that lacked full classification information and which were classified by the authors. P-values ≤ 0.005 are highlighted in orange.

CHAPTER 3

Loss of β-carotene-15,15'-dioxygenase alters hepatic vitamin A and lipid metabolism in mice

Abstract

Dietary provitamin A carotenoids are converted to retinol by β-carotene-15,15'-dioxygenase (BCO1). Much work has gone into the description of enzymatic carotenoid cleavage activities of the enzyme, but although pleiotropic effects of *Bco1* loss on lipid metabolism *in vivo* have occasionally been described, few investigators have reported extensively on this. We sought to describe the effects of *Bco1* loss on hepatic vitamin A status, lipid composition, and gene expression profile. Additionally, we describe phenotypic effects of *Bco1* loss on organ weight across the lifespan. We found that vitamin-A sufficient, chow-fed adult (20 - 22 weeks of age) male *Bco1*$^{-/-}$ mice accumulate > 2-fold more hepatic vitamin A than wild-type (WT) controls, an effect driven exclusively by retinyl ester accumulation. Notably, *Bco1* status significantly interacts with age across a wide range of developmental stages (<9 – 71 weeks of age) to alter hepatic retinyl ester accumulation in a highly age-dependent fashion. Furthermore, *Bco1*$^{-/-}$ mice experience alterations in hepatic lipid metabolism, including a 2-fold increase of cholesteryl palmitate. Levels of this cholesteryl ester correlate with total vitamin A content, and gene expression analysis suggests that a retinoid – *Pparg* – *Slc27a4* mechanism may increase palmitoyl-CoA levels to drive cholesteryl palmitate synthesis. Additionally, PPAR/RXR signaling may explain at least a part of the hepatic lipid phenotype observed in *Bco1*$^{-/-}$ mice, including the steatosis reported by several independent investigators. In summary, we report that *Bco1* loss interacts with developmental age to alter hepatic retinyl ester accumulation, even when maintained on vitamin-sufficient diet. This effect may in turn result in altered RXR/PPAR signaling and a disruption of hepatic lipid metabolism. Investigators should be aware of retinoid

and lipid perturbations present in the *Bco1*$^{-/-}$ strain when using this mouse model to study the metabolism and distribution of lipophilic carotenoids and retinoids.

Introduction

In 2007, Hessel et al. were the first to describe the effects of genomic *Bco1* ablation in a mammal [1]. They reported that the *Bco1*$^{-/-}$ genotype abolished retinol production in mice fed β-carotene as the major source of vitamin A; these data validated the hypothesis that BCO1 was the primary enzyme responsible for conversion of provitamin A carotenoids to retinol. Of the 68 articles that have cited the Hessel paper (per PubMed as of 2/27/16), nearly all have cited it purely in relation to its biochemical function in carotenoid cleavage. Although retinol production from provitamin A carotenoids clearly seems to be the conserved evolutionary role for the enzyme, the Hessel paper also reported that *Bco1*$^{-/-}$ mice experience perturbations in hepatic lipid metabolism, *even when provided adequate dietary levels of pre-formed vitamin A*. Later reports also pointed to disruptions of lipid metabolism in *Bco1*$^{-/-}$ mice [2–5].

These results, suggesting that *Bco1* loss alters physiology through a mechanism not reliant on its function in β-carotene cleavage, are important for the interpretation of data arising from use of this model. If the loss of BCO1 function truly impacts biological outcomes independently from cleavage of dietary provitamin A carotenoids, studies on single nucleotide polymorphisms (SNPs) in the human *BCO1* gene (which are common, with minor allele frequencies between 0.25 and 0.50) should take these broader effects into account. Of the 11 studies that have investigated the effects of *BCO1* SNPs [6–16], only 3 have investigated endpoints other than carotenoid metabolism and distribution [7,11,15] and only one explicitly examined markers of lipid status [7]. Even in studies limited in scope to carotenoid metabolism and

distribution, it would seem important to acknowledge and account for potential changes in lipid metabolism, as carotenoids are lipophilic compounds that are absorbed and transported along with exogenous and endogenous lipids.

As the "central hub" of mammalian metabolism, the liver is responsible for regulation of anabolism, catabolism, and peripheral distribution of lipids. Previous reports have described effects of *Bco1* loss on hepatic lipid metabolism, but have either not investigated alterations in metabolism to the depth of individual lipid species [1], or have done so only in embryonic, and not adult, mice [3,4]. Therefore, our goal was threefold: 1) in adult mice, describe the effects of *Bco1* loss on the composition of hepatic lipid pools at the level of individual fatty acid species, 2) investigate changes in gene expression which may be responsible for such alterations, and 3) report any changes in gross organ weight across the lifespan of *Bco1*$^{-/-}$ mice, as these key phenotypic data are currently missing from the literature. If scientists are to truly understand the role of BCO1 in the metabolism and distribution of the lipophilic dietary carotenoids, it is critical to elucidate its impact on lipid metabolism, especially in the liver.

Materials and Methods

Animals and study designs

All animal procedures were approved by the University of Illinois Institutional Animal Care and Use Committee.

Generation of *Bco1*$^{-/-}$ animals has been described previously [1]. C57BL/6J x 129/SvJ F1 cross (WT) mice were purchased from The Jackson Laboratory (Bar Harbor, ME) and used in all experiments. Mice were housed in shoebox cages in a temperature- and humidity-controlled facility with *ad libitum* access to water. For the studies described, we have focused our studies

only on male mice, although the importance of expanding these investigations to female mice in the future is acknowledged.

Two studies were completed. Study #1 investigated the effects of *Bco1* loss on hepatic retinyl esters, composition of distinct lipid pools, and expression of genes governing lipid and cholesterol metabolism in mice fed a chow diet. In this study, male *Bco1*$^{-/-}$ mice (n = 8) were weaned from the breeding colony at 3 weeks of age onto a standard rodent chow (Harlan Teklad, Indianapolis, IN) and sacrificed at 21 – 22 weeks of age (one mouse was 36 weeks of age). Male WT mice (n = 8) were received from Jackson Laboratories at 4 - 8 weeks of age and consumed chow diet until sacrifice at 20 weeks of age. Tissues were harvested, weighed, frozen in liquid nitrogen, and stored at -80 ˚C until analysis. Chow pellets were replenished weekly. Study #2 was designed to probe the effects of *Bco1*$^{-/-}$ genotype hepatic vitamin A status in mice consuming a nutritionally defined (vitamin A-sufficient, carotenoid-free, and semi-purified) diet. In addition, the interaction of *Bco1*$^{-/-}$ genotype with age was assessed through evaluation of WT and *Bco1*$^{-/-}$ mice at ≤9, 9, 31, 51, and 71 weeks of age. In this study, male *Bco1*$^{-/-}$ mice (n = 8/age) were weaned from the breeding colony at 3 weeks of age onto a powdered, semi-purified AIN-93G-based diet and sacrificed at ≤9 (range, 5 - 8), 9, 31, 51, or 71 weeks of age. Male WT mice (n = 8/age) consumed the semi-purified diet upon arrival at 4 - 8 weeks of age until sacrifice at the same ages as *Bco1*$^{-/-}$ mice. Tissues were harvested, frozen in liquid nitrogen, and stored at -80 ˚C until analysis. The diet in Study #2 was devoid of carotenoids and contained 1,500 IU retinyl palmitate/kg, which is sufficient to prevent deficiency [1,17]. Composition of the diet in Study #2 was identical to the CON diet described in **Chapter 2** of this dissertation.

Hepatic retinyl ester and free retinol analysis

Briefly, 100 – 150 mg of liver tissue was homogenized in a 1:1 mixture of PBS:absolute ethanol + 0.1% BHT (w/v). Retinyl acetate (1 μg) was spiked into homogenates for calculation of extraction efficiency. To preserve retinyl esters, samples were not saponified. The samples were extracted three times with 5 mL hexane, the nonpolar supernatant was separated by centrifugation (5 min @ 1056 x *g*, 4 ˚C), transferred to a new tube, and dried in a centrifugal evaporator (Savant, Thermo Scientific, Waltham, MA) and with compressed argon. Extracts were stored at -20 ˚C for <48 h before analysis.

An HPLC system consisting of an Alliance e2695 separations module and 2998 photodiode array (PDA) detector (Waters, Milford, MA), with column cooling set to 22 ˚C and sample cooling at 4 ˚C, was used for all analyses. The HPLC conditions for free retinol and retinyl ester separation were modified from a previously published method [18]. A three-component gradient method was composed as follows: mobile phase A: acetonitrile/H_20/glacial acetic acid, 90/10/2; mobile phase B: acetonitrile/methanol, 90/10; mobile phase C: tetrahydrofuran, 100%. Separation was performed on a Supelco® Supelcosil LC-18 250 mm x 4.6 mm x 5 μm analytical column (Sigma-Aldrich, St. Louis, MO) over a total run time of 36.2 minutes, at 0.79 mL/min flow rate, and using the following linear gradient profile: 0 – 6.27 min at 100% A, 6.27 – 9.06 min to 100% B, 9.06 – 16.72 min to 60% B/40% C, 16.72 – 20.90 min hold at 60% B/40% C, 20.90 – 27.87 min to 100% B, 27.87 – 36.23 min back to 100% A. Retinyl palmitate, free retinol, and the retinyl acetate internal standard were identified by comparison to authentic standards (Sigma-Aldrich) and quantified using an external standard curve. Seven additional peaks surrounding the retinyl palmitate peak were identified as putative retinyl esters (retinyl laurate, retinyl linoleate/retinyl palmitoleate co-eluted peaks, retinyl

myristate, retinyl pentadecanoate, retinyl oleate, retinyl heptadecanoate, retinyl stearate) based on comparison to chromatograms from the published literature of retinyl esters positively identified using mass spectrometry [19]. As all retinyl esters share the same chromatophore, the putative retinyl esters were quantified using the retinyl palmitate standard curve.

Hepatic lipid analysis

Total hepatic lipids were extracted with the method of Folch et al. [20]. For TLC-GC lipid analysis, internal standards (50 μg) for cholesteryl esters (C15:0; Sigma-Aldrich), phosphatidylcholine (C17:0, Avanti Polar Lipids, Alabaster, AL) and triglycerides (C17:0, Sigma-Aldrich) were added before extraction. Extracts were separated into cholesteryl ester (CE), phospholipid (PL), triglyceride (TG), and free fatty acid (FFA) pools on channeled Uniplate Silica Gel G (500 μm gel thickness) thin-layer chromatography (TLC) plates (Analtech, Newark DE), resolved with 80:20:1 petroleum ether:ethyl ether:acetic acid. Lipid bands were visualized under UV light with dichlorofluoroscein, scraped into new tubes, and derivatized to fatty acid methyl esters (FAMEs) with 3 mL methanolic HCl and 0.5 mL benzene at 75 ˚C for 90 minutes. FAMEs were extracted with 1.8 mL petroleum ether after addition of 2mL K_2CO_3, dried under argon, and analyzed via gas chromatography (GC). GC analysis was performed on a GC-2010 Plus instrument (Shimadzu Corporation, Kyoto, Japan) equipped with a flame ionization detector set to 250 ˚C. Separation was achieved on a DB-FFAP 15 m x 0.1 mm x 0.1 μm column (Agilent Technologies, Santa Clara, CA). FAMEs were identified by comparison of retention times to 20 authentic standards and quantified as a percent of total fatty acids, as previously demonstrated [21].

Gene expression

Total RNA was extracted from liver tissue of animals in Study #1 using RNEasy Mini spin columns (Qiagen, Valencia, CA) according to manufacturer's instructions. cDNA was synthesized using the High-Capacity Reverse Transcription Kit (Life Technologies, Grand Island, NY). qPCR was carried out with SYBR Green chemistry (Life Technologies) on an ABI 7900 HT qPCR platform (Life Technologies), using pre-designed primer assays (*Scd1, Fasn, Rpl19*; SA Biosciences, Valencia, CA) and pre-designed PCR arrays ("PPAR Targets" and "Lipoprotein and Cholesterol Metabolism" arrays, SA Biosciences). Relative expression (to *Rpl19*) was calculated using the $2^{-\Delta\Delta Ct}$ method. For analysis of the two PCR arrays, identical PCR cycling and threshold parameters were used, raw Ct data were combined into one dataset analyzed together relative to the mean of *Actb* and *B2m* expression, which was averaged across both arrays.

Statistical analysis

Data are presented as mean ± SEM. Statistical analysis was done in SAS v9.3 (SAS Institute, Cary, NC). With the exception of the qPCR array analysis, all data were analyzed with two-way ANOVA and results were considered statistically significant at $p \leq 0.05$. Repeated measures analysis was used to probe the effects of age in Study #2. Letters denoting statistical significance were assigned using a SAS macro that has been previously described [22]. Data were transformed logarithmically when normality assumptions were violated. Individual group variances were used in place of the pooled variance when homogeneity of variance assumptions were violated. Correlations were calculated with PROC CORR and considered significant at $p \leq 0.05$. For qPCR array analysis, pairwise T-tests for each gene were calculated in Excel and considered significant at $p \leq 0.005$.

Results

Effects of *Bco1*$^{-/-}$ genotype on body and organ weight throughout the lifespan of male mice

In Study#1, *Bco1* loss did not alter the body or liver weights of adult (20 - 22 weeks old) chow-fed mice (**Fig. 3.1A, B**). Significant effects of genotype were observed in spleen and brain weights, both of which were reduced in *Bco1*$^{-/-}$ mice, compared to WT (**Fig. 3.1C**). At this age, weights of lungs, kidney, testes, and seminal vesicles were not affected by genotype. Prostate weights were not recorded in this study. In mice of <9, 9, 31, 51, or 71 weeks of age fed a semi-purified, vitamin A-sufficient, carotenoid-free diet (Study #2), significant main effects of genotype and age were observed, as well as significant genotype*age interactions (**Fig. 3.1D-I**). Due to the significant effects of age on body weight (**Fig. 3.1D**), raw organ weights in Study #2 were normalized to body weight and expressed as a percent of total body weight. Significant genotype*age interactions were observed in the liver (**Fig. 3.1E**), brain (**Fig. 3.1F**), testes (**Fig. 3.1G**), seminal vesicles (**Fig. 3.1H**), and kidneys (data not shown). As in Study #1, a significant main effect of genotype reduced brain weight (**Fig. 3.1F**). Prostate weights were not recorded in this study. In every organ collected other than the heart (liver, lung, spleen, kidney, brain, testes, seminal vesicles), a significant main effect of age was observed. Weight of the heart, as a percent of body weight, trended lower in *Bco1*$^{-/-}$ mice at 51 and 71 weeks of age, compared to age-matched WT mice (**Appendix Fig. B.1**). However, heart tissues were not collected in the <9 and 9 week-old groups, and no statistically significant interaction or main effects of genotype and age were observed.

Bco1 loss alters hepatic vitamin A accumulation

BCO1 has a well-established role in mammalian vitamin A metabolism. Therefore, we measured hepatic retinyl ester and free retinol levels, as the liver is the main storage depot for

this vitamin. In Study #1, in which mice did not consume a nutritionally defined diet, *Bco1* loss increased hepatic retinyl ester levels more than two-fold (**Fig. 3.2A**). As expected, retinyl palmitate, identified by comparison to an authentic standard, was by far the predominant retinyl ester present, accounting for >80% of total vitamin A stores (**Fig. 3.2C**). Six additional retinyl esters, putatively identified by comparison of retention times with results from mass spectrometry experiments in the published literature [18,19], demonstrated significantly increased levels of accumulation, in ratios similar to retinyl palmitate. Conversely, levels of free retinol were not significantly modulated by *Bco1* genotype (**Fig. 3.2A**). Overall, although *Bco1* loss doubled total vitamin A stores, the relative abundances of free retinol and retinyl esters were not changed (**Fig. 3.2C**).

Next, in order to rule out the possibility that variations in dietary preformed vitamin A were a cause of the observed increase in hepatic retinyl esters, we repeated the experiment in mice from Study #2, which were fed a nutritionally defined diet. Diets were devoid of provitamin A carotenoids, but were sufficient in preformed vitamin A. Additionally, tissues from Study #2 allowed us to assess potential interactions between genotype and age. *Bco1*$^{-/-}$ genotype strikingly interacted with age to significantly modulate hepatic retinoid storage. As seen in **Fig. 3.2B**, *Bco1* loss at <9 or 9 weeks of age significantly *reduced* hepatic total vitamin A concentrations, whereas loss of the gene at 51 or 71 weeks of age significantly *increased* accumulation by more than 6-fold. Although not significant, *Bco1* loss in 31-week old animals induced a numerical increase in vitamin A levels (>2-fold). As in Study #1, no changes in the relative abundances of retinol or retinyl esters were observed (**Fig. 3.2D**, **Appendix Table B.1**) and changes were driven almost entirely by levels of retinyl palmitate, which accounted for >80% vitamin A at every age (**Appendix Table B.1**). Each of the other six detected retinyl esters were modulated in

the same pattern as retinyl palmitate and total vitamin A stores (**Appendix Table B.1**). *Bco1*$^{-/-}$ genotype did not alter levels of retinol at any age (**Appendix Table B.1**).

Bco1 loss increases hepatic total lipids in adult male mice

Using the Folch method, we assessed total hepatic lipids in both Study #1 and Study #2. As seen in **Figure 3.3A**, *Bco1* loss in adult (20-22 weeks old) male mice resulted in a modest, but statistically significant, increase in total lipid content of the liver. This effect appears to be somewhat variable in middle-aged adults, as lipid accumulation was not different between genotypes at 31 weeks of age in Study #2 (**Fig. 3.3B**). However, separation between the two genotypes appears to progress during aging and is statistically significant at 51 and 71 weeks of age (**Fig. 3.3B**).

Bco1$^{-/-}$ genotype alters the composition of hepatic lipid pools in adult male

Retinoid signaling plays an important role in regulation of lipid metabolism. Therefore, given the observed changes in hepatic vitamin A accumulation, we assessed the percent abundance of 20 unique fatty acid species (derivatized to FAMEs) across four hepatic lipid pools (cholesteryl esters [CE], phospholipids [PL], triglycerides [TG], and free fatty acids [FFA]) in 20 - 22-week old chow-fed WT and *Bco1*$^{-/-}$ mice (**Table 3.1**). Internal standards for CE, PL, and TG were spiked into the sample extraction mixture in known quantities (50 μg), allowing for estimation of the total mass of each of these three lipid pools. We observed numeric increases in total mass of each of the CE, PL, and TG pools in *Bco1*$^{-/-}$ mice, but none of the differences reached statistical significance ($p = 0.26$, $p = 0.19$, and $p = 0.15$, respectively; **Table 3.1**). Within the CE pool, palmitate increased from 10.6 ± 0.58% abundance in WT mice to 24.9 ± 2.32% in *Bco1*$^{-/-}$ mice. Three other minor species (cholesteryl gondoate, cholesteryl eicosadienoate, and cholesteryl erucate), ranging in abundance from 0.02 – 0.12%, were also increased in *Bco1*$^{-/-}$

mice. As FAME species were calculated on the basis of percentage of the total lipid pool, the large increase in cholesteryl palmitate in *Bco1*$^{-/-}$ mice was accompanied by a significant reduction in unidentified peaks (79.4 ± 1.11% vs. 61.3 ± 5.89%). Palmitate was the predominant species in the CE lipid pool, but five additional species (palmitate, stearate, linoleate, arachidonate, and docosahexaenoate) were also in high abundance (>10%) in the PL pool. Changes in this pool were much more subtle than with CEs, and only one of the five high-abundance FAMEs, stearate, was significantly modulated by *Bco1*$^{-/-}$ genotype (15.2 ± 0.31% in WT vs. 16.5 ± 0.29% in *Bco1*$^{-/-}$). Four other minor species (linoleate, gondoate, eicosadienoate, and behenate) were significantly modulated by *Bco1* loss. No lipid species were significantly modulated in the TG pool, which experienced relatively high variability. Finally, free fatty acids were also assayed. Similarly to CEs, levels of palmitate in this lipid pool were increased by *Bco1* loss (17.3 ± 0.95% vs. 20.6 ± 0.31%). Levels of free arachidonate were significantly decreased in *Bco1*$^{-/-}$ mice (2.34 ± 0.36 vs. 1.42 ± 0.04%).

Genes controlling lipid and cholesterol metabolism are altered in livers of adult male *Bco1*$^{-/-}$ mice

To further elucidate the effects of *Bco1* loss, we analyzed mRNA expression of genes controlling hepatic lipid metabolism in 20 - 22-week old chow-fed WT and *Bco1*$^{-/-}$ mice. First, with single-gene qPCR, we measured the expression of *Scd1*, which governs the ∂-9 desaturation of saturated fatty acids such as palmitate, and *Fasn,* which is the rate limiting step for fatty acid synthesis, and which yields palmitate. As seen in **Figure 3.4A**, neither *Scd1* nor *Fasn* mRNA expression was altered by *Bco1*$^{-/-}$ genotype. To further characterize lipid metabolism in *Bco1*$^{-/-}$ mice, we assessed the mRNA expression of 163 genes involved in lipid, lipoprotein, and cholesterol metabolism (**Appendix Table B.2**). These genes were assayed with two separate

qPCR arrays, one focused on PPAR signaling, and the other on lipoprotein and cholesterol metabolism. Data output from both arrays were pooled, normalized, and analyzed together, as described in the **Materials and Methods** section. All 163 genes are shown in a volcano plot in **Figure 3.4**, with expression of the *Bco1*$^{-/-}$ group relative to WT mice as log(fold change) plotted against –log(p-value). Three genes which were regulated at $p \leq 0.05$ but nonetheless had a basal (WT) expression of Ct > 30 (*Mmp9, Src, Smarcd3*) were not considered to be meaningfully expressed and were excluded from further analysis. These are noted as gray x's on the volcano plot. Seven genes were significantly regulated ($p \leq 0.005$; *Apoa4*, *Sorl1*, *Acox3*, *Hsp90ab1*, *Fabp5*, *Gapdh,* and *Slc27a4*), whereas an additional thirteen genes were regulated at $0.005 < p \leq 0.05$ (**Table 3.2**). Most (15 / 20) of the regulated genes were present on only the PPAR signaling targeted qPCR array, whereas only 2 were present only on the lipoprotein and cholesterol metabolism array. Three regulated genes were present on both arrays, and their expression from each array was averaged. Regulated genes encoded lipoproteins or lipoprotein receptors (*Apoa4, Apoa5, Sorl1*), fatty acid binding or transport proteins (*Fabp2, Fabp5, Slc27a1, Slc27a4*), or were involved in β-oxidation (*Cpt1b*, *Acox3, Mlycd*) and PPAR signaling (*Pparg, Ppard, Pprc1*). The predominant liver PPAR isoform, *Ppara*, was not regulated by *Bco1* loss. Genes involved in glycolysis (*Gapdh*) and gluconeogenesis (*Pck1*) were also modulated. Interestingly, *Rxra* and *Rxrb* were upregulated; the proteins translated from these genes are receptors for 9-*cis*-retinoic acid and are transcription factors that heterodimerize with a wide array of nuclear receptors, including PPARs. Notably, genes controlling cholesterol esterification (*Soat1, Soat2, Lcat*) and synthesis (*Hmgcr, Hmgcs1, Hmgcs2*) were not affected. *Scd1* was present in the arrays and was not altered, confirming the previous single-gene qPCR result. Notably, seven genes were regulated ≥ |2|-fold by *Bco1* genotype: *Sorl1* (-3.92, $p = 0.0001$), *Apoa4* (-3.54, $p < 0.0001$),

Fabp5 (-2.85, p = 0.0017), *Slc27a1* (+2.67, p = 0.0095), *Pprc1* (+2.33, p = 0.0105), *Pparg* (+2.32 p = 0.0126), and *Cpt1b* (+2.09, p = 0.0182).

Correlations between hepatic vitamin A stores, lipid species, and gene expression in adult male mice

To gain insight into the potential mechanisms by which *Bco1* loss alters hepatic lipid metabolism, correlation analysis was performed on several endpoints measured in the 20 - 22-week old chow-fed WT and *Bco1*$^{-/-}$ mice. Endpoints were included on the basis of significant regulation by *Bco1*, or as "negative control" variables to validate proposed relationships. All variables included were obtained from measurements in livers of chow-fed animals. Pearson correlation coefficients were calculated between endpoints of vitamin A status (total vitamin A, retinyl palmitate, retinyl stearate, free retinol), lipid species (cholesteryl palmitate, cholesteryl stearate, phospholipid palmitate, phospholipid stearate, free palmitate), gene expression (*Acox3, Cpt1b, Fabp5, Gapdh, Hsp90ab1, Mlycd, Pck1, Ppard, Pparg, Pprc1, Rxra, Rxrb, Slc22a5, Slc27a1, Slc27a4, Sorl1*), and organ weight (brain weight). A complete table of all factorial correlations is shown in **Appendix Table B.1**. Selected correlations are presented in **Fig. 3.5.** Total vitamin A stores, as expected, correlate almost perfectly with retinyl palmitate, the predominant retinyl ester (**Fig. 3.5A**). As seen in **Fig. 3.5B**, no specificity in retinyl esterification is seen, as retinyl stearate also correlated very strongly with total vitamin A levels. Validating this analysis, as expected, free retinol, does not accumulate linearly with total vitamin A stores (**Fig. 3.5C**). In contrast, total vitamin A stores correlate very strongly with cholesteryl palmitate (**Fig. 3.5D**), but not at all with cholesterol stearate (**Fig. 3.5E**), and inversely with phospholipid palmitate (**Appendix Table B.1**), suggesting possible specificity linking vitamin A levels to metabolism of particular lipid species. Furthermore, total vitamin A levels correlate strongly with

genes involved in retinoid signaling (*Rxrb*; **Fig. 3.5G**) and PPAR signaling (*Pparg, Pprc1*; **Fig. 3.5H,I**). Hepatic cholesteryl palmitate levels are significantly correlated with expression of genes governing lipoprotein metabolism (*Sorl1, Apoa4*), fatty acid transport (*Slc27a1*, **Appendix Table B.2**; *Slc27a4* **Fig. 3.5M**), β-oxidation (*Cpt1b, Acox3, Mlycd;* **Appendix Table B.2**), and retinoid and PPAR signaling (*Rxrb, Rxra, Pparg, Pprc1;* **Appendix Table B.2**).

Discussion

The goal of this work was to identify alterations in lipid metabolism occurring as a result of genomic *Bco1* ablation. Given that the liver is the central organ for metabolic regulation, including control of lipid homeostasis, we hypothesized that *Bco1* loss would result in dysregulated hepatic lipid metabolism, as demonstrated by alterations in relative abundance of specific fatty acyl species, as well as by changes in expression of genes governing lipid synthesis, trafficking, and utilization.

First, we observed that chow-fed *Bco1*$^{-/-}$ mice had a roughly 2-fold increase in hepatic vitamin A content, entirely due to increases in concentrations of retinyl esters, and not free retinol. Additionally, despite the difference in absolute abundance between genotypes, no change in retinol esterification substrate preference was detected, as the relative abundances of hepatic retinyl esters in WT and *Bco1*$^{-/-}$ mice were similar, and levels of retinyl palmitate correlated strongly with other retinyl ester species. Importantly, we observed that age dramatically influenced the directionality of the impact of *Bco1* loss on hepatic retinyl ester stores. Whereas young mice (≤9 weeks old) demonstrated a reduction in retinyl ester stores with *Bco1* loss, *Bco1*$^{-/-}$ mice at 51 or 71 weeks of age experienced up to a 6.7-fold increase in accumulation. *Bco1*$^{-/-}$ mice at 31 weeks of age accumulated numerically more retinyl esters than age-matched

WT mice (+2-fold), but this was not statistically significant. This suggests the existence of a physiologically relevant interaction between *Bco1* and factors changing within the liver during the development and aging process. Furthermore, in animals > 9 weeks of age, we observed the same pattern of retinyl ester accumulation in mice fed either rodent chow (Study #1) or a nutritionally defined, carotenoid-free, modified AIN-93G diet (Study #2). This is notable, as the rodent chow used in Study #1 contained roughly 10-fold more preformed vitamin A than the nutritionally defined diet used in Study #2 (1,500 IU/kg diet). Importantly, the levels provided in Study #2 are sufficient to prevent hypovitaminosis A in mice [23]. Our data show that *Bco1* loss results in a doubling of hepatic retinyl ester content in adult male mice, even when fed diets ranging from 1,500 IU vitamin A/kg diet to at least 16,000 IU vitamin A/kg diet. Secondly, and perhaps most importantly, *Bco1* impacts hepatic vitamin A storage in a highly age-dependent manner.

To date, twenty studies have utilized the *Bco1*$^{-/-}$ mouse model [1–5,17,24–37]. Vitamin A source (preformed vs. provitamin A carotenoid) is a crucial detail when comparing the results from the current study to others in the literature that have utilized the *Bco1*$^{-/-}$ model. Ten of the twenty published *Bco1*$^{-/-}$ studies did not report levels of hepatic vitamin A [5,25,27,28,30–32,35–37]. Of the ten studies that have reported levels of hepatic retinol or retinyl esters, one study [33] provided β-carotene to WT and *Bco1*$^{-/-}$ as the sole source of dietary vitamin A, precluding comparisons between *Bco1*$^{-/-}$ mice in that study and those in our current investigation. However, wild-type mice in that study (which were of the same strain as those used in our current study) accumulated hepatic retinyl esters and free retinol at approximately 1,000 and 5 nmol/g tissue, respectively. These values are both very similar to levels we observed in our WT mice. In another study allowing direct comparison, van Helden et al. provided WT and *Bco1*$^{-/-}$ mice with 1,500 IU

preformed vitamin A/kg diet (as in the current Study #2) and reported hepatic free retinol levels of approximately 6 and 8 nmol/g in WT and *Bco1*$^{-/-}$ mice, respectively [31]. Again, these levels are very similar to those we have observed. However, it does not appear that the authors measured hepatic levels of retinyl esters or total vitamin A, preventing further comparison. The final publication amenable to direct comparison also fed a basal diet of 1,500 vitamin A IU/kg, but reported no change in hepatic "stored retinol" levels [2]. However, this was included as "data not shown" and details on hepatic tissue extraction methods (i.e., saponification) are not provided, making interpretation difficult. Seven remaining studies exist in which hepatic vitamin A levels are reported, but they vary in levels of dietary vitamin A provided, β-carotene supplementation, and age of mice used (embryonic, juvenile, or adult). Hessel et al., when feeding 14,000 IU vitamin A/kg in chow, reported no difference between 25-week-old WT and *Bco1*$^{-/-}$ mice in total hepatic vitamin A – both genotypes accumulated 3 ± 0.2 μmol/g [1]. These levels are approximately 100% higher than we have observed in *Bco1*$^{-/-}$ mice and 200% greater than recorded in WT mice. Others reported that breeding *Bco1*$^{-/-}$ dams maintained on a purified 25,000 IU/kg diet experienced a non-significant increase in hepatic retinyl esters, compared to WT [29], but levels were much lower (622 nmol/g) than reported in either of our current studies. In another study from the same authors, adult (16 week-old) female mice fed an 18,000 IU/kg chow diet experienced no change in hepatic retinyl esters, but the authors did observe significant increases (>2-fold) in renal and splenic retinyl esters [4]. Deletion of the enzyme primarily responsible for retinol esterification, lecithin:retinol acyltransferase (*Lrat*), abolished this effect in *Bco1*$^{-/-}$/*Lrat*$^{-/-}$ mice, suggesting that *Bco1* may influence retinyl esterification through *Lrat*. In conflict with this, however, is the fact that retinyl ester levels in the liver are highly dependent upon *Lrat* [38], and yet, Kim et al. observed no alterations in hepatic retinyl ester accumulation in

the *Bco1*$^{-/-}$/*Lrat*$^{+/+}$ strain. Tissue-specific activities of a separate acyl CoA:retinol acyltransferases (ARAT) may explain these discrepancies. A study in juvenile mice (6 weeks old) found no alterations in hepatic retinyl ester levels in male or female *Bco1*$^{-/-}$ mice maintained on 25,000 IU/kg vitamin A chow [24]. Finally, studies in embryos have shown that loss of *Bco1* reduced retinyl esters in fetal total homogenates [3], although tissue-specific measurements demonstrated a non-significant reduction in embryonic liver [4]. Vitamin A levels in chow diets fed to dams in these two studies were 29,000 IU/kg and 18,000 IU/kg, respectively. Although *Lrat* mRNA expression was reduced in whole *Bco1*$^{-/-}$ embryos and livers of *Bco1*$^{-/-}$ embryos [4,29], *Bco1* loss did not fully abolish retinol esterification in embryos *in vitro* or *in vivo* [3,29], suggesting that LRAT may work in conjunction with other ARAT enzymes to link *Bco1* status to retinyl esterification. Others have shown LRAT to play a role in the effects of *Bco1* loss on retinyl esterification, but as we have not yet investigated *Lrat* expression in the livers of our mice, we can only speculate on this point at this time.

Several other mechanisms to explain increased accumulation of retinyl esters in adult *Bco1*$^{-/-}$ may be mechanistically plausible. Elevated food intake in *Bco1*$^{-/-}$ mice, compared to WT, would putatively increase supply of dietary vitamin A and thus could lead to increased hepatic storage. We did not measure food intake in either of our present studies. However, to match patterns of accumulation seen, young *Bco1*$^{-/-}$ mice would have to consume much less diet than their WT counterparts, whereas older mice would need to consume a great deal more. Apart from the lack of a parsimonious mechanistic explanation for such changes in food intake, body weights were very similar at all ages and do not reflect the vast differences in caloric intake that would seem necessary for dietary vitamin A intake to be causative of the hepatic accumulations observed. Therefore, it is unlikely that changes in food intake are a cause of the effects seen.

Another possibility may involve decreased turnover of retinoids in the livers of *Bco1*$^{-/-}$ mice, thus requiring increased esterification for storage and prevention of retinoid-induced toxicity. Bco2 catalyzes the eccentric cleavage of a diverse array of carotenoids at the 9′,10′ (or 9,10) double bond [39]. Bco2 can cleave both the 9,10 as well as the 9',10' double bonds from a *single* molecule of β-carotene [39], suggesting that Bco2 may degrade retinol or retinal. *Bco2* expression is increased in both hepatocytes and hepatic stellate cells isolated from 11-week-old *Bco1*$^{-/-}$ mice [26]. If the observed ≤9 week-old retinyl ester accumulation phenotype persists until 11 weeks of age, it is plausible that Bco2 clearance of retinol/retinal may account for the changes seen at these ages. However, for the mechanism to be internally consistent, Bco2 expression would need to be depressed by ~20 weeks of age and persist (or decrease yet further) through 71 weeks of age. This remains to be seen.

Differences in retinyl ester stores in the liver may be affected by distribution of retinol to extra-hepatic tissues. Decreased export of retinol in complex with retinol binding protein 4 (RBP4) may lead to elevated hepatic retinyl ester levels. This hypothesis also fails scrutiny, however. Hessel et al., in the first paper describing the *Bco1*$^{-/-}$ model, show that RBP4 protein levels are equivalent or slightly increased in *Bco1*$^{-/-}$ mice, compared to WT mice, even when raised on a vitamin A-sufficient diet [1]. Although we have not measured hepatic RBP4 expression or retinyl esters in extraheptic tissues in our mice, the data from Hessel et al. do not support the likelihood of a defect in retinol export to peripheral tissues.

Finally, a fourth mechanism may affect retinyl ester accumulation in the liver. Retinyl ester hydrolases (REHs) are a functional group of enzymes (rather than family of sequence homologues), which are involved in multiple steps of vitamin A absorption and metabolism [40,41]. In the liver, REHs hydrolyze retinyl esters to liberate retinol for transport to peripheral tissues.

Lipoprotein lipase, which serves as an REH in the liver [40], was not significantly modulated by *Bco1*$^{-/-}$ genotype in our mice (**Appendix Table B.3**). However, other enzymes with REH activity may have been altered. In particular, adipose triglyceride lipase (ATGL), which is expressed in the liver, is a highly effective triglyceride hydrolase and REH *in vitro* [42]; *in vivo*, liver-specific knockdown of ATGL increases hepatic TG accumulation (it appears that no studies have examined retinyl esters in liver-specific ATGL knockdown/knockout mice) [43,44]. Thus, hepatic depression of ATGL expression in *Bco1*$^{-/-}$ mice may unify changes observed in both lipid and retinyl ester accumulation. This warrants future investigation.

Potentially relevant to the alterations in retinyl esters, we observed alterations in the weights of several organs in *Bco1*$^{-/-}$ mice. Brain weight was decreased by a main effect of *Bco1*$^{-/-}$ genotype in both Studies #1 and #2, spleen weight was decreased by genotype in Study #1 only, and seminal vesicle weight was modulated by a genotype*age interaction in Study #2. It is well established that vitamin A is necessary for proper embryological development due to the pro-differentiative effects of retinoic acid. Kim et al. have previously shown that, when dams are maintained on a vitamin A deficient diet, adding *Bco1*$^{-/-}$ to an *Rbp*$^{-/-}$ background can produce structural abnormalities in fetuses, including exencephaly [29]. Moreover, vitamin A deficiency can produce decreases in cerebral volume that correlate very highly with retinol status [45], and depletion of retinoic acid in adult mice inhibits neurogenesis [46]. Vitamin A deficiency alters cell number and immunological capacity in the spleen [47,48], and we have already demonstrated that *Bco1*$^{-/-}$ loss affects seminal vesicle weight in young (9-14-week old) mice through modulation of serum testosterone levels (**Chapter 2** of this dissertation). Androgen status is known to modulate the metabolism of carotenoids in the liver [49] and low retinoid status has been shown to impact testicular steroidogenesis [50,51]. Further speculation would be unwise without more evaluations of

the affected peripheral organs, but it is plausible that modulation of vitamin A status in *Bco1*$^{-/-}$ mice may directly or indirectly alter brain, seminal vesicle, and spleen biology.

Three points arise from evaluation of previous and current work: 1) levels of dietary vitamin A >1,500 IU/kg diet do not alter the effect of *Bco1* genotype on hepatic retinyl accumulation, 2) *Bco1* genotype may modulate hepatic retinol esterification through LRAT or REH activity, whereas in extra-hepatic tissues, other enzymes with ARAT activity may be important, and 3) directionality of this effect appears to be dependent on age or developmental stage.

Next, focusing on the livers from 20 - 22 week-old chow-fed mice, we measured the relative abundance of 20 FAME species in each of four distinct hepatic lipid pools, as well as gene expression of 164 genes involved in lipid and cholesterol metabolism. Although not statistically significant, *Bco1* loss numerically increased the total pools of CEs, PLs, and TGs by 73%, 27%, and 60%, respectively (an internal standard was not used in the free fatty acid pool, precluding a similar estimation). In agreement with this, Hessel et al. have previously reported that 25-week-old *Bco1*$^{-/-}$ on vitamin A-sufficient chow (14,000 IU/kg diet) experience significant increases in hepatic TGs, and more generally, total lipids [1]. This effect is amplified when exposed to vitamin A-deficient and high-fat diets [1,26]. We have previously reported that histological assessment of livers from female *Bco1*$^{-/-}$ mice reveals increases in lipidosis [5], and analysis of male mice from both studies revealed significant increases in hepatic total lipids with *Bco1* loss (**Fig. 3.3**).

In contrast to our measurements in retinyl esters, we observed that *Bco1*$^{-/-}$ genotype significantly modulated the abundance of *specific* lipid species, most notably by significantly doubling cholesteryl palmitate abundance, increasing phospholipid stearate, increasing free

palmitic acid, and reducing free arachidonic acid. Within livers of chow-fed animals, cholesteryl palmitate levels, but not levels of cholesteryl stearate, correlated very strongly with total levels of vitamin A, suggesting that total stores of vitamin A may influence the formation of specific species of cholesteryl esters. Additionally, levels of cholesteryl palmitate did not correlate with levels of free retinol. Free retinol accounts for <1% of total retinoid in the liver, is tightly bound to cellular retinol binding proteins (CRBPs), and is little more than a transient intermediate in the tightly regulated conversion of stored retinyl esters to retinoic acid, which is at cellular concentrations 100- to 1,000-fold lower than even retinol [52]. Thus, although hepatic retinyl esters are an inert bulk storage form of vitamin A, they represent retinoid capacity much more accurately than does the level of free retinol. Blaner and colleagues demonstrate this elegantly, showing that although hepatic retinyl esters are nearly completely eliminated in *Lrat*$^{-/-}$ mice, retinoic acid levels are also reduced, rather than increased [53]. A correlation with hepatic total vitamin A suggests that retinoid signaling may be associated with levels of cholesteryl palmitate, and the lack of correlation with free retinol bolsters this hypothesis by serving as a "negative control".

Whereas we observed a doubling in cholesteryl palmitate levels and a non-significant increase in total CEs in adult *Bco1*$^{-/-}$ mice, others have reported *Bco1* loss to significantly decrease both of these endpoints in day 14.5 *post coitus* embryos [3,4]. The same authors also report that *Bco1*$^{-/-}$ embryos had 22 - 32% lower ($p < 0.05$) levels of phosphatidylcholines and phosphatidylethanolamines with 36:4 total carbons:unsaturated double bonds, which would be predicted to contain either 18:1 and 18:3 fatty acids or two 18:2 fatty acids [3]. Our results show that *Bco1*$^{-/-}$ genotype resulted in a 22% decrease in phospholipid pool linoleate (18:3), in line with these previous results. Additionally, Dixon et al. report that 40:6 phosphatidylcholines and

phosphatidylethanolamines, which likely contain one each of the 22:6 and 18:0 lipid species, are reduced 30 – 35% by *Bco1*$^{-/-}$ genotype. We observed no changes in phospholipid docosahexaenoate (22:6), but find that levels of stearate (18:0) in phospholipids were significantly elevated by approximately 9%. A methodological difference is worth noting: as these authors [3] utilized LC/MS on non-methylated lipid extracts, species detected were intact phospholipids and not individual fatty acids; our method used derivitization to FAMEs and GC-FID measurement of individual fatty acid species. Overall, our results in adult *Bco1*$^{-/-}$ mice – although at times contradictory to the directionality of effects observed in *Bco1*$^{-/-}$ embryos – support the hypothesis that *Bco1* genotype alters lipid esterification and may do so in a developmentally divergent manner. This is made more plausible by the earlier observation of an age-dependent effect of *Bco1* genotype on accumulation of hepatic retinyl esters.

Fatty acid synthase (*Fasn*) catalyzes the conversion of acetyl-CoA to malonyl-CoA for lipid biosynthesis, whereas stearyl-CoA desaturase 1 (*Scd1)* is responsible for the first step in desaturation of saturated fatty acids, such as palmitate [54]. Thus, these two genes play important roles in the control of *de novo* lipid biosynthesis. We observed an accumulation of palmitate in the hepatic CE and FFA pools of *Bco1*$^{-/-}$ mice, as well as accumulation of stearate in PLs. Hessel et al. reported a reduction in hepatic *Scd1* expression in *Bco1*$^{-/-}$ mice, which might be expected to reduce the conversion of saturated fatty acids like palmitate and stearate to their monounsaturated products, resulting in accumulation of the saturated fatty acid substrate. Contrary to this hypothesis, we did not observe a similar reduction in gene expression as observed by Hessel et al., either when we measured *Scd1* mRNA expression in single-gene qPCR experiments, or *via* PCR array. However, similar to the previous report [1], we observed no change in *Fasn* expression. Therefore, it seems that regulation of *de novo* lipogenesis and

desaturation cannot explain the accumulation of saturated FAMEs that we observed in the CE, PL, and FFA pools.

Uptake of free fatty acids into tissues from the circulation occurs *via* both unregulated and receptor-mediated mechanisms. Thus, increased tissue levels of free fatty acids may alternatively reflect increased uptake, rather than increased *de novo* synthesis. Interestingly, others have reported that cardiac free fatty acids, including free palmitate, were increased in *Bco1*$^{-/-}$ mice, as was mRNA expression of *Lpl* and the lipid transporter *Cd36* [35]. Similarly, we observed both a significant increase in hepatic free palmitate, as well as a 1.6-fold increase in hepatic *Cd36* expression; however, this change in *Cd36* gene expression was not statistically significant.

Cholesterol esterification is accomplished through the actions of cellular acyl-CoA cholesterol acyl transferase (ACAT, also called SOAT; not to be confused with the ACAT enzymes involved in β-oxidation), of which two isoforms exist (referred to hereafter by gene names *Soat1* and *Soat2*). Another enzyme, LCAT, is produced in the liver, secreted into circulation in association with lipoproteins, and serves to convert free cholesterol to CEs in maturing HDL lipoproteins. Fatty acid species display varying efficiencies of incorporation into CEs, with V_{max} for palmitate being ~53-fold higher than for stearate [55]. This may be due to substrate-specific differences in enzyme activity [56,57], or due to changes in enzyme expression under various fatty acid exposures [58]. While cholesteryl palmitate levels more than doubled in chow-fed *Bco1*$^{-/-}$ mice compared to WT, no significant changes in expression of genes controlling cholesterol synthesis (*Hmgcr, Hmgcs1, Hmgcs2*) or esterification (*Soat1, Soat2, Lcat)* were observed (**Appendix Table B.2**). However, other than palmitate, only linoleate (29.0%) was routinely detected in WT livers at ≥5% of total free fatty acids, and palmitate is esterified to

cholesterol more readily than is linoleate [55,57]. Whether arising from passive uptake, receptor-mediated uptake (*Cd36* or hepatic lipase *Lipc*), or another mechanism, minor increases in hepatic free palmitate levels observed in *Bco1*$^{-/-}$ mice (20%) may be amplified to larger differences in levels of the esterified fatty acid due to substrate preferences of cholesterol esterifying enzymes.

Apolipoprotein A-IV (*Apoa4*) is normally induced by SREBP-1a in response to lipid accumulation, increasing TG export through VLDL expansion [59]. Thus, *Apoa4* serves to reduce hepatic lipid burden. However, despite strong down regulation of *Apoa4* in our chow-fed *Bco1*$^{-/-}$ mice compared to WT, total hepatic TGs trended higher (+60%, p = 0.15; **Table 1**). These data appear to be contradictory; however, it is possible that *Apoa4* expression is reduced as a cause, and not consequence, of changes in hepatic TG content. Knockout of *Apoa4* results in a non-significant increase in hepatic TGs, whereas overexpression significantly decreases hepatic TG levels [59]. Forced down regulation of *Apoa4* could inhibit TG export to VLDL, potentially resulting in hepatic TG accumulation. Multiple transcriptional regulators of *Apoa4* have been identified, including genes identified in this study as modulated by *Bco1*$^{-/-}$ genotype (*Rxra, Rxrb, Ppard*; [60–62]). Lending further support to this hypothesis, ApoA-IV protein suppresses gluconeogenesis through transcriptional repression of *Pck1* and *G6pc* in primary mouse hepatocytes through the nuclear receptor NR1D1 [63]; we find that hepatic *Pck1* expression is significantly upregulated in *Bco1*$^{-/-}$ mice (1.72, p = 0.018). Whether – and how – repression of *Apoa4* is a direct contributor to the hepatic lipidosis that has been repeatedly observed in the *Bco1*$^{-/-}$ strain requires further study, but it provides a mechanistically plausible hypothesis for investigation.

Gene expression analysis also revealed that expression of sortilin-related receptor LDLR class A (*Sorl1*) was repressed nearly 4-fold in *Bco1*$^{-/-}$ livers, compared to WT. This gene was the

most strongly regulated of all 164 genes investigated and encodes a lipoprotein receptor (which has at times been called SORLA, SorLA-1, LR11, and LRP9) responsible for the uptake of apoE-rich VLDL [64–66]. Vongpromek et al. have shown that triglyceride-rich lipoproteins, but not LDL or HDL, induce *Sorl1* mRNA and protein expression in HepG2 cells [64] and Sugiyama et al. showed that provision of ^{14}C-labeled oleate in apoE-rich VLDLs resulted in accumulation of cholesteroyl ^{14}C-oleate in cells overexpressing *Sorl1* [65]. Thus, like *Apoa4,* the decrease that we observe in *Sorl1* expression in *Bco1*$^{-/-}$ liver tissue is perplexing. Indeed, contrary to expectation, relative *Sorl1* expression correlates negatively with cholesterol palmitate levels in chow-fed mice (**Appendix Table B.1**). However, the administration of PPARγ ligands (conjugated linoleic acid, troglitazone, and 15-deoxy-Δ-12,14-prostaglandin J_2) both i*n vitro* and *in vivo* reduced *Sorl1* mRNA and protein expression, and effects which were abolished *in vitro* by treatment with a PPARγ antagonist [67]. Thus, PPARγ, which is significantly upregulated at the transcript level in livers of *Bco1*$^{-/-}$ mice (+2.32-fold, $p = 0.013$), negatively regulates *Sorl1*. It appears that the inverse relationship observed between *Sorl1* expression and cholesteryl palmitate is likely an artifact of the mediating effects of PPARγ, as PPAR signaling likely accounts for other accepts of the phenotype observed in *Bco1*$^{-/-}$ as well.

Fatty acid transfer protein (FATP) 4, gene name *Slc27a4*, was significantly ($p = 0.0029$) up regulated in the livers of chow-fed *Bco1*$^{-/-}$ mice. PPARγ ligands induce expression of *Slc27a4* and do so synergistically with 9-*cis*-retinoic acid, the ligand for RXRs [68,69]. Additionally, although *Slc27a4* belongs to the FATP family, it is actually a weak fatty acid transporter [70] and functions rather as an acyl-CoA synthetase with substrate specificity towards long- and very long-chain fatty acid synthesis [71]. Indeed, overexpression of *Slc27a4* into hepatic Huh-7 cells demonstrated a preference for palmitoyl-CoA synthetase activity over oleoyl-CoA synthetase

activity [72]. Thus, PPARγ-induced *Slc27a4* expression increases capacity for palmitoyl CoA synthesis, increasing levels of free palmitate and providing substrate for enhanced esterification of palmitate to cholesterol. This may explain the >2-fold accumulation of cholesteryl palmitate we observe in chow-fed *Bco1*$^{-/-}$ mice, although the mechanism by which circulating FFAs contribute to the hepatic palmitate pool, described earlier, may also play a minor role.

A conceptual model summarizing the effects of *Bco1* loss on hepatic lipid and retinoid metabolism is shown in **Fig. 3.5**. Our current data demonstrates that *Bco1* loss evokes age-dependent effects on hepatic retinyl ester accumulation; although the mechanism for this is not yet clear, several plausible mediators may be involved. We have also shown that expression of *Pprc1, Pparg, Rxra,* and *Rxrb* are induced in adult *Bco1*$^{-/-}$ mice, potentially mediating expression of downstream PPRE-containing target genes through 9-*cis*-RA-mediated signaling. Hepatic *Rxrb, Rxra, Pparg,* and *Pprc1* mRNA expression all correlate strongly with total hepatic vitamin A levels, which other investigators have shown are positively associated with concentrations of the active retinoid signaling metabolites. In accordance with this model, we have observed that hepatic cholesteryl palmitate is elevated in *Bco1*$^{-/-}$ mice; this is a major product of the PPARγ-induced acyl-CoA synthetase, FATP4 (gene name *Slc27a4*); expression of *Slc27a4* correlates with both cholesteryl palmitate concentrations and mRNA expression of *Pparg*, *Rxrb,* and *Rxra*. We have documented elevated levels of hepatic free palmitate in *Bco1*$^{-/-}$ mice, which may provide substrate to FATP4 for cholesteryl palmitate synthesis. Free palmitate, in turn, may arise from either passive or active uptake. We observed a non-significant increase in hepatic expression of the fatty acid transporter CD36 with *Bco1* loss, while others have observed this to be significantly elevated in both adipose and heart tissues of *Bco1*$^{-/-}$ mice [1,35]. While we did not measure circulating free fatty acids, others have reported increased plasma concentrations with

Bco1 ablation [1]. Absorbed free fatty acids may be shunted through the triglyceride synthesis pathway and the rate-limiting enzyme, DGAT, to induce TG storage; this would agree with the hepatic lipidosis we and others have observed with *Bco1* loss. While hepatic *Apoa4* and *Sorl1* were the most strongly regulated genes identified in our analysis (both downregulated nearly 4-fold), due to the counteracting effects of their translated proteins on TG-rich lipoprotein import/export, *Bco1* loss may mediate hepatic lipid accumulation through altered lipid metabolism *in situ*, rather than *via* lipoprotein-mediated lipid transport.

Conclusions

Several conclusions can now be made, although other hypotheses must still be tested. First, adult male *Bco1*$^{-/-}$ mice accumulate 2-6-fold more hepatic retinyl esters than do WT mice, with no detectable fatty acyl substrate preference. Second, this accumulation is highly dependent on developmental age, as data from juvenile mice in our studies, and embryonic data from others, demonstrate significant decreases in retinyl esters as a result of *Bco1* loss. Third, it is clear from our own work and that of others that a wide span of dietary vitamin A (ranging from 1,500 IU/kg to nearly 30,000 IU/kg) does not modify the effect of *Bco1*$^{-/-}$ genotype on retinyl ester accumulation. Fourth, in adult mice, total hepatic lipid content is increased and patterns of lipid esterification are altered by *Bco1* loss, as evidenced by alterations in unique fatty acid species, most notably in our study being cholesteryl palmitate. Although details of this latter result have not been consistent across comparisons to work in other labs, other investigators have indeed reported changes in unique fatty acid species due to *Bco1* loss. Variability in outcomes may be a result of an interaction between *Bco1*$^{-/-}$ genotype and developmental stage, as in patterns of retinyl ester accumulation. Further work is needed to clarify this issue. Fifth, changes

in organ weights (brain, spleen, and seminal vesicle) may be a direct result of altered vitamin A status, or an indirect result (e.g., seminal vesicles per the mechanism described in **Chapter 2**); however, more work is needed before further speculation on this matter. Finally, PPAR/RXR signaling may explain the altered hepatic metabolism observed in *Bco1*$^{-/-}$ mice. *Apoa4* mRNA expression is significantly down regulated in chow-fed *Bco1*$^{-/-}$ livers, nearly 4-fold, potentially reducing the capacity for TG export to VLDL and providing a mechanism that may explain the commonly reported hepatic lipidosis observed in *Bco1*$^{-/-}$ mice. A retinoid-*Pparg*-*Slc27a4* mechanism is proposed to account for a PPAR/RXR role in lipid metabolism: in *Bco1*$^{-/-}$ mice, altered retinoid signaling at RXR/PPARγ heterodimers induces the expression of *Slc27a4*, a long-chain acyl-CoA synthetase, driving palmitoyl-CoA formation, which is incorporated into cholesteryl palmitate esters.

This work has provided some clarity to the impact of *Bco1* on hepatic retinoid and lipid metabolism, but now more questions have emerged. Future studies are needed to answer some of these new questions; for example, do LRAT or tissue-specific ARAT enzymes mediate the age-dependent effect of *Bco1* loss on retinyl ester accumulation? What is the mechanism of interaction between *Bco1* and *Lrat*? Is altered expression of retinyl ester hydrolases or *Bco2* also involved? Does inhibition of PPARγ signaling ablate the effects of *Bco1* loss on hepatic lipid metabolism? Despite these critical uncertainties, at this point, we can conclude that *Bco1*$^{-/-}$ genotype 1) impacts hepatic retinyl ester pools in an age-dependent manner, 2) alters hepatic lipid metabolism, and 3) may do so through alterations in PPAR signaling. Additionally, we observe that PPAR signaling is associated with retinyl ester concentrations, suggesting a potential mechanism involving retinoid-PPAR activity. The manner through which *Bco1* impacts

retinol and lipid metabolism independent of its carotenoid cleavage function will continue to be an area of intense interest.

References cited

1. Hessel, S. *et al.* CMO1 deficiency abolishes vitamin A production from beta-carotene and alters lipid metabolism in mice. *J. Biol. Chem.* **282,** 33553–61 (2007).
2. Amengual, J. *et al.* Beta-carotene reduces body adiposity of mice via BCMO1. *PLoS One* **6,** e20644 (2011).
3. Dixon, J. L., Kim, Y.-K., Brinker, A. & Quadro, L. Loss of β-carotene 15,15'-oxygenase in developing mouse tissues alters esterification of retinol, cholesterol and diacylglycerols. *Biochim. Biophys. Acta* **1841,** 34–43 (2014).
4. Kim, Y.-K., Zuccaro, M. V., Costabile, B. K., Rodas, R. & Quadro, L. Tissue- and sex-specific effects of β-carotene 15,15′ oxygenase (BCO1) on retinoid and lipid metabolism in adult and developing mice. *Arch. Biochem. Biophys.* **572,** 11–18 (2015).
5. Ford, N. A., Elsen, A. C. & Erdman Jr., J. W. Genetic ablation of carotene oxygenases and consumption of lycopene or tomato powder diets modulate carotenoid and lipid metabolism in mice. *Nutr. Res.* **33,** 733–42 (2013).
6. Borel, P. *et al.* Genetic variants in BCMO1 and CD36 are associated with plasma lutein concentrations and macular pigment optical density in humans. *Ann. Med.* **43,** 47–59 (2011).
7. Clifford, A. J. *et al.* Single nucleotide polymorphisms in CETP, SLC46A1, SLC19A1, CD36, BCMO1, APOA5, and ABCA1 are significant predictors of plasma HDL in healthy adults. *Lipids Health Dis.* **12,** 66 (2013).
8. Feigl, B., Morris, C. P., Voisey, J., Kwan, A. & Zele, A. J. The relationship between BCMO1 gene variants and macular pigment optical density in persons with and without age-related macular degeneration. *PLoS One* **9,** e89069 (2014).

9. Ferrucci, L. *et al.* Common variation in the beta-carotene 15,15'-monooxygenase 1 gene affects circulating levels of carotenoids: a genome-wide association study. *Am. J. Hum. Genet.* **84,** 123–33 (2009).

10. Hendrickson, S. J. *et al.* Beta-carotene-15,15'-monooxygenase 1 single nucleotide polymorphisms in relation to plasma carotenoid and retinol concentrations in women of European descent. *Am. J. Clin. Nutr.* **96,** 1379–1389 (2012).

11. Hendrickson, S. J. *et al.* Plasma carotenoid- and retinol-weighted multi-snp scores and risk of breast cancer in the national cancer institute breast and prostate cancer cohort consortium. *Cancer Epidemiol. Biomarkers Prev.* **22,** 927–936 (2013).

12. Leung, W. C. *et al.* Two common single nucleotide polymorphisms in the gene encoding beta-carotene 15,15'-monoxygenase alter beta-carotene metabolism in female volunteers. *FASEB J.* **23,** 1041–53 (2009).

13. Lietz, G., Oxley, A., Leung, W. & Hesketh, J. Single nucleotide polymorphisms upstream from the beta-carotene-15,15'-monooxygenase gene influence provitamin A conversion efficiency in female volunteers. *J. Nutr.* **142,** 161S–165S (2012).

14. Lobo, G. P. *et al.* Genetics and diet regulate vitamin A production via the homeobox transcription factor ISX. *J. Biol. Chem.* **288,** 9017–27 (2013).

15. Perry, J. R. B. *et al.* Circulating beta-carotene levels and type 2 diabetes-cause or effect? *Diabetologia* **52,** 2117–21 (2009).

16. Wang, T. T. Y., Edwards, A. J. & Clevidence, B. A. Strong and weak plasma response to dietary carotenoids identified by cluster analysis and linked to beta-carotene 15,15'-monooxygenase 1 single nucleotide polymorphisms. *J. Nutr. Biochem.* **24,** 1538–46 (2013).

17. Lindshield, B. L. *et al.* Lycopene biodistribution is altered in 15,15'-carotenoid monooxygenase knockout mice. *J. Nutr.* **138,** 2367–2371 (2008).

18. Schäffer, M. W. *et al.* Qualitative and quantitative analysis of retinol, retinyl esters, tocopherols and selected carotenoids out of various internal organs form different species by HPLC. *Anal. Methods* **2,** 1320–1332 (2010).

19. Wingerath, T., Kirsch, D., Spengler, B., Kaufmann, R. & Stahl, W. High-performance liquid chromatography and laser desorption / ionization mass spectrometry of retinyl esters. *Anal. Chem.* **69,** 3855–3860 (1997).

20. Folch, J., Lees, M. & Stanley, G. H. S. A simple method for the isolation and purification of total lipids from animal tissues. *J. Biol. Chem.* **226,** 497–509 (1957).

21. Masood, A., Stark, K. D. & Salem Jr., N. A simplified and efficient method for the analysis of fatty acid methyl esters suitable for large clinical studies. *J. Lipid Res.* **46,** 2299–2305 (2005).

22. Piepho, H. P. A SAS macro for generating letter displays of pairwise mean comparisons. *Commun. Biometry Crop Sci.* **7,** 4–13 (2012).

23. National Research Council. *Nutrient requirements of laboratory animals, Revised fourth edition.* (National Academies Press, 1995).

24. Fierce, Y. *et al.* In vitro and in vivo characterization of retinoid synthesis from beta-carotene. *Arch. Biochem. Biophys.* **472,** 126–38 (2008).

25. Lobo, G. P. *et al.* ISX is a retinoic acid-sensitive gatekeeper that controls intestinal beta,beta-carotene absorption and vitamin A production. *FASEB J.* **24,** 1656–66 (2010).

26. Shmarakov, I. *et al.* Hepatic stellate cells are an important cellular site for β-carotene conversion to retinoid. *Arch. Biochem. Biophys.* **504,** 3–10 (2010).

27. van Helden, Y. G. J. *et al.* Knockout of the Bcmo1 gene results in an inflammatory response in female lung, which is suppressed by dietary beta-carotene. *Cell. Mol. Life Sci.* **67,** 2039–56 (2010).

28. van Helden, Y. G. J. *et al.* Downregulation of Fzd6 and Cthrc1 and upregulation of olfactory receptors and protocadherins by dietary beta-carotene in lungs of Bcmo1-/- mice. *Carcinogenesis* **31,** 1329–1337 (2010).

29. Kim, Y.-K. *et al.* β-Carotene and its cleavage enzyme β-carotene-15,15'-oxygenase (CMOI) affect retinoid metabolism in developing tissues. *FASEB J.* **25,** 1641–1652 (2011).

30. van Helden, Y. G. J. *et al.* Beta-carotene affects gene expression in lungs of male and female Bcmo1 (-/-) mice in opposite directions. *Cell. Mol. Life Sci.* **68,** 489–504 (2011).

31. van Helden, Y. G. J. *et al.* Gene expression response of mouse lung, liver and white adipose tissue to β-carotene supplementation, knockout of Bcmo1 and sex. *Mol. Nutr. Food Res.* **55,** 1466-1474 (2011).

32. Ford, N. A., Moran, N. E., Smith, J. W., Clinton, S. K. & Erdman Jr., J. W. An interaction between carotene-15,15'-monooxygenase expression and consumption of a tomato or lycopene-containing diet impacts serum and testicular testosterone. *Int. J. Cancer* **131,** E143–8 (2012).

33. Amengual, J. *et al.* Two carotenoid oxygenases contribute to mammalian provitamin A metabolism. *J. Biol. Chem.* **288,** 34081–96 (2013).

34. van Helden, Y. G. J., Godschalk, R. W. L., van Schooten, F. J. & Keijer, J. Organ specificity of beta-carotene induced lung gene-expression changes in Bcmo1-/- mice. *Mol. Nutr. Food Res.* **57,** 307–319 (2013).

35. Lee, S.-A. *et al.* Cardiac dysfunction in beta-carotene-15,15'-dioxygenase-deficient mice is associated with altered retinoid and lipid metabolism. *Am. J. Physiol. - Hear. Circ. Physiol.* **307,** H1675–H1684 (2014).

36. Piga, R., Van Dartel, D., Bunschoten, A., Van der Stelt, I. & Keijer, J. Role of Frizzled6 in the molecular mechanism of beta-carotene action in the lung. *Toxicology* **320,** 67–73 (2014).

37. Widjaja-Adhi, M. A. K., Lobo, G. P., Golczak, M. & Von Lintig, J. A genetic dissection of intestinal fat-soluble vitamin and carotenoid absorption. *Hum. Mol. Genet.* **24,** 3206–19 (2015).

38. O'Byrne, S. M. *et al.* Retinoid absorption and storage is impaired in mice lacking lecithin:retinol acyltransferase (LRAT). *J. Biol. Chem.* **280,** 35647–35657 (2005).

39. Amengual, J. *et al.* A mitochondrial enzyme degrades carotenoids and protects against oxidative stress. *FASEB J.* **25,** 948–959 (2011).

40. Schreiber, R. *et al.* Retinyl ester hydrolases and their roles in vitamin A homeostasis. *Biochim. Biophys. Acta - Mol. Cell Biol. Lipids* **1821,** 113–123 (2012).

41. Harrison, E. H. Lipases and carboxylesterases: Possible roles in the hepatic utilization of vitamin A. *J. Nutr.* **130,** 321S–322S (2000).

42. Taschler, U. *et al.* Adipose triglyceride lipase is involved in the mobilization of triglyceride and retinoid stores of hepatic stellate cells. *Biochim. Biophys. Acta - Mol. Cell Biol. Lipids* **1851,** 937–945 (2015).

43. Ong, K. T., Mashek, M. T., Bu, S. Y. & Mashek, D. G. Hepatic ATGL knockdown uncouples glucose intolerance from liver TAG accumulation. *FASEB J.* **27,** 313–321 (2013).

44. Wu, J. W. *et al.* Deficiency of liver adipose triglyceride lipase in mice causes progressive hepatic steatosis. *Hepatology* **54,** 122–132 (2011).

45. Ghenimi, N. *et al.* Vitamin A deficiency in rats induces anatomic and metabolic changes comparable with those of neurodegenerative disorders. *J Nutr* **139,** 696–702 (2009).

46. Jacobs, S. *et al.* Retinoic acid is required early during adult neurogenesis in the dentate gyrus. *Proc Natl Acad Sci U S A* **103,** 3902–3907 (2006).

47. Nauss, K. M., Phua, C.-C., Ambrogi, L. & Newberne, P. M. Immunological changes during progressive stages of vitamin A deficiency in the rat. *J. Nutr.* **115,** 909–918 (1985).

48. Liu, X. *et al.* Gestational vitamin A deficiency reduces the intestinal immuneresponse by decreasing the number of immune cells inrat offspring. *Nutrition* **30,** 350–357 (2014).

49. Boileau, T. W.-M. *et al.* Testosterone and food restriction modulate hepatic lycopene isomer concentrations in male F344 rats. *J. Nutr.* **131,** 1746–52 (2001).

50. Chaudhary, L. R., Hutson, J. C. & Stocco, D. M. Effect of retinol and retinoic acid on testosterone production. *Biochem. Biophys. Res. Commun.* **158,** 400–406 (1989).

51. Bosakowski, T., Levin, A. A. & Edgcomb, J. H. Studies on the testicular effects of vitamin A palmitate in the Sprague-Dawley rat. *Food Chem. Toxicol.* **26,** 767–773 (1988).

52. O'Byrne, S. M. & Blaner, W. S. Retinol and retinyl esters: Biochemistry and physiology. *J. Lipid Res.* **54,** 1731–43 (2013).

53. Wongsiriroj, N. *et al.* Genetic dissection of retinoid esterification and accumulation in the liver and adipose tissue. *J. Lipid Res.* **55,** 104–14 (2014).

54. Flowers, M. T. & Ntambi, J. M. Role of stearoyl-coenzyme A desaturase in regulating lipid metabolism. *Curr. Opin. Lipidol.* **19,** 248–256 (2008).

55. Kvilekval, K., Lin, J., Cheng, W. & Abumrad, N. Fatty acids as determinants of triglyceride and cholesteryl ester synthesis by isolated hepatocytes: kinetics as a function of various fatty acids. *J. Lipid Res.* **35,** 1786–94 (1994).

56. Cheema, S. K. & Agellon, L. B. Metabolism of cholesterol is altered in the liver of C3H mice fed fats enriched with different C-18 fatty acids. *J Nutr* **129,** 1718–1724 (1999).

57. Lee, J.-Y. & Carr, T. P. Biochemical and molecular actions of nutrients dietary fatty acids regulate acyl-coa:cholesterol acyltransferase and cytosolic cholesteryl ester hydrolase in hamsters. *J. Nutr* **134,** 3239–3244 (2004).

58. Fungwe, T. V, Kudchodkar, B. J., Lacko, A. G. & Dory, L. Fatty acids modulate lecithin:cholesterol acyltransferase secretion independently of effects on triglyceride secretion in primary rat hepatocytes. *J Nutr* **128,** 1270–1275 (1998).

59. Verhague, M. A., Cheng, D., Weinberg, R. B. & Shelness, G. S. Apolipoprotein A-IV expression in mouse liver enhances triglyceride secretion and reduces hepatic lipid content by promoting very low density lipoprotein particle expansion. *Arterioscler. Thromb. Vasc. Biol.* **33,** 2501–2508 (2013).

60. Melhuish, T. A., Chung, D. D., Bjerke, G. A. & Wotton, D. Tgif1 represses apolipoprotein gene expression in liver. *J. Cell. Biochem.* **111,** 380–390 (2010).

61. Hanniman, E. A., Lambert, G., Inoue, Y., Gonzalez, F. J. & Sinal, C. J. Apolipoprotein A-IV is regulated by nutritional and metabolic stress: involvement of glucocorticoids, HNF-4 alpha, and PGC-1 alpha. *J. Lipid Res.* **47,** 2503–2514 (2006).

62. Sanderson, L. M., Boekschoten, M. V, Desvergne, B., Müller, M. & Kersten, S. Transcriptional profiling reveals divergent roles of PPAR alpha and PPAR beta/delta in regulation of gene expression in mouse liver. *Physiol Genomics* **41,** 42–52 (2010).

63. Li, X. *et al.* Apolipoprotein A-IV reduces hepatic gluconeogenesis through nuclear receptor NR1D1. *J. Biol. Chem.* **289,** 2396–2404 (2014).

64. Vongpromek, R. *et al.* LR11/SorLA links triglyceride-rich lipoproteins to risk of developing cardiovascular disease in FH patients. *Atherosclerosis* **243,** 429–437 (2015).

65. Sugiyama, T. *et al.* A novel low-density lipoprotein receptor-related protein mediating cellular uptake of apolipoprotein E-enriched β-VLDL in vitro. *Biochemistry* **39,** 15817–15825 (2000).

66. Taira, K. *et al.* LR11, a mosaic LDL receptor family member, mediates the uptake of apoE-rich lipoproteins in vitro. *Arterioscler. Thromb. Vasc. Biol.* **21,** 1501–1506 (2001).

67. McCarthy, C. *et al.* SorLA modulates atheroprotective properties of CLA by regulating monocyte migration. *Atherosclerosis* **213,** 400–407 (2010).

68. Schaiff, W. T. *et al.* Peroxisome proliferator-activated receptor-gamma and retinoid X receptor signaling regulate fatty acid uptake by primary human placental trophoblasts. *J. Clin. Endocrinol. Metab.* **90,** 4267–4275 (2005).

69. Schaiff, W. T. *et al.* Ligand-activated peroxisome proliferator activated receptor γ alters placental morphology and placental fatty acid uptake in mice. *Endocrinology* **148,** 3625–3634 (2007).

70. Shim, J. *et al.* Fatty acid transport protein 4 is dispensable for intestinal lipid absorption in mice. *J. Lipid Res.* **50,** 491–500 (2009).

71. Herrmann, T. *et al.* Mouse fatty acid transport protein 4 (FATP4): Characterization of the gene and functional assessment as a very long chain acyl-CoA synthetase. *Gene* **270,** 31–40 (2001).

72. Seeble, J., Liebisch, G., Schmitz, G., Stremmel, W. & Chamulitrat, W. Palmitate activation by fatty acid transport protein 4 as a model system for hepatocellular apoptosis and steatosis. in *Biochim. Biophys. Acta - Mol. Cell Biol. Lipids* **1851,** 549–565 (2015).

Figures

Figure 3.1.

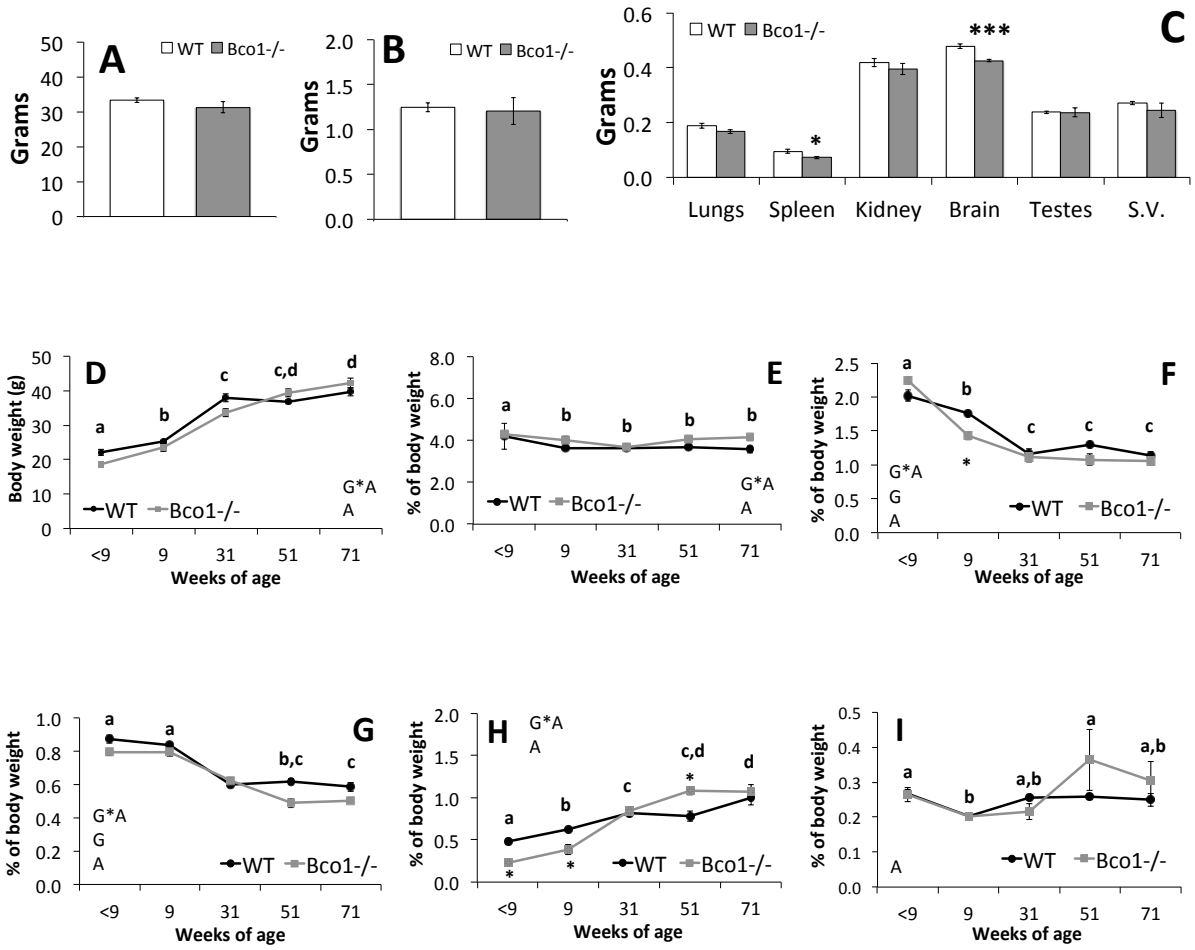

Figure 3.1. Impact of *Bco1*$^{-/-}$ genotype on weight body and organ weights in chow-fed mice (**A-C**) and in mice fed a semi-purified, vitamin A-sufficient, carotenoid-free diet from weaning until <9, 9, 31, 51, or 71 weeks of age (**D-I**). Body weight (**A**), liver weight (**B**), and organ weights (**C**) in chow-fed mice. Body weight (**D**) and liver (**E**), brain (**F**), testes (**G**), seminal vesicles (**H**), and spleen (**I**) weights as percentages of total body weight. Data are presented as group mean ± SEM. Group n = 8 (**A-C**) or n = 7 - 10/genotype/age (**D-I**). *p < 0.05, ***p < 0.001 between genotypes. G, A, and G*A indicate statistical main effects of genotype, age, or an interaction between genotype and age. Different lowercase letters above ages indicate significant (p < 0.05) results of mean separations tests for the main effect of age.

Figure 3.2.

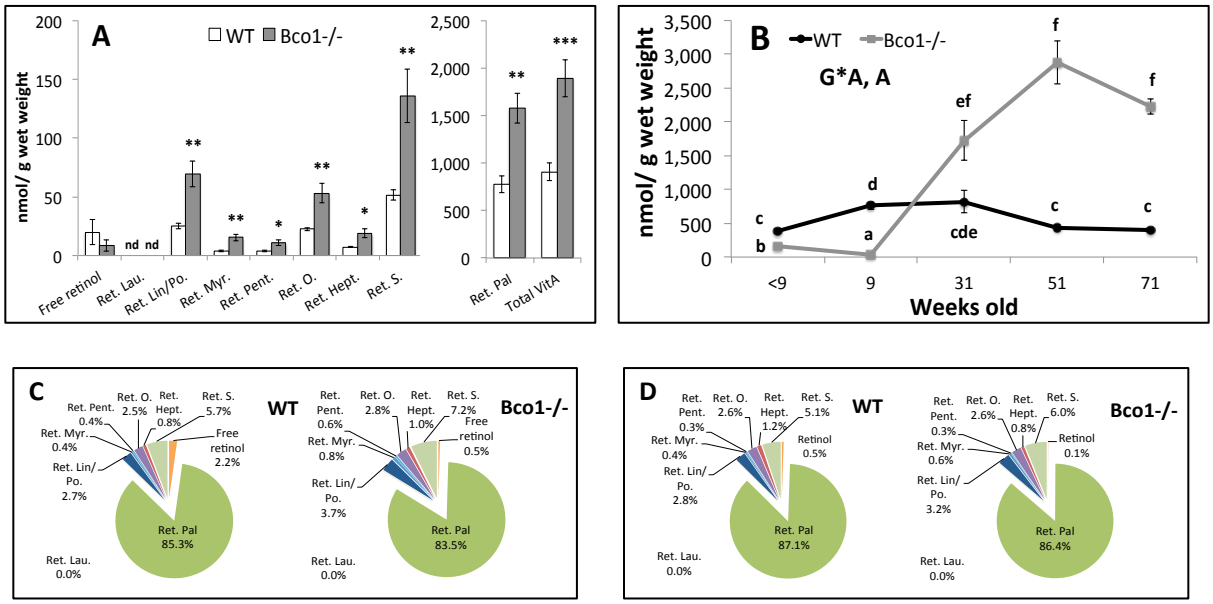

Figure 3.2. Loss of *Bco1* interacts with age to modulate total hepatic vitamin A stores, but does not alter the relative abundance of hepatic retinol/retinyl esters. Hepatic free retinol and major retinyl ester species in 20 – 22-week old chow-fed mice (**A**, **C**) and 51-week old mice fed a semi-purified, vitamin A-sufficient, carotenoid-free diet (**D**). Total vitamin A (free retinol plus all measured retinyl esters) in WT and *Bco1*$^{-/-}$ mice <9, 9, 31, 51, or 71 weeks of age (**B**). Composition of hepatic vitamin A pools are shown in (**C**) for chow-fed mice and (**D**) for 51 week-old mice fed a semi-purified, vitamin A-sufficient, carotenoid-free diet. Data in (**A,B**) are displayed as mean nmol/g tissue ± SEM. Some error bars are too small to be visible. Group n = 4 - 6. Data in (**C**, **D**) display vitamers as a percent of the total hepatic vitamin A pool within each genotype. Ret. Lau., retinyl laurate; Ret. Lin/Po., retinyl linoleate/retinyl palmitoleate co-eluted peaks;, Ret. Myr., retinyl myristate;, Ret. Pent., retinyl pentadecanoate;, Ret. O., retinyl oleate;, Ret. Hept., retinyl heptadecanoate;, Ret. S., retinyl stearate;, Ret. Pal., retinyl palmitate. *p < 0.05 vs. WT, **p < 0.01 vs. WT, ***p < 0.005 vs. WT. G*A denotes significant interaction between genotype and age; A denotes significant main effect of age. Means with different letters are statistically significant from one another. nd, not detected.

Figure 3.3.

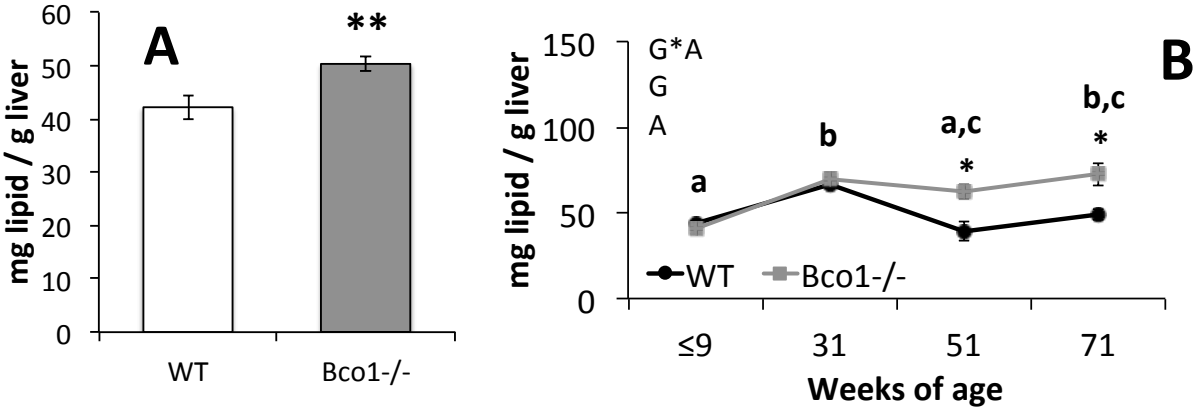

Figure 3.3. *Bco1* loss increases total hepatic lipids in adult male mice. Total hepatic lipids in chow-fed adult 20- 22-week-old male mice (**A**). Data are presented as group mean ± SEM. n = 6/group. **p = 0.011. Total hepatic lipid content in mice fed a vitamin A-sufficient, carotenoid-free, semi-purified diet (**B**). Data are presented as group mean ± SEM. n = 7 - 10/genotype/age. *p < 0.05 between genotypes. G, A, and G*A indicate statistical main effects of genotype, age, or an interaction between genotype and age. Different lowercase letters above ages indicate significant results of mean separations tests for the main effect of age (p < 0.05).

Table 3.1.

		Cholesteryl esters[ab]		Phospholipids		Triglycerides		Free Fatty Acids	
Fatty acid methyl ester		**WT**	***Bco1*$^{-/-}$**	**WT**	***Bco1*$^{-/-}$**	**WT**	***Bco1*$^{-/-}$**	**WT**	***Bco1*$^{-/-}$**
Internal Standard (IS)	15:0 or 17:0	0.08 ± 0.03	0.04 ± 0.01	1.40 ± 0.20	1.05 ± 0.15	2.53 ± 0.54	1.79 ± 0.52	n/a[f]	n/a[f]
Myristic	14:0	0.17 ± 0.05	0.19 ± 0.02	0.10 ± 0.02	0.09 ± 0.02	1.00 ± 0.18	0.89 ± 0.21	0.49 ± 0.04	0.45 ± 0.05
Myristoleic	14:1n5	0.11 ± 0.01	0.10 ± 0.01 [d]	0.02 ± <0.00	0.01 ± <0.00	0.09 ± 0.03	0.09 ± 0.03	0.01 ± <0.00 [d]	0.01 ± <0.00
Palmitic	16:0	10.6 ± 0.58	24.9 ± 2.32 *	21.3 ± 0.33	20.9 ± 0.13	12.2 ± 1.82	14.5 ± 2.77	17.3 ± 0.95	20.6 ± 0.31 *
Palmitoleic	16:1n7	0.43 ± 0.07	0.75 ± 0.19	0.54 ± 0.06	0.54 ± 0.04	0.54 ± 0.31	1.02 ± 0.58	1.71 ± 0.23	2.17 ± 0.33
Stearic	18:0	2.34 ± 0.60	2.67 ± 0.24	15.2 ± 0.31	16.5 ± 0.29 *	10.7 ± 2.65	8.98 ± 2.87	2.85 ± 0.53	1.87 ± 0.38 [d]
Oleic	18:1n9	3.95 ± 1.32	4.40 ± 1.85	6.34 ± 0.51 [d]	5.99 [e]	2.51 ± 0.88 [d]	2.57 ± 1.08 [d]	17.9 ± 0.93 [d]	nd
Vaccenic	18:1n7	nd [c]	0.05 [e]	nd	nd	nd	nd	nd	nd
Linoleic	18:2n6	1.95 ± 0.18	2.73 ± 0.52	18.4 ± 0.25	18.0 ± 0.41	8.96 ± 5.05	10.9 ± 5.97	29.0 ± 3.19	35.6 ± 1.03
Linolenic	18:3n3	0.10 ± 0.01	0.11 ± 0.02	0.18 ± 0.01	0.14 ± 0.01 *	0.44 ± 0.15	0.50 ± 0.19	1.81 ± 0.32	1.82 ± 0.22
Arachidic	20:0	0.04 ± 0.01	0.05 ± 0.02	0.36 ± 0.02	0.36 ± 0.02	0.20 ± 0.02	0.26 ± 0.05	0.17 ± 0.03	0.19 ± 0.03
Gondoic	20:1n9	0.02 ± <0.00	0.08 ± 0.02 *	0.21 ± 0.01	0.18 ± 0.01 ^	0.26 ± 0.08	0.34 ± 0.09	0.42 ± 0.07	0.46 ± 0.05
Eicosadienoic	20:2n6	0.12 ± 0.01	0.08 ± 0.02 ^	0.35 ± 0.02	0.27 ± 0.01 ^	0.12 ± 0.06	0.13 ± 0.01 [d]	0.34 ± 0.03	0.27 ± 0.02
Eicosatrienoic acid	20:3n3	0.02 ± <0.00	0.01 ± <0.00 [d]	0.01 ± 0.01	0.01 ± 0.01	0.06 ± 0.01	0.07 ± 0.02	0.04 ± <0.00 [d]	0.04 ± <0.00
Arachidonic	20:4n6	0.05 ± 0.04	0.56 ± 0.12	15.4 ± 0.44	15.5 ± 0.44	0.78 ± 0.35	0.53 ± 0.19	2.34 ± 0.36	1.42 ± 0.04 ^
Eicosapentaenoic	20:5n3	0.05 ± 0.02	0.08 ± 0.03	0.42 ± 0.02	0.48 ± 0.03	0.30 ± 0.08	0.37 ± 0.12	0.92 ± 0.17	0.98 ± 0.15
Behenic	22:0	0.02 ± 0.01	0.02 ± 0.01	0.67 ± 0.02	0.82 ± 0.05 ^	0.09 ± 0.01	0.10 ± 0.02	0.15 ± 0.03	0.14 ± 0.04
Erucic	22:1n9	0.03 ± 0.01	0.05 ± 0.01 ^	0.02 ± <0.00	0.02 ± <0.00	0.27 ± 0.13	0.14 ± 0.05	0.07 ± 0.01	0.06 ± 0.01
Docosahexaenoic	22:6n3	0.17 ± 0.04	0.26 ± 0.07	11.6 ± 0.28	11.6 ± 0.38	0.73 ± 0.39	0.65 ± 0.35	4.06 ± 0.77	2.65 ± 0.27
Lignoceric	24:0	nd	nd	0.26 ± 0.09 [d]	0.09 ± 0.08 [d]	0.05 ± 0.01	0.05 ± 0.01 [d]	0.05 ± 0.02	0.02 ± <0.00
Nervonic	24:1n9	0.02 ± <0.00 [d]	0.10 ± 0.08	0.26 ± 0.08	0.07 ± 0.07	nd	0.01 ± <0.00 [d]	0.01 [e]	0.02 ± <0.00 [d]
Unidentified fatty acids	Various	79.4 ± 1.11	61.3 ± 5.89 *	12.1 ± 1.74	13.4 ± 1.27	60.6 ± 6.49	58.4 ± 7.76	32.3 ± 5.08	31.9 ± 1.03
Total lipid pool (µmol/g) [g]	Various	1,236 ± 423	2,147 ± 617	57.8 ± 8.55	73.6 ± 7.22	42.1 ± 12.2	67.5 ± 11.3	n/a[f]	n/a[f]

Table 3.1. Loss of *Bco1* differentially impacts the composition of hepatic lipid pools. Fatty acid methyl esters derived from hepatic TLC-isolated CE, PL, TG, or FFA pools in chow-fed mice were analyzed by GC and compared to authentic standards for twenty fatty acid species. Odd-chain length internal standards (IS) were used to track recovery: CE: cholesteryl pentadecanoate; PL: 1,2-diheptadecanoyl-*sn*-glycero-3-phosphocholine; TG: glyceryl triheptadecanoate. N = 6 - 7/genotype. [a] Data are mean % of lipid pool ± SEM. [b] Values in a column may not sum to exactly 100% due to averaging and rounding. [c] not detected in any sample within group. [d] not detected in one or more samples within group. [e] detected in only one sample within group. [f] IS not used. [g] calculated as mean of (µmol of IS FAME added / IS FAME % abundance) / sample weight. *Statistically different from WT $p \leq 0.01$; ^statistically different from WT $p \leq 0.05$.

Figure 3.4.

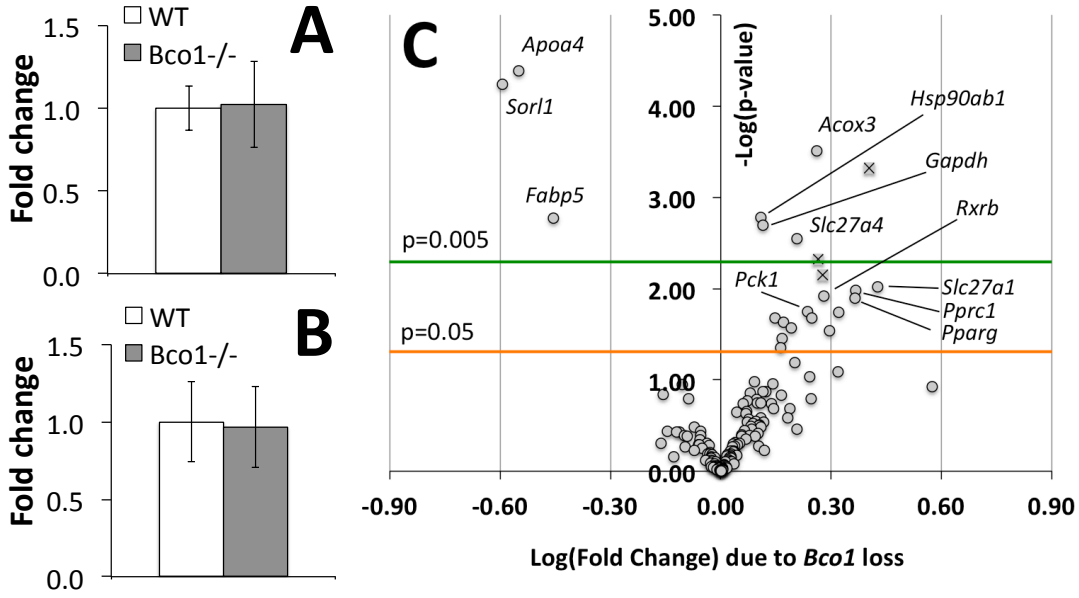

Figure 3.4. *Bco1*$^{-/-}$ genotype alters hepatic expression of genes involved in lipid and cholesterol metabolism in chow-fed mice. *Fasn* (**A**) and *Scd1* (**B**) expression, normalized to *Rpl19*, are unchanged by *Bco1* loss; n=6-8/genotype. Gene expression was assayed using qPCR arrays focused on PPAR signaling and lipoprotein and cholesterol metabolism (**C**). Log(fold change) and –log(p-value) [derived from pairwise t-tests] for 163 lipid- and cholesterol metabolism-related gene is plotted in a volcano plot. Absolute log(fold change) values of 0.30, 0.60, and 0.90 approximately equal absolute fold-change values of 2.0, 4.0, and 6.0. Selected genes are noted. Genes which had p-values below or approaching p = 0.005 but which had extremely low basal expression (Ct > 30.0; *Mmp9, Smarcd3,* and *Src*) are marked with x's.

Table 3.2.

Array	Refseq	Symbol	Name	Fold Regulation Mean	SEM	p-value
LipoproChol	NM_007468	Apoa4	Apolipoprotein A-IV	**-3.54**	0.03	0.0000
LipoproChol	NM_011436	Sorl1	Sortilin-related receptor	**-3.92**	0.03	0.0001
PPAR	NM_030721	Acox3	Peroxisomal acyl coenzyme A oxidase	1.83	0.07	0.0003
Both	NM_008302	Hsp90ab1	Heat shock protein 90 beta	1.28	0.05	0.0017
PPAR	NM_010634	Fabp5	Fatty acid binding protein, epidermal	**-2.85**	0.06	0.0017
Both	NM_008084	Gapdh	Glyceraldehyde-3-phosphate dehydrogenase	1.30	0.07	0.0020
PPAR	NM_011989	Slc27a4	Long-chain fatty acid transport potein 4	1.61	0.08	0.0029
PPAR	NM_011977	Slc27a1	Long-chain fatty acid transport protein 1	**2.67**	0.57	0.0095
PPAR	NM_001081214	Pprc1	Peroxisome proliferator-activated receptor gamma coactivator related protein 1	**2.33**	0.45	0.0105
PPAR	NM_011306	Rxrb	Retinoid X receptor, beta	1.91	0.24	0.0120
PPAR	NM_011146	Pparg	Peroxisome proliferator-activated receptor, gamma	**2.32**	0.47	0.0126
PPAR	NM_011044	Pck1	Phosphoenolpyruvate carboxykinase, cytosolic	1.72	0.26	0.0177
PPAR	NM_009948	Cpt1b	Carnitine O-palmitoyltransferase 1, muscle	**2.09**	0.39	0.0182
PPAR	NM_024264	Cyp27a1	Sterol 26-hydroxylase, mitochondrial	1.40	0.07	0.0209
PPAR	NM_080434	Apoa5	Apolipoprotein A-V	1.77	0.29	0.0211
PPAR	NM_011305	Rxra	Retinoid X receptor, alpha	1.48	0.15	0.0233
PPAR	NM_019966	Mlycd	Malonyl-CoA decarboxylase, mitochondrial	1.56	0.17	0.0270
PPAR	NM_011396	Slc22a5	Solute carrier family 22 member 5	1.98	0.39	0.0287
PPAR	NM_007980	Fabp2	Fatty acid binding protein, intestinal	1.47	0.14	0.0352
Both	NM_011145	Ppard	Peroxisome proliferator-activated receptor, delta	1.45	0.21	0.0443

Table 3.2. *Bco1*$^{-/-}$ genotype alters hepatic expression of genes involved in lipid and cholesterol metabolism. Gene expression was assayed using qPCR arrays focused on PPAR signaling (PPAR) and lipoprotein and cholesterol metabolism (LipoproChol); several genes were present on both arrays (Both). Genes $p \leq 0.05$ are shown here; yellow highlighting indicates $0.005 < p < 0.05$, whereas green highlighting indicates $p \leq 0.005$. Fold regulation and SEM are displayed, with fold regulation ≥ 2 in red and ≤ -2 in blue. NCBI RefSeq identifiers are provided for each gene.

Figure 3.5.

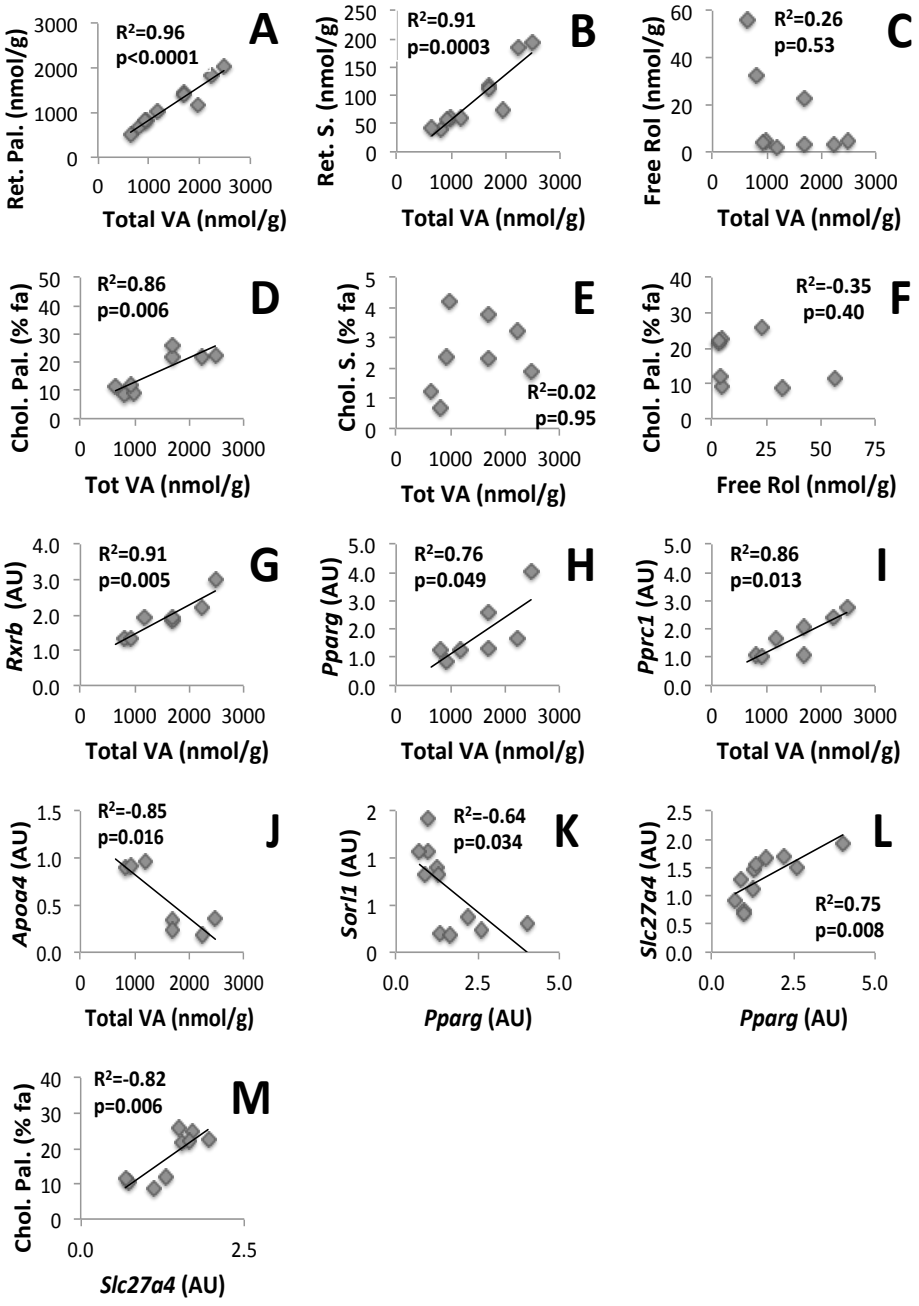

Figure 3.5. Correlation between measured outcomes in livers of chow-fed mice. Retinyl palmitate (**A**) and retinyl stearate (**B**) both correlate with total vitamin A stores, while free retinol does not (**C**). Cholesteryl palmitate (**D**), but not cholesteryl stearate (**E**), correlates with total hepatic vitamin A stores. Free retinol does not correlate with cholesteryl palmitate levels (**F**). Total hepatic vitamin A stores are positively associated with mRNA expression of *Rxrb* (**G**), *Pparg* (**H**), and *Pprc1* (**I**). mRNA expression of *Apoa4* is inversely associated with total vitamin A levels (**J**), mRNA expression of *Sor1l* (**K**) and *Slc27a4* (**L**) are inversely and positively correlated with *Pparg* expression, respectively, while *Slc27a4* expression is positively associated with cholesteryl palmitate (**M**).

Figure 3.6.

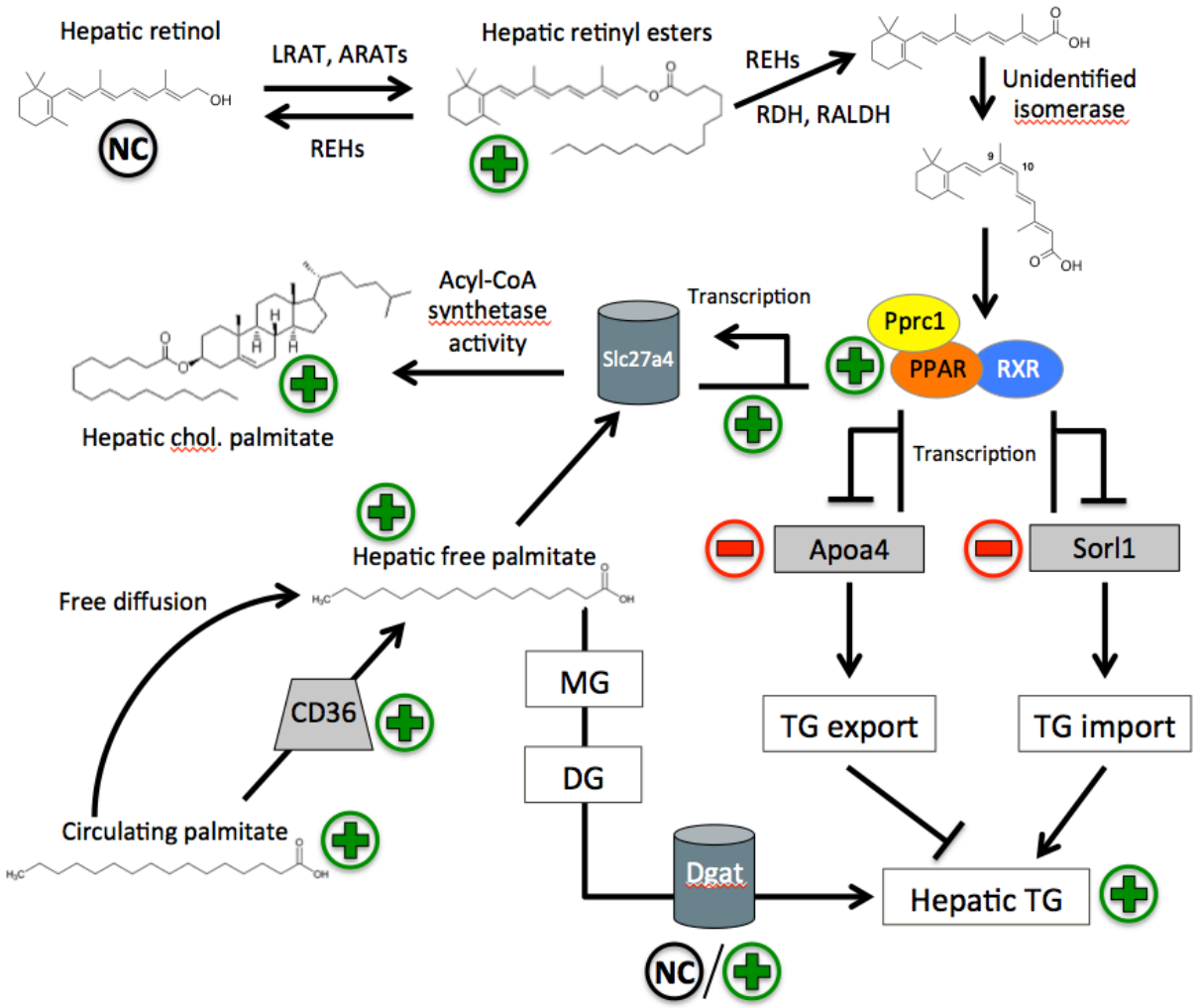

Figure 3.6. Conceptual model of *Bco1* loss-induced changes in hepatic lipid and retinoid metabolism in adult mice (*Bco1* loss reduces retinyl esters in embryonic and juvenile samples). Arrows indicate induction, blunted lines indicate inhibition. Green plus signs indicate induction in *Bco1*$^{-/-}$ mice, red minus signs indicate repression in *Bco1*$^{-/-}$ mice, and black "NC" signs indicate no change observed in *Bco1*$^{-/-}$ mice. Model incorporates findings from the current study, as well as previous work from the literature. ARAT, acyl CoA:retinol-acyltransferase; LRAT, lecithin:retinol acyltransferase; REHs, retinyl ester hydrolases; RDH, retinol dehydrogenase; RALDH, retinaldehyde dehydrogenase; MG, monoacylglyceride; DG, diacylglyceride; TG, triacylglyceride.

CHAPTER 4

Dietary tomato reduces castration-resistant prostate cancer progression in the TRAMP model

Abstract

Observational data in humans continue to support the hypothesis that tomato intake is associated with a reduced risk of primary prostate cancer (PCa). However, few studies have examined the effects of dietary tomato on castration-resistant prostate cancer (CRPC), which constitutes the late and lethal stage of PCa. CRPC is defined as PCa progression after surgical castration or pharmacological reduction of circulating androgens through androgen deprivation therapy (ADT). One mechanism that has previously been implicated in the transition from PCa to CRPC is the acquired ability for local androgen synthesis. We have previously shown in animal models that dietary tomato powder can reduce incidence of primary PCa, and that tomato feeding modulated genes controlling tumoral androgen in the direction of reduced steroidogenic capacity. Therefore, we hypothesized that lifelong dietary intake of tomato, as well as a dietary intervention following castration, would reduce cancer progression in a mouse model of CRPC. Transgenic adenocarcinoma of the mouse prostate (TRAMP) mice were acclimated to a powdered, AIN-93G diet (CON) for one week and then randomized to consume CON (n = 28) or 10% w/w lyophilized tomato paste (TP; n = 30) from 4 weeks of age until euthanization. A third group, modeling adjuvant dietary intervention, consumed CON diet from 4 weeks of age until 12 weeks of age, and then 10% w/w lyophilized tomato paste from week 12 until euthanization (TP-I; n = 27). All animals were castrated at 12 weeks of age. Beginning at 10 weeks of age, mice were monitored longitudinally with biweekly ultrasound scans for tumor detection. For each ultrasound scan, serial 2D image slices were used to generate a 3D volume measurement. Upon tumor detection, mice were switched from biweekly to weekly scans and imaged 4 additional

times for volumetric tumor measurement and determination of tumor growth rate.

Two criteria were implemented for euthanasia: after 5 tumor scans (tumor detection + 4 weekly), or if no tumor had been detected by 30 weeks of age. No differences between TP or TP-I treatments in hepatic, prostatic, or tumoral carotenoid accumulation were observed. TP-I, but not TP, significantly reduced *in vivo* tumor growth rate ($p < 0.0001$) and tumor volume ($p < 0.05$) by approximately 50%, compared to CON. At necropsy, compared to CON, tumor weight trended ($p = 0.07$) towards a reduction with TP-I treatment, but not TP. TP-I reduced gross metastasis to lungs ($p < 0.05$) and preserved body weight ($p < 0.01$) and gonadal adipose depot weight ($p < 0.05$), compared to CON. However, no significant effect by dietary treatment was observed in tumoral mRNA expression of androgen receptor or androgen biosynthetic genes. In conclusion, we have shown, for the first time, that dietary tomato can reduce CRPC progression in an animal model. Epidemiological work suggests that the human equivalent lycopene dose provided by tomato diets in the present study is both easily achievable and potentially protective against both incident and lethal PCa in humans. Future work should address the efficacy of adjuvant combinations of dietary tomato with the front-line therapies currently in clinical use against CRPC, in order to assess the potential for this approach to translate into clinical benefits for men with this lethal disease.

Introduction

Tomato intake has been linked to a reduced risk of PCa since the first observational studies noting an inverse association were published in the late 1990s [1–4]. Notably, these studies often reported that the strongest inverse associations were between tomato or lycopene intake and lethal or aggressive cancers [1–6]. This is important, because PCa is often diagnosed at a

Gleason grade of 7 [4,6,7], and tumors with a grade ≥ 7 are associated with higher rates of mortality [8]. Moreover, cancers that are at an advanced stage at diagnosis (classified by the TNM staging system [9]) suffer worse prognosis than those with localized disease [10]. Men with low-grade cancer are likely to survive in spite of their diagnosis [8], and so identification of dietary agents that are especially effective against aggressive and lethal cancers is especially desirable.

Several animal studies have provided data to support the observational association between tomato intake and a reduced risk of PCa. Pannellini et al. showed that a 10% w/w tomato paste diet reduced incidence in TRAMP mice [11], and we have shown that tomato feeding reduces PCa tumorigenesis [12,13] and carcinogenesis [14]. However, although these studies support the hypothesis of the incorporation of dietary tomato to reduce a lifetime risk of primary disease, they do not directly address the efficacy of tomato on the lethal phase of clinical PCa, castration resistant prostate cancer (CRPC). Men with primary PCa are treated with radiation or prostatectomy, but some cancers will recur, either locally or with distant metastasis [15]. First-line therapy for these cancers has been androgen-deprivation therapy (ADT), which involves the pharmacological ablation of circulating androgens (formerly surgical castration), or the pharmacological blockade of androgen receptor (AR) signaling. ADT is initially successful, but which eventually gives rise to CRPC in 2 to 3 years; CRPC is fatal [16]. Some pharmacological agents have shown promise in prolonging survival [17,18], but other effective approaches, including adjuvant therapies, are needed.

Due to the positive data linking tomato intake to reduced rates of primary PCa, some researchers have turned to dietary tomato for the prevention or treatment of CRPC. Indeed, men may change dietary habits following a PCa diagnosis [19], and increased consumption of tomato products after PCa diagnosis has been shown to reduce the risk of progression [6]. However, very

few human studies have examined tomato or lycopene interventions in men with CRPC. One study provided 15 mg lycopene twice daily in the form of a tomato supplement, but it did not include a control group and the majority of patients experienced cancer progression [20]. Another compared surgical castration alone to surgical castration + lycopene (2 mg twice daily), and reported that men in the castration + lycopene group experienced greater survival [21]. However, this study was small (27 men) and suffered from errors in data reporting, which severely detracted from its reliability [22,23]. Although a few animal studies have examined the effects of lycopene or tomato on growth of androgen-insensitive human cell xenografts [24,25], these models of tumorigenesis do not recapitulate the carcinogenic process, nor do they avoid the limitations of anatomical fidelity that are inherent with xenograft studies. To our knowledge, no previous experimental study has examined the effects of dietary tomato on CRPC carcinogenesis *in vivo*. Moreover, we wondered whether lifelong vs. adjuvant intervention may be equally effective.

Materials and Methods

Diets

Tomato paste (Contadina®, San Francisco, CA) was purchased from a local Schnuck's® supermarket between September 2014 and July 2015. Tomato paste from freshly opened cans was spread into aluminum pans, covered loosely with aluminum foil, and lyophilized in a VirTis Freezemobile 12SL/Unitop 600 SL freeze dryer (SP Scientific, Warminster, PA). Dried yield was approximately 25% of wet weight. Dried tomato paste was broken into pieces and ground for 1 minute to fine powder in a tabletop food processor. Lyophilized tomato paste powder (LTP) was transferred to resealable gallon storage bags, air removed, and kept in the dark at 4 ˚C until diet mixing. New diet was made approximately every 1.5 months. 7 batches of 10% LTP diet

were made throughout the course of the study and each was analyzed for carotenoid content by HPLC.

Proximate analysis was performed on the 100% LTP (data not shown) and diet formulas were balanced for total energy, carbohydrates, protein, fat, and fiber. Two experimental diets were used in this study: a powdered, AIN-93G-based diet and a powdered, AIN-93G-based diet supplemented with 10% (w/w) LTP (**Table 4.1**). Proximate analysis of the two diets revealed that total carbohydrates were within 5% (w/w), whereas crude protein, crude fat, crude fiber, organic matter, ash, dry matter, and moisture contents were all within 3% (w/w; data not shown).

Animals and experimental design

The University of Illinois Laboratory Institutional Animal Care and Use Committee reviewed and approved all animal procedures. Male C57BL/6-Tg(TRAMP)8247Ng/J, female C57BL/6J, and female FVB/NJ mice were purchased from The Jackson Laboratory (Bar Harbor, ME). The C57BL/6-Tg(TRAMP)8247Ng/J strain is heterozygotic for the SV40Tag transgene, which is responsible for prostatic transformation and carcinogenesis in this model [26]. A breeding colony was maintained with crosses of C57BL/6J females and C57BL/6-Tg(TRAMP)8247Ng/J males, and F_1 offspring of C57BL/6-Tg(TRAMP)8247Ng/J and FVB/NJ mice were enrolled on study via rolling admission (hereafter referred to as TRAMP mice). Tail DNA of pups was isolated with an Extract-N-Amp™ Tissue PCR kits (Sigma-Aldrich, St. Louis, MO) and mice were genotyped with the following PCR primers: *Pbsn* Fwd, 5′- CCG GTC GAC CGG AAG CTT CCA CAA GTG CAT TTA -3′; SV40Tag Fwd, 5′- CTC CTT TCA AGA CCT AGA AGG TCC A -3′; *Csn2* (β-casein) Fwd, 5′- GAT GTG CTC CAG GCT AAA GTT -3′; *Csn2* Rev, 5′- AGA AAC GGA ATG TTG TGG AGT -3′. TRAMP pups were weaned to a powdered, modified AIN-93G diet at 3 weeks of age. At 4 weeks of age, mice were randomized to consume a

modified AIN-93G diet CON (n = 34) or 10% w/w lyophilized tomato paste (TP; n = 34) from 4 weeks of age until euthanization. A third group, modeling adjuvant dietary intervention, consumed CON diet from 4 weeks of age until 12 weeks of age, and then 10% w/w lyophilized tomato paste from week 12 until euthanization (TP-I; n = 31). Non-transgenic littermates (WT; n = 5) were maintained on CON diet for the duration of study. Mice were housed in shoebox cages under controlled conditions (12 hour light/dark cycle, 22˚C, 55% humidity). Mice were weighed weekly (Mondays) and diet was refreshed 3x/week (M, W, F). Diet removal from bowls was recorded on each day that fresh diet was provided. Mice were provided with separate nesting bowls for enrichment and in an effort to reduce burrowing and nesting activities in powdered diet.

TRAMP mice were castrated by surgical orchiectomy at 12 - 13 weeks of age through an abdominal incision while under 2% inhalation isofluorane. At this age, TRAMP mice are expected to have high-grade prostatic intraepithelial neoplasia (PIN) or well- to moderately-differentiated adenocarcinoma [27,28]. Animals were provided pre- and post-op analgesic (buprenorphine, 0.05 mg/kg IP) and all peri-surgical procedures complied with recommendations of the NIH Guide for the Care and Use of Laboratory Animals [29]. TRAMP mice in the TP-I group were not switched to the 10% w/w tomato paste diet until after castration.

Beginning at 10 weeks of age, mice were monitored longitudinally *via* ultrasound imaging for tumor development. Animals were scanned biweekly until tumor detection, at which time scans were switched to a weekly schedule for 5 consecutive weeks (detection + 4 subsequent). Mice were anesthetized in a chamber with 4 - 5% isofluorane for induction of anesthesia and then with 2% isofluorane (or to effect) for maintenance via facemask. The depth of anesthesia was monitored by pedal reflex and respiratory rate. Prior to ultrasonic scanning,

hair over the lower abdomen was shaved, followed by application of a depilatory agent and ultrasound coupling gel (Aquasonic, Parker Laboratories, Inc., Fairfield NJ) to maximize sound transmission. Anesthetized mice were scanned while in dorsal recumbency on a heated table. Scans were obtained through the ventral body wall using the Vevo 2100 pre-clinical imaging platform (VisualSonics, Inc., Toronto, Canada) and various transducers; the MS550D (22 – 55 MHz) was used for most scans, whereas the MS250 or MS200 (13 – 24 MHz or 9 – 18 MHz, respectively) were used for larger tumors. Scans were conducted in 3D B-mode, which enables the automated stepwise collection of serial 2-dimensional frames. For each animal, between 30 and 100 frames were collected in a caudal to cranial direction at intervals of approximately 0.3 mm. Serial 2-dimensional image slices were used to generate prostatic or tumor volume estimates as previously described [30]. Previous work in our lab has shown that *in vivo* volume estimates using this method correlate very strongly with tumor volume estimates obtained using three-axis calipers measurement at necropsy [31].

Mice were euthanized if they reached 30 weeks of age with no detectable tumor, or after 5 consecutive tumor ultrasound scans (tumor detection + 4 weekly). Euthanization was performed by rendering the animal unconscious by 5% inhalation isofluorane, followed by CO_2 asphyxiation while unconscious. Blood was collected by cardiac puncture (processed to obtain serum portion) and tissues were removed and weighed. Animals and tissues were dissected on an ice-chilled petri dish to reduce sample degradation. Gross metastases were identified by visual inspection. Entire cross-sections of tumors, half of each prostatic lobe, lungs, liver, regional lymph node metastases (medial iliac, lumbar aortic; when metastases present), and various distant organ metastases (when present) were fixed in 10% neutral-buffered formalin for 12 - 24 h and held in 70% aqueous ethanol until paraffin embedding. Necrotic tumor tissue was

identified by visual inspection, dissected away from vascularized tissue, and discarded. Remaining tissues (tumor, half of each prostate lobe, lymph node metastases, seminal vesicles, liver, gonadal adipose, and serum) were frozen in liquid N_2 and stored at -80 ˚C until analysis.

Thirteen mice were found dead while on study protocol and were not available for tissue analysis, but did contribute data points to weight gain and food intake (3 CON, 5 TP, 5 TP-I). None of these animals developed a tumor as detected by ultrasound before their death. 14 mice were removed from the study early for various reasons: loss of ≥15% body weight in 1 week (1 CON), hydrocephaly (1 TP-I), kidney tumor detected before prostatic tumor (1 CON), neck tumor detected before prostatic tumor (1 CON, 1 TP), or prostate tumor detected *via* ultrasound before castration (3 CON, 3 TP, 3 TP-I). These 14 mice were enrolled on study, but were not included in any subsequent analysis. Therefore, final group sizes were n = 28, n = 30, and n = 27 for CON, TP, and TP-I, respectively.

Carotenoid measurement

Carotenoids were extracted from diet, anterior prostate, tumor, and liver tissue and analyzed *via* HPLC as previously described [32,33]. Approximately 300 mg tumor tissue, 100 mg liver tissue, and 25 mg diet were used for analysis. Due to castration, anterior prostates were too small to be assayed individually and thus were pooled to achieve quantifiable signal. Anterior prostates from 8 - 12 mice (one lobe per mouse) were pooled into individual replicates and two such replicates per diet group were measured via HPLC. Total mass of each replicate ranged from 44 – 91 mg. On-column lower limits of quantification (LLOQ) were 2.0 ng phytoene, 2.0 ng phytofluene, 500 pg ζ-carotene, 500 pg lycopene (250 pg on-column lower limit of detection, LLOD), 2.0 ng α-carotene, 3.4 ng β-carotene, and 3.4 ng lutein.

Histopathology

Tissues were embedded in paraffin and 4 μm sections were stained with hematoxylin and eosin for pathological grading. A blinded examiner (S.K. Clinton; Division of Medical Oncology, Department of Medicine, College of Medicine, The Ohio State University) evaluated the extent and severity of neoplasia in prostate and tumor sections. Regional lymph node gross metastases were confirmed or rejected by histopathology.

Immunohistochemistry

Immunohistochemistry to detect endogenous expression of Ki67 was performed on 4 μm paraffin sections of dorsolateral prostate lobes. Ki67 staining was performed using a monoclonal antibody (D3B5, catalog #12202, Cell Signaling Technology, Danvers, MA). Slides were deparaffinized and rehydrated, followed by antigen retrieval in citrate buffer (pH 6.0) under steam heat for 60 min. Endogenous peroxidase was inhibited with H_2O_2 for 10 min, washed with TBS-Tween 20, and blocked with Background Punisher blocking agent (Biocare Medical, Concord, CA) for 15 min. Slides were incubated with the primary antibody for 60 min at 1:600 dilution, rinsed 3 times for 5 min each in TBS-Tween 20, and incubated with the secondary antibody (Rabbit on Rodent HRP-Polymer, Biocare Medical) for 30 min. Slides were again rinsed 3 times for 5 min each in TBS-Tween 20, followed by staining with DAB (5 min) and counterstain with hematoxylin. Small intestine was used as a positive control. Negative controls were prepared by omitting the primary antibody. Slides were digitized with a NanoZoomer 2.0-HT slide scanner (Hamamatsu, Bridgewater, NJ) equipped with an Olympus Uplansapo 20X objective (Tokyo, Japan). Images were captured with NDP View software (Hamamatsu) and dietary assignment was blinded. Images were processed in Fiji [34]. Stromal cells were manually removed from the RGB TIFF images and Ki67-positive DAB signal was extracted using a

previously described color deconvolution plugin [35]. Total epithelial images and extracted epithelial Ki67 signal images were thresholded to binary, and positive pixels were counted. Proliferative index (PI) was calculated as PI = epithelial Ki67-positive pixels/total epithelial pixels. All images were captured at 20x magnification.

Gene expression analysis

Total RNA was extracted from ~30 mg tumor tissue using RNEasy Mini spin columns (Qiagen, Valencia, CA) according to manufacturer's instructions. RNA was quantified spectrophotometrically and integrity verified using agarose gel electrophoresis. cDNA was synthesized using a High-Capacity Reverse Transcription Kit (Life Technologies, Grand Island, NY). qPCR was carried out with SYBR Green chemistry (Life Technologies) on an ABI 7900 HT qPCR platform (Life Technologies), using pre-designed primer assays (*Ar, Srd5a1, Srd5a2, Hsd17b2, Hsd17b3, Akr1c6, Vegfa, Bco2,* and *Rpl19*; SA Biosciences, Valencia, CA). *Rpl19* was used as the reference gene for $2^{-\Delta\Delta Ct}$ relative expression analysis.

Statistical analysis

Tumor growth rate was compared by exponential non-linear regression in GraphPad Prism 6 (GraphPad Software, Inc., La Jolla, CA). All other analysis was conducted in SAS version 9.3 (SAS Institute, Cary, NC). Repeated-measures ANOVA with Toeplitz covariance structure was used for analysis of body weight over time. Individual *post hoc* contrast statements were used to compare body weight at each time point under CON and TP-I treatments. Bonferroni's adjusted α was calculated and used for this test ($\alpha = 0.05 / 27$ tests $= 0.0018$). CON-fed animals were not included in statistical comparisons of tissue carotenoid accumulation. Tissue carotenoids, tissue weights, PI index, and gene expression were compared using mixed model two-way analysis of variance with multiple-comparison adjustment by Tukey's method.

Tumor weight and tumor volume were compared similarly, but with date of birth and castration-tumor interval (time in weeks between castration and tumor detection via ultrasound) as covariates. Sacrifice age was used as a covariate on measures of tissue weight. Data were log transformed when not meeting assumptions of normality and individual group variances were used in place of the pooled variance when the Brown-Forsyth test indicated heterogeneity of variances. Tumor incidence, metastasis incidence, and histopathological cancer incidence were compared using a two-tailed Fisher's Exact Test.

Results

Carotenoid profile of diet and accumulation in tissue *in vivo*

Carotenoid composition of the 10% LTP diet is shown in **Figure 4.1**. Lycopene was the predominant carotenoid, accounting for 45% of the total carotenoids. Likely due to the presence of some under-ripe tomatoes in the commercial tomato paste used, a large proportion of dietary carotenoids were the lycopene precursors phytoene (29%) and phytofluene (18%). Lycopene, phytoene, and phytofluene were present at 37.5, 25.1, and 16.0 nmol/g diet, respectively. ζ-carotene, another lycopene precursor, constituted only 3% of total carotenoids; three other minor carotenoids (α-carotene, β-carotene, and lutein) also contributed <5% of total dietary carotenoid content. With the HPLC method used, it was not possible to separate all-*trans* from 5-*cis* lycopene. However, aside from the 5-*cis* species, dietary lycopene was not commonly isomerized, as only 20% of total lycopene were present in other *cis* conformations.

Tissue carotenoid profiles contrasted starkly with dietary carotenoids. In the livers of animals in the TP group, whereas lycopene, phytoene, and phytofluene were still the predominant carotenoids, the proportions of phytoene and phytofluene were approximately

switched, making phytofluene the second-most abundant hepatic carotenoid behind lycopene (**Fig. 4.2A**). β-carotene and lutein were not detected at all in the liver (**Table 4.2**), and α-carotene was present at <1% of total hepatic carotenoids (**Fig. 4.2A**). These patterns were similar between TP and TP-I treatments (**Table 4.2**). We did detect small amounts of all-*trans*/5-*cis* lycopene in the livers of CON-fed mice, but these levels were more than 700-fold lower than levels of total lycopene in the TP- and TP-I-fed mice (**Table 4.2**). We suspect that these signals were the result of trace cross-sample contamination during the sample extraction and preparation procedures; this is feasible since our HPLC assay is very sensitive for lycopene (≤500 pg on-column LLOD). No significant differences in hepatic carotenoid accumulation were observed between the TP and TP-I groups (**Table 4.2**).

Tumors and anterior prostate (AP) samples demonstrated an even more selective carotenoid distribution pattern than the liver. Although lycopene was still the most abundant carotenoid in both tissues (48% and 44%, respectively), ζ-carotene accumulation increased to 21% and 39% of total carotenoids, respectively (**Fig. 4.2B, C**). Notably, although present at 29% in the diet and 16% in the liver, phytoene was not detected in any tumor or AP samples (**Table 4.2**). Like the liver, no significant differences between TP and TP-I treatments were observed in tumoral carotenoid accumulation (**Table 4.2**). Due to tissue limitations, only two pooled replicates per group (8 - 12 mice/replicate) were possible for AP analysis; therefore, we did not analyze these data statistically. However, for all detected carotenoids, the replicates in the TP or TP-I groups overlap with replicates in the other group (**Table 4.2**), suggesting that no significant differences would be observed had greater replication been possible.

Finally, levels of accumulation suggest that tumors and AP tissues experienced carotenoid saturation, whereas the liver did not. Average lycopene accumulation in the liver was

in the range of 14.5 – 17.5 nmol/g, whereas accumulation was ≥31-fold lower in AP samples (0.291 – 0.474 nmol/g) and ≥121-fold lower in tumors (0.010 – 0.012 nmol/g; **Table 4.2**). Moreover, across both TP and TP-I groups, hepatic total lycopene accumulation exhibited linear correlation with age at sacrifice (**Fig. 4.2D**). This relationship was also present with phytofluene (**Fig. 4.2E**), phytoene (data not shown), and ζ-carotene (**Fig. 4.2F**). In contrast, tumoral carotenoid accumulation did not demonstrate correlation with age at sacrifice (**Fig. 4.2G, H, I**). It is important to note that since no significant difference in sacrifice age was present between the treatment groups (CON: 28.1 ± 0.8 weeks, TP: 26.5 ± 0.8 weeks, TP-I: 27.4 ± 1.0 weeks), the only difference between the TP and TP-I treatments in length of dietary exposure to tomato carotenoids was due to the earlier exposure of animals in the TP group (at 4 weeks of age) compared to the TP-I group (12 weeks of age). Despite this, liver accumulation was not different between the two treatment groups (**Table 4.2**) and no differences in correlation between sacrifice age and liver carotenoid accumulation were observed (data not shown).

TP-I treatment preserves body weight compared to CON and TP treatments

Average group body weights were calculated from animals alive at each study week. As seen in **Figure 4.3**, a main effect of diet indicated that TP-I treatment preserved body weight ($p < 0.01$) compared to both the CON and TP treatment groups. Intact WT littermates are shown as a reference. Although there was no significant treatment*time interaction effect, *a priori*-defined contrast statements were used to compare the TP-I treatment to CON at each week of age. Six time points (weeks 19, 26, 27, 28, 29, and 30) reached $p \leq 0.01$ and one passed the Bonferroni's adjusted α (week 29, $p < 0.0018$; **Fig. 4.3**). Comparisons for every time point after 11 weeks of age were lower than $p < 0.05$ (data not shown).

TP-I treatment reduces CRPC tumor growth *in vivo*

Longitudinal 3D ultrasound measurements began at 10 weeks of age and continued biweekly until tumor detection. At the week of tumor detection ("Week 0"), tumor-bearing animals were switched to weekly scans for four subsequent weeks (Weeks +1, +2, +3, and +4) for construction of tumor growth curves *in vivo*. Age at tumor detection raged from 14 to 30 weeks of age (data not shown). Animals were sacrificed within one week of the final (Week +4) scan. Compared to both CON and TP, TP-I treatment significantly reduced the growth rate of CRPC tumors *in vivo* ($p \leq 0.0001$; **Fig. 4.4A**). Volumes at the last tumor scan, Week +4, were significantly reduced by TP-I compared to CON, but not compared to TP ($p = 0.05$; **Fig. 4.4B**).

TP-I treatment modulates tissue weights of mice at necropsy

At necropsy, TP-I trended towards a reduction in tumor weight, compared to CON ($p = 0.07$, **Fig. 4.5A**). Compared to CON, TP-I also decreased non-tumor-involved dorsolateral prostate weight ($p = 0.05$; **Fig. 4.5B**) and increased non-tumor-involved ventral prostate weight ($p = 0.03$, **Fig. 4.5C**). TP reduced DLP weight, relative to CON ($p = 0.04$; **Fig. 4.5B**). The difference between TP-I and TP in non-tumor-involved ventral prostate weight was also significant ($p = 0.01$; **Fig. 4.5C**). No significant differences were seen in seminal vesicle or non-tumor-involved anterior prostate weights (**Fig. 4.5D**, **E**). Although not significant, TP-I induced a numerical decrease in total weight of regional lymph node metastases (**Fig. 4.5F**); variability in this measure was driven by large metastases in the CON group. Finally, TP-I induced alterations in gonadal adipose depot weight in a tumor-dependent manner. No differences between treatments were observed in animals not bearing a tumor, but gonadal adipose depot weight in tumor-bearing mice was higher with TP-I treatment, compared to CON ($p \leq 0.01$, **Fig. 4.5G**).

This difference was also observed when analyzing all mice together (tumor-bearing and non-tumor-bearing mice; **Fig. 4.5G**).

TP-I does not significantly alter tumor or PCa incidence, but does inhibit metastasis to distant organs

No diet effects were observed in tumor incidence or histopathologically confirmed PCa incidence (**Fig. 4.6**). Sizable numerical decreases by TP-I treatment were observed in the incidences of neuroendocrine phenotypes in tumors and prostatic lobe-confined PCa, but these did not reach statistical significance (**Fig. 4.6**). However, whereas CON animals experienced a 20% incidence of gross lung metastasis, no mice in the TP-I group experienced gross metastasis to this organ (**Fig. 4.7**); this effect was statistically significant. TP-I non-significantly prevented gross metastasis to the liver; this lack of statistical effect likely owed to the low hepatic metastasis incidence observed in the CON group. TP treatment numerically reduced metastasis to the lungs and liver, but these changes were not significant. Incidence of regional lymph node metastasis was high (68% positive in CON) and although TP-I and TP both reduced this figure (-18 and -8 percentage points, respectively), these changes were not statistically significant (**Fig. 4.7**).

TP-I does not appear to inhibit CRPC progression through modulation of genes controlling androgen synthesis

We measured the tumoral expression of five genes that play a critical role in paracrine/autocrine androgen synthesis (*Hsd17b2, Hsd17b3, Akr1c6, Srd5a1, Srd5a2*), as well as the androgen receptor (*Ar*). No changes by dietary treatment were observed (**Fig. 4.8A**). In addition, we measured the expression of a mediator of angiogenesis (*Vegfa*) and carotenoid metabolism (*Bco2*) – neither gene was significantly modulated (**Fig. 4.8A**).

In addition, we assessed immunohistochemical Ki67 staining in non-tumor-involved dorsolateral prostatic tissue to determine whether dietary treatments may alter rates of cell division in the prostate. As seen in **Figure 4.8B**, although both TP and TP-I numerically reduced rates of proliferation, no significant differences were seen. The lack of effect may be due to high degree of variability seen in CON mice.

Discussion

In response to observational research suggesting that tomato intake may reduce the risk of PCa [1–6,36–38], several experimental animal studies have found that tomato feeding reduces carcinogenesis and tumorigenesis in models of primary PCa [11–13]. Although providing results to support the hypothesis that dietary sources of lycopene, like tomato, may reduce the risk of primary PCa, they do not address the role of dietary tomato in the etiology of CRPC, which is the late and lethal stage of the disease. To our knowledge, no studies have investigated the use of dietary tomato or lycopene in a model of CRPC carcinogenesis *in vivo*. Therefore, the objective of this work was to evaluate the effect of dietary tomato, imitating either lifelong consumption (TP) or adjuvant intervention (TP-I), on the incidence and progression of CRPC in the TRAMP model. Although the TP and TP-I treatment schemes produced no measureable differences in tissue carotenoid accumulation, we observed that TP-I and not TP treatment effectively reduced CRPC progression. TP-I reduced tumor growth *in vivo*, inhibited distant organ metastasis, and preserved body weight and gonadal adipose stores.

Levels of tomato feeding used in this study were intended to model achievable quantities of dietary lycopene intake and accumulation, as well as provide a translatable source and composition of tomato carotenoids. Epidemiological studies suggest that median/mean intakes of

13 – 19 mg lycopene/day [1,3,4] have been associated with a reduced risk of primary PCa. As one serving of tomato sauce (1 cup) or tomato paste (0.25 cup) contains 34 mg or 19 mg lycopene, respectively (per the U.S.D.A. Nutrient Composition Database), achievable levels of tomato intake may have protective effects. Indeed, consumption of as little as 1 serving of tomato sauce/week has been inversely associated with PCa risk [1,3]. At 10% w/w of the diet, the tomato paste used in this study provided, on average, 0.1 mg lycopene/day to a mouse; converted to a human equivalent dose [39], this would be comparable to approximately 19 mg/day in a 90-kg adult human. This would be equivalent to consumption of about ½ serving of tomato sauce, or about 1 serving of tomato paste. Thus, the level of dietary tomato inclusion in the current study reflects levels of human lycopene intake that are both physiologically relevant and likely protective. Tomatoes contain many bioactives aside from lycopene [40] and evidence suggests that tomatoes may be more effective in reducing PCa carcinogenesis and tumorigenesis than lycopene alone [12,13,41]. Our choice to use a whole tomato product, and moreover one which is commercially available to consumers, reflects our desire to investigate dietary treatments with the greatest translatability possible in an animal study.

Rates of tumor incidence were slightly lower than previously reported [28], even after the original protocol was extended from 24 weeks to 30 weeks due to low tumor incidence at 24 weeks (data not shown). Neuroendocrine tumor pathology incidence was also lower than previously reported [42].

Compared to CON, TP-I reduced tumor growth and volume *in vivo,* while simultaneously resulting in greater body weight and gonadal adipose. Notably, this effect on gonadal adipose weight was not present in non-tumor-bearing animals. The main-effect difference in body weight between CON and TP-I treatments was approximately 1.9 grams; nearly one third of that gap

was accounted for by the difference in gonadal adipose depot weight (0.6 grams). Cancer cachexia is characterized by wasting of adipose and skeletal muscle, reduced quality of life, and decreased survival [43]. Cancer cachexia is driven primarily by metabolic derangements and a mix of tumor and host-derived inflammatory cytokines [44]. Within CRPC patients, elevated BMI (>25) is inversely associated with PCa-specific mortality [45], suggesting that preservation of body mass is indicative of either lower cancer burden or alteration of cancer biology. TP-I treatment may have lessened a pro-cachectic tumor burden, thus helping to preserve adipose stores and body weight. It is interesting to note that, temporally, the first indication of an effect ($p < 0.05$) of TP-I on longitudinal body weight (relative to CON) was observed at the 12-week time point, when animals were castrated and the transition from control diet to 10% LTP occurred in the TP-I group. Although provision of diet was measured and recorded three times a week, due to burrowing activity and waste on the floor of the cage, accurate food intake data were not available from which to draw conclusions. Regardless, these differences in body weight and adipose depot weight suggest a unique role of the TP-I treatment in reducing the impact of CRPC in this model.

Surprisingly, TP did not reduce mean CRPC tumor growth rate and volume *in vivo,* as seen with TP-I treatment. We hypothesized that the longer dietary exposure provided by the TP treatment would result in a stronger effect than the TP-I treatment, which was designed to model adjuvant intervention. The present results were unexpected, given that a tomato powder intervention (initiated at 8 weeks of age) had previously failed to prevent primary PCa in the TRAMP model [27]. One possibility to explain our findings is that heterogeneity in tumor responses may have masked positive effects of the TP treatment. Although comparison of group mean tumor growth curves (**Fig. 4.4A**) show the CON and TP groups to have nearly identical

growth rates, examination of individual curves demonstrates the potential existence of phenotypic non-responders (**Appendix Fig. C.1**). Both fast- and slow-growing tumors can be seen in the CON group and rates of growth are evenly distributed; in contrast, TP and TP-I treatments both demonstrate a predominance of slow-growing tumors, with the exception of three tumors in the TP group and one in the TP-I treatment group. These divergent tumors can also be seen on graphs of the Week +4 tumor volume (**Fig. 4.4B**) and tumor weight at necropsy (**Fig. 4.5A**; two of these mice in the TP group died between their last ultrasound scan and necropsy, making tumor weight data unavailable). If these animals were to be excluded from group mean tumor growth rates, the TP growth rate curve approximated the TP-I curve more so than the CON growth curve (**Appendix Fig. C.2**). It can also be seen in **Figs. 4.4B** and **4.5A** that these data points drive their respective group means upward. Data which follow binomial distributions, such as incidence data, are inherently unbiased by individual values and thus may reflect average group behavior in the presence of outliers more faithfully than continuous data. In binomial measures of metastasis incidence, TP performs similarly to TP-I in lung metastasis, liver metastasis, and all distant organ metastasis, albeit non-significantly relative to CON (**Fig. 4.7**).

It is known that genomic and transcriptomic signatures of CRPC tumors demonstrate large patient-to-patient variability [46] and that molecular subtype can be prognostic for clinical outcomes [47–51]. Among these signatures are markers of hormonal responsiveness; most CRPC tumors are androgen-sensitive [52,53] and often rely on local production of androgens despite ablation of circulating androgens by androgen deprivation therapy [54–56]. It has been shown that tomato carotenoids may modulate androgen-metabolic genes [57–59] and unpublished data from our own lab suggest that dietary tomato inhibits primary PCa in the TRAMP model while altering

expression of androgen biosynthetic genes *Hsd17b2* and *Hsd17b3* (Zuniga, unpublished data). However, gene expression analysis on CRPC tumors in the present study revealed no significant differences between treatment groups in the mRNA expression of *Hsd17b2, Hsd17b3, Srd5a1, Srd5a2,* or *Ar* (**Fig. 4.8A**). Moreover, expression of these genes did not correlate with tumor weight at necropsy (data not shown). Angiogenesis markers have been associated with increased risk of PCa metastasis and mortality [7], and dietary lycopene is associated with lower levels of angiogenesis and mortality [4]. However, tumoral mRNA expression of *Vegfa* was not modulated by treatment group (**Fig. 4.8A**), nor did it correlate with tumor growth (data not shown). Protein expression analysis of several of these genes is underway. The current study captures too few non-responder tumors to definitely conclude that divergent tumor phenotypes contributed to heterogeneity in the TP treatment group. Furthermore, the gene expression endpoints investigated thus far do not support the existence of heterogeneity in transcriptional subtypes within the TP treatment group. Additional analysis is needed to clarify the mechanism of reduced tumor growth by TP-I and whether a heterogeneity of tumor phenotypes exists within the TP treatment group.

Tissue carotenoid accumulation in the present study supports previous reports in various rodent models. Liver represents a major site of carotenoid metabolism, as well as a major depot of storage [60–63]. The two previous TRAMP studies from our lab provided 533 and 23.8 nmol nmol lycopene/g diet from tomato powder, resulting in hepatic lycopene concentrations of 4.6 and 1.9 nmol/g after 14 and 12 weeks of feeding, respectively [14,27]. In contrast, whereas the current study provided only 37.5 nmol/g dietary lycopene, hepatic accumulation of this carotenoid was 14.5 or 17.5 nmol/g with TP or TP-I treatment, respectively. These hepatic concentrations were up to 3.8-fold higher than reported by Zuniga et al, despite feeding 14-fold

lower levels of dietary lycopene. This difference is very likely due to the difference in castration status between the to studies – prior work has shown that castrated rats accumulated roughly double that of intact rats, even when fed 10-fold lower levels of dietary lycopene [64,65]. Hepatic concentrations of the four major carotenoids significantly correlated with length of exposure in the current study. These data additionally suggest that carotenoids accumulated in the liver as a function of time on diet and that the accumulation was still in a linear phase (i.e., no saturation occurring) up to 30 weeks of exposure within this study. Moreover, hepatic accumulation of phytoene and ζ-carotene was significantly ($p < 0.05$) increased ~ 1.7-fold in non-tumor-bearing animals compared to tumor-bearing animals; lycopene and phytofluene exhibited similar, but non-significant trends (data not shown). This, too, was almost certainly an effect of dietary exposure length, as non-tumor-bearing mice were sacrificed at 30 wk of age (per protocol) and tumor-bearing animals were, by design, not on study as long (average age 23.3 ± 0.8 wk). An alternative explanation could be that the presence of a tumor increased systemic inflammation, oxidative stress, or metabolic rate, thus resulting in greater catabolism of hepatic carotenoids. Although dietary exposure length and tumor presence are confounded in this endpoint, precluding a definitive conclusion, exposure length is a more parsimonious explanation for the patterns of hepatic accumulation observed. Despite the strong effect of dietary exposure length on hepatic carotenoid accumulation, hepatic carotenoid accumulation did not differ between the TP and TP-I treatments, which differed in average dietary exposure by approximately 8 weeks of age. However, Conlon et al. also reported no significant difference between mice fed tomato diets for 8 or 12 weeks [27].

Interestingly, carotenoid accumulation in serum and extra-hepatic tissues, in contrast to the liver, is *not* affected by androgen status [64,65]. This suggests that either carotenoid metabolism

in the liver is uniquely responsive to circulating androgens, that extra-hepatic tissues experience saturation at levels of exposure much lower than the liver, or both. Comparing data from the report by Conlon et al. (feeding 23.8 nmol lycopene/g tomato diet to TRAMP mice for 4, 8, or 12 wk) to the current study (feeding 37.5 nmol lycopene/g tomato diet to castrated TRAMP mice for 2 – 30 wk) sheds light on this issue. Lycopene accumulation in anterior prostate tissue from castrated TRAMP mice (0.3 – 0.5 nmol/g, **Table 4.2**) is equivalent to that in intact TRAMP mice (0.4 nmol/g, [27]). This suggests that despite atrophy of the anterior prostate after androgen deprivation by castration, relative accumulation of carotenoids proceeds unimpaired. Moreover, carotenoid accumulation in the anterior prostate [27] and prostatic tumor tissue (**Fig. 4.2G-I**) does not increase with longer dietary exposure, in contrast to the liver. This demonstrates that these tissues indeed do saturate at carotenoid exposures lower than those necessary to saturate the liver.

In agreement with previous reports in gerbils, mice, and rats, phytoene was not detected in prostates or tumors [14,27,33,66]. As previously reported in gerbils [66], ζ-carotene was a highly abundant carotenoid in prostatic tissues, despite its presence at <5% of the diet. Mechanisms responsible for these differences in carotenoid distribution remain unresolved. This area continues to be one of active research, and genetic factors, tissue-specific receptors, or differences in lipoprotein handling may play a role [61].

Conclusions

In conclusion, we have shown, for the first time, that dietary tomato can reduce CRPC progression in an animal model. CRPC tumor volume and rate of CRPC tumor growth were reduced nearly 50% by adjuvant dietary tomato intervention following surgical castration. In

addition, compared to control feeding, adjuvant tomato treatment reduced distant gross metastasis to the lungs, and preserved gonadal adipose and body weights. Importantly, CRPC progression was reduced with clearly achievable levels of dietary tomato intake, and through use of a common tomato food source that is already commercially available to consumers. These effects should be replicated and extended in future animal studies to examine the effects of adjuvant dietary tomato in conjunction with pharmacological androgen deprivation therapy, which is the current first-line therapy in men with metastatic recurrent PCa. Additionally, it would be important to ascertain whether a dose escalation intervention - e.g., lifelong basal tomato exposure + elevated exposure at intervention – would yield similar results, as few men abstain from all tomato intake prior to PCa diagnosis and treatment. Hopefully, these data can eventually be translated into improved clinical outcomes for men with CRPC.

References cited

1. Giovannucci, E. L. *et al.* Intake of carotenoids and retinol in relation to risk of prostate cancer. *J. Natl. Cancer Inst.* **87,** 1767–76 (1995).
2. Giovannucci, E. L., Liu, Y., Platz, E. A., Stampfer, M. J. & Willett, W. C. Risk factors for prostate cancer incidence and progression in the health professionals follow-up study. *Int. J. Cancer* **121,** 1571–8 (2007).
3. Giovannucci, E. L., Rimm, E. B., Liu, Y., Stampfer, M. J. & Willett, W. C. A prospective study of tomato products, lycopene, and prostate cancer risk. *J. Natl. Cancer Inst.* **94,** 391–8 (2002).
4. Zu, K. *et al.* Dietary lycopene, angiogenesis, and prostate cancer: A prospective study in the prostate-specific antigen era. *J. Natl. Cancer Inst.* **106,** djt430 (2014).
5. Vogt, T. M. *et al.* Serum lycopene, other serum carotenoids, and risk of prostate cancer in U.S. blacks and whites. *Am. J. Epidemiol.* **155,** 1023–1032 (2002).
6. Chan, J. M. *et al.* Diet after diagnosis and the risk of prostate cancer progression, recurrence, and death (United States). *Cancer Causes Control* **17,** 199–208 (2006).
7. Mucci, L. A. *et al.* Prospective study of prostate tumor angiogenesis and cancer-specific mortality in the Health Professionals Follow-Up Study. *J. Clin. Oncol.* **27,** 5627–5633 (2009).
8. Stark, J. R. *et al.* Gleason score and lethal prostate cancer: Does 3 + 4 = 4 + 3? *J. Clin. Oncol.* **27,** 3459–64 (2009).
9. Schröder, F. H. *et al.* The TNM classification of prostate cancer. *Prostate. Suppl.* **4,** 129–38 (1992).

10. Siegel, R. L., Miller, K. D. & Jemal, A. Cancer Statistics, 2016. *CA. Cancer J. Clin.* **66,** 7–30 (2016).

11. Pannellini, T. *et al.* A dietary tomato supplement prevents prostate cancer in TRAMP mice. *Cancer Prev. Res.* **3,** 1284–91 (2010).

12. Boileau, T. W.-M. *et al.* Prostate carcinogenesis in N-methyl-N-nitrosourea (NMU)-testosterone-treated rats fed tomato powder, lycopene, or energy-restricted diets. *J. Natl. Cancer Inst.* **95,** 1578–1586 (2003).

13. Canene-Adams, K. *et al.* Combinations of tomato and broccoli enhance antitumor activity in Dunning R3327-H prostate adenocarcinomas. *Cancer Res.* **67,** 836–43 (2007).

14. Zuniga, K. E., Clinton, S. K. & Erdman, J. W. The interactions of dietary tomato powder and soy germ on prostate carcinogenesis in the TRAMP model. *Cancer Prev. Res.* **6,** 548–57 (2013).

15. Attard, G. *et al.* Prostate cancer. *Lancet* **387,** 70–82 (2015).

16. Geethakumari, P. R., Cookson, M. S. & Kevin, W. The evolving biology of castration-resistant prostate cancer: Review of recommendations from the Prostate Cancer Clinical Trials Working Group 3. *Oncology* **30,** 187–95 (2016).

17. Beer, T. M. *et al.* Enzalutamide in metastatic prostate cancer before chemotherapy. *N. Engl. J. Med.* **371,** 424–433 (2014).

18. de Bono, J. S. *et al.* Abiraterone and increased survival in metastatic prostate cancer. *N. Engl. J. Med.* **364,** 1995–2005 (2011).

19. Butler, S. *et al.* Use of complementary and alternative medicine among men with prostate cancer in a rural setting. *J. Community Health* **36,** 1004–1010 (2011).

20. Jatoi, A. *et al.* A tomato-based, lycopene-containing intervention for androgen-independent prostate cancer: results of a Phase II study from the North Central Cancer Treatment Group. *Urology* **69,** 289–94 (2007).

21. Ansari, M. S. & Gupta, N. P. A comparison of lycopene and orchidectomy vs orchidectomy alone in the management of advanced prostate cancer. *BJU Int.* **92,** 375–378 (2003).

22. Bratt, O. A comparison of lycopene and orchidectomy vs orchidectomy alone in the management of advanced prostate cancer - Letter. *BJU Int.* 192 (2005).

23. Ansari, M. S. & Gupta, N. P. Reply to Bratt - A comparison of lycopene and orchidectomy vs. orchidectomy alone in the management of advanced prostate cancer. *BJU Int.* **93,** 678 (2004).

24. Tang, Y. *et al.* Lycopene enhances docetaxel's effect in castration-resistant prostate cancer associated with insulin-like growth factor I receptor levels. *Neoplasia* **13,** 108–119 (2011).

25. Tang, L., Jin, T., Zeng, X. & Wang, J. Lycopene inhibits the growth of human androgen-independent prostate cancer cells in vitro and in BALB/c nude mice. *J. Nutr.* **135,** 287–290 (2005).

26. Greenberg, N. M. *et al.* Prostate cancer in a transgenic mouse. *Proc. Natl. Acad. Sci.* **92,** 3439–3443 (1995).

27. Conlon, L. E., Wallig, M. A. & Erdman, J. W. Low-lycopene containing tomato powder diet does not protect against prostate cancer in TRAMP mice. *Nutr. Res.* **35,** 882–890 (2015).

28. Gingrich, J. R. *et al.* Androgen-independent Prostate Cancer Progression in the TRAMP Model. *Cancer Res.* **57,** 4687–4691 (1997).

29. National Research Council, *Guide for the Care and Use of Laboratory Animals: Eighth Edition*. (The National Academies Press, 2011).

30. Wirtzfeld, L. A. *et al.* A new three-dimensional ultrasound microimaging technology for preclinical studies using a transgenic prostate cancer mouse model. *Cancer Res.* **65,** 6337–6345 (2005).

31. Conlon, L. E. Reducing the risk of prostate cancer with tomatoes and soy. *Dissertation, University of Illinois at Urbana-Champaign*. 149 pages (2015).

32. Lu, C.-H., Engelmann, N. J., Lila, M. A. & Erdman, J. W. Optimization of lycopene extraction from tomato cell suspension culture by response surface methodology. *J. Agric. Food Chem.* **56,** 7710–4 (2008).

33. Zuniga, K. E. & Erdman, J. W. Combined consumption of soy germ and tomato powders results in altered isoflavone and carotenoid bioavailability in rats. *J. Agric. Food Chem.* **59,** 5335–41 (2011).

34. Schindelin, J. *et al.* Fiji: an open-source platform for biological-image analysis. *Nat. Methods* **9,** 676–82 (2012).

35. Varghese, F., Bukhari, A. B., Malhotra, R. & De, A. IHC profiler: An open source plugin for the quantitative evaluation and automated scoring of immunohistochemistry images of human tissue samples. *PLoS One* **9,** (2014).

36. Etminan, M., Takkouche, B. & Caamaño-Isorna, F. The role of tomato products and lycopene in the prevention of prostate cancer: A meta-analysis of observational studies. *Cancer Epidemiol. Biomarkers Prev.* **13,** 340–345 (2004).

37. Nordström, T. *et al.* Associations between circulating carotenoids, genomic instability and the risk of high-grade prostate cancer. *Prostate* **348,** 339–348 (2015).

38. Wang, Y., Jacobs, E. J., Newton, C. C. & McCullough, M. L. Lycopene, tomato products and prostate cancer-specific mortality among men diagnosed with nonmetastatic prostate cancer in the Cancer Prevention Study-II Nutrition Cohort. *Int. J. Cancer* **138,** 2846-2855 (2016).

39. Reagan-Shaw, S., Nihal, M. & Ahmad, N. Dose translation from animal to human studies revisited. *FASEB J.* **22,** 659–61 (2008).

40. Canene-Adams, K., Campbell, J. K., Zaripheh, S., Jeffery, E. H. & Erdman Jr., J. W. The tomato as a functional food. *J. Nutr.* **135,** 1226–1230 (2005).

41. Gitenay, D. *et al.* Serum from rats fed red or yellow tomatoes induces connexin43 expression independently from lycopene in a prostate cancer cell line. *Biochem. Biophys. Res. Commun.* **364,** 578–82 (2007).

42. Huss, W. J. *et al.* Origin of androgen-insensitive poorly differentiated tumors in the transgenic adenocarcinoma of mouse prostate model. *Neoplasia* **9,** 938–950 (2007).

43. Tisdale, M. J. Mechanisms of cancer cachexia. *Physiol. Rev.* **89,** 381–410 (2009).

44. Argilés, J. M., Busquets, S., Stemmler, B. & López-Soriano, F. J. Cancer cachexia: Understanding the molecular basis. *Nat. Rev. Cancer* **14,** 754–762 (2014).

45. Halabi, S., Ou, S.-S., Vogelzang, N. J. & Small, E. J. Inverse correlation between body mass index and clinical outcomes in men with advanced castration–recurrent prostate cancer. *Cancer* **110,** 1478–1484 (2007).

46. Kumar, A. *et al.* Substantial interindividual and limited intraindividual genomic diversity among tumors from men with metastatic prostate cancer. *Nat. Med.* **22,** 369-378 (2016).

47. Huang, S.-P. *et al.* Genetic variants in CASP3, BMP5, and IRS2 genes may influence survival in prostate cancer patients receiving androgen-deprivation therapy. *PLoS One* **7,** e41219 (2012).

48. Sun, T. *et al.* The impact of common genetic variations in genes of the sex hormone metabolic pathways on steroid hormone levels and prostate cancer aggressiveness. *Cancer Prev. Res.* **4,** 2044–50 (2011).

49. Fujimoto, N. *et al.* Polymorphisms of the androgen transporting gene SLCO2B1 may influence the castration resistance of prostate cancer and the racial differences in response to androgen deprivation. *Prostate Cancer Prostatic Dis.* **16,** 336–40 (2013).

50. Nakabayashi, M. *et al.* Clinical predictors of survival in men with castration-resistant prostate cancer: Evidence that Gleason score 6 cancer can evolve to lethal disease. *Cancer* **119,** 2990–2998 (2013).

51. Grasso, C. S. *et al.* The mutational landscape of lethal castration-resistant prostate cancer. *Nature* **487,** 239–243 (2012).

52. Feldman, B. J. & Feldman, D. The development of androgen-independent prostate cancer. *Nat. Rev. Cancer* **1,** 34–45 (2001).

53. Mellado, B., Codony, J., Ribal, M. J., Visa, L. & Gascón, P. Molecular biology of androgen-independent prostate cancer: The role of the androgen receptor pathway. *Clin. Transl. Oncol.* **11,** 5–10 (2009).

54. Montgomery, R. B. *et al.* Maintenance of intratumoral androgens in metastatic prostate cancer: A mechanism for castration-resistant tumor growth. *Cancer Res.* **68,** 4447–54 (2008).

55. Locke, J. A. *et al.* Androgen levels increase by intratumoral de novo steroidogenesis during progression of castration-resistant prostate cancer. *Cancer Res.* **68,** 6407–15 (2008).

56. Chang, K.-H. *et al.* Dihydrotestosterone synthesis bypasses testosterone to drive castration-resistant prostate cancer. *Proc. Natl. Acad. Sci.* **108,** 13728-13733 (2011).

57. Siler, U. *et al.* Lycopene and vitamin E interfere with autocrine/paracrine loops in the Dunning prostate cancer model. *FASEB J.* **18,** 1019–21 (2004).

58. Herzog, A. *et al.* Lycopene reduced gene expression of steroid targets and inflammatory markers in normal rat prostate. *FASEB J.* **24,** 1–24 (2004).

59. Wan, L. *et al.* Dietary tomato and lycopene impact androgen signaling- and carcinogenesis-related gene expression during early TRAMP prostate carcinogenesis. *Cancer Prev. Res.* **7,** 1228–1239 (2014).

60. Olson, J. A. & Hayaishi, O. The enzymatic cleavage of beta-carotene into vitamin A by soluble enzymes of rat liver and intestine. *Proc. Natl. Acad. Sci.* **54,** 1364–1370 (1965).

61. Moran, N. E., Erdman, J. W. & Clinton, S. K. Complex interactions between dietary and genetic factors impact lycopene metabolism and distribution. *Arch. Biochem. Biophys.* **539,** 171-180 (2013).

62. Tan, H. *et al.* Beta-carotene-9', 10'-oxygenase status modulates the impact of dietary tomato and lycopene on hepatic nuclear receptor- , stress- , and metabolism-related gene expression in mice. *J. Nutr.* **144,** 431-439 (2014).

63. Gajic, M., Zaripheh, S., Sun, F. & Erdman, J. W. Apo-8'-lycopenal and apo-12'-lycopenal are metabolic products of lycopene in rat liver. *J. Nutr.* **136,** 1552–1557 (2006).

64. Boileau, T. W.-M., Clinton, S. K. & Erdman, J. W. Tissue lycopene concentrations and isomer patterns are affected by androgen status and dietary lycopene concentration in male F344 rats. *J. Nutr.* **130,** 1613–8 (2000).

65. Boileau, T. W.-M. *et al.* Testosterone and food restriction modulate hepatic lycopene isomer concentrations in male F344 rats. *J. Nutr.* **131,** 1746–52 (2001).

66. Moran, N. E., Clinton, S. K. & Erdman Jr., J. W. Differential bioavailability, clearance, and tissue distribution of the acyclic tomato carotenoids lycopene and phytoene in mongolian gerbils. *J. Nutr.* **143,** 1920–1926 (2013).

Table 4.1.

	g/100 g diet	
	CON	**10% LTP [d]**
Cornstarch	39.0	36.3
Maltodextrin	13.0	10.5
Sucrose	9.8	9.7
Casein	19.6	17.7
Cellulose	4.9	4.1
Mineral Mix [a]	3.4	3.4
Vitamin Mix [b]	1.0	1.0
L-Cystine	0.3	0.3
Choline bitartrate	0.2	0.2
Soybean oil	7.0	6.8
LTP	0.0	10.0 [e]
Water	1.8	0.0
Total	*100.0*	*100.0*
Energy density (kcal/g diet) [c]	3.88	3.84

Table 4.1. Composition of experimental diets.

[a] AIN-93-MX formulation

[b] AIN-93-VX formulation

[c] Calculated.

[d] Lyophilized tomato paste (Contadina® Foods, San Francisco, CA)

[e] As determined by proximate analysis, 10.0 g LTP provided 4.5 g total carbohydrates, 1.7 g crude protein, 0.1 g crude fat, 0.8 g crude fiber, 1.8 g water, and 1.1 g ash.

Figure 4.1.

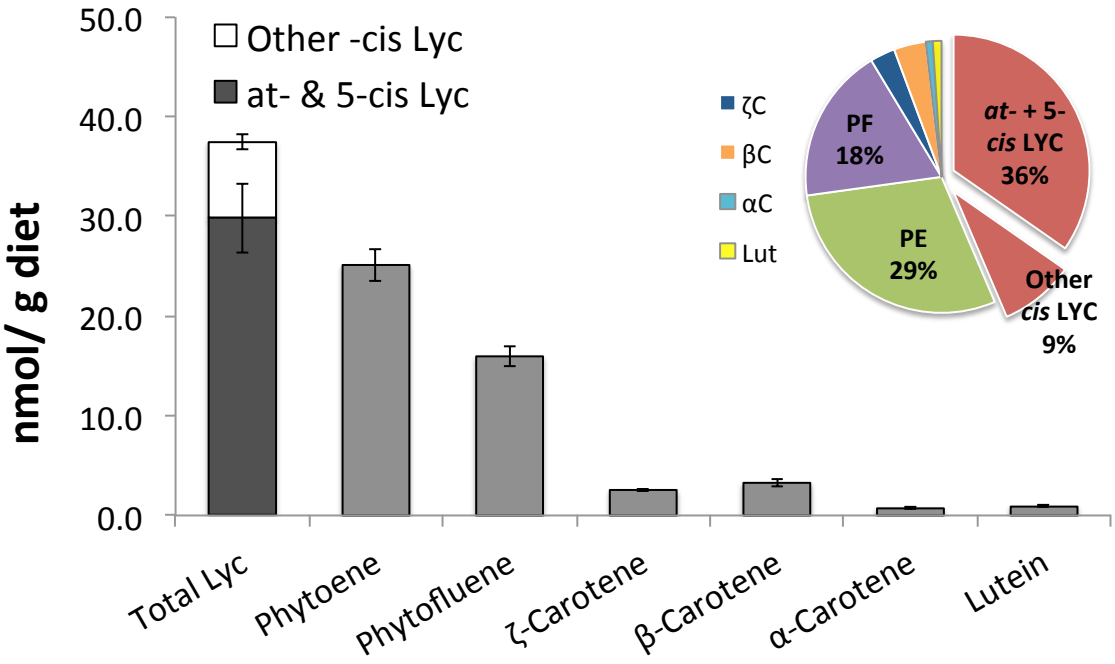

Figure 4.1. 10% LTP diet carotenoid composition. Data are group means ± SEM across all 7 diet batches. n = 2 replicates/batch. Inset displays average diet profile. Four minor carotenoids (<5%) are listed in the legend to the side of the pie chart. *at,* all *trans;* LYC, lycopene; PE, phytoene; PF, phytofluene; ζ C, ζ-Carotene; βC, β-Carotene; α C, α-Carotene; Lut, lutein.

Table 4.2.

	nmol/g		
	CON	**TP**	**TP-I**
Liver			
Total carotenoids	0.02 ± 0.01	30.6 ± 1.77	36.4 ± 2.17
Total Lycopene	0.02 ± 0.01	14.5 ± 1.96	17.51 ± 2.09
at- + 5-*cis* Lycopene	0.02 ± 0.01	10.9 ± 1.49	13.3 ± 1.60
Other *cis* Lycopene	n.d.	3.60 ± 0.47	4.19 ± 0.49
Phytoene	n.d.	5.01 ± 0.83	5.80 ± 0.70
Phytofluene	n.d.	9.54 ± 1.48	11.43 ± 1.42
ζ-Carotene	n.d.	1.50 ± 0.19	1.59 ± 0.18
β-Carotene	n.d.	n.d.	n.d.
α-Carotene	n.d.	0.03 ± 0.00	0.02 ± 0.00
Lutein	n.d.	n.d.	n.d.
Anterior Prostate			
Total carotenoids	n.d., 0.010	0.695, 1.055	0.785, 0.838
Total Lycopene	n.d., 0.010	0.291, 0.474	0.324, 0.407
at- + 5-*cis* Lycopene	n.d., 0.010	0.165, 0.283	0.194, 0.251
Other *cis* Lycopene	n.d., n.d.	0.126, 0.191	0.130, 0.156
Phytoene	n.d., n.d.	n.d., n.d.	n.d., n.d.
Phytofluene	n.d., n.d.	0.131, 0.169	0.111, 0.134
ζ-Carotene	n.d., n.d.	0.274, 0.412	0.296, 0.350
β-Carotene	n.d., n.d.	n.d., n.d.	n.d., n.d.
α-Carotene	n.d., n.d.	n.d., n.d.	n.d., n.d.
Lutein	n.d., n.d.	n.d., n.d.	n.d., n.d.
Tumor			
Total carotenoids	n.d.	0.19 ± 0.05	0.31 ± 0.06
Total Lycopene	n.d.	0.10 ± 0.02	0.12 ± 0.02
at- + 5-*cis* Lycopene	n.d.	0.06 ± 0.01	0.08 ± 0.01
Other *cis* Lycopene	n.d.	0.03 ± 0.01	0.04 ± 0.01
Phytoene	n.d.	n.d.	n.d.
Phytofluene	n.d.	0.05 ± 0.02	0.13 ± 0.03
ζ-Carotene	n.d.	0.04 ± 0.01	0.06 ± 0.01
β-Carotene	n.d.	n.d.	n.d.
α-Carotene	n.d.	n.d.	n.d.
Lutein	n.d.	n.d.	n.d.

Table 4.2. Tissue carotenoid accumulation. Values for liver and tumor are mean ± SEM, whereas both duplicates analyzed are reported for anterior prostate. Liver n = 14 for TP and TP-I, n = 3 for CON; tumors n = 5 for TP and TP-I, n = 3 for CON; anterior prostate n = 2 pools of 8 - 12 mice/group. n.d., not detectable. There were no significant differences in accumulation between the TP and TP-I diets.

Figure 4.2.

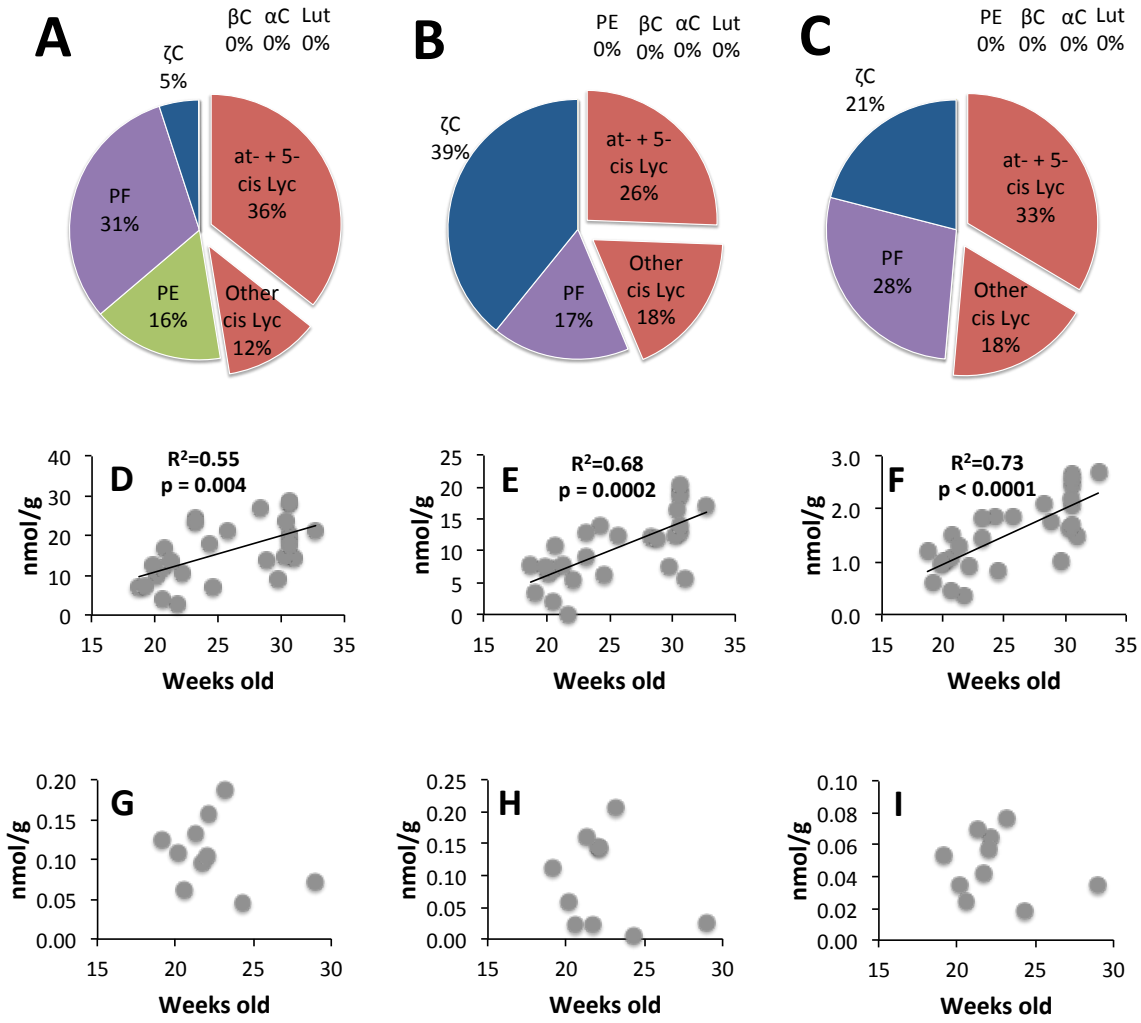

Figure 4.2. Carotenoids accumulate in a tissue-specific manner in the CRPC TRAMP model. Liver (**A**), anterior prostate (**B**), and tumor (**C**) accumulation profiles in TP mice. Mice in the TP-I dietary group had similar patterns of accumulation (data not shown). Liver accumulation of lycopene (**D**), phytofluene (**E**), and ζ-carotene (ζC, **F**) correlates with length of dietary exposure ("Weeks old" indicates weeks old at sacrifice), whereas tumor accumulation of lycopene (**G**), phytofluene (**H**), and ζC (**I**) does not.

Figure 4.3

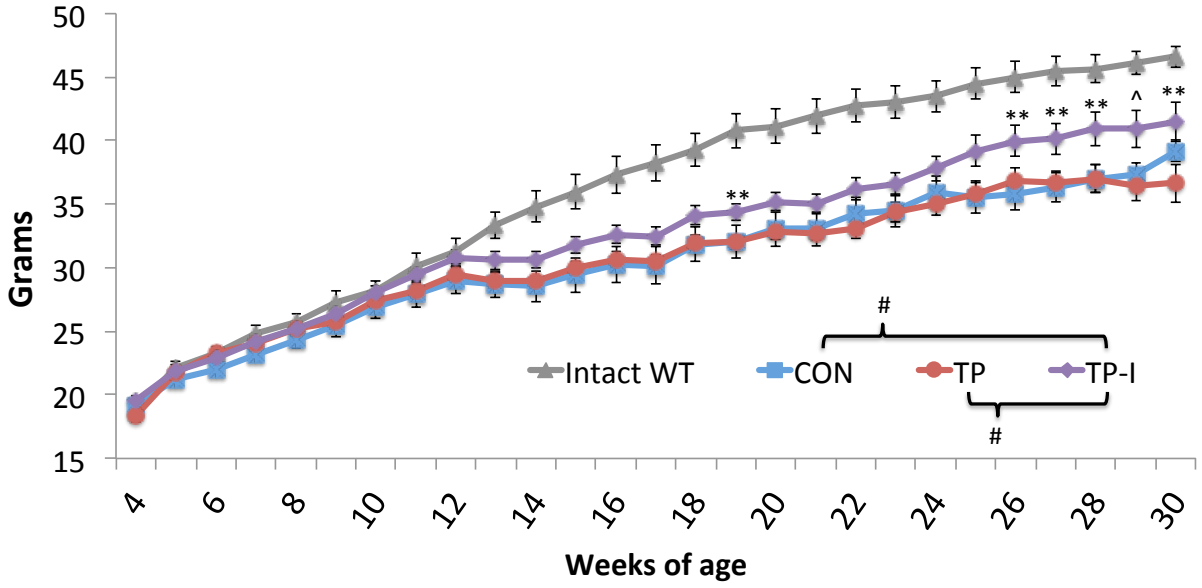

Figure 4.3. TP-I treatment preserves body weight compared to CON and TP in the CRPC TRAMP model. Data represent weekly weight ± SEM. Intact (non-castrated) WT littermates are shown for reference. Longitudinal comparison of CON and TP-I treatment was tested with 27 individual contrasts (Bonferroni's adjusted $\alpha = 0.0018$); ^ TP-I vs. CON $p < 0.0018$; ** TP-I vs. CON $p \leq 0.01$. # Indicates significant main effect of diet ($p < 0.01$ for both CON vs. TP-I and TP vs. TP-I).

Figure 4.4.

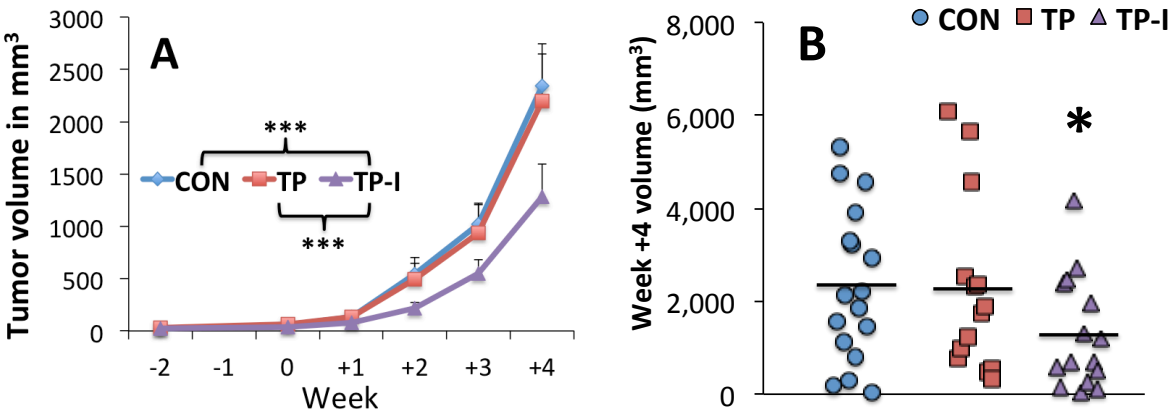

Figure 4.4. TP-I reduces CRPC tumor growth *in vivo*. **A**, TP-I reduces rate of tumor growth as measured by longitudinal 3D ultrasound. Week of tumor detection is set at "0". Data shown are means ± SEM. Group n = 15 - 17. Non-linear exponential regression was used to determine best-fit curves from all data points within a group. ***$p \leq 0.0001$ for the test of the null hypothesis that one best-fit curve describes both groups. **B**, Tumor volume at the Week +4 scan (calculated by 3D ultrasound) is reduced in TP-I animals, compared to CON-fed animals. Data represent individual mice. Group n = 15 – 17. The black line marks the group mean. *$p \leq 0.05$ vs. CON.

Figure 4.5.

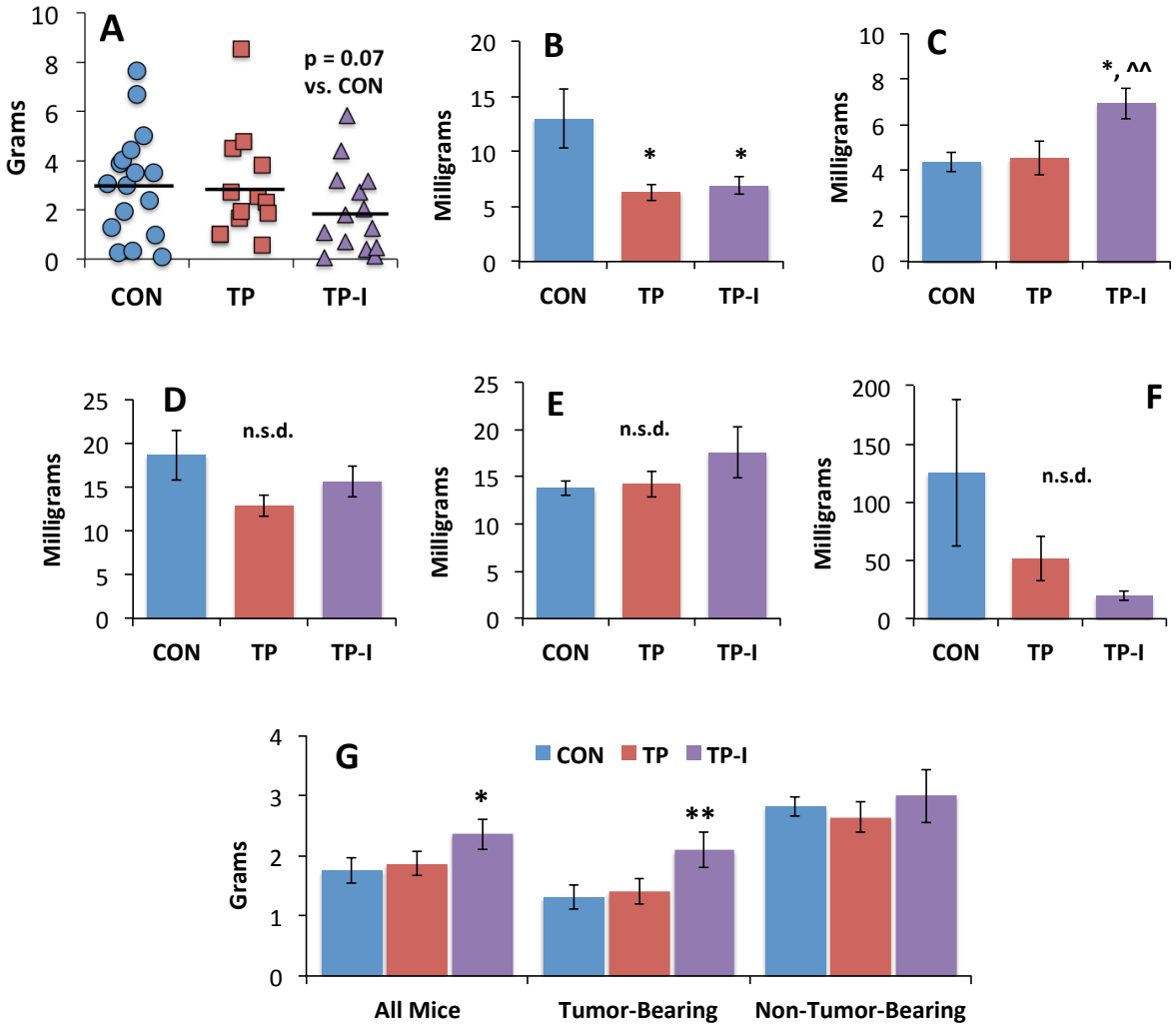

Figure 4.5. Selected tissue weights in TRAMP CRPC mice. Tumor weight (**A**) trends lower in TP-I mice, relative to CON. Data points represent individual mice and the black line marks the group mean. TP and TP-I reduce dorsolateral prostate weight (**B**), whereas TP-I increases ventral prostate weight (**C**). No significant differences were observed in the weights of anterior prostate (**D**), seminal vesicles (**E**), or gross regional lymph node metastases (**F**), although within gross lymph node metastases, there was a trend for main effect of diet ($p = 0.07$). TP-I increases gonadal adipose depot weights in a tumor-dependent manner (**G**). *$p \leq 0.05$ vs. CON; **$p \leq 0.01$ vs. CON, ^^$p \leq 0.01$ vs. TP. n.s.d., no significant differences.

Figure 4.6.

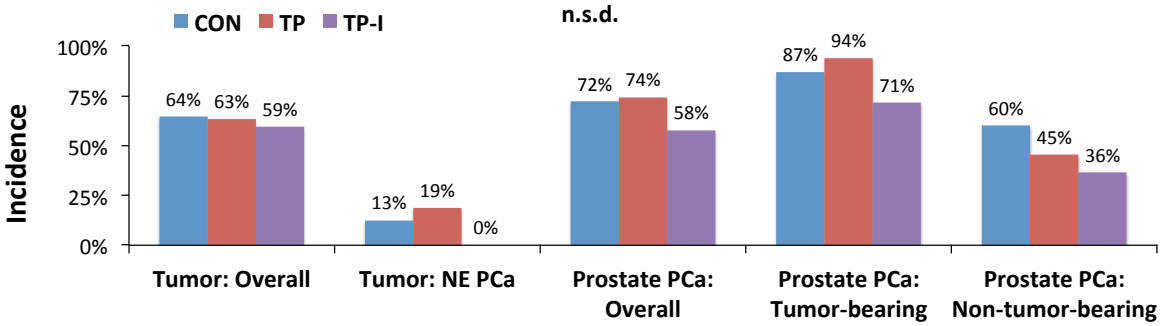

Figure 4.6. Tomato diets do not significantly reduce CRPC incidence. Tumor incidence was identified by visual inspection during necropsy. All tumors were confirmed by histopathology (data not shown). Neuroendocrine (NE) incidence and PCa incidence in non-tumor-involved prostatic lobes were determined by histopathology by a blinded examiner. Prostatic lobe PCa was considered positive if observed in any of the dorsolateral, ventral, or anterior lobes. Statistical analysis was done by two-tailed Fisher's Exact Test. n.s.d., no significant differences.

Figure 4.7.

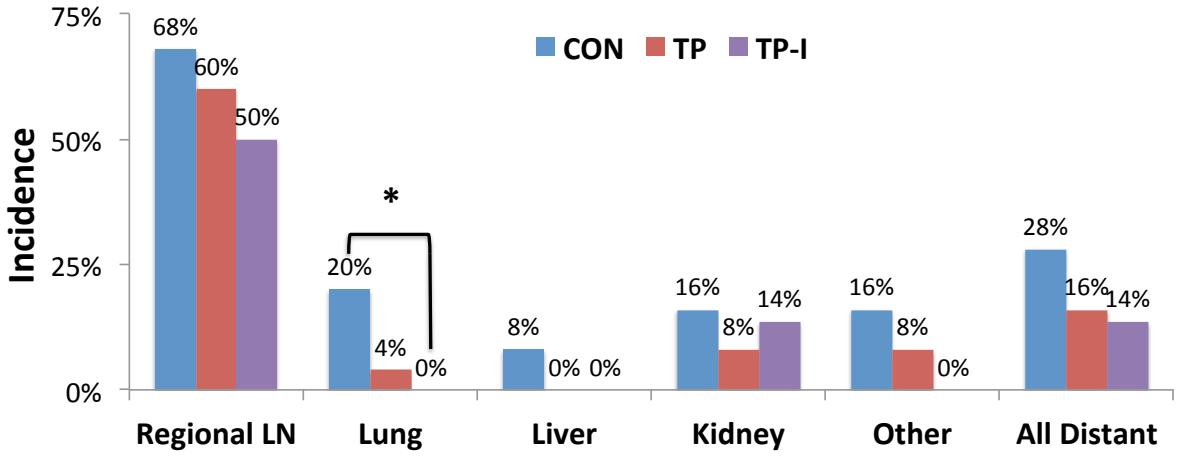

Figure 4.7. TP-I reduces CRPC gross lung cancer metastasis. Gross metastases were identified on visual inspection during necropsy. * $p < 0.05$. by two-tailed Fisher's Exact Test.

Figure 4.8.

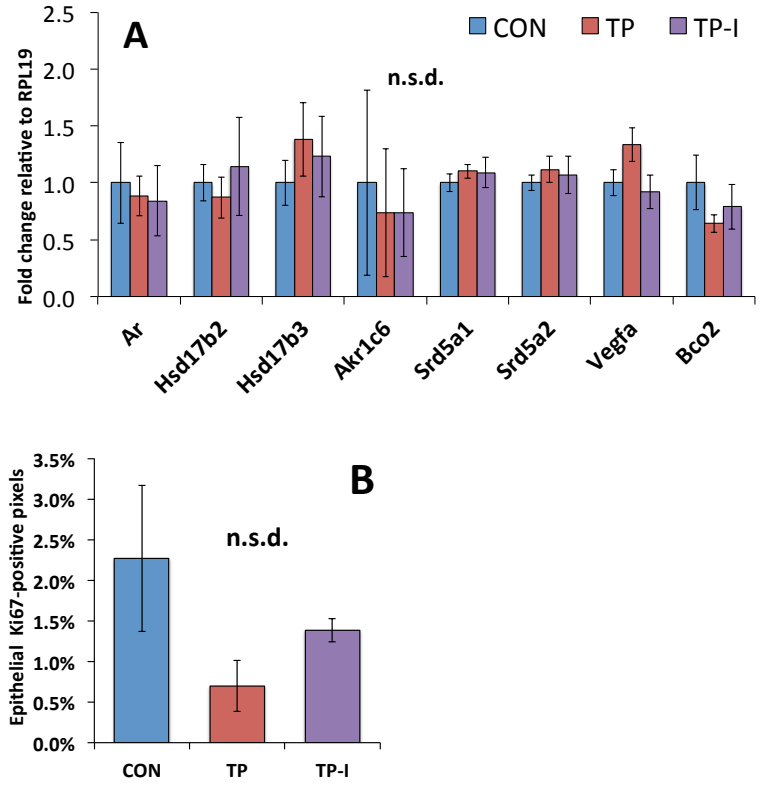

Figure 4.8. Dorsolateral prostate Ki67 staining and selected tumoral mRNA expression are not modified by tomato diets. Genes involved in androgen synthesis and signaling (*Ar, Hsd17b2, Hsd17b3, Akr1c6, Srd5a1, Srd5a2*), carotenoid metabolism (*Bco2*) and angiogenesis (*Vegfa*) were measured *via* qPCR in tumoral tissue (**A**). Data are $2^{-\Delta\Delta Ct}$ means ± SEM of n = 11 - 16/diet. Genes were measured relative to *Rpl19*, which was stable across all diet treatments and qPCR runs (data not shown). Immunohistochemical epithelial Ki67 labeling in dorsolateral prostate was not altered by diet (**B**). Data are group means ± SEM. n = 3 - 4 replicates/group. Each replicate is the average of 2 - 3 images. n.s.d., no significant differences.

CHAPTER 5

Summary and future directions

There is substantial evidence in the literature that inversely links PCa incidence to intake of dietary tomato carotenoids; additionally, much work has been done since the early 20th century to elucidate the mechanisms of carotenoid metabolism and distribution *in vivo*. It has become clear that each of these areas of research contributes to the other: without a thorough understanding of the molecular mechanisms of carotenoid metabolism, research on the dietary prevention of PCa would be ill-equipped; likewise, without firm mechanistic knowledge of the role of carotenoids in PCa etiology, the significance and impact of research on metabolism of dietary tomato carotenoids is lessened. The aim of this dissertation, broadly, was to contribute to both of these fields and perhaps shed light onto their intersection. More specifically, the aims of this dissertation were to:

1. Elucidate the impact of *Bco1* loss on prostatic physiology, with a focus on androgen status and signaling,
2. Determine the impact of *Bco1* loss on lipid, cholesterol, and retinoid metabolism in the liver, a key organ in the metabolism and biodistribution of dietary carotenoids, and
3. Evaluate the effects of dietary tomato feeding in an animal model of CRPC and determine its efficacy in preventing disease progression.

In Chapters 2 and 3, we aimed to review the background literature and clarify the *in vivo* role of a major mediator of carotenoid metabolism, BCO1. Conserved through much of the animal kingdom, BCO1 is the primary mediator of central provitamin A carotenoid cleavage for

the production of retinal, and subsequently, the active form of vitamin A, all-*trans* retinoic acid [1]. However, subsequent work has shown that this enzyme is not limited to production of retinal from non-substituted cyclized carotenes, but rather can cleave non-provitamin A carotenoids, such as lycopene [2]. Given the abundance of work linking dietary tomato carotenoid intake to a reduced risk of PCa, we questioned whether interactions between *Bco1* genotype and dietary tomato carotenoids might modulate aspects of prostatic biology. Originally, the plan of work was to analyze interactions at both short- and long-term tomato exposures; whereas long-term exposures more realistically approximate a human diet, evaluation of short-term exposures would allow for the potential identification of "primary" molecular targets of lycopene, or its BCO1-mediated metabolites. However, a quote from Richard Feynman, the Nobel Prize-winning physicist, presaged the sharp change in trajectory that this dissertation would soon take: *"We are not to tell nature what she's gotta be. She's always got better imagination than we have."* Although short-term (4 day) tomato carotenoid feeding did interact with *Bco1* genotype to modulate some endpoints (HMG-CoA reductase protein expression and StAR mRNA expression were altered by tomato or lycopene in a *Bco1*-dependent manner), the major finding was that *Bco1* loss, independent of dietary carotenoid feeding, significantly and dramatically reduced circulating testosterone concentrations, accompanied by significant decreases in prostatic organ weight, proliferation, cell cycle progression, and androgen signaling. In concert with these changes, testicular mRNA expression of *Hsd17b3*, a major regulator of testosterone synthesis, was significantly reduced, as were populations of Leydig cells, the primary cells in the body responsible for maintenance of serum testosterone levels in males. These changes were unexpected, as few researchers had envisioned a role for BCO1 apart from its function in carotenoid cleavage. Multiple implications were raised with these findings. First, relevance to

human populations lies within the fact that single nucleotide polymorphisms in the human *BCO1* gene are common (with major allele frequencies of 0.25 – 0.50) and occur within protein coding regions of the gene [3]. Moreover, loss-of-function alleles that result in decreased provitamin A conversion have been identified, showing that these polymorphisms are not silent [4,5]. Secondly, although no studies have investigated the effects of *BCO1* polymorphisms on androgen status in human populations, the level of serum testosterone decrease observed could be clinically significant. Ever since the seminal studies by Huggins in the 1940s [6], many scientists have assumed that modulation of endogenous circulating testosterone levels in eugonadal men subsequently modulated PCa risk; in fact, several epidemiological studies supported this hypothesis [7–9]. However, these associations were apparently spurious. Subsequent analysis and refined understanding has led the scientific community to appreciate that, due to the saturation of AR binding sites under endogenous levels of circulating testosterone [10,11], modifications of serum testosterone within the reference range does not result in changes in PCa risk. We observed a large and significant reduction in serum testosterone levels in *Bco1*$^{-/-}$ mice compared to WT, accompanied by a significant decrease in an immunohistochemical marker of prostatic proliferation. Despite these changes in androgen status and prostatic proliferative index, due to the AR saturation effect, WT mice were almost certainly at no higher risk of PCa than *Bco1*$^{-/-}$ mice; in fact, we have never observed a spontaneous case of PCa in WT or *Bco1*$^{-/-}$ mice up to 71 weeks of age. Consequently, reductions in serum testosterone in humans due to the putative effects of *BCO1* variation would likely not directly reduce prostate cancer risk. However, given the broad impacts of circulating androgens, such an effect of BCO1 may impact a myriad of other endpoints. Hypogonadism may be a causal factor for dyslipidemia and metabolic syndrome in males [12,13] and androgen status has been shown to modulate carotenoid accumulation

in vivo [14,15]. Similarly, a common *BCO1* variant (0.49 minor allele frequency) significantly predicts circulating HDL concentrations in humans [16], and loss of *Bco1* in mice alters lycopene accumulation – strikingly, increasing prostatic accumulation 4-fold [17]! Other studies have demonstrated effects of *Bco1* loss on various endpoints of lipid metabolism *in vivo* [18–22]. Given the fact that carotenoid metabolism and distribution is in turn highly dependent on the mechanisms of lipid metabolism [23], it would be unwise to reject a potential network linking BCO1 status, androgens, and lipids. Our study in Chapter 2 contributed to the elucidation of this relationship. Future work is required to assess whether polymorphisms in the human *BCO1* gene have similar effects on androgen status in humans, as well as to identify a direct mechanism through which ablation of *Bco1* alters testicular testosterone production.

More work in humans is needed to expand on the hypothesis that *BCO1* status may alter lipid metabolism, but we pursued this question in Chapter 3, again using the *Bco1*$^{-/-}$ mouse model. Other labs had identified changes in lipid esterification, cholesterol metabolism, retinol esterification, and hepatic steatosis as a result of *Bco1* loss [18–21], but results were sometimes contradictory. Furthermore, although each study had used descendants of the same *Bco1*$^{-/-}$ founder pair, ages, sex of animals studied, and the carotenoid/retinoid content of study diets varied widely. Given the impact of *Bco1* loss on hormonal status uncovered in Chapter 2, and concerned about changes in phenotype that might occur over the wide range of ages used in previous studies, we decided to assess how *Bco1* loss altered hepatic lipid and retinoid metabolism in male mice, as well as include analysis of a wide range of developmental stages. Two primary findings arose from our work in Chapter 3. First, we found that adult male *Bco1*$^{-/-}$ mice accumulate roughly 2 - 6 greater levels of hepatic retinyl esters than did age-matched WT mice, but that this effect was reversed in juveniles. Notably, whereas others had previously

reported a similar effect of *Bco1* loss on retinol esterification in younger mice, our finding demonstrates that *Bco1* interacts with hepatic retinol metabolism in an age-dependent manner, a novel finding with potentially more broad implications. Secondly, we found that hepatic retinoid metabolism was altered in concert with changes in cholesterol and phospholipid esterification, and we propose that altered retinoid levels may act through PPAR/RXR signaling pathways to mediate the changes that we and others have observed in hepatic lipid metabolism. Third, our finding that *Bco1*-dependent changes in retinol metabolism are not only present from youth through old age, but also are developmentally regulated, may help to explain other findings from Chapter 2 as well. In Chapter 2, we reported that, in young mice (9 – 14 weeks old), weight of the androgen-dependent seminal vesicles were reduced by *Bco1* loss, in concert with testicular production of testosterone. In Chapter 3, we also found that seminal vesicles were reduced in weight in young mice (≤9 weeks of age), but conversely, that *Bco1*$^{-/-}$ seminal vesicle weight was greater than WT in older mice (≥51 weeks of age). Moreover, it was striking that this change occurred in almost lockstep with hepatic retinyl ester accumulation. As vitamin A has long been known to impact testicular steroidogenesis and function [24], modulation of systemic and testicular retinoid status may mediate the effects previously seen on testosterone status with *Bco1* loss. This, of course, is currently only speculative, and it remains to be seen whether hepatic changes in retinoid status would have any impact on testicular and subsequently androgen-sensitive tissues, but this possibility should be investigated.

It is important to note that the genetic techniques used to create genetically modified models, such as the *Bco1*$^{-/-}$ mouse, may directly introduce off-target effects that are unrelated to the gene under study. Indeed, in a very similar mouse model, the β-carotene-9',10'-dioxygenase (*Bco2*) knockout, prostatic mRNA expression of interleukin 18 (*Il18*) was reduced 25-fold,

compared to WT mice (unpublished data). The murine *Bco2* exon 1, which was replaced with a *lacZ* cassette during generation of the *Bco2*$^{-/-}$ strain [25], overlaps with the complementary sequence on chromosome 9 that encodes the murine *Il18* gene (NCBI); this may account for our observations in *Il18* expression. In fact, a similar juxtaposition of *IL18* and *BCO2* is present on the human chromosome 11 and a large genome-wide association study found that four of the top seven SNPs associated with circulating IL18 levels were located within the *IL18* gene, whereas the other three, including the most strongly associated SNP, were present in the *BCO2* gene [26]. The regions of the *Bco1* gene that were modified to create the *Bco1*$^{-/-}$ strain [18] do not have similar juxtapositions (they are roughly 15 Kb upstream from the closest gene; NCBI), but even the basic gene targeting techniques used in genetic modification can alter expression of genes located up to 3.1 Mb from the site of insertion [27]. This is not to suggest that the presence of off-target effects inherently negates the value of a genetically engineered model; the *Bco2*$^{-/-}$ strain, despite the likely off-target effect on IL18 levels, has proven to be hugely informative for our understanding of lycopene metabolism [28]. Rather, it is clear that the more thoroughly a mouse model can be described, "warts and all", the better the data arising from its use can be interpreted. Additionally, the accretion of evidence consistent with a singular mechanism (for example, of altered retinoid metabolism) would help to assuage fears of off-target effects. Nonetheless, these concerns must always be kept in mind when using genetically engineered models generated with techniques similar to those used to create the *Bco1*$^{-/-}$ and *Bco2*$^{-/-}$ models.

Finally, in Chapter 4, we aimed to assess the impact of dietary tomato treatments, administered to model either lifelong consumption or adjuvant intervention, on the progression of castration-resistant prostate cancer. We administered a physiologically relevant dose of a commercially available tomato food (Contadina® brand tomato paste), in order to maximize

translatability of this animal study. Specifically, the 19 mg/day human equivalent dose provided to mice in this study (calculated for a 90-kg man using previously described body surface area conversions [29]) would be achievable through the consumption of 0.6 servings of tomato sauce per day (1.0 C/serving; U.S.D.A. Nutrient Database), or 1 serving of tomato paste per day (0.25 C/serving). To our knowledge, this is the first report of the effects of dietary tomato in an animal model of CRPC carcinogenesis. We found that tomato intervention, and not lifelong consumption, was effective in reducing CRPC tumor growth and metastasis. No differences in tissue carotenoid accumulation were observed between the treatment groups, nor were any differences observed in mRNA markers of tumoral steroidogenesis and androgen signaling. Despite these null effects in mRNA expression of genes related to androgen metabolism, due to the abundance of literature in the area, we are continuing with our *a priori* plans to investigate protein expression of several of these enzymes, as well as measure intratumoral androgen profiles with mass spectrometry techniques. Both of those projects are currently underway. However, the difference in TP and TP-I results were contradictory to our hypothesis, as epidemiological studies and conventional thought would suggest that lifelong consumption, and not a shorter intervention, would be most effective. Additionally, the TP-I intervention was initiated at 12 weeks, when the majority of animals would already have had high-grade pre-neoplastic intraepithelial neoplasia, or low-grade adenocarcinoma [30,31]. Although the intervention was purposely administered at such a stage of early carcinogenesis, again, conventional wisdom would suggest that such timing would miss the "critical window" to prevent progression. Indeed, in a previous study from our group, it appears that a tomato powder intervention in primary PCa in the TRAMP model was ineffective due to administration of tomato diets outside of such a window [31]. Apart from the hypothesis proposed in Chapter 4 – that the TP diet was actually not

wholly ineffective, but rather suffered from bias by "non-responder" outliers – we can think of another plausible mechanism which may explain the results. Castration in the TRAMP model has been shown to induce treatment effects in the cancer genome, inducing androgen receptor mutations and other molecular alterations, which otherwise may not have been acquired [32,33]. Similar effects may be seen with ADT in humans with CRPC [34]. It may be possible that tomato consumption prior to castration "primes" the nascent cancer to evade its effects, and this only becomes evident once the evolutionarily selective pressure of castration is applied and forces the selection of the "fittest" cellular populations. We have engaged in discussions with multiple unit leaders at the Roy J. Carver Center for Biotechnology to lay groundwork for a project to sequence the AR from each tumor. If differential types or numbers of AR mutations were to be revealed between the TP and TP-I treatment groups, it would lend credence to this hypothesis.

Despite the uncertainty about both the mechanism of action of the TP-I group, as well as uncertainty surrounding the reason for a lack of effect in the TP group, important conclusions can be drawn from the data presented in Chapter 4. For the first time, we have shown that dietary tomato can reduce CRPC progression in an animal model, particularly when provided as an adjuvant dietary intervention. This is encouraging, and provides preliminary data for larger follow-on studies. We see two key studies as being necessary: first, it will be important to assess whether a dose-escalation tomato intervention – for example, increasing consumption from 2% at weaning to 10% at castration – would be effective. Although our current TP-I group was meant to model men who increase tomato consumption following a cancer diagnosis, most men in such a situation would likely have consumed some sub-protective level of tomato prior to diagnosis, rather than completely abstaining form tomato intake. Thus, it would be important to further refine the model to more closely match human dietary patterns. Second, studies

combining dietary tomato with pharmacological ADT, rather than surgical castration, would more fully recapitulate clinical treatment combinations available as first-line therapy to men with CRPC. These would need to be successfully completed and replicated before any attempt to translate our results to clinical trials.

In conclusion, this work has revealed that BCO1, a key enzyme involved in carotenoid metabolism, impacts steroid, lipid, and retinoid metabolism *independent of its role in carotenoid cleavage*. Further work in animal models and humans is needed, but we have shed additional light on a somewhat unexamined corner of the carotenoid field. Future work should incorporate our findings in mice and assess their relevance in humans. Secondly, we have demonstrated that a relevant level and source of dietary tomato can reduce CRPC progression in mice. This work requires confirmation and further expansion in order to be considered for translation to humans. In total, this dissertation has contributed novel findings to our understanding of carotenoid metabolism and bioactivity *in vivo*.

References cited

1. von Lintig, J. Colors with functions: Elucidating the biochemical and molecular basis of carotenoid metabolism. *Annu. Rev. Nutr.* **30,** 35–56 (2010).
2. dela Seña, C. *et al.* Substrate specificity of purified recombinant human β-carotene 15,15'-oxygenase (BCO1). *J. Biol. Chem.* **288,** 37094–103 (2013).
3. Lietz, G., Oxley, A., Boesch-Saadatmandi, C. & Kobayashi, D. Importance of β,β-carotene 15,15'-monooxygenase 1 (BCMO1) and β,β-carotene 9',10'-dioxygenase 2 (BCDO2) in nutrition and health. *Mol. Nutr. Food Res.* **55,** (2011).
4. Lindqvist, A., Sharvill, J., Sharvill, D. E. & Andersson, S. Loss-of-function mutation in carotenoid 15,15'-monooxygenase identified in a patient with hypercarotenemia and hypovitaminosis A. *J. Nutr.* **137,** 2346–2350 (2007).
5. Ferrucci, L. *et al.* Common variation in the beta-carotene 15,15'-monooxygenase 1 gene affects circulating levels of carotenoids: A genome-wide association study. *Am. J. Hum. Genet.* **84,** 123–33 (2009).
6. Huggins, C. Endocrine-induced regression of cancers. *Cancer Res.* **27,** 1925–1930 (1967).
7. Barrett-Connor, E., Garland, C., McPhillips, J. B., Khaw, K.-T. & Wingard, D. L. A prospective, population-based study of androstenedione, estrogens, and prostatic cancer. *Cancer Res.* **50,** 169–173 (1990).
8. Gann, P. H., Hennekens, C. H., Ma, J., Longcope, C. & Stampfer, M. J. Prospective study of sex hormone levels and risk of prostate cancer. *J. Natl. Cancer Inst.* **88,** 1118–1126 (1996).
9. Shaneyfelt, T., Husein, R., Bubley, G. & Mantzoros, C. S. Hormonal predictors of prostate cancer: A meta-analysis. *J. Clin. Oncol.* **18,** 847–53 (2000).

10. Morgentaler, A. Testosterone and prostate cancer: An historical perspective on a modern myth. *Eur. Urol.* **50,** 935–939 (2006).

11. Morgentaler, A. & Traish, A. M. Shifting the paradigm of testosterone and prostate cancer: The saturation model and the limits of androgen-dependent growth. *Eur. Urol.* **55,** 310–20 (2009).

12. Yassin, A., Al Mehmadi, Y., Yassin, D. J., Doros, G. & Traish, A. Effects of continuous long-term testosterone replacement therapy (TRT) up to 11 years in 115 hypogonadal elderly men on anthropometric, endocrine and metabolic parameters: Real-life experience from an observational registry study. *J. Urol.* **1),** e303 (2015).

13. Naifar, M. *et al.* Male hypogonadism and metabolic syndrome. *Andrologia* **47,** 579–586 (2015).

14. Boileau, T. W.-M., Clinton, S. K. & Erdman, J. W. Tissue lycopene concentrations and isomer patterns are affected by androgen status and dietary lycopene concentration in male F344 rats. *J. Nutr.* **130,** 1613–8 (2000).

15. Boileau, T. W.-M. *et al.* Testosterone and food restriction modulate hepatic lycopene isomer concentrations in male F344 rats. *J. Nutr.* **131,** 1746–52 (2001).

16. Clifford, A. J. *et al.* Single nucleotide polymorphisms in CETP, SLC46A1, SLC19A1, CD36, BCMO1, APOA5, and ABCA1 are significant predictors of plasma HDL in healthy adults. *Lipids Health Dis.* **12,** 66 (2013).

17. Lindshield, B. L. *et al.* Lycopene biodistribution is altered in 15,15'-carotenoid monooxygenase knockout mice. *J. Nutr.* **138,** 2367–2371 (2008).

18. Hessel, S. *et al.* CMO1 deficiency abolishes vitamin A production from beta-carotene and alters lipid metabolism in mice. *J. Biol. Chem.* **282,** 33553–61 (2007).

19. Dixon, J. L., Kim, Y.-K., Brinker, A. & Quadro, L. Loss of β-carotene 15,15'-oxygenase in developing mouse tissues alters esterification of retinol, cholesterol and diacylglycerols. *Biochim. Biophys. Acta* **1841,** 34–43 (2014).

20. Kim, Y.-K., Zuccaro, M. V., Costabile, B. K., Rodas, R. & Quadro, L. Tissue- and sex-specific effects of β-carotene 15,15′ oxygenase (BCO1) on retinoid and lipid metabolism in adult and developing mice. *Arch. Biochem. Biophys.* **572,** 11–18 (2015).

21. Lee, S.-A. *et al.* Cardiac dysfunction in Beta-carotene-15,15'-dioxygenase-deficient mice is associated with altered retinoid and lipid metabolism. *Am. J. Physiol. - Hear. Circ. Physiol.* **307,** H1675–H1684 (2014).

22. Ford, N. A., Elsen, A. C. & Erdman Jr., J. W. Genetic ablation of carotene oxygenases and consumption of lycopene or tomato powder diets modulate carotenoid and lipid metabolism in mice. *Nutr. Res.* **33,** 733–42 (2013).

23. Harrison, E. H. Mechanisms involved in the intestinal absorption of dietary vitamin A and provitamin A carotenoids. *Biochim. Biophys. Acta - Mol. Cell Biol. Lipids* **1821,** 70–77 (2012).

24. Chaudhary, L. R., Hutson, J. C. & Stocco, D. M. Effect of retinol and retinoic acid on testosterone production. *Biochem. Biophys. Res. Commun.* **158,** 400–406 (1989).

25. Amengual, J. *et al.* A mitochondrial enzyme degrades carotenoids and protects against oxidative stress. *FASEB J.* **25,** 948–959 (2011).

26. He, M. *et al.* Genome-wide association study identifies variants at the IL18-BCO2 locus associated with interleukin-18 levels. *Arterioscler. Thromb. Vasc. Biol.* **30,** 885–890 (2010).

27. Meier, I. D. *et al.* Short DNA sequences inserted for gene targeting can accidentally interfere with off-target gene expression. *FASEB J.* **24,** 1714 –1724 (2010).

28. Ford, N. A., Clinton, S. K., Lintig, J. Von, Wyss, A. & Erdman Jr., J. W. Loss of carotene-9',10'-monooxygenase expression increases serum and tissue lycopene concentrations in lycopene-fed mice. *J. Nutr.* **140,** 2134–2138 (2010).

29. Reagan-Shaw, S., Nihal, M. & Ahmad, N. Dose translation from animal to human studies revisited. *FASEB J.* **22,** 659–61 (2008).

30. Gingrich, J. R. *et al.* Androgen-independent prostate cancer progression in the TRAMP model. *Cancer Res.* **57,** 4687–4691 (1997).

31. Conlon, L. E., Wallig, M. A. & Erdman, J. W. Low-lycopene containing tomato powder diet does not protect against prostate cancer in TRAMP mice. *Nutr. Res.* **35,** 882–890 (2015).

32. O'Mahony, O. a *et al.* Profiling human androgen receptor mutations reveals treatment effects in a mouse model of prostate cancer. *Mol. Cancer Res.* **6,** 1691–1701 (2008).

33. Tang, Y. *et al.* Divergent effects of castration on prostate cancer in TRAMP mice: possible implications for therapy. *Clin. Cancer Res.* **14,** 2936–43 (2008).

34. Katzenwadel, A. & Wolf, P. Androgen deprivation of prostate cancer: Leading to a therapeutic dead end. *Cancer Lett.* **367,** 12–17 (2015).

Appendix A

Supplemental tables and figures for Ch. 2

Figure A.1. Designs of Studies 1, 2, and 3.

A. Study 1.

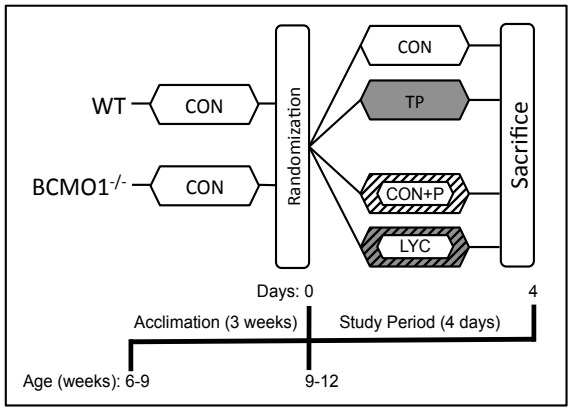

B. Study 2.

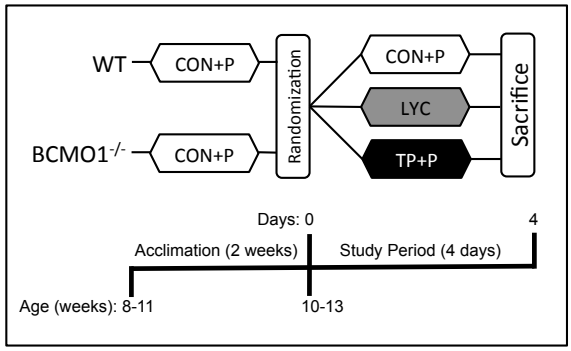

C. Study 3.

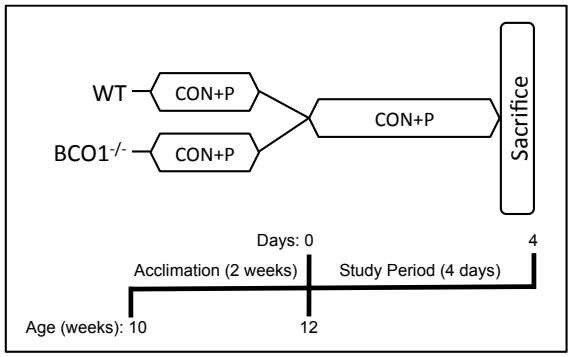

Figure A.2.

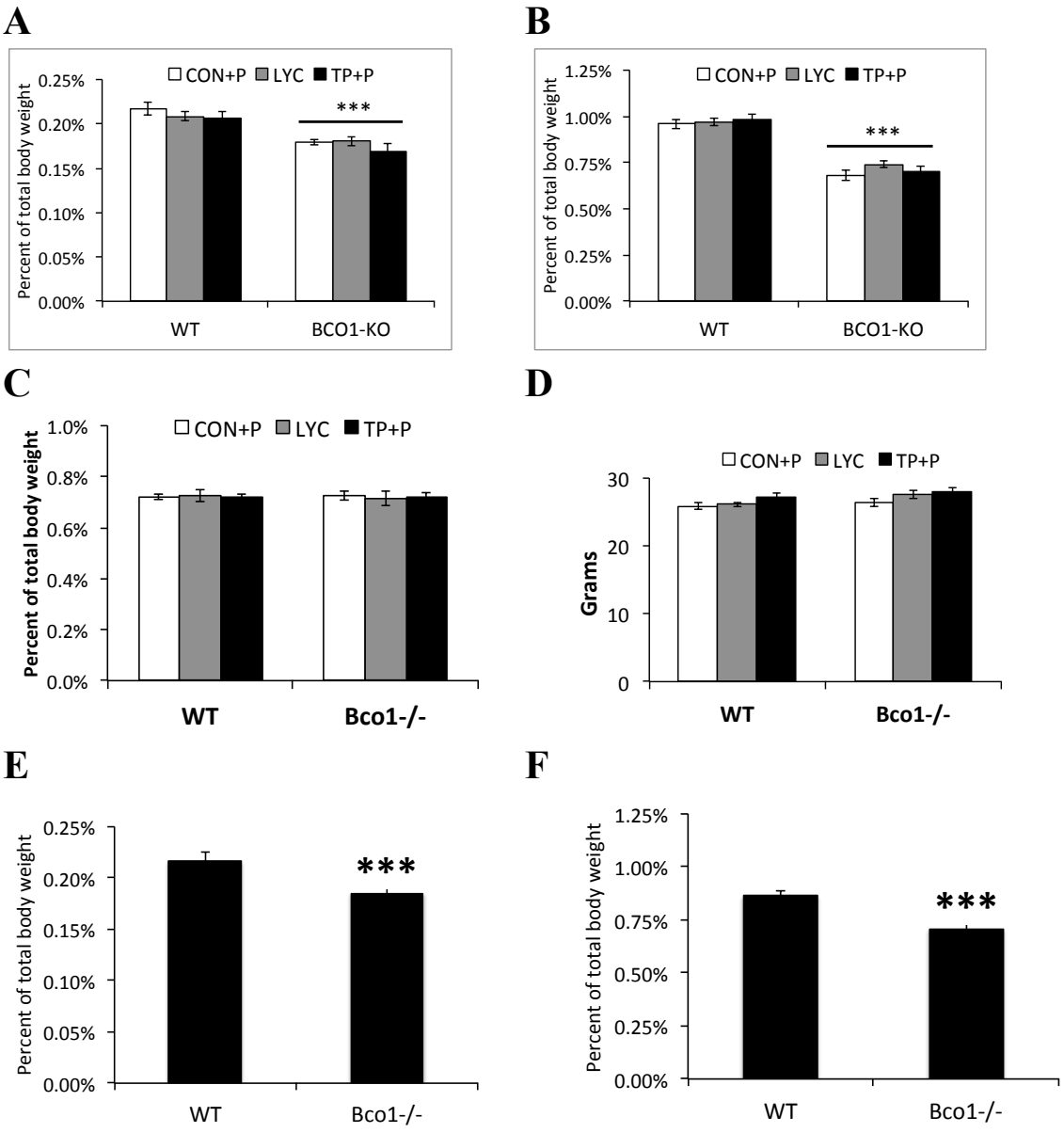

Figure A.2. Body weights and testes, prostate, and seminal vesicle weight as percent of total body weight (%BW). Study 2 prostate (A) and seminal vesicle %BW (B). Study 2 testes %BW (C) and total BW (D). Data are presented as mean group %BW relative to the mean %BW of the control group, ± SEM. n = 14 - 18; ***p < 0.001. Prostate (E) and seminal vesicle (F) data from Study #3 were similar, as were testes and total body weight (data not shown)

Figure A.3.

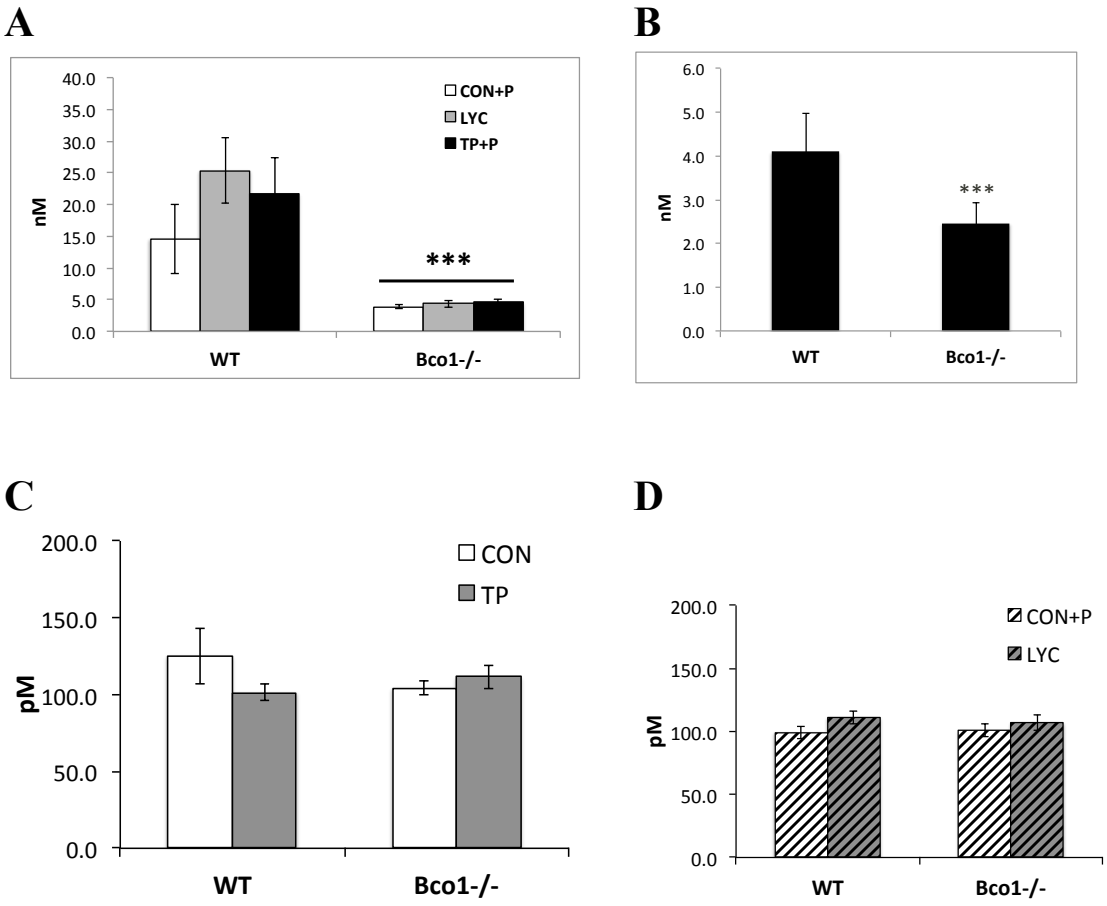

Figure A.3. Serum testosterone, but not serum estradiol, is reduced by Bco1 loss. Data are presented as means ± SEM; n = 10 - 15. ***$p < 0.001$. Data are from Study 1 (C, D), Study 2 (A), and Study 3 (B).

Figure A.4.

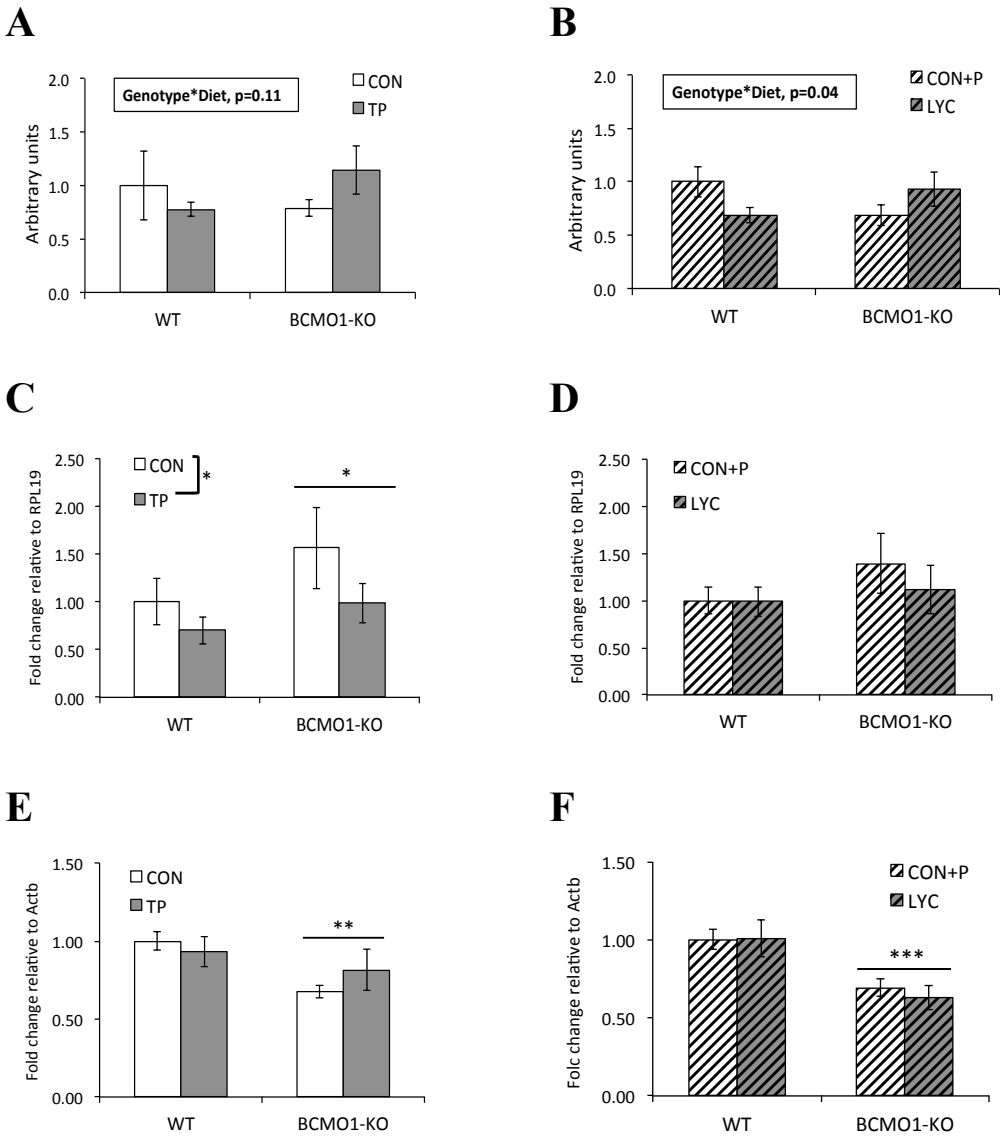

Figure A.4. *Bco1* loss alters expression of testicular steroidogenic genes. A significant genotype-diet interaction decreased HMG-CoA reductase protein expression in lycopene-fed WT mice, but elevated expression in lycopene-fed *Bco1*$^{-/-}$ mice (B). A similar, but non-significant, trend is observed with tomato feeding (A). Gene expression of *Star* is up-regulated by *Bco1* loss, but down-regulated by TP diet (C, D). *Bco1*, loss, but not tomato or lycopene feeding, reduced *Hsd17b3* mRNA expression (E, F). Data are presented as means ± SEM, *$p < 0.05$, **$p < 0.01$, ***$p < 0.001$. All data are from Study 1.

Figure A.5.

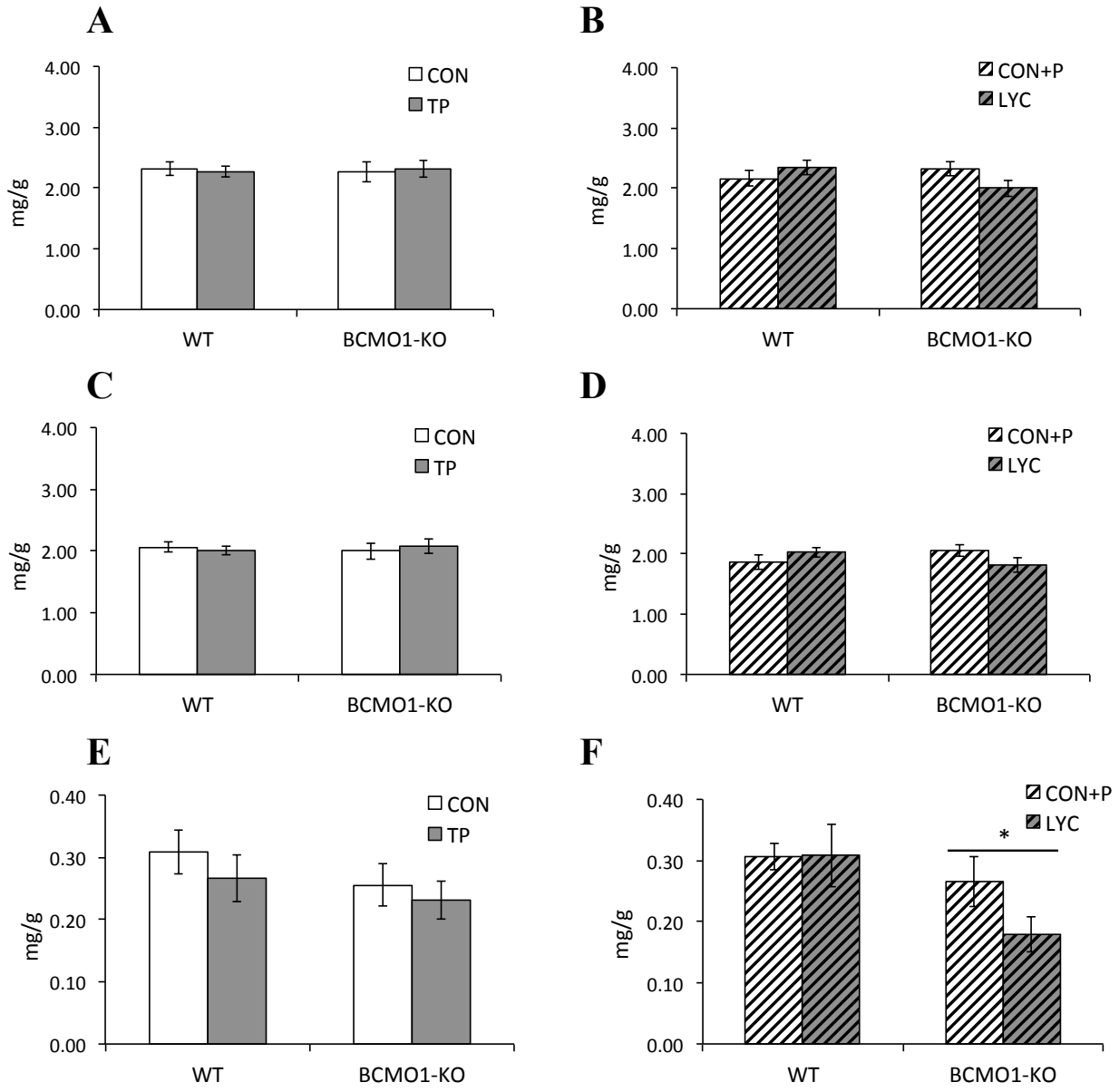

Figure A.5. *Bco1* loss does not alter testicular total cholesterol (A, B) or free cholesterol (C, D), but has inconsistent effects on levels of esterified cholesterol (E, F).

Figure A.6.

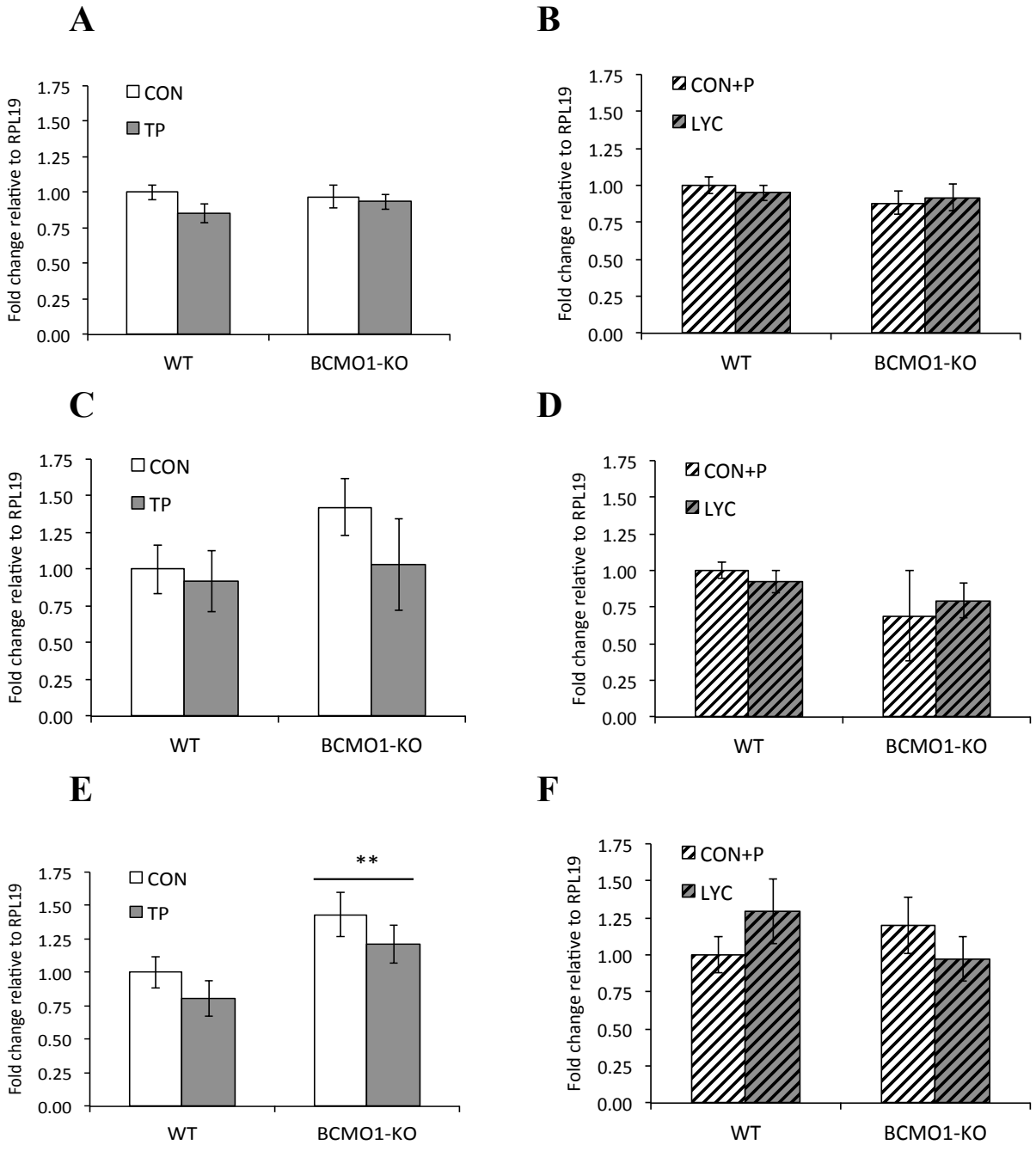

Figure A.6. *Bco1* loss does not alter testicular mRNA expression of the cholesterol esterases *Soat1* (A, B) or *Soat2* (C, D), but has inconsistent effects on expression of *Lcat* (E, F).

Figure A.7.

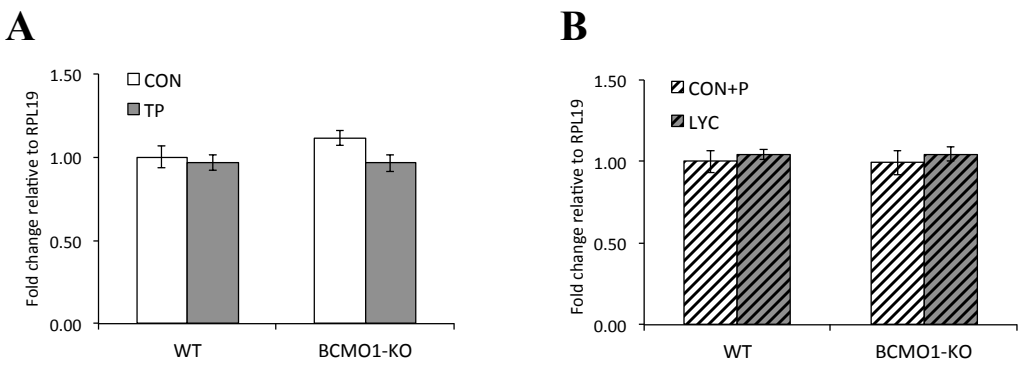

Figure A.7. AR mRNA expression is unchanged in *Bco1*$^{-/-}$ mice (A, B). Data are presented as means ± SEM; n = 11 - 14 (A,B). Data in (A, B) are from Study 1.

Figure A.8.

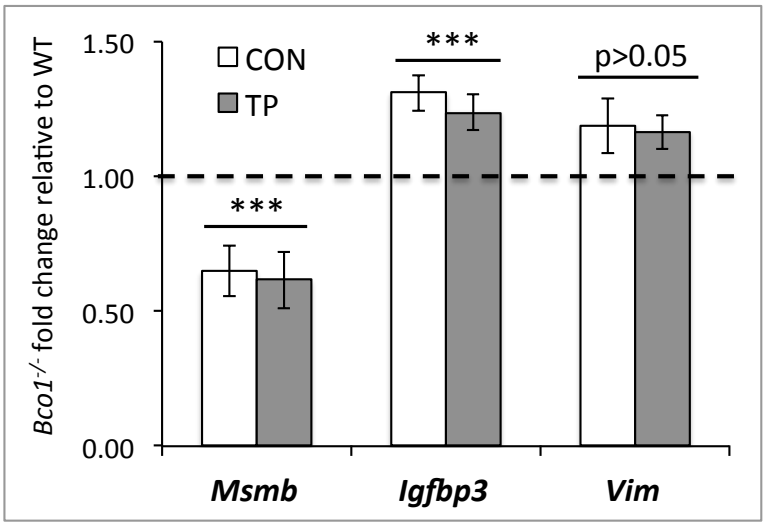

Figure A.8. Gene expression of *Msmb*, *Igfbp3*, and *Vim* in the prostates of mice from Study 1, n = 7 - 14 (A). ***p < 0.001.

Figure A.9.

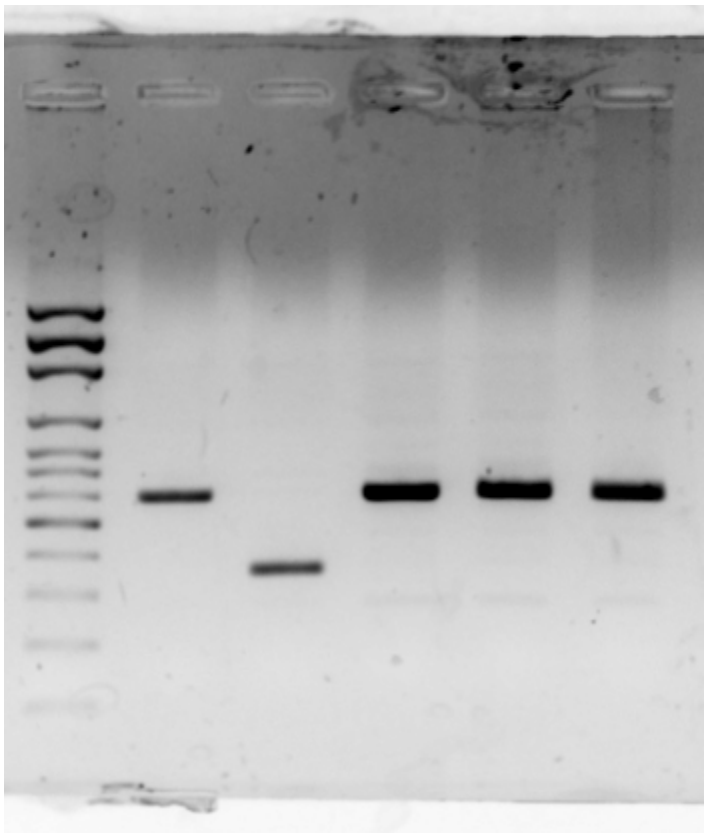

Figure A.9. PCR genotyping confirms *Bco1* ablation in several tissues of male *Bco1*$^{-/-}$ mice. Lane 1: DNA ladder; lane 2: tail snip from *Bco1*$^{-/-}$ breeding dam; lane 3: tail snip from WT breeding dam (Jackson Laboratories); lane 4: liver sample from male *Bco1*$^{-/-}$ study animal; lane 5: testicle sample from *Bco1*$^{-/-}$ study animal; lane 6: anterior prostate sample from *Bco1*$^{-/-}$ study animal. WT and *Bco1*$^{-/-}$ band weights correspond to those reported by Hessel et al (Hessel S et al., *J Biol Chem*. 2007; 282(46):33553-61).

Table A.1. Formulation of experimental diets.

	Study 1				Study 2			Study 3
Component (g/kg)	**CON**	**TP [1]**	**CON+P**	**LYC [2]**	**CON+P**	**TP+P [3]**	**LYC [4]**	**CON+P**
Cornstarch	397.5	331.5	397.5	397.5	397.5	331.1	397.5	397.5
Casein	200.0	187.5	200.0	200.0	200.0	187.5	200.0	200.0
Maltodextrin	102.0	132.0	102.0	102.0	102.0	102.0	102.0	102.0
Sucrose	100.0	100.0	100.0	100.0	100.0	100.0	100.0	100.0
Cellulose	50.0	34.0	50.0	50.0	50.0	33.8	50.0	50.0
Mineral Mix [5]	35.0	35.0	35.0	35.0	35.0	35.0	35.0	35.0
Vitamin Mix [6]	10.0	10.0	10.0	10.0	10.0	10.0	10.0	10.0
L-Cystine	3.0	3.0	3.0	3.0	3.0	3.0	3.0	3.0
Choline bitartrate	2.5	2.5	2.5	2.5	2.5	2.5	2.5	2.5
Soybean oil	100.0	65.0	100.0	100.0	100.0	95.1	100.0	100.0
Tomato powder	0.0	100.0	0.0	0.0	0.0	100.0	0.0	0.0
10% lycopene beadlets	0.0	0.0	0.0	1.0	0.0	0.0	1.2	0.0
Placebo beadlets	0.0	0.0	1.0	0.0	1.2	1.2	0.0	1.2
Energy density (kcal/g) [7]	4.11	3.98	4.11	4.11	4.11	4.13	4.11	4.11

[1] As measured by HPLC-PDA, Study 1 TP diet contained 204 nmol lycopene/g diet, 10.1 nmol phytoene/g diet, 2.6 nmol phytofluene/g diet, and 0.8 nmol β-carotene/g diet.
[2] As measured by HPLC-PDA, Study 1 LYC diet contained 248 nmol lycopene/g diet.
[3] As measured by HPLC-PDA, Study 2 TP+P diet contained 214 nmol lycopene/g diet, 24.6 nmol phytoene/g diet, 14.6 nmol phytofluene/g diet, and 1.9 nmol beta-carotene/g diet.
[4] As measured by HPLC-PDA, Study 2 LYC diet contained 185 nmol lycopene/g diet.
[5] AIN-93-MX formulation (Reeves PG et al., *J Nutr*. 1993; 123:1939-51).
[6] AIN-93-VX formulation (Reeves PG et al., *J Nutr*. 1993; 123:1939-51), modified to contain reduced levels of vitamin A (1,500 IU retinyl palmitate/g diet).
[7] Calculated from composition as formulated**.**

Table A.2. Primer sequences (purchased from Integrated DNA Technologies) used for single-gene qPCR.

Star	Forward	5'-TTGGGCATACTCAACAACCA-3'
	Reverse	5'-CCTTGACATTTGGGTTCCAC-3'
Ar	Forward	5'-TCTTTCAAGGGAGGTTACGC-3'
	Reverse	5'-AGGACGGGATCTCAAGTGTC-3'
Msmb	Forward	5'-GTCAATCACCTGCTGTACCAAC-3'
	Reverse	5'-CTGGGTTCTTCCGATCCAC-3'
Igfbp3	Forward	5'-TCCACTCCATGCCAAGATG-3'
	Reverse	5'-CTGTCTCCCGCTTAGACTCG-3'
Rpl19	Forward	5'-AAATCGCCAATGCCAACTC-3'
	Reverse	5'-ACCCTTCCTCTTCCCTATGC-3'

Table A.3. Complete results from NanoString array codeset.

Test	Gene symbol	Accession #	Mean WT count	SD WT	Mean Bco1$^{-/-}$ count	SD Bco1$^{-/-}$	BCO1$^{-/-}$ vs. WT	Raw p	Adj p	FDR
1	*Gpx3*	NM_008161	3,286.62	944.17	10,053.72	3,472.64	3.06	<0.0001	0.0020	0.0004
2	*Kras*	NM_021284	198.07	22.25	104.69	22.23	-1.89	<0.0001	0.0020	0.0004
3	*Met*	NM_008591	361.32	52.85	598.01	83.79	1.66	<0.0001	0.0020	0.0004
4	*Tgfb2*	NM_009367	521.18	71.24	328.74	37.83	-1.59	<0.0001	0.0020	0.0004
5	*Vegfa*	NM_001025250	350.03	20.25	526.87	70.63	1.51	<0.0001	0.0020	0.0004
6	*Bco1*	NM_001163028	9.58	6.91	78.70	16.59	8.21	0.0001	0.0200	0.0033
7	*Aurkb*	NM_011496	37.89	12.18	17.27	7.11	-2.19	0.0005	0.1200	0.0171
8	*Prom1*	NM_008935	2,763.65	308.31	1,997.24	337.06	-1.38	0.0006	0.2000	0.0250
9	*Esr2*	NM_010157	105.51	34.93	168.79	28.32	1.60	0.0016	0.3200	0.0356
10	*Ccnb2*	NM_007630	59.36	10.83	29.31	15.03	-2.03	0.0021	0.4200	0.0420
11	*Mki67*	NM_001081117	125.32	24.18	70.72	30.89	-1.77	0.0025	0.5000	0.0450
12	*Pcna*	NM_011045	1,062.05	77.57	938.59	66.39	-1.13	0.0027	0.5400	0.0450
13	*Bax*	NM_007527	296.56	27.41	244.34	28.51	-1.21	0.0030	0.6000	0.0462
14	*Hif1a*	NM_010431	1,027.56	62.70	1,232.14	193.33	1.20	0.0078	1.0000	0.1013
15	*Trp63*	NM_011641	143.06	21.81	187.08	38.91	1.31	0.0079	1.0000	0.1013

Table A3. Gene symbols, accession numbers (NCBI), and expression values are provided for the entire NanoString codeset. Data are presented as mean and standard deviation (SD) of transcript count. Fold regulation by *Bco1*$^{-/-}$ genotype (relative to WT) and raw p-values (*via* T-test) were calculated with NanoString nSolver Analysis Software. Bonferroni's-corrected p-values (Adj p) and false discovery rates (FDR) were calculated in SAS 9.3 using PROC MULTTEST. Green highlight indicates raw $p \leq 0.005$, Bonferroni's-corrected $p \leq 0.05$, or FDR ≤ 0.05. Red highlight indicates transcript count values were lower than average negative control values for WT, *Bco1*$^{-/-}$, or both genotypes. WT n = 9, *Bco1*$^{-/-}$ n = 8.

* In this analysis, *Bco1* expression was increased 8.21-fold (p=0.0001) in *Bco1*$^{-/-}$ mice compared to WT mice. When this genetically engineered mouse model was created, disruption of *Bco1* gene function was achieved through homozygous replacement of exons 2 and 3 of the *Bco1* gene (approximately 8.8 kb) with *IRES-lacZ* and a *neomycin*^{R} cassette (Hessel S et al., *J Biol Chem*. 2007; 282(46):33553-61). This was confirmed by PCR genotyping (see also **Figure A.9**). Mice of this strain do not express BCO1 protein (Hessel S et al., 2007 *J Biol Chem*) and they accumulate β-carotene when fed tomato powder (Lindshield BL et al., *J Nutr*. 2008;138:2367-71), consistent with a lack of BCO1 cleavage function. However, the *Bco1* probe used in this NanoString array targets 100 nt within exons 9 and 10 (see footnote †) – a portion of the gene that was not modified during generation of this model. The increased expression detected with this specific *Bco1* probe is likely a feedback response to the absence of functional BCO1 protein. *Bco1*$^{-/-}$ genotype of mice in this study was confirmed by PCR (**Figure A.9**).

† Sequence of *Bco1* probe: 5' –
CTTACAACGGGAAGCCATATCGCTACATCTTTGCAGCTGAAGTACAGTGGAGTCCAGTCCCAACCAAGATACTGAAATATGACATTCTCACAAAGTCCTC – 3'

Table A.3, (continued). Complete results from NanoString array codeset.

Test	Gene symbol	Accession #	Mean WT count	SD WT	Mean Bco1$^{-/-}$ count	SD Bco1$^{-/-}$	BCO1$^{-/-}$ vs. WT	Raw p	Adj p	FDR
16	*Sod1*	NM_011434	10,849.24	1,165.58	9,312.06	875.78	-1.17	0.0081	1.0000	0.1013
17	*Mcl1*	NM_008562	1,702.52	105.75	1,531.22	132.00	-1.11	0.0146	1.0000	0.1568
18	*Birc5*	NM_009689	27.62	7.01	16.70	8.49	-1.65	0.0154	1.0000	0.1568
19	*Foxm1*	NM_008021	24.01	6.72	13.74	6.77	-1.75	0.0157	1.0000	0.1568
20	*Nkx3-1*	NM_010921	6,740.67	1,298.23	5,031.51	1,260.41	-1.34	0.0165	1.0000	0.1568
21	*Vegfb*	NM_011697	712.93	67.58	623.56	71.70	-1.14	0.0179	1.0000	0.1568
22	*Acpp*	NM_207668	26.47	15.73	93.58	170.85	3.54	0.0181	1.0000	0.1568
23	*Prlr*	NM_011169	4,372.66	1,028.15	5,620.04	937.36	1.29	0.0182	1.0000	0.1568
24	*B2m*	NM_009735	76,292.03	11,538.21	109,993.51	50,653.70	1.44	0.0190	1.0000	0.1568
25	*Igf1r*	NM_010513	966.03	171.07	1,208.09	233.20	1.25	0.0196	1.0000	0.1568
26	*Parp1*	NM_007415	416.73	49.95	371.02	22.75	-1.12	0.0204	1.0000	0.1569
27	*Vdr*	NM_009504	46.27	10.22	55.90	6.26	1.21	0.0232	1.0000	0.1719
28	*Tert*	NM_009354	22.82	6.33	30.45	6.49	1.33	0.0263	1.0000	0.1879
29	*Akt2*	NM_001110208	146.86	24.35	181.12	38.08	1.23	0.0276	1.0000	0.1903
30	*Ccne2*	NM_001037134	44.91	7.68	35.32	8.86	-1.27	0.0291	1.0000	0.1940
31	*Becn1*	NM_019584	2,208.44	266.79	1,965.73	164.08	-1.12	0.0307	1.0000	0.1981
32	*Casp3*	NM_009810	232.96	14.35	216.56	13.66	-1.08	0.0320	1.0000	0.1994
33	*Igfbp5*	NM_010518	7,878.26	1,614.37	9,979.93	2,028.14	1.27	0.0336	1.0000	0.1994
34	*Itgav*	NM_008402	735.64	64.19	672.58	44.19	-1.09	0.0339	1.0000	0.1994
35	*Egfr*	NM_007912	583.51	52.85	503.75	71.71	-1.16	0.0376	1.0000	0.2149

Table A.3, (continued). Complete results from NanoString array codeset.

Test	Gene symbol	Accession #	Mean WT count	SD WT	Mean Bco1$^{-/-}$ count	SD Bco1$^{-/-}$	BCO1$^{-/-}$ vs. WT	Raw p	Adj p	FDR
36	*Selp*	NM_011347	12.41	4.54	7.16	4.18	-1.73	0.0401	1.0000	0.2189
37	*Foxo1*	NM_019739	174.26	17.65	194.42	17.65	1.12	0.0405	1.0000	0.2189
38	*Aurka*	NM_011497	33.85	8.19	22.90	8.85	-1.48	0.0449	1.0000	0.2363
39	*Jun*	NM_010591	497.89	90.40	406.28	89.29	-1.23	0.0484	1.0000	0.2430
40	*Akt1*	NM_009652	1,741.89	168.09	1,581.92	143.38	-1.10	0.0486	1.0000	0.2430
41	*Casp1*	NM_009807	20.29	7.16	13.33	6.46	-1.52	0.0568	1.0000	0.2771
42	*E2f1*	NM_007891	22.36	8.36	13.85	8.17	-1.61	0.0708	1.0000	0.3371
43	*Casp2*	NM_007610	89.09	13.53	101.37	12.82	1.14	0.0758	1.0000	0.3433
44	*Ar*	NM_013476	545.12	61.78	620.38	104.29	1.14	0.0778	1.0000	0.3433
45	*Gpx1*	NM_008160	2,752.99	324.80	2,516.30	207.88	-1.09	0.0791	1.0000	0.3433
46	*Il18*	NM_008360	128.04	28.86	95.87	38.38	-1.34	0.0807	1.0000	0.3433
47	*Cdkn1a*	NM_007669	89.54	19.02	113.24	35.70	1.26	0.0810	1.0000	0.3433
48	*Erg*	NM_133659	26.83	8.24	20.81	6.00	-1.29	0.0824	1.0000	0.3433
49	*Cdc25b*	NM_001111075	18.53	8.97	26.40	9.75	1.42	0.0849	1.0000	0.3465
50	*Mapk1*	NM_011949	2,509.49	277.48	2,286.04	216.99	-1.10	0.0887	1.0000	0.3504
51	*Gstp1*	NM_013541	2,533.88	85.04	2,414.00	152.79	-1.05	0.0915	1.0000	0.3504
52	*Pten*	NM_008960	1,570.42	132.12	1,452.83	131.07	-1.08	0.0923	1.0000	0.3504
53	*Krt5*	NM_027011	120.56	48.88	155.31	41.82	1.29	0.0943	1.0000	0.3504
54	*Slc2a1*	NM_011400	230.77	17.26	275.35	76.47	1.19	0.0946	1.0000	0.3504
55	*Mmp9*	NM_013599	81.79	18.70	61.49	22.55	-1.33	0.0977	1.0000	0.3518

Table A.3, (continued). Complete results from NanoString array codeset.

Test	Gene symbol	Accession #	Mean WT count	SD WT	Mean Bco1$^{-/-}$ count	SD Bco1$^{-/-}$	BCO1$^{-/-}$ vs. WT	Raw p	Adj p	FDR
56	*Rb1*	NM_009029	236.03	26.69	257.65	22.36	1.09	0.0985	1.0000	0.3518
57	*Hdac6*	NM_010413	57.78	13.14	70.86	16.38	1.23	0.1026	1.0000	0.3600
58	*Igfbp3*	NM_008343	202.20	55.96	240.78	43.25	1.19	0.1092	1.0000	0.3756
59	*Cdc25c*	NM_009860	14.18	3.66	8.98	6.16	-1.58	0.1108	1.0000	0.3756
60	*Bcl2*	NM_009741	56.10	13.77	69.34	21.27	1.24	0.1201	1.0000	0.4003
61	*Cdh1*	NM_009864	2,596.86	327.79	2,348.31	327.98	-1.11	0.1282	1.0000	0.4203
62	*Csf1*	NM_001113530	236.72	33.79	210.45	31.51	-1.12	0.1351	1.0000	0.4358
63	*Tgfbr2*	NM_009371	392.58	59.46	346.30	60.73	-1.13	0.1409	1.0000	0.4469
64	*Arntl*	NM_007489	112.23	23.21	92.39	27.96	-1.21	0.1430	1.0000	0.4469
65	*Erbb2*	NM_001003817	296.84	50.23	333.43	51.82	1.12	0.1489	1.0000	0.4576
66	*Cyp7b1*	NM_007825	90.57	11.36	100.16	14.88	1.11	0.1510	1.0000	0.4576
67	*Cyp27a1*	NM_024264	166.85	30.70	147.88	21.55	-1.13	0.1574	1.0000	0.4699
68	*Etv1*	NM_007960	38.62	10.11	46.13	11.13	1.19	0.1633	1.0000	0.4803
69	*Srd5a1*	NM_175283	73.42	14.96	63.88	12.22	-1.15	0.1702	1.0000	0.4933
70	*Mtor*	NM_020009	94.66	18.83	84.49	11.53	-1.12	0.1838	1.0000	0.5251
71	*Ptgs2*	NM_011198	61.41	338.88	190.61	853.04	3.10	0.1893	1.0000	0.5278
72	*Hdac2*	NM_008229	445.67	23.11	429.91	24.32	-1.04	0.1900	1.0000	0.5278
73	*Il1a*	NM_010554	29.97	9.95	24.59	6.51	-1.22	0.1935	1.0000	0.5301
74	*Hsp90ab1*	NM_008302	11,523.73	1,699.68	10,512.53	1,622.53	-1.10	0.2106	1.0000	0.5692
75	*Srebf1*	NM_011480	1,345.05	217.85	1,481.86	238.83	1.10	0.2196	1.0000	0.5856

Table A.3, (continued). Complete results from NanoString array codeset.

Test	Gene symbol	Accession #	Mean WT count	SD WT	Mean Bco1$^{-/-}$ count	SD Bco1$^{-/-}$	BCO1$^{-/-}$ vs. WT	Raw p	Adj p	FDR
76	*Pthlh*	NM_008970	33.44	8.04	39.36	16.24	1.18	0.2337	1.0000	0.6150
77	*Dnmt1*	NM_010066	145.03	16.56	155.53	19.37	1.07	0.2421	1.0000	0.6249
78	*Esr1*	NM_007956	528.14	92.13	480.11	77.04	-1.10	0.2437	1.0000	0.6249
79	*Pxn*	NM_133915	419.93	35.80	449.71	68.42	1.07	0.2533	1.0000	0.6339
80	*Syp*	NM_009305	184.87	102.79	130.92	89.47	-1.41	0.2561	1.0000	0.6339
81	*Flt1*	NM_010228	68.46	22.45	77.96	7.67	1.14	0.2572	1.0000	0.6339
82	*Stat5a*	NM_011488	2,993.95	566.70	3,295.51	573.01	1.10	0.2599	1.0000	0.6339
83	*Aldh1a1*	NM_013467	1,651.30	483.28	1,419.00	436.02	-1.16	0.2651	1.0000	0.6367
84	*Bid*	NM_007544	53.19	9.98	63.14	26.73	1.19	0.2685	1.0000	0.6367
85	*Odc1*	NM_013614	49.02	11.01	42.65	14.03	-1.15	0.2718	1.0000	0.6367
86	*Atg5*	NM_053069	711.92	74.75	669.97	73.28	-1.06	0.2738	1.0000	0.6367
87	*Ccna1*	NM_007628	2.00	1.54	3.12	3.17	1.56	0.2867	1.0000	0.6503
88	*Hmgcr*	NM_008255	261.59	28.58	284.67	50.81	1.09	0.2880	1.0000	0.6503
89	*Casp8*	NM_009812	396.09	49.89	372.01	44.05	-1.06	0.2894	1.0000	0.6503
90	*Rxra*	NM_011305	148.69	20.98	161.99	32.92	1.09	0.3047	1.0000	0.6771
91	*Gata2*	NM_008090	4,385.97	823.83	4,851.34	1,076.70	1.11	0.3181	1.0000	0.6991
92	*Ezh2*	NM_007971	170.12	19.95	155.07	35.42	-1.10	0.3253	1.0000	0.7052
93	*Cd44*	NM_009851	561.05	93.50	616.17	139.91	1.10	0.3334	1.0000	0.7052
94	*Igfbp2*	NM_008342	282.35	64.79	250.29	61.37	-1.13	0.3337	1.0000	0.7052
95	*Mapk3*	NM_011952	2,431.24	388.68	2,652.08	562.51	1.09	0.3352	1.0000	0.7052

Table A.3, (continued). Complete results from NanoString array codeset.

Test	Gene symbol	Accession #	Mean WT count	SD WT	Mean Bco1$^{-/-}$ count	SD Bco1$^{-/-}$	BCO1$^{-/-}$ vs. WT	Raw p	Adj p	FDR
96	*Cdk2*	NM_016756	107.29	20.99	98.63	17.23	-1.09	0.3385	1.0000	0.7052
97	*Ep300*	NM_177821	824.97	64.43	798.54	48.19	-1.03	0.3505	1.0000	0.7134
98	*Cdkn1b*	NM_009875	1,799.30	119.59	1,725.71	184.90	-1.04	0.3551	1.0000	0.7134
99	*Atg7*	NM_028835	203.96	20.23	196.18	12.77	-1.04	0.3568	1.0000	0.7134
100	*Igf1*	NM_001111274	161.85	56.01	133.91	58.64	-1.21	0.3591	1.0000	0.7134
101	*H6pd*	NM_173371	403.10	62.47	436.96	95.68	1.08	0.3665	1.0000	0.7134
102	*Ccng1*	NM_009831	1,892.81	189.56	1,808.73	195.34	-1.05	0.3702	1.0000	0.7134
103	*Ngfr*	NM_033217	344.94	140.06	244.96	211.50	-1.41	0.3703	1.0000	0.7134
104	*Sirt1*	NM_019812	336.65	13.92	325.91	27.90	-1.03	0.3738	1.0000	0.7134
105	*Ran*	NM_009391	130.64	18.20	139.22	18.17	1.07	0.3773	1.0000	0.7134
106	*Ccnb1*	NM_172301	2.17	1.60	3.20	4.79	1.48	0.3781	1.0000	0.7134
107	*Hsd3b2*	NM_153193	1.37	2.48	1.11	0.17	-1.24	0.3869	1.0000	0.7232
108	*Il6*	NM_031168	1.09	0.14	1.25	0.83	1.15	0.4000	1.0000	0.7407
109	*Cyp24a1*	NM_009996	11.74	5.18	9.51	4.25	-1.23	0.4048	1.0000	0.7428
110	*Cdk4*	NM_009870	1,016.14	124.44	973.93	89.72	-1.04	0.4228	1.0000	0.7586
111	*Gstm1*	NM_010358	44.16	9.15	40.31	10.03	-1.10	0.4233	1.0000	0.7586
112	*Irs1*	NM_010570	189.41	54.42	208.38	58.76	1.10	0.4248	1.0000	0.7586
113	*Ugt1a1*	NM_201645	9.40	38.18	6.43	3.73	-1.46	0.4468	1.0000	0.7898
114	*Cdkn2a*	NM_001040654	1.74	1.24	1.41	1.14	-1.23	0.4502	1.0000	0.7898
115	*Notch1*	NM_008714	589.51	77.13	614.97	69.22	1.04	0.4566	1.0000	0.7941

Table A.3, (continued). Complete results from NanoString array codeset.

Test	Gene symbol	Accession #	Mean WT count	SD WT	Mean Bco1$^{-/-}$ count	SD Bco1$^{-/-}$	BCO1$^{-/-}$ vs. WT	Raw p	Adj p	FDR
116	*Vim*	NM_011701	1,000.75	264.77	914.77	156.16	-1.09	0.4633	1.0000	0.7988
117	*Smad3*	NM_016769	171.38	25.32	179.21	16.86	1.05	0.4787	1.0000	0.8127
118	*Ncoa1*	NM_010881	392.92	31.22	406.63	46.61	1.03	0.4795	1.0000	0.8127
119	*Cav1*	NM_007616	1,632.79	209.29	1,562.95	205.84	-1.04	0.4983	1.0000	0.8367
120	*Gapdh*	NM_008084	5,763.76	592.61	6,073.88	1,247.30	1.05	0.5027	1.0000	0.8367
121	*Wnt1*	NM_021279	6.64	4.89	5.16	2.72	-1.29	0.5062	1.0000	0.8367
122	*Etv4*	NM_008815	19.90	6.00	21.89	6.08	1.10	0.5157	1.0000	0.8454
123	*Tgfb1i1*	NM_009365	93.51	12.93	99.62	25.08	1.07	0.5297	1.0000	0.8561
124	*Mdk*	NM_001012335	42.01	21.69	46.95	13.66	1.12	0.5308	1.0000	0.8561
125	*Myc*	NM_001177352	174.22	24.35	184.61	42.96	1.06	0.5456	1.0000	0.8730
126	*Cdh2*	NM_007664	68.32	43.83	49.10	45.24	-1.39	0.5598	1.0000	0.8886
127	*Kit*	NM_001122733	19.13	11.30	22.35	15.15	1.17	0.5661	1.0000	0.8904
128	*Ccnd1*	NM_007631	766.60	434.61	916.16	1,022.09	1.20	0.5703	1.0000	0.8904
129	*Bmp6*	NM_007556	30.75	9.19	27.78	10.75	-1.11	0.5779	1.0000	0.8904
130	*Hgf*	NM_010427	53.36	5.56	55.53	9.67	1.04	0.5822	1.0000	0.8904
131	*Plaur*	NM_011113	26.98	9.92	30.97	25.14	1.15	0.5912	1.0000	0.8904
132	*Shh*	NM_009170	86.94	43.69	77.84	50.91	-1.12	0.5920	1.0000	0.8904
133	*Mmp2*	NM_008610	199.68	57.20	184.23	55.51	-1.08	0.5921	1.0000	0.8904
134	*Egf*	NM_010113	8,259.22	1,545.95	7,872.64	1,388.03	-1.05	0.6016	1.0000	0.8930
135	*Sele*	NM_011345	14.29	5.47	12.70	7.19	-1.12	0.6028	1.0000	0.8930

Table A.3, (continued). Complete results from NanoString array codeset.

Test	Gene symbol	Accession #	Mean WT count	SD WT	Mean Bco1$^{-/-}$ count	SD Bco1$^{-/-}$	BCO1$^{-/-}$ vs. WT	Raw p	Adj p	FDR
136	*Stat3*	NM_011486	191.38	24.57	197.66	27.05	1.03	0.6113	1.0000	0.8985
137	*Hdac4*	NM_207225	100.02	12.71	96.94	11.75	-1.03	0.6155	1.0000	0.8985
138	*Hoxb13*	NM_008267	1,618.69	407.62	1,522.96	471.01	-1.06	0.6330	1.0000	0.9145
139	*Atm*	NM_007499	129.25	11.31	133.70	24.28	1.03	0.6356	1.0000	0.9145
140	*Cyp19a1*	NM_007810	1.61	2.03	1.88	1.84	1.17	0.6551	1.0000	0.9321
141	*Pbsn*	NM_017471	166,923.14	32,045.77	159,204.27	37,507.88	-1.05	0.6571	1.0000	0.9321
142	*Bad*	NM_007522	120.13	12.96	117.10	14.87	-1.03	0.6658	1.0000	0.9377
143	*Ncor1*	NM_011308	608.83	44.85	620.39	65.94	1.02	0.6740	1.0000	0.9406
144	*Cyp2r1*	NM_177382	28.56	7.81	27.19	6.04	-1.05	0.6783	1.0000	0.9406
145	*Pou5f1*	NM_013633	1.13	0.15	1.22	1.17	1.08	0.6819	1.0000	0.9406
146	*Tgfb1*	NM_011577	118.27	20.19	114.23	23.37	-1.04	0.7120	1.0000	0.9420
147	*Rbp1*	NM_011254	25.51	5.48	26.52	5.61	1.04	0.7132	1.0000	0.9420
148	*Tmprss2*	NM_015775	2,674.15	452.17	2,769.21	607.11	1.04	0.7146	1.0000	0.9420
149	*Krt18*	NM_010664	4,828.25	845.28	4,707.34	504.30	-1.03	0.7158	1.0000	0.9420
150	*Pdha1*	NM_008810	1,347.06	88.97	1,366.52	125.50	1.01	0.7195	1.0000	0.9420
151	*Fgfr1*	NM_001079908	101.23	15.83	104.25	18.84	1.03	0.7276	1.0000	0.9420
152	*Spp1*	NM_009263	18.20	19.67	15.13	47.80	-1.20	0.7362	1.0000	0.9420
153	*Fasn*	NM_007988	1,046.94	414.58	1,109.78	720.32	1.06	0.7453	1.0000	0.9420
154	*Ncoa4*	NM_001033988	5,277.69	1,419.30	5,027.93	1,873.21	-1.05	0.7502	1.0000	0.9420
155	*Casp9*	NM_015733	121.04	22.57	124.35	21.46	1.03	0.7516	1.0000	0.9420

Table A.3, (continued). Complete results from NanoString array codeset.

Test	Gene symbol	Accession #	Mean WT count	SD WT	Mean Bco1$^{-/-}$ count	SD Bco1$^{-/-}$	BCO1$^{-/-}$ vs. WT	Raw p	Adj p	FDR
156	*Bcl2l1*	NM_009743	567.27	71.09	579.28	82.80	1.02	0.7536	1.0000	0.9420
157	*Pdgfra*	NM_001083316	242.70	66.32	253.08	52.77	1.04	0.7569	1.0000	0.9420
158	*Braf*	NM_139294	396.41	54.83	389.83	26.38	-1.02	0.7579	1.0000	0.9420
159	*Foxa1*	NM_008259	371.64	100.43	385.41	110.22	1.04	0.7670	1.0000	0.9420
160	*Ctnnb1*	NM_007614	2,924.97	262.29	2,889.87	235.62	-1.01	0.7737	1.0000	0.9420
161	*Ccl2*	NM_011333	21.68	13.83	20.01	8.28	-1.08	0.7741	1.0000	0.9420
162	*Cflar*	NM_009805	883.71	92.13	870.15	107.48	-1.02	0.7832	1.0000	0.9420
163	*Srd5a2*	NM_053188	105.63	21.80	101.46	36.12	-1.04	0.7832	1.0000	0.9420
164	*Ptgs1*	NM_008969	1,305.90	161.02	1,329.90	198.13	1.02	0.7835	1.0000	0.9420
165	*Rarb*	NM_011243	41.68	10.57	42.83	7.05	1.03	0.7840	1.0000	0.9420
166	*Il6ra*	NM_010559	148.87	20.57	153.00	39.00	1.03	0.7844	1.0000	0.9420
167	*Pparg*	NM_011146	7.87	7.24	8.75	10.42	1.11	0.7866	1.0000	0.9420
168	*Hk1*	NM_001146100	39.54	10.80	40.76	8.90	1.03	0.8019	1.0000	0.9546
169	*Gsk3b*	NM_019827	1,095.73	94.55	1,106.68	99.65	1.01	0.8114	1.0000	0.9553
170	*Trp53*	NM_011640	93.37	16.97	95.26	17.56	1.02	0.8180	1.0000	0.9553
171	*Pdgfrb*	NM_008809	34.87	9.50	35.80	7.94	1.03	0.8249	1.0000	0.9553
172	*Pecam1*	NM_008816	384.56	117.54	372.85	80.45	-1.03	0.8270	1.0000	0.9553
173	*Cdk6*	NM_009873	50.74	11.47	49.20	17.40	-1.03	0.8272	1.0000	0.9553
174	*Fasl*	NM_010177	1.30	1.36	1.25	0.40	-1.04	0.8311	1.0000	0.9553
175	*Bco2*	NM_133217	22.44	6.18	23.02	6.76	1.03	0.8399	1.0000	0.9564

Table A.3, (continued). Complete results from NanoString array codeset.

Test	Gene symbol	Accession #	Mean WT count	SD WT	Mean Bco1$^{-/-}$ count	SD Bco1$^{-/-}$	BCO1$^{-/-}$ vs. WT	Raw p	Adj p	FDR
176	*Alox5*	NM_009662	19.68	8.85	20.44	5.72	1.04	0.8416	1.0000	0.9564
177	*Brca1*	NM_009764	39.11	11.11	40.15	10.52	1.03	0.8509	1.0000	0.9566
178	*Brca2*	NM_009765	24.88	6.89	25.49	6.38	1.02	0.8514	1.0000	0.9566
179	*Ccnd2*	NM_009829	383.79	63.24	388.23	46.14	1.01	0.8712	1.0000	0.9658
180	*Spdef*	NM_013891	558.00	97.71	551.53	88.92	-1.01	0.8827	1.0000	0.9658
181	*Cd34*	NM_001111059	646.89	271.67	668.16	199.63	1.03	0.8833	1.0000	0.9658
182	*Insr*	NM_010568	327.95	38.02	325.57	32.23	-1.01	0.8913	1.0000	0.9658
183	*Smad4*	NM_008540	1,157.48	145.75	1,166.31	121.27	1.01	0.8977	1.0000	0.9658
184	*Ncoa2*	NM_008678	307.03	26.62	305.61	19.84	-1.00	0.9014	1.0000	0.9658
185	*Gadd45a*	NM_007836	300.72	38.78	303.48	52.80	1.01	0.9059	1.0000	0.9658
186	*Egr1*	NM_007913	211.05	72.66	204.09	325.85	-1.03	0.9085	1.0000	0.9658
187	*Sod2*	NM_013671	640.52	36.72	642.62	40.36	1.00	0.9088	1.0000	0.9658
188	*Hsd3b1*	NM_008293	3.40	2.84	3.29	1.14	-1.03	0.9168	1.0000	0.9658
189	*Tnf*	NM_013693	2.32	3.03	2.23	2.46	-1.04	0.9231	1.0000	0.9658
190	*Fgf2*	NM_008006	126.27	29.44	125.09	17.22	-1.01	0.9249	1.0000	0.9658
191	*Hdac1*	NM_008228	694.56	71.43	697.77	63.52	1.00	0.9253	1.0000	0.9658
192	*Ncoa3*	NM_008679	600.69	32.69	602.93	64.10	1.00	0.9307	1.0000	0.9658
193	*Prkab1*	NM_031869	897.84	128.70	892.63	120.85	-1.01	0.9320	1.0000	0.9658
194	*Hdac3*	NM_010411	745.48	89.32	741.95	97.54	-1.00	0.9390	1.0000	0.9680
195	*Gja1*	NM_010288	158.86	31.06	158.05	43.50	-1.01	0.9646	1.0000	0.9893
196	*Actb*	NM_007393	21,207.69	1,435.81	21,177.38	1,984.89	-1.00	0.9728	1.0000	0.9902
197	*Acaca*	NM_133360	512.75	110.44	514.72	201.48	1.00	0.9753	1.0000	0.9902
198	*Ly6a*	NM_010738	718.57	313.22	716.24	276.32	-1.00	0.9884	1.0000	0.9916
199	*Nfkb1*	NM_008689	501.33	63.93	500.95	57.02	-1.00	0.9897	1.0000	0.9916
200	*Cdk1*	NM_007659	14.57	6.97	14.53	6.07	-1.00	0.9916	1.0000	0.9916

Appendix B

Supplemental tables and figures for Ch. 3

Figure B.1.

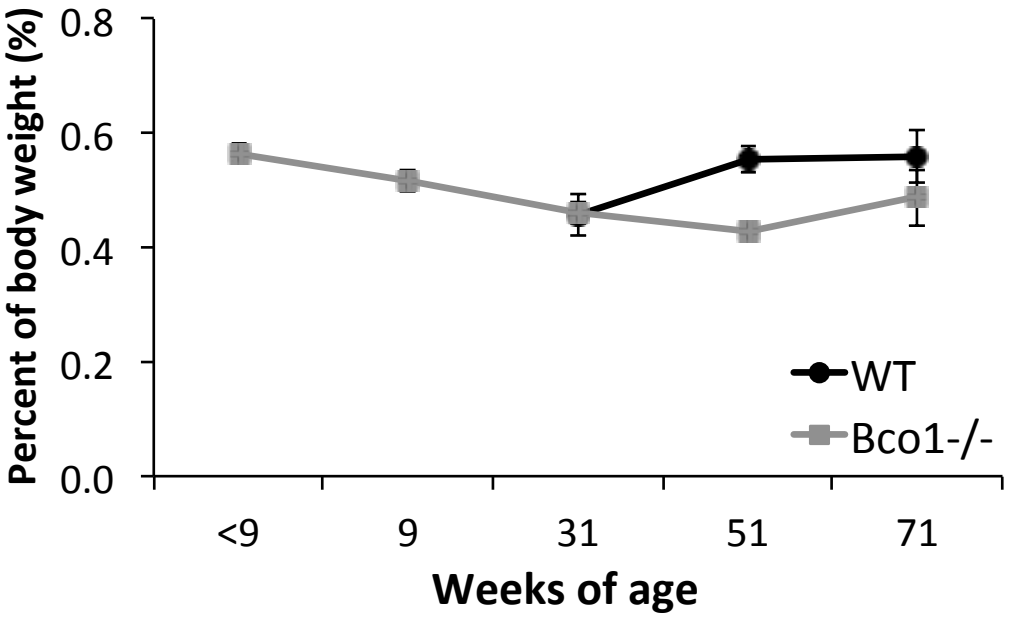

Figure B.1. Heart weight as a percent of body weight in mice fed a semi-purified, vitamin A-sufficient, carotenoid-free diet (Study #2). WT heart tissues were not collected at ages <9 or 9 weeks of age. No statistical differences were observed.

Figure B.2.

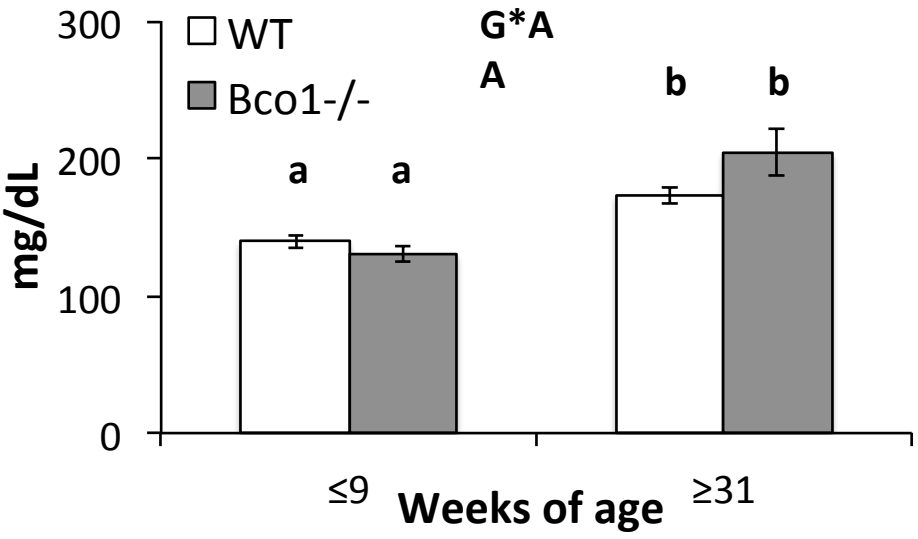

Figure B.2. Serum cholesterol in mice fed vitamin A-sufficient, carotenoid-free semi-purified diets. G*A and A indicate statistical main effect of age or an interaction between genotype and age. Different lowercase letters above groups indicate significant ($p < 0.05$) results of mean separations tests for interaction effect.

Table B.1.

			Retinol	Ret. Pal	Ret. Lau.	Ret. Lin/Po.	Ret. Myr.	Ret. Pent.	Ret. O.	Ret. Hept.	Ret. S.	Total VitA
<9 weeks	WT	nmol/g	4.62 ± 0.82 b	326.5 ± 30.90 c	nd	11.50 ± 1.36 c	1.72 ± 0.22 c	1.35 ± 0.12 bc	10.29 ± 1.33 b	3.68 ± 0.33 c	22.70 ± 2.35 c	382.4 ± 36.96 c
		% total	1.2%	85.4%	0.0%	3.0%	0.5%	0.4%	2.7%	1.0%	5.9%	100.0%
	Bco1-/-	nmol/g	2.36 ± 0.77 ab	146.3 ± 18.72 b	nd	4.44 ± 0.57 b	0.78 ± 0.13 ab	0.32 ± 0.04 a	3.42 ± 0.50 a	0.93 ± 0.12 a	9.97 ± 1.68 b	168.5 ± 21.55 b
		% total	1.4%	86.8%	0.0%	2.6%	0.5%	0.2%	2.0%	0.6%	5.9%	100.0%
9 weeks	WT	nmol/g	2.28 ± 0.22 ab	662.8 ± 46.66 d	nd	20.06 ± 1.55 d	3.52 ± 0.29 d	3.65 ± 0.28 d	18.33 ± 1.23 c	8.67 ± 0.59 be	40.04 ± 2.15 d	759.4 ± 52.79 d
		% total	0.3%	87.3%	0.0%	2.6%	0.5%	0.5%	2.4%	1.1%	5.3%	100.0%
	Bco1-/-	nmol/g	nd	25.50 ± 15.26 a	nd	0.94 ± 0.53 a	0.19 ± 0.10 a	0.19	0.84 ± 0.39 a	1.68 ± 1.10 abcd	1.87 ± 0.87 a	29.82 ± 17.17 a
		% total	0.0%	85.5%	0.0%	3.1%	0.6%	0.6%	2.8%	5.6%	6.3%	100.0%
31 weeks	WT	nmol/g	24.84 ± 4.37 c	696.0 ± 137.68 cde	nd	24.04 ± 6.74 cde	3.89 ± 1.06 cd	2.39 ± 0.56 bcd	22.28 ± 7.13 bc	5.24 ± 1.12 bc	39.57 ± 8.39 cd	818.3 ± 162.7 cde
		% total	3.0%	85.1%	0.0%	2.9%	0.5%	0.3%	2.7%	0.6%	4.8%	100.0%
	Bco1-/-	nmol/g	42.83 ± 13.44 c	1,495.3 ± 264.9 ef	nd	47.47 ± 8.17 ef	7.76 ± 2.02 def	3.21 ± 0.85 cde	34.94 ± 5.36 cd	7.95 ± 1.82 ce	76.90 ± 12.89 de	1,724.7 ± 297.4 ef
		% total	2.5%	86.7%	0.0%	2.8%	0.4%	0.2%	2.0%	0.5%	4.5%	100.0%
51 weeks	WT	nmol/g	2.19 ± 0.15 ab	375.8 ± 37.20 c	nd	12.15 ± 1.21 c	1.62 ± 0.03 c	1.35 ± 0.01 c	11.39 ± 1.01 b	5.11 ± 1.27 ce	22.05 ± 2.63 c	430.48 ± 43.48 c
		% total	0.5%	87.3%	0.0%	2.8%	0.4%	0.3%	2.6%	1.2%	5.1%	100.0%
	Bco1-/-	nmol/g	2.60 ± 0.38 ab	2,486.1 ± 281.0 f	nd	93.52 ± 9.03 g	17.23 ± 1.98 f	7.34 ± 1.12 e	75.44 ± 8.87 e	23.35 ± 5.00 d	173.0 ± 22.59 f	2,878.5 ± 323.2 f
		% total	0.1%	86.4%	0.0%	3.2%	0.6%	0.3%	2.6%	0.8%	6.0%	100.0%
71 weeks	WT	nmol/g	1.63 ± 0.23 a	347.0 ± 32.17 c	nd	11.09 ± 0.74 c	1.14 ± 0.13 bc	0.90 ± 0.08 b	11.15 ± 0.78 b	3.27 ± 0.62 c	19.78 ± 2.12 c	395.13 ± 34.25 c
		% total	0.4%	87.8%	0.0%	2.8%	0.3%	0.2%	2.8%	0.8%	5.0%	100.0%
	Bco1-/-	nmol/g	16.90 ± 12.52 abc	1,953.1 ± 88.00 f	nd	61.64 ± 6.10 fg	9.89 ± 0.49 e	4.27 ± 0.38 de	59.11 ± 6.25 de	13.45 ± 1.41 de	106.7 ± 9.38 ef	2,225.1 ± 111.1 f
		% total	0.8%	87.8%	0.0%	2.8%	0.4%	0.2%	2.7%	0.6%	4.8%	100.0%
ANOVA p-values		Genotype	0.0786	0.6565	-	0.9732	0.0905	0.1841	0.4329	0.6226	0.9831	0.6606
		Age	<0.0001	<0.0001	-	<0.0001	<0.0001	<0.0001	<0.0001	<0.0001	<0.0001	<0.0001
		G*A	0.0062	<0.0001	-	<0.0001	<0.0001	<0.0001	<0.0001	<0.0001	<0.0001	<0.0001

Table B.1. Loss of *Bco1* interacts with age to modulate total hepatic vitamin A stores, but does not alter the relative abundance of hepatic retinol/retinyl esters. Data are mean nmol/g ± SEM. The percent of the total vitamin A pool (retinol plus all quantified retinyl esters) within each genotype-age combination is denoted by % total. Group n = 4 - 6, except for ret. pent., which was detected in only one 9-week old *Bco1*$^{-/-}$ mouse. All data were log transformed and analyzed with individual group variances, due to heterogeneity of variance. Repeated-measure ANOVA p-values for main effects of genotype and age, and the interaction between genotype and age (G*A), are shown at the bottom of the table. Means in each column with different letters are significantly different using *post hoc* Tukey-Kramer adjustment for multiple comparisons. Ret. Pal., retinyl palmitate; Ret. Lau., retinyl laurate; Ret. Lin/Po., retinyl linoleate/retinyl palmitoleate co-eluted peaks; Ret. Myr., retinyl myristate; Ret. Pent., retinyl pentadecanoate; Ret. O., retinyl oleate; Ret. Hept., retinyl heptadecanoate; Ret. S., retinyl stearate; Total VitA, sum of retinol + all quantified retinyl esters. nd, not detected.

Table B.2.

	BrainWt	TotVA	RetPal	RetS	FrRol	CEPal	PLPal	PLS	FFAPal	Acox3	Apoa4	Cpt1b	Fabp5	Gapdh	Hsp90ab1	Mlycd	Pck1	Ppard	Pparg	Pprc1	Rxra	Rxrb	Slc22a5	Slc27a1	Slc27a4	Sorl1
BrainWt																										
TotVA	**-0.75** 0.012																									
RetPal	-0.68 0.031	0.96 <.0001																								
RetS	-0.56 0.090	0.91 0.000	0.97 <.0001																							
FrRol	-0.36 0.313	0.23 0.528	-0.05 0.886	-0.16 0.657																						
CEPal	-0.76 0.003	0.86 0.006	0.86 0.006	0.82 0.012	-0.35 0.396																					
PLPal	0.30 0.339	**-0.84** 0.019	**-0.84** 0.017	**-0.81** 0.028	0.64 0.125	-0.23 0.479																				
PLS	-0.36 0.256	0.55 0.201	0.56 0.191	0.52 0.232	-0.43 0.330	0.56 0.059	-0.70 0.011																			
FFAPal	-0.53 0.078	0.71 0.048	0.73 0.040	0.69 0.060	-0.75 0.031	0.72 0.009	-0.59 0.056	0.76 0.007																		
Acox3	-0.70 0.017	0.82 0.023	0.83 0.022	0.79 0.035	-0.11 0.815	0.88 0.002	-0.24 0.575	0.70 0.054	0.51 0.161																	
Apoa4	0.71 0.014	**-0.85** 0.016	**-0.84** 0.018	**-0.85** 0.017	0.11 0.810	**-0.91** 0.001	0.02 0.965	-0.61 0.109	-0.55 0.124	**-0.91** <.0001																
Cpt1b	-0.73 0.010	0.71 0.073	0.73 0.065	0.64 0.124	-0.26 0.568	0.70 0.035	-0.12 0.786	0.25 0.553	0.37 0.322	0.59 0.058	-0.59 0.058															
Fabp5	0.85 0.001	-0.76 0.049	-0.74 0.055	-0.73 0.061	-0.24 0.608	-0.77 0.014	-0.19 0.652	-0.33 0.420	-0.32 0.406	-0.63 0.038	0.76 0.007	-0.74 0.009														
Gapdh	-0.74 0.010	0.66 0.110	0.67 0.102	0.60 0.152	-0.07 0.877	0.88 0.002	-0.11 0.804	0.56 0.147	0.63 0.068	0.75 0.007	**-0.82** 0.002	0.75 0.008	-0.73 0.011													
Hsp90ab1	-0.54 0.088	0.78 0.039	0.79 0.035	0.77 0.042	-0.71 0.072	0.81 0.008	-0.20 0.639	0.59 0.126	0.62 0.075	0.76 0.006	**-0.83** 0.001	0.64 0.032	-0.56 0.073	0.66 0.029												
Mlycd	-0.68 0.022	0.61 0.149	0.63 0.129	0.51 0.238	-0.34 0.459	0.81 0.008	-0.07 0.870	0.39 0.335	0.47 0.200	0.74 0.010	-0.68 0.022	0.89 0.000	-0.58 0.064	0.82 0.002	0.68 0.020											
Pck1	-0.72 0.012	0.71 0.075	0.72 0.067	0.65 0.113	-0.25 0.593	0.76 0.018	-0.12 0.778	0.33 0.428	0.52 0.153	0.64 0.034	-0.65 0.030	0.91 <.0001	-0.67 0.024	0.88 0.000	0.61 0.045	0.93 <.0001										
Ppard	-0.26 0.432	0.48 0.277	0.48 0.276	0.46 0.295	-0.18 0.706	0.41 0.270	-0.08 0.853	0.29 0.480	0.08 0.841	0.52 0.099	-0.55 0.083	0.50 0.116	-0.54 0.084	0.43 0.188	0.59 0.055	0.34 0.306	0.31 0.346									
Pparg	-0.72 0.012	0.76 0.049	0.76 0.048	0.71 0.072	0.00 0.997	0.69 0.040	-0.16 0.703	0.27 0.511	0.35 0.353	0.66 0.026	-0.63 0.037	0.87 0.001	-0.77 0.006	0.76 0.006	0.46 0.151	0.79 0.004	0.88 0.000	0.44 0.180								
Pprc1	**-0.85** 0.001	0.86 0.013	0.86 0.013	0.85 0.016	-0.21 0.654	0.77 0.015	-0.03 0.952	0.31 0.448	0.55 0.129	0.64 0.034	-0.72 0.012	0.78 0.005	-0.71 0.013	0.78 0.005	0.68 0.022	0.81 0.002	0.87 0.000	0.12 0.735	0.72 0.013							
Rxra	-0.65 0.030	0.72 0.067	0.73 0.062	0.70 0.080	-0.36 0.431	0.75 0.019	-0.08 0.848	0.37 0.371	0.48 0.187	0.76 0.007	-0.72 0.013	0.77 0.006	-0.52 0.099	0.81 0.002	0.68 0.020	0.93 <.0001	0.92 <.0001	0.25 0.451	0.76 0.006	0.86 0.001						
Rxrb	-0.55 0.078	0.91 0.005	0.91 0.004	0.87 0.012	-0.41 0.363	0.74 0.023	-0.08 0.852	0.38 0.349	0.36 0.346	0.84 0.001	-0.76 0.006	0.76 0.006	-0.61 0.048	0.65 0.031	0.72 0.013	0.84 0.001	0.75 0.008	0.53 0.096	0.81 0.003	0.65 0.031	0.81 0.002					
Slc22a5	-0.74 0.010	0.63 0.130	0.65 0.116	0.55 0.203	-0.16 0.731	0.73 0.026	-0.22 0.600	0.34 0.414	0.44 0.236	0.63 0.038	-0.56 0.075	0.95 <.0001	-0.64 0.033	0.81 0.003	0.53 0.091	0.93 <.0001	0.96 <.0001	0.35 0.298	0.90 0.000	0.79 0.004	0.85 0.001	0.75 0.008				
Slc27a1	-0.79 0.004	0.69 0.086	0.70 0.082	0.64 0.124	0.02 0.965	0.81 0.008	-0.17 0.695	0.43 0.293	0.52 0.155	0.74 0.009	-0.71 0.014	0.81 0.003	-0.65 0.029	0.90 0.000	0.55 0.080	0.89 0.000	0.95 <.0001	0.26 0.444	0.87 0.000	0.85 0.001	0.91 <.0001	0.72 0.013	0.92 <.0001			
Slc27a4	-0.66 0.028	0.95 0.001	0.96 0.001	0.92 0.004	-0.55 0.198	0.82 0.006	-0.15 0.730	0.50 0.203	0.48 0.195	0.90 0.000	**-0.83** 0.002	0.77 0.005	-0.63 0.039	0.74 0.009	0.83 0.002	0.89 0.000	0.80 0.003	0.51 0.109	0.75 0.008	0.76 0.006	0.90 0.000	0.94 <.0001	0.77 0.005	0.78 0.005		
Sorl1	0.71 0.015	**-0.86** 0.014	**-0.86** 0.014	**-0.84** 0.017	0.25 0.589	**-0.88** 0.002	0.34 0.408	-0.74 0.038	-0.55 0.125	**-0.97** <.0001	0.89 0.000	-0.60 0.050	0.66 0.027	-0.71 0.014	**-0.82** 0.002	-0.69 0.019	-0.62 0.043	-0.59 0.057	-0.64 0.034	-0.64 0.033	-0.72 0.013	**-0.80** 0.003	-0.61 0.047	-0.69 0.020	**-0.90** 0.000	

Table B.2. Pearson correlation coefficients (R^2) and p-values for endpoints measured in livers of chow-fed WT and *Bco1*$^{-/-}$ mice. Correlations were calculated using values from both genotypes; n = 8 - 16. R^2 values > 0.8 are highlighted in red, while R^2 values <-0.8 are highlighted in blue. P-values < 0.05 are highlighted in green. BrainWt, brain weight; TotVA, total retinyl esters + retinol; RetPal, retinyl palmitate; RetS, retinyl stearate; FrRol, free retinol; CEPal, cholesteryl palmitate; PLPal, phospholipid palmitate; PLS, phospholipid stearate; FFAPal, free palmitate; *Acox3, Apoa4, Cpt1b, Fabp5, Gapdh, Hsp90ab1, Mlycd, Pck1, Ppard, Pparg, Pprc1, Rxra, Rxrb, Slc22a5, Slc27a1, Slc27a4, Sorl1:* gene names.

Table B.3. Hepatic expression of lipid metabolism- and cholesterol metabolism-related genes.

Test	Array	Refseq	Gene	Fold Regulation	Raw p	Adj p	FDR
1	LipoproChol	NM_007468	Apoa4	**-3.54**	0.0000	0.0067	0.0047
2	LipoproChol	NM_011436	Sorl1	**-3.92**	0.0001	0.0095	0.0047
3	PPAR	NM_030721	Acox3	1.83	0.0003	0.0502	0.0167
4	PPAR	NM_013599	Mmp9	**2.53**	0.0005	0.0778	0.0195
5	Both	NM_008302	Hsp90ab1	1.28	0.0017	0.2721	0.0459
6	PPAR	NM_010634	Fabp5	**-2.85**	0.0017	0.2754	0.0459
7	Both	NM_008084	Gapdh	1.30	0.0020	0.3267	0.0467
8	PPAR	NM_011989	Slc27a4	1.61	0.0029	0.4648	0.0581
9	PPAR	NM_009271	Src	1.84	0.0047	0.7741	0.0860
10	PPAR	NM_025891	Smarcd3	1.89	0.0071	1.0000	0.1152
11	PPAR	NM_011977	Slc27a1	**2.67**	0.0095	1.0000	0.1413
12	PPAR	NM_001081214	Pprc1	**2.33**	0.0105	1.0000	0.1429
13	PPAR	NM_011306	Rxrb	1.91	0.0120	1.0000	0.1472
14	PPAR	NM_011146	Pparg	**2.32**	0.0126	1.0000	0.1472
15	PPAR	NM_011044	Pck1	1.72	0.0177	1.0000	0.1853
16	PPAR	NM_009948	Cpt1b	**2.09**	0.0182	1.0000	0.1853
17	PPAR	NM_024264	Cyp27a1	1.40	0.0209	1.0000	0.1907
18	PPAR	NM_080434	Apoa5	1.77	0.0211	1.0000	0.1907
19	PPAR	NM_011305	Rxra	1.48	0.0233	1.0000	0.1995
20	PPAR	NM_019966	Mlycd	1.56	0.0270	1.0000	0.2200
21	PPAR	NM_011396	Slc22a5	1.98	0.0287	1.0000	0.2225
22	PPAR	NM_007980	Fabp2	1.47	0.0352	1.0000	0.2609
23	Both	NM_011145	Ppard	1.45	0.0443	1.0000	0.3141
24	PPAR	NM_010174	Fabp3	1.59	0.0641	1.0000	0.4351
25	LipoproChol	NM_013703	Vldlr	**2.08**	0.0819	1.0000	0.5343

Table B.3. *Bco1*$^{-/-}$ genotype alters hepatic expression of genes involved in lipid and cholesterol metabolism. Gene expression was assayed using qPCR arrays focused on PPAR signaling (PPAR) and lipoprotein and cholesterol metabolism (LipoproChol); several genes were present on both arrays (Both). Results for all genes measured are displayed. Fold regulation values are displayed, with fold regulation ≥ 2 in red and ≤ -2 in blue. NCBI RefSeq identifiers are provided for each gene. Raw p values, Bonferroni's adjusted p-values (Adj p), and FDR q-values (FDR) are displayed for each gene; Bonferroni's adjusted p-values and FDR q-values were calculated after ranking genes by raw p-value, smallest first. For raw p-values, yellow highlighting indicates $0.005 < p \leq 0.05$, while green highlighting indicates $p \leq 0.005$. For Bonferroni's adjusted p-values and FDR q-values, green highlighting indicates values < 0.05. Several genes did not have Ct values above 35 for more than two replicates per group, and so fold regulation calculations were either inaccurate (*Cela3b, Apod, Adipoq*) or not quantifiable (n.q., several). Statistical tests were not done for those genes.

Table B.3, (continued). Hepatic expression of lipid metabolism- and cholesterol metabolism-related genes.

Test	Array	Refseq	Gene	Fold Regulation	Raw p	Adj p	FDR
26	LipoproChol	NM_011850	Nr0b2	1.74	0.0931	1.0000	0.5837
27	Both	NM_177470	Acaa2	1.23	0.1055	1.0000	0.6358
28	PPAR	NM_019699	Fads2	1.38	0.1113	1.0000	0.6358
29	PPAR	NM_024406	Fabp4	-1.27	0.1131	1.0000	0.6358
30	PPAR	NM_010011	Cyp4a10	**3.75**	0.1193	1.0000	0.6481
31	PPAR	NM_007925	Eln	1.33	0.1334	1.0000	0.6817
32	PPAR	NM_010046	Dgat1	1.30	0.1353	1.0000	0.6817
33	PPAR	NM_013839	Nr1h3	1.20	0.1380	1.0000	0.6817
34	LipoproChol	NM_011480	Srebf1	-1.43	0.1449	1.0000	0.6826
35	PPAR	NM_020581	Angptl4	1.46	0.1466	1.0000	0.6826
36	LipoproChol	NM_178082	Insig2	1.76	0.1594	1.0000	0.6935
37	Both	NM_023114	Apoc3	-1.22	0.1601	1.0000	0.6935
38	PPAR	NM_008679	Ncoa3	1.25	0.1642	1.0000	0.6935
39	LipoproChol	NM_020010	Cyp51	1.18	0.1689	1.0000	0.6935
40	PPAR	NM_183162	Helz2	1.26	0.1776	1.0000	0.6935
41	PPAR	NM_016772	Ech1	1.28	0.1780	1.0000	0.6935
42	LipoproChol	NM_007379	Abca2	1.15	0.1805	1.0000	0.6935
43	PPAR	NM_013495	Cpt1a	1.37	0.1829	1.0000	0.6935
44	LipoproChol	NM_145942	Hmgcs1	1.54	0.2046	1.0000	0.7447
45	PPAR	NM_015729	Acox1	1.39	0.2056	1.0000	0.7447
46	PPAR	NM_009949	Cpt2	1.18	0.2216	1.0000	0.7851
47	Both	NM_009696	Apoe	1.11	0.2272	1.0000	0.7877
48	LipoproChol	NM_145364	Akr1d1	1.17	0.2320	1.0000	0.7877
49	PPAR	NM_019825	Ncoa6	1.29	0.2597	1.0000	0.8472
50	PPAR	NM_011125	Pltp	1.52	0.2599	1.0000	0.8472

Table B.3, (continued). Hepatic expression of lipid metabolism- and cholesterol metabolism-related genes.

Test	Array	Refseq	Gene	Fold Regulation	Raw p	Adj p	FDR
51	PPAR	NM_001025432	Crebbp	1.19	0.2689	1.0000	0.8595
52	PPAR	NM_011062	Pdpk1	1.25	0.2830	1.0000	0.8736
53	PPAR	NM_133828	Creb1	1.18	0.2896	1.0000	0.8736
54	LipoproChol	NM_138656	Mvd	1.31	0.2904	1.0000	0.8736
55	PPAR	NM_007381	Acadl	1.23	0.3005	1.0000	0.8736
56	PPAR	NM_023737	Ehhadh	1.27	0.3135	1.0000	0.8736
57	PPAR	NM_011978	Slc27a2	1.27	0.3151	1.0000	0.8736
58	LipoproChol	NM_009885	Cel	**-34.82**	0.3218	1.0000	0.8736
59	LipoproChol	NM_001004157	Scarf1	1.21	0.3222	1.0000	0.8736
60	Both	NM_009692	Apoa1	-1.18	0.3260	1.0000	0.8736
61	LipoproChol	NM_019707	Cdh13	1.28	0.3269	1.0000	0.8736
62	PPAR	NM_177821	Ep300	1.21	0.3479	1.0000	0.8926
63	PPAR	NM_007643	Cd36	1.61	0.3486	1.0000	0.8926
64	PPAR	NM_008194	Gk	1.16	0.3608	1.0000	0.8926
65	LipoproChol	NM_172814	Lrp12	-1.14	0.3630	1.0000	0.8926
66	Both	NM_138648	Olr1	-1.40	0.3685	1.0000	0.8926
67	PPAR	NM_008904	Ppargc1a	-1.29	0.3730	1.0000	0.8926
68	LipoproChol	NM_172622	Trerf1	-1.32	0.3750	1.0000	0.8926
69	LipoproChol	NM_009230	Soat1	1.26	0.3875	1.0000	0.8926
70	LipoproChol	NM_153565	Pcsk9	1.14	0.4005	1.0000	0.8926
71	PPAR	NM_001033606	Acsl3	1.20	0.4035	1.0000	0.8926
72	LipoproChol	NM_010719	Lipe	-1.13	0.4038	1.0000	0.8926
73	PPAR	NM_008509	Lpl	-1.26	0.4049	1.0000	0.8926
74	LipoproChol	NM_130449	Colec12	1.14	0.4118	1.0000	0.8926
75	PPAR	NM_017399	Fabp1	-1.24	0.4152	1.0000	0.8926

Table B.3, (continued). Hepatic expression of lipid metabolism- and cholesterol metabolism-related genes.

Test	Array	Refseq	Gene	Fold Regulation	Raw p	Adj p	FDR
76	LipoproChol	NM_007825	Cyp7b1	1.24	0.4162	1.0000	0.8926
77	PPAR	NM_054089	Tgs1	1.17	0.4410	1.0000	0.9335
78	PPAR	NM_007981	Acsl1	-1.14	0.4519	1.0000	0.9443
79	LipoproChol	NM_178143	Prkaa2	1.10	0.4878	1.0000	0.9599
80	LipoproChol	NM_033218	Srebf2	1.10	0.4901	1.0000	0.9599
81	LipoproChol	NM_001081970	Apol8	-1.45	0.4935	1.0000	0.9599
82	PPAR	NM_019477	Acsl4	1.13	0.4949	1.0000	0.9599
83	LipoproChol	NM_029787	Cyb5r3	-1.09	0.4966	1.0000	0.9599
84	LipoproChol	NM_022993	Lrp10	1.08	0.5065	1.0000	0.9599
85	LipoproChol	NM_013913	Angptl3	1.11	0.5090	1.0000	0.9599
86	LipoproChol	NM_001001144	Scap	-1.15	0.5093	1.0000	0.9599
87	PPAR	NM_028994	Pck2	-1.14	0.5133	1.0000	0.9599
88	LipoproChol	NM_013454	Abca1	-1.07	0.5203	1.0000	0.9599
89	LipoproChol	NM_009693	Apob	1.09	0.5294	1.0000	0.9599
90	PPAR	NM_001081072	Slc27a6	1.27	0.5330	1.0000	0.9599
91	PPAR	NM_013634	Med1	1.07	0.5411	1.0000	0.9599
92	PPAR	NM_013692	Klf10	-1.25	0.5418	1.0000	0.9599
93	LipoproChol	NM_007856	Dhcr7	-1.12	0.5634	1.0000	0.9875
94	LipoproChol	NM_018887	Cyp39a1	-1.18	0.5883	1.0000	0.9931
95	LipoproChol	NM_021283	Il4	1.31	0.5908	1.0000	0.9931
96	LipoproChol	NM_010191	Fdft1	1.08	0.5973	1.0000	0.9931
97	LipoproChol	NM_019709	Mbtps1	1.08	0.5999	1.0000	0.9931
98	Both	NM_008256	Hmgcs2	1.08	0.6029	1.0000	0.9931
99	LipoproChol	NM_001013367	Prkaa1	1.06	0.6077	1.0000	0.9931
100	PPAR	NM_177224	Chd9	1.08	0.6093	1.0000	0.9931

Table B.3, (continued). Hepatic expression of lipid metabolism- and cholesterol metabolism-related genes.

Test	Array	Refseq	Gene	Fold Regulation	Raw p	Adj p	FDR
101	LipoproChol	NM_134469	Fdps	-1.07	0.6271	1.0000	1.0000
102	LipoproChol	NM_013493	Cnbp	1.07	0.6431	1.0000	1.0000
103	LipoproChol	NM_207530	Osbpl1a	-1.09	0.6453	1.0000	1.0000
104	LipoproChol	NM_026784	Pmvk	-1.07	0.6507	1.0000	1.0000
105	Both	NM_010368	Gusb	1.04	0.6590	1.0000	1.0000
106	LipoproChol	NM_007768	Crp	-1.06	0.6640	1.0000	1.0000
107	LipoproChol	NM_008255	Hmgcr	1.11	0.6687	1.0000	1.0000
108	LipoproChol	NM_021547	Stard3	1.06	0.6712	1.0000	1.0000
109	LipoproChol	NM_007898	Ebp	1.04	0.6772	1.0000	1.0000
110	PPAR	NM_010208	Fgr	-1.34	0.6985	1.0000	1.0000
111	LipoproChol	NM_153526	Insig1	1.07	0.6999	1.0000	1.0000
112	LipoproChol	NM_146064	Soat2	-1.06	0.7004	1.0000	1.0000
113	LipoproChol	NM_153680	Snx17	1.06	0.7037	1.0000	1.0000
114	LipoproChol	NM_133997	Apof	-1.04	0.7113	1.0000	1.0000
115	PPAR	NM_009512	Slc27a5	-1.07	0.7214	1.0000	1.0000
116	PPAR	NM_013492	Clu	1.07	0.7217	1.0000	1.0000
117	LipoproChol	NM_023158	Cxcl16	-1.06	0.7259	1.0000	1.0000
118	PPAR	NM_010562	Ilk	1.05	0.7417	1.0000	1.0000
119	LipoproChol	NM_009108	Nr1h4	-1.06	0.7603	1.0000	1.0000
120	PPAR	NM_133249	Ppargc1b	-1.10	0.7637	1.0000	1.0000
121	PPAR	NM_019812	Sirt1	1.06	0.7694	1.0000	1.0000
122	LipoproChol	NM_010700	Ldlr	1.04	0.7730	1.0000	1.0000
123	PPAR	NM_008960	Pten	-1.05	0.7731	1.0000	1.0000
124	PPAR	NM_011144	Ppara	1.07	0.7827	1.0000	1.0000
125	LipoproChol	NM_145554	Ldlrap1	1.03	0.7896	1.0000	1.0000

Table B.3, (continued). Hepatic expression of lipid metabolism- and cholesterol metabolism-related genes.

Test	Array	Refseq	Gene	Fold Regulation	Raw p	Adj p	FDR
126	LipoproChol	NM_010941	Nsdhl	-1.03	0.7898	1.0000	1.0000
127	PPAR	NM_009166	Sorbs1	-1.06	0.8209	1.0000	1.0000
128	LipoproChol	NM_024289	Osbpl5	1.08	0.8240	1.0000	1.0000
129	LipoproChol	NM_145360	Idi1	-1.04	0.8300	1.0000	1.0000
130	LipoproChol	NM_013587	Lrpap1	1.02	0.8485	1.0000	1.0000
131	LipoproChol	NM_028454	Tm7sf2	1.02	0.8677	1.0000	1.0000
132	LipoproChol	NM_023472	Ankra2	-1.03	0.8697	1.0000	1.0000
133	PPAR	NM_009107	Rxrg	-1.05	0.8720	1.0000	1.0000
134	PPAR	NM_010477	Hspd1	1.02	0.8769	1.0000	1.0000
135	LipoproChol	NM_009593	Abcg1	-1.03	0.8795	1.0000	1.0000
136	LipoproChol	NM_013474	Apoa2	-1.03	0.8823	1.0000	1.0000
137	LipoproChol	NM_177197	Idi2	1.03	0.8854	1.0000	1.0000
138	PPAR	NM_023719	Txnip	-1.06	0.8886	1.0000	1.0000
139	LipoproChol	NM_138673	Stab2	-1.02	0.8964	1.0000	1.0000
140	Both	NM_007824	Cyp7a1	-1.05	0.9013	1.0000	1.0000
141	LipoproChol	NM_133808	Hdlbp	-1.01	0.9072	1.0000	1.0000
142	LipoproChol	NM_145401	Prkag2	1.03	0.9182	1.0000	1.0000
143	LipoproChol	NM_207242	Npc1l1	1.04	0.9242	1.0000	1.0000
144	LipoproChol	NM_008514	Lrp6	1.01	0.9286	1.0000	1.0000
145	LipoproChol	NM_008490	Lcat	-1.01	0.9320	1.0000	1.0000
146	PPAR	NM_010431	Hif1a	1.01	0.9364	1.0000	1.0000
147	LipoproChol	NM_010010	Cyp46a1	-1.03	0.9528	1.0000	1.0000
148	PPAR	NM_025794	Etfdh	1.01	0.9579	1.0000	1.0000
149	LipoproChol	NM_023556	Mvk	1.01	0.9664	1.0000	1.0000
150	PPAR	NM_027976	Acsl5	-1.01	0.9710	1.0000	1.0000

Table B.3, (continued). Hepatic expression of lipid metabolism- and cholesterol metabolism-related genes.

Test	Array	Refseq	Gene	Fold Regulation	Raw p	Adj p	FDR
151	PPAR	NM_009127	Scd1	1.01	0.9780	1.0000	1.0000
152	PPAR	NM_007382	Acadm	1.00	0.9859	1.0000	1.0000
153	LipoproChol	NM_138672	Stab1	1.00	0.9913	1.0000	1.0000
154	PPAR	NM_021272	Fabp7	1.00	0.9935	1.0000	1.0000
155	LipoproChol	NM_053272	Dhcr24	1.00	0.9938	1.0000	1.0000
156	LipoproChol	NM_026419	Cela3b	**-10.88**	-	1.0000	1.0000
157	LipoproChol	NM_007470	Apod	**-9.52**	-	1.0000	1.0000
158	PPAR	NM_009605	Adipoq	**3.08**	-	1.0000	1.0000
159	LipoproChol	NM_019779	Cyp11a1	n.q.	-	1.0000	1.0000
160	PPAR	NM_008375	Fabp6	n.q.	-	1.0000	1.0000
161	LipoproChol	NM_008493	Lep	n.q.	-	1.0000	1.0000
162	LipoproChol	NM_053011	Lrp1b	n.q.	-	1.0000	1.0000
163	PPAR	NM_009463	Ucp1	n.q.	-	1.0000	1.0000

Appendix C

Supplemental tables and figures for Ch. 4

Figure C.1.

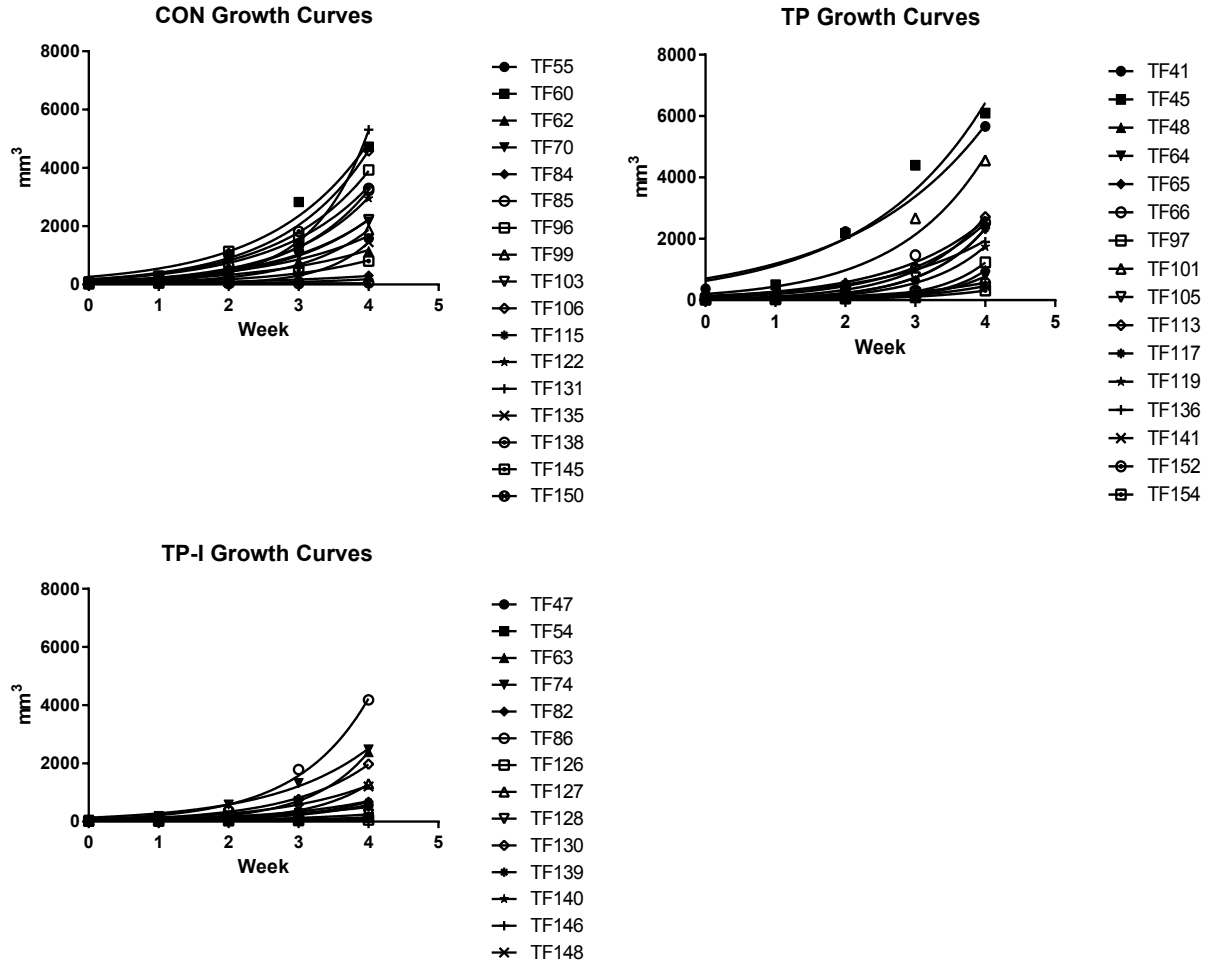

Fig. C.1. Tumor growth curves for individual mice in CON (top left), TP (top right), and TP-I (bottom left) groups. Animals TF41, TF45, TF101, and TF86 appear to display divergent "non-responder" growth behavior compared to other mice in their respective treatment groups.

Figure C.2

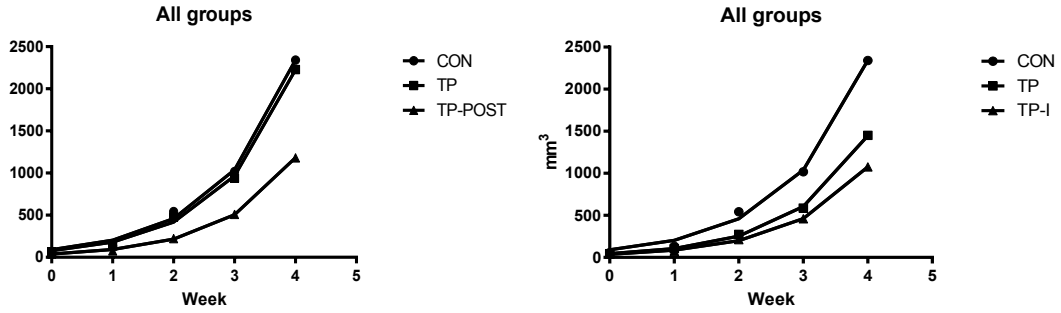

Figure C.2. Average tumor growth rate curves including (left) and excluding (right) "non-responder" tumors putatively identified in **Fig. C.1.**